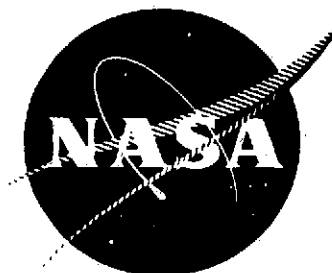AVAILABLE TO THE
PUBLIC

ANALYTICAL AND EXPERIMENTAL INVESTIGATION

OF FLOW FIELDS OF ANNULAR JETS

WITH AND WITHOUT SWIRLING FLOW

by

GENERAL ELECTRIC COMPANY

Prepared For

**National Aeronautics and Space Administration**

NASA — Ames Research Center
Contract NAS 2-5462

| 1. Report No.  NASA CR-137536 | 2. Government Accession No. | 3. Recipient's Catalog No. |
|---|---|---|
| 4. Title and Subtitle  ANALYTICAL AND EXPERIMENTAL INVESTIGATION OF FLOW FIELDS OF ANNULAR JETS WITH AND WITHOUT SWIRLING FLOW | | 5. Report Date  June, 1974 |
| | | 6. Performing Organization Code |
| 7. Author(s)  M. R. Simonson, E. G. Smith, W. R. Uhl | | 8. Performing Organization Report No.  R74AEG265 |
| 9. Performing Organization Name and Address  General Electric Company  Aircraft Engine Group  Cincinnati, Ohio 45215 | | 10. Work Unit No. |
| | | 11. Contract or Grant No.  NAS 2-5462 |
| 12. Sponsoring Agency Name and Address  National Aeronautics and Space Administration  Washington, D. C. 20546 | | 13. Type of Report and Period Covered  Contractor Report |
| | | 14. Sponsoring Agency Code |

15. Supplementary Notes

16. Abstract

Analytical and experimental studies were performed to define the flowfield of annular jets, with and without swirling flow. The analytical model treated configurations with variations of flow angularities, radius ratio and swirl distributions. Swirl distributions characteristic of stator vanes and rotor blade rows, where the total pressure and swirl distributions are related were incorporated in the mathematical model.

The experimental studies included tests of eleven nozzle models, both with and, without swirling exhaust flow. Flowfield surveys were obtained and used for comparison with the analytical model. This comparison of experimental and analytical studies served as the basis for evaluation of several empirical constants as required for application of the analysis to the general flow configuration.

The analytical model developed during these studies is applicable to the evaluation of the flowfield and overall performance of the exhaust of statorless lift fan systems that contain various levels of exhaust swirl.

| 17. Key Words (Suggested by Author(s))  Lift Fans, Annular Jets, Base Pressures, Swirl | 18. Distribution Statement  Unclassified – Unlimited | | |
|---|---|---|---|
| 19. Security Classif. (of this report)  Unclassified | 20. Security Classif. (of this page)  Unclassified | 21. No. of Pages  157 | 22. Price* |

## TABLE OF CONTENTS

## TABLE OF CONTENTS

iv

# LIST OF TABLES

# LIST OF FIGURES

vii

## SUMMARY

This is the final report presenting the results of the analytical and experimental investigations of flow fields downstream of annular jets, both with axial and swirling flows.

An analytical model was developed to predict the base pressures established by axial or swirling flow through annular jets having blunt bases. The model made predictions for configurations having various flow angularities, radius ratios and swirl distributions. Approximately 50 hours of scale model testing were conducted to determine several empirical constants that were required for the analytical model.

The scale models tested consisted of 11 sets of interchangeable inner and outer exhaust flowpaths encompassing flow angles of 10 degrees radially outward to 20 degrees radially inward and radius ratios of 0.40 to 0.70. All of the models were designed to have a constant nozzle exit area of 6.41 square inches (41.35 square centimeters). Various model configurations were tested with:

- Axial flow
- Swirling flow
- Variable pressure ratio
- Simulated louvers (blockage)
- Skewed flow distribution

Having evaluated the necessary empirical constants using the experimental results from the configurations tested with axial and swirling flows, a comparison of the theory with test results was made to verify the selection of the constants. A fair agreement was obtained considering the relatively small sampling of test configurations and the complexity of the analysis. Based on the comparison of test and analytical parameters such as velocity, flow and pressure coefficients, the analytical model appears to be an adequate representation of the exhaust flow downstream of annular nozzle with blunt bases.

## INTRODUCTION

During the initial testing of a rotor-alone turbotip lift fan system, a deficiency in fan thrust was observed and identified as an excessively low hub base pressure. A program was initiated under NASA Contract NAS2-5462 to investigate, both analytically and experimentally, the effects of various types of flow fields upon the base pressures of an annular jet. This report covers this investigation.

An analytical model was developed to predict the level of base pressures which would exist for various flow angularities and nozzle exit radius ratios of annular jets. The analytical model was supported by approximately 50 hours of scale model testing conducted as a General Electric Company, Evendale test facility. Empirical constants from the experimental results were evaluated and used to verify the analytical results with the experimental results. Two of the test configurations were used as an independent check on the validity of the empirical constant selection.

Based on the comparison of test and analytical parameters such as velocity, flow and base pressure coefficients, the analytical model appears to be an adequate representation of the exhaust flow downstream of annular nozzles.

# ANALYTICAL INVESTIGATIONS

## ANALYTICAL MODEL

### General Discussion

When flow exits from an annular nozzle with a blunt centerbody, the pressure over the aft face of the centerbody may be considerably different from the ambient pressure into which the jet is exhausting. This base pressure may have a significant effect on the flow and thrust coefficients of the nozzle. If the jet exits axially without swirl base pressure coefficients, based on average jet velocity head, on the order of -.10 to -.15 are typical. However, if the jet has radial or circumferential velocity components, it is found that the base pressure coefficients may vary widely from these values. This analysis was undertaken to develop an analytical model which could be used to predict base pressure, thrust, and flow coefficients for annular nozzles with nonaxial exit flow. The analysis also considers the effects of radial distribution of swirl, nozzle radius ratio and nozzle pressure ratio.

Conceptually, the reduction of the base pressure below ambient pressure can be thought of as being the result of three separate factors. First, in a jet with axial exit velocity, the shear forces between the high velocity main stream flow and the relatively stagnant air mass composing the centerbody wake must be balanced by an equal and opposite force acting across the base area. This component of base pressure is a true drag force and results in a thrust loss.

Second, there is a component of base pressure due to the meridonal curvature of the flow streamlines in the vicinity of the nozzle exit. This streamline curvature causes a radial static pressure gradient in the flow and, thus causes the base pressure to differ from ambient pressure. If the flow exits axially, the streamline curvatures are small; but if the flow is angled radially inward or outward, the streamline curvatures are much larger, and the effect on the base pressure may be significant. This component of the base pressure has no effect on the nozzle velocity coefficient since it is essentially a potential flow phenomenon.

Third, if the jet has a swirl velocity component, a radial pressure gradient must exist in the flow stream to support the centrifugal forces generated by the swirl. This then results in a base pressure lower than the ambient pressure. Furthermore, the swirling jet induces a rotational motion to the centerbody wake which in turn causes a radial pressure gradient across the base area and a further reduction in average base pressure. This component of base pressure can cause a large loss in nozzle thrust coefficient and represents the energy lost in the swirl velocity component.

It is evident that the above three effects are closely interrelated so that they cannot be treated independently in a mathematical analysis of the problem; however, it is conceptually enlightening to recognize the separate factors affecting the base pressure.

ANALYSIS

## Assumptions and Boundary Conditions

Figure 1 shows the general scheme of the flow model assumed in this analysis. The flow downstream of the nozzle exit is divided into two distinct regions, the main stream flow and the centerbody wake. The dividing line between these two regions is the hub streamline of the main flow. It is recognized that there is actually flow interchange across this boundary, but it can be taken as the line across which the time averaged flow is zero. Thus, the total time averaged mass of air within the wake region is constant. It is assumed that static pressures in the two regions are equal along this streamline and that shear forces between the two regions may exist along this line.

The outer streamline of the main flow is assumed to be an isobaric surface where the static pressure equals the ambient pressure into which the jet is exhausting. Shear stresses and mixing along this outer boundary are assumed to have negligible effect on the base pressure of the centerbody.

At Station 1, the upstream boundary of the main flow, it is assumed that the radial distributions of total pressure, total temperature and angular momentum can be specified as will be explained later. At Station 2, the downstream boundary of the main flow, it is assumed that the slope and curvature of all streamlines are zero. Total temperature and swirl angle distributions at this station are derived from the upstream values assuming that energy and angular momentum are conserved along each stream-line. The total pressure distribution at Station 2 is derived from the upstream total pressure and the assumption that the loss due to the shear stress between the main flow and wake is distributed uniformly across the main stream.

Other assumptions are that the flow is steady, axisymetric and has the properties of an ideal gas. At the inlet station, it is assumed that the radial distribution of angular momentum can be sufficiently well represented as a linear relationship to the stream function.

## General Approach

The general approach used in this analysis is as follows:

First, it is assumed that the shape of the 50% streamline can be represented by an exponential equation of the form.

$$R_m = \left[A + B\,(Z/L) + C\,(Z/L)^2\right] e^{-(Z/L)} + R_{m2} \tag{1}$$

It is readily seen that A and B are determined by the initial radius and slope of the 50% streamline. The constants C and $R_{m2}$ are determined empirically and will be explained in more detail later. L is a length parameter that controls the rate at which $R_m$ approaches its asymptotic value, $R_{m2}$, and will be adjusted during the solution to satisfy axial momentum requirements.

- Starting with an initial guess for L, the radius, slope and curvature of 50% streamline are calculated at a series of axial locations starting with Z = 0 and continuing until $R_m$ approaches $R_{m2}$ sufficiently close.

- An initial guess for the mass flow rate, $\dot{M}$ , is then made, and at each of the above axial locations, a calculation is made along a line normal to the 50% streamline to determine flow properties and radial locations of the other main flow streamlines. Appendix I discusses the equations used for this calculation and the computer program section of this report discusses some of the calculation details. Briefly, however, good approximations to the streamline curvatures are made from the mean streamline slope and curvature and then the equations of momentum, continuity and energy are applied in a direction normal to the flow while satisfying the boundary condition of ambient static pressure on the outer streamline. These calculations begin at the nozzle exit and progress downstream and add an incremental total pressure loss at each step to account for the centerbody wake mixing loss. This incremental pressure loss is calculated from the local hub streamline velocity, density and incremental mixing surface area. This loss is assumed to be distributed uniformly through the main flow at each axial station however.

- Next, using the static pressures and velocities calculated above, axial components of the pressure and momentum forces are integrated across the upstream Station 1 and the downstream Station 2. The pressure forces across the wake area are calculated using the hub streamline static pressures and an empirical correction based on the level of swirl at the hub streamline. The momentum forces across the wake areas are zero since the net amount of fluid in the wake does not change.

- A check is then made on the overall balance between axial pressure and momentum forces acting on the fluid contained between Stations 1 and 2. The radius ratio at the nozzle exit station is also compared to the desired radius ratio. If the axial force balance and radius ratio are not close enough, new estimates are made for $L$ and $\dot{M}$ and the procedure is repeated until the parameters are in agreement within a specified tolerance.

  It is readily seen that the mass flow rate, $\dot{M}$, has a first order effect on the radius ratio. In general, the length parameter $L$ has its first order effect on the force balance since it directly affects the mean streamline curvature and the surface area of the wake-main flow mixing surface. Both parameters do, however, have significant influence on both radius ratio and the force balance and the iteration scheme must recognize this.

- After values for $L$ and $\dot{M}$ are found which simultaneously satisfy the desired radius ratio and the axial force balance, then the desired values for flow coefficient, thrust coefficient, base pressure coefficients, etc., are calculated from the converged solution.

## Mean Streamline Shape

An exponential equation in the form of Equation 1 was selected to represent the shape of the 50% streamline. This equation can be made to have any initial radius and slope at $Z = 0$ and asymptotically approaches zero slope and curvature far downstream as we would expect of the real flow.

The length parameter L controls the rate at which the mean streamline radius approaches its asymptotic value of $R_{m2}$ and, in effect, then controls the rate at which the centerbody wake washes out. It can easily be shown that A and B are determined by the desired initial radius and slope and are given by

$$A = 1 - R_{m2} \tag{2}$$

$$B = A + L \tan \beta_{m1} \tag{3}$$

if we assume an initial radius, $R_{m1}$ of 1.

The third term in Equation 1 whose magnitude is controlled by the constant C is not needed to match the end conditions but was added to achieve a more realistic axial distribution of curvature along the mean streamline. If C is set equal to zero, the third derivitive of $R_m$ from Equation 1 is very high when Z is small. This implies a high axial gradient · of mean streamline curvature and thus a high axial gradient of static pressure in the centerbody wake. Initially, it was felt that selecting C so that the third derivitive of $R_m$ would be zero at Z = 0 would result in a more realistic curvature distribution for the mean streamline. To achieve this then it can be shown that

$$C = (-A + 3B)/6 \tag{4}$$

Finally, in the comparing the calculated mean streamline shapes with the model test data, it was found that a better correlation could be obtained if C was defined as

$$C = (-A + 3B + C_9)/6 \tag{5}$$

where $C_9$ was determined experimentally and discussed in the Application of Analytical Methods Section of this report. $C_9$ then controls the initial value of the axial curvature gradient of the mean streamline and has the same sign.

The value of $R_{m2}$ is indirectly based on experimental data. The Application of Analytical Methods Section of this report describes how the inner streamline radius at the downstream station was found to vary in the test program. If the inner streamline radius is known at the downstream

station, it is a relatively simple matter to calculate the mean streamline
radius knowing the flow, swirl distribution, etc. and assuming zero slope
and curvature at all streamlines.

## Station Calculations Normal to Mean Streamline

### Streamline Curvatures

In order to apply the momentum equation in the direction normal to
streamlines, the streamline curvatures must be known along a potential
line. Since we are assuming a shape for the mean streamline, we know only
its slope and curvature and must estimate a curvature for the other stream-
lines. If we assume that the flow area between the mean streamline and any
other streamline is approximately constant over a short distance, then we
may superimpose the two cases illustrated in Figure 2. This then will
approximately relate the curvature of any streamline to the mean streamline
slope and curvature on the same calculation line by the following equation:

$$1/r = 1/ \left[ r_m + (R_m - R)/\cos \beta_m \right]$$

$$+ (R^2 - R_m^2) \sin^2 \beta_m /(R^2 + R_m^2 \sin \beta_m )^{1.5} \qquad (6)$$

### Summary of Other Equations

In addition to the above equation for streamline curvature, five more
equations are derived in Appendix I which are required to define the main
stream flow properties along a calculation line normal to the mean stream-
line. These additional five equations involve the six unknowns - $r$, $RV_\theta$,
$\rho$, $T$, $R$ and $V_m$ and are summarized below:

$$RV_\theta = (RV_\theta)_T + \lambda \dot{M} (1 - \Psi) \qquad (I1)$$

$$\rho/\rho_{T0} = (P/P_{T0})(T/T_{T0}) \qquad (I4)$$

$$T/T_{T0} = 1 + [Q\ V_{T1}^2 (RV_\theta/(RV_\theta)_T) - (RV_\theta)^2/R^2 - V_m^2] \qquad (I5)$$

$$\frac{\partial R}{\partial \Psi} = \frac{\dot{M} \cos \beta_m}{2\pi\ \rho\ V_m\ R} \qquad (I6)$$

$$\frac{\partial V_m}{\partial \Psi} = \frac{\dot{M}}{2\pi\ \rho\ R\ r} + \frac{\dot{M}\ \lambda}{V_m} \left[ \frac{V_{T1}^2}{2} \frac{Q}{(RV_\theta)_T} - \frac{(RV_\theta)^2}{R^2} \right] \qquad (I10)$$

-9-

Since the last two of the above equations are partial differential equations, they must be integrated along the calculation line. This was done using a second order Runge Kutta procedure and is described in more detail in the Computer Program Section of this report. The other four above equations are used as auxiliary equations in the integration procedure.

## Axial Force Balance

If we remember that the outer surface of the main stream is at ambient pressure and that there is no net flow into or out of the wake region, we may write the following equation expressing equilibrium between the resultant axial pressure force and the change in axial momentum of the main stream.

$$\dot{M} \int_0^1 (V_{Z1} - V_{Z2}) \, d\Psi = 2\pi \int_0^{R_{T1}} R(P_a - P_1) \, dR + 2\pi \int_0^{R_{T2}} R(P_a - P_2) \, dR \quad (7)$$

The two terms on the right-hand side of Equation 7 may each be written as two terms, one of which represents the pressure force in the wake region and the other of which represents the pressure force in the main stream flow as follows:

$$\dot{M} \int_0^1 (V_{Z1} - V_{Z2}) \, d\Psi = 2\pi \int_0^{R_{H1}} R(P_a - P_1) \, dR + 2\pi \int_{R_{H1}}^{R_{T1}} R(P_a - P_1) \, dR$$

$$+ 2\pi \int_0^{R_{H2}} R(P_a - P_2) \, dR + 2\pi \int_{R_{H2}}^{R_{T2}} R(P_a - P_2) \, dR \quad (8)$$

In this analysis, the first integral on the left is calculated as follows:

$$\dot{M} \int_0^1 (V_{Z1} - V_{Z2}) \, d\Psi = \dot{M} \int_0^1 (V_{m1} \cos \beta_{m1} - V_{m2}) \, d\Psi \quad (9)$$

Where it has been assumed that

$$\beta_1 \approx \beta_{m1}$$

and

$$\beta_2 = 0$$

-10-

the first integral on the right is calculated by

$$2\pi \int_0^{R_{H1}} R(P_a - P_1) dR = \pi R_{H1}^2 (P_a - P_{H1}) - C_{PL} \left[ \frac{\pi}{2} \rho_1 (RV_\theta)_{H1}^2 \right] \tag{10}$$

where $C_{PL}$ is an empirical coefficient which accounts for the effect of swirl in the wake region on the hub base pressure. The third integral on the right of Equation 8 is calculated by

$$2\pi \int_0^{R_{H2}} R(P_a - P_2) dR = \pi R_{H2}^2 (P_a - P_{H2}) \tag{11}$$

Collecting Equations 8, 9, 10 and 11 and rearranging gives the final axial force balance equation used in this analysis:

$$\frac{\dot{M}}{2\pi} \int_0^1 (V_{m1} \cos \beta_{m1} - V_{m2}) d\psi - \int_{R_{H1}}^{R_{T1}} R(P_a - P_1) dR$$

$$- \int_{R_{H2}}^{R_{T2}} R(P_a - P_2) dR - \frac{1}{2} \left\{ R_{H1}^2 (P_a - P_{H1}) - C_{PL} \left[ \frac{\rho_1}{2} (RV_\theta)_{H1}^2 \right] \right\} \tag{12}$$

$$- \frac{1}{2} R_{H2}^2 (P_a - P_{H2}) = 0$$

## Overall Performance Calculations

After a converged solution to the flow problem is obtained, we must still calculate flow, thrust, velocity and base pressure coefficients since they are the nozzle characteristics of primary interest. To do this, the following procedure was used:

● First, a mass averaged ideal jet velocity, $V_i$, was calculated using total pressure and temperature at Station 1 expanding to ambient pressure. Also, a corresponding ideal density, $\rho_i$, was calculated.

● An ideal mass flow was calculated as

$$\dot{M}_i = \rho_i A_n V_i \tag{13}$$

where $A_n$ is the geometric annular area at the nozzle exit with no angularity factor applied.

● An ideal thrust was calculated as

$$F_i = \dot{M}_i V_i \tag{14}$$

-11-

- The real mass flow and thrust are taken from the converged flow solution and used to calculate flow, thrust and velocity coefficients as follows:

$$C_F = \dot{M}/\dot{M}_i \tag{15}$$

$$C_T = F/F_i \tag{16}$$

$$C_V = C_T/C_F \tag{17}$$

- A mean total pressure at Station 1, $\overline{P}_{T1}$, was calculated from $V_1$ and base pressure coefficients calculated as:

$$C_{P1} = \frac{P_{H1} - P_a}{\overline{P}_{T1} - P_a} \tag{18}$$

$$C_{P2} = (\overline{P}_H - P_a)/(\overline{P}_{T1} - P_a) \tag{19}$$

Thus, $C_{P1}$ is the base pressure coefficient at the outer radius of the centerbody and $C_{P2}$ represents the average base pressure coefficient over the centerbody area. Both are based on an average nozzle exit dynamic pressure.

# COMPUTER PROGRAM

## General Description

The computer program was written to carry out the iterative solution to the equations presented in the previous section. Time-sharing Fortran was used. In general, input to the program consists of:

- Geometric parameters describing the nozzle exit.
- Total pressure, total temperature, and swirl distributions at the nozzle exit.
- A wake shear stress factor.
- Three empirical constants.
- An initial guess for L.
- Parameters used to calculate rotor loading coefficients if the swirl is generated by a rotor.
- Two control indicators.

All input is supplied at the time-sharing terminal at the time of program execution. Output of the program consists of:

- A general description of the flow field.
- Nozzle base pressure, flow, velocity and thrust coefficients.
- An approximate description of the rotor blade environment and loading coefficients if the swirl is generated by a rotor.

Figure 3 is a schematic block diagram of the program showing the general calculation procedure and flow of information. The solid lines show information flow between main program elements while the dotted lines show information flow between the main program and subroutines or between subroutines. Numbers in the upper left-hand corner of some blocks refer to statement numbers in the program listing given in Appendix III.

There are two options in running this program - the rotor option and the stator option. For the stator option, it is assumed that the

swirl is generated by a "no loss" stator with uniform inlet total pressure and temperature. For the rotor option, it is assumed that the swirl is generated by a rotor with uniform upstream total pressure and temperature and zero upstream swirl. The energy addition process is assumed to be isentropic but will result in a radial variation of total pressure and temperature at the nozzle exit station if a nonconstant angular momentum is specified at this station.

## "ROTFLO" Subroutine

A key element of this program is the subroutine "ROTFLO" which performs the station calculations normal to the mean streamline. This subroutine uses a second order Runge Kutta method to simultaneously integrate Equations I6 and I10 along a station calculation line. Equations I1, I4 and I5 are used as auxiliary equations during this integration.

"ROTFLO" can either begin with the radius given for the inner streamline and integrate outward to the tip streamline or begin with the radius given for the mean streamline and integrate both ways to the tip and hub streamlines. In either case, the initial value of the meridonal velocity, $V_m$, is iterated upon until the static pressure on the tip streamline equals the ambient pressure. Twelve streamlines are used in the integration procedure and are located at 0, 4, 10, 20, 30, 40, 50, 60, 70, 80, 90 and 100 percent of the flow starting at the hub streamline. The streamlines are spaced closer together in the inner portion of the flow since the flow tends to vary more rapidly in this region.

## Iteration Scheme

In order to arrive at a solution, both the mass flow rate, $\dot{M}$, and the length parameter, L, must be iterated upon until the nozzle exit

radius ratio and axial force balance equation are satisfied. The scheme selected to do this has been called the secant method and will be briefly described for the case of two variables.

Let "$e_1$" be the percent error in radius ratio and "$e_2$" be the percent error in the axial force balance and plot these errors against $\dot{M}$ and L for three previous iterations as shown in Figures 4a and 4b. These points lie on error function surfaces. If we pass a plane through each of these two sets of points, we will have "secant" planes to the two error function surfaces. Suppose that in Figure 4a the secant plane intersects the $\dot{M}$-L plane in the Line ab. Combinations of $\dot{M}$ and L which lie on Line ab can usually be expected to reduce the error $e_1$ to a lower value than the previous tries. Similarly points which lie along line cd in Figure 4b can be expected to reduce the error $e_2$. A combination of $\dot{M}$ and L then which lies on both ab and cd should then be an improved estimate for the next iteration. This then is the scheme which the subroutine "INT2" uses to give improved estimates for $\dot{M}$ and L at each step in the iteration.

In order to start the iteration procedure, initial estimates of $\dot{M}$ and L are made and then each in turn is perturbated by a small amount in order to give three starting points.

Input Definitions

| | |
|---|---|
| $R_H/R_T$ | Nozzle exit radius ratio, dimensionless. |
| $\beta_{ml}$ | Mean streamline angle from axial; deg. + = outward, – = inward. |
| FF | Wake mixing shear stress coefficient; based on hub streamline meridonal velocity head; dimensionless. |
| L | Initial guess for the length parameter, L, feet. |
| $C_{PL}$ | The difference between average base pressure and hub streamline base pressure divided by hub streamline tangential velocity head; dimensionless. |

RCUO      Angular momentum, $RV_\theta$ , on tip streamline; $ft^2/sec$.

DRCUO      Angular momentum difference between hub and tip, $(RV_\theta)_H$ - $(RV_\theta)_T$; $ft^2/sec$. The distribution of $RV_\theta$ is assumed linear with stream function between hub and tip.

$(P_T/P_a)$      Nozzle exit pressure ratio at tip; dimensionless.

$T_{TO}$      Inlet temperature - upstream of rotor for rotor case; deg. R.

ROT      0 if swirl is generated by a stator; 1 if swirl is generated by a rotor.

IPT      1 if downstream flowfield printout is desired; 0 if not.

$C_2$      Ratio of downstream hub streamline radius to nozzle exit tip radius; dimensionless. (See Figure 91 for values recommended from data.)

$C_9$      Empirical constant determining mean streamline curvature gradient at nozzle exit station. (See Figure 92.)

The following four inputs are used only for the rotor option but must have dummy values for stator option also:

$\sigma_T$      Rotor tip solidity; dimensionless.

$\sigma_H$      Rotor hub solidity, dimensionless.

VIN      Average rotor inlet absolute velocity; ft/sec.

$n_R$      Average rotor efficiency.

## Output Definitions

Output from the program is in three blocks. The first, which is optional (depending on IPT), describes the flowfield downstream of the nozzle exit. At each axial station, it lists in this order:

$$Z, \; R_m, \; \beta_m, \; c_m, \; R_T, \; R_H, \; V_T, \; V_{mT}, \; V_{mH}, \; P_H - P_a$$

The second output block is generated only for the rotor case and approximately describes the rotor blade environment, the rotor blade static pressure rise coefficient and "D" factor at each streamline.

At each streamline (starting at the hub), it lists in this order across the page:

S.L. No., R, $P-P_a$, $W_1$, $V_{Z1}$, U, $\sigma$, $C_{PR}$, DF

The third output block lists most of the input on the first line for reference. On the second line, it lists the overall performance parameters and other items of interest in this order:

$C_P$, $C_V$, $C_T$, $C_{PL}$, $C_{P2}$, Z, AP, L, $\dot{M}$, $F_i$

where Z is the value at the downstream Station 2 and L is the final value of the length parameter.

# EXPERIMENTAL INVESTIGATIONS

## TEST HARDWARE AND INSTRUMENTATION

### Base Pressure Models

The base pressure model consisted of a 4 inch (10.16 centimeter) inner diameter stainless steel casing in which a 2 inch (5.08 centimeter) aluminum center body was positioned by one support strut as shown in Figure 5. To the inlet of the model, a small bellmouth was attached. Vanes to generate axial or swirling flow shown in Figure 6 were fitted behind the center body with the swirl vanes designed to produce a comparable level of swirl as observed in the full scale testing of the LF336E (Reference 1). Inter-changeable inner and outer aluminum flowpaths could be positioned at the model exit plane. A total of 11 sets of different inner and outer flow-paths was designed with varying radius ratios and flow angles with a positive flow angle designated as radially outward. Table I contains perti-nent data on the exit flowpath and Table II gives the contour geometry of each set. Figure 7 shows a schematic of the test model cross section.

For simplification, the model configurations will be hereafter desig-nated by the model number as given in Table I and a prefix of either an "A" or "S" will be used to identify axial or swirling flow, respectively. Thus, S5 is the test configuration designation for Model 5 tested with swirling flow and A5 is for Model 5 with axial flow.

### Test Facility

The base pressure tests were performed at the probe calibration facility at the General Electric Company, Evendale, Ohio. This test facility has the capability of adapting the probe stand for small scale model testing. With the base pressure model positioned in the test stand as shown in Figure 8, total pressure ratios of slightly greater than 1.4 and flow rates between 2-3 lbs/sec (0.9-1.4 Kg/sec) could be attained using the shop air system.

The test facility contained instrumentation systems to provide constant temperature inlet air operation for each test and provided the actuation systems for the exit plane traversing probe in immersion, yaw and pitch.

-18-

## Instrumentation

Instrumentation on the base pressure model was kept at a minimum level with the major portion of the performance data being recorded by three port exhaust traversing probes. Eight static pressure taps were located 90° from the center body support strut and equally spaced from the inlet of which the first five were used to record wall statics for upstream flow measurements.

The three port exhaust traversing probe was mounted in a facility actuation system which had the capability of immersing, pitching and yawing the probe. For the base pressure tests, the probe was installed such that the probe static pressure ports could be nulled, i.e., probe aligned in the direction of the flow which yielded the magnitude and direction of the swirl angle. The data pressure null was indicated by a pressure balancing transducer with a null meter readout with each static pressure connected to each side.

The exhaust traversing probe was mounted aft of the model such that the axial distance could be varied to at least four model diameters downstream.

# TESTING AND PROCEDURES

## Test Scope

The main purpose of this test was to investigate the effects of various flow field conditions of annular jets on the base pressures of blunt bases so that experimental data could be correlated with an analytical model in order to develop a useful tool in the future design of turbotip lift fan systems. The new analytical model, including empirical constants from the tests, could then be used to predict the base pressure levels of new lift fan designs, thus reflecting permissible or nonpermissible levels of base pressure or exit geometry.

A total of 50 hours of testing was conducted consisting of three to four traverse probe axial positions with axial and swirling flows, variable pressure ratios, blockage at the exit plane to simulate louvers, and skewed swirl distributions. Table III gives a complete summary of the different configurations that were tested.

## Test Procedures

Since a minimum of instrumentation was used for the tests and due to an unavailability of an adequate pressure recording system, the total and static pressures from the traversing probe and the wall statics were recorded manually from mercury manometers. Traverse data was recorded for approximately 20 radial locations from the tip to center of the base. Digital counters on the traverse probe yaw and immersion actuators were used for determination of the swirl angle and the probe radial location.

## Probe Calibration

One three-port cobra probe was used to obtain a survey of the total and static pressures and the yaw (swirl) angle across the model exhaust plane. Figure 9 shows a schematic of the probe head with several pertinent dimensions.

The probe was calibrated in the probe calibration stand over a range

-20-

of pitch angles (+10° to -20°) and Mach numbers (0.6 and 0.8). The calibration was performed with the yaw angle kept constant (0°) since the actual model tests would be performed with the static pressures nulled, i.e., the probe aligned in the direction of the flow.

The recorded pressures were reduced into a coefficient form such that

$$K1 = \frac{P_{TO} - P_a}{P_{TP} - P_{SP}}$$

where,

$P_{TO}$ — plenum total pressure

$P_a$ — barometric pressure

$P_{TP}$ — total pressure indicated by probe

$P_{SP}$ — static pressure indicated by probe

Also, a correction factor (K2) was included due to the effect of the flow angularity (pitch), where

$$K2 = \frac{P_{SP}}{P_{SP} \ (\beta = 0°)}$$

The results of the probe calibration are shown in Figure 10. These calibration characteristics provided the basis for converting the measured pressure data into the appropriate corrected pressures, where

$$P_S = P_{TP} - (P_{TP} - P_{SP})(K1/K2)$$

Data Processing

Data reduction of the recorded parameters was done by a time-sharing computer program which calculated and integrated various flow field parameters. Further details of the procedures used for attaining overall model performance are given in Appendix II.

# TEST RESULTS

The results of the Base Pressure Tests are presented in the following section of this report. The discussion will be separated into major categories covering:

- Model performance with axial flow
- Model performance with swirling flow
- Model performance with variable pressure ratio
- Model performance with simulated louvers (blockage)
- Model performance with skewed swirl distribution

## Performance With Axial Flow

Data was recorded for the axial configurations at several traverse axial distances. Figures 11 through 16 show the total and static pressure coefficient distribution for the closeup traverse position and Figures 17 and 22 show the same parameters but with the traverse plane being located 0.656 model diameters downstream. As indicated from these figures, the configurations with a positive flow angle, radially outward, exhibit a higher static pressure in the flow stream and a lower static pressure in the base region as those configurations with axial or less than axial flow angularity.

Integration of the exhaust plane at several axial distances made it possible to locate the flow streamlines in the exhaust region of the models. Figures 23 through 28 show a graphical representation of the exhaust flow fields for all the models tested with axial flow. The 100% streamline location was determined at the point where the integrated flow equalled the upstream flow with the integration starting at the centerline and proceeding radially outward. The zero percent streamline was determined at the location at which the total pressure was equal to zero. The mixing region, as indicated on the figures, is the difference between the total integrated flow and the upstream flow. In this region, the moving jet interacts with the stationary surrounding air, transfers momentum to the stationary air, thus entraining flow. Figures 29 through 31 show the amount of flow entrainment for all the models with axial flow.

Figures 32 through 34 contain the wake mixing loss characteristics for the models with axial flow with the mixing loss coefficient defined as,

$$\overline{\omega} = \frac{P_{TO} - \overline{\omega}_0(P_{TO} - P_{Sm}) - \overline{P}_T}{P_{TO} - \overline{\omega}_0(P_{TO} - P_{Sm}) - P_a}$$

where

$P_{TO}$ — upstream total pressure

$P_{Sm}$ — flow section static pressure

$\overline{P}_T$ — mass averaged total pressure

$\overline{\omega}_0$ — loss coefficient due to components of model (bellmouth, vanes, etc.)

$P_a$ — ambient pressure

Figures 35 through 38 show the effects of model geometry on the average hub base pressure, the main flow thrust coefficient, the overall thrust coefficient and on the flow coefficient for axial flow. The calculation procedures for these parameters are discussed in Appendix II.

Performance With Swirling Flow

Figures 39 through 44 show the total and static pressure coefficients and swirl angle distributions for the set of models tested with swirling flow with the exhaust plane survey being made at the closeup traverse position. The same parameters for the same test conditions, but with the exhaust traverse plane being 0.656 model diameters downstream are presented in Figures 45 through 50. An immediate observation is the difference in the levels of the static pressure coefficients between configurations with axial and swirling flows. For the swirl cases, the static pressure coefficients are at least twice as low than those with axial flow.

The graphical representations of the flow fields for the models with swirling flow are shown in Figures 51 through 56. The same calculation schemes were used to establish the 100 and the zero percent streamlines and the mixing regions as with the axial cases. Figures 57 through 59 contain the flow entrainment characteristics for the configurations tested with swirling flow. Again, an immediate observation shows that the flow entrainment characteristics of the configurations with swirl are 20 to 30 percent higher than the same configurations with axial flow.

The wake mixing loss characteristics for the swirl cases are shown in Figures 60 through 62. The mixing loss coefficients are calculated in the same manner as those for the axial cases.

The effects of model geometry on the level of the average base pressure and on the base pressure at the hub outer radius are shown in Figures 63 through 65. As can be seen, swirling flow has a tremendous effect upon the levels of base pressures that were observed. Compared to the axial cases, the swirl configurations are, on an average, four to six times lower, i.e., more negative.

The effects of geometry on the main flow thrust and on the overall thrust coefficients are shown in Figures 66 and 67. Figure 68 contains the variation of the flow coefficient with model geometry.

The unstable regions as indicated in Figures 63 through 68 were observed while testing the 0.4 radius ratio models at -10 and -20 degree flow angles. Intermittent, unstable conditions existed several times with these two configurations which were signified by changes in the audible noise frequency and a fluctuation of the total and static pressures in the exhaust flow. Inserting a tool or a hand into the exhaust stream removed the unstability.

## Performance With Variable Pressure Ratio

The three models with zero degree flow angles were tested at two other pressure ratios, 1.2 and 1.4, with swirling flow to investigate the effects of variable pressure ratio upon the base pressures. Figures 69 through 71 show the effects of pressure ratio on the total and static pressure coefficients and on the swirl distributions. As indicated, the swirl angle and total pressure coefficients are unchanged by pressure ratio while the static pressure coefficients do show a slight change. Figures 72 and 73 show the effects of pressure ratio on the base pressure coefficients averaged over the base and at the base outer radius. The trends that are shown indicate that the average base pressure increases slightly with pressure ratio while the base pressure at the base outer radius exhibits the opposite trend.

The effects of pressure ratio upon the main flow and the overall thrust coefficients are presented in Figures 74 and 75. As shown, the thrust coefficients increase with increasing pressure ratio. Figure 76 shows that increasing pressure ratio has no significant effect upon the measured flow coefficient.

## Performance With Blockage

The possibility that the base pressures could be increased by the addition of a blockage system, simulating exhaust louvers, was investigated. The blockage system consisted of a wooden support frame containing eight rows of 0.0645 inch (0.1638 cm) outside diameter, stainless steel tubing. The tubing spacing was selected at 0.5 inch (1.27 cm) such that a 14 percent blockage existed. The blockage system was mounted 0.5 inch (1.27 cm) aft of the nozzle exit plane. Figure 77 shows photographs of the test setup with the blockage system mounted in position.

The models with zero flow angles were tested with the blockage system installed with and without swirling flow. Figures 78 through 80 show the effects of blockage with axial flow. The only result that the blockage produced was a small increase in the flow stream static pressure of approximately 5 percent for all three configurations. The influence of the blockage upon the base pressure and the flow coefficient is insignificant as shown in Figure 81.

Figures 82 through 84 contain the effects of blockage on the total and static pressure coefficients and on the swirl angle for those models tested with swirling flow. As with the axial flow configurations, a similar trend is observed in regard to the stream static pressure, that is, a slight increase in that static pressure. Figures 85 and 86 show the influence of the blockage and the base pressures and on the flow coefficinet. The blockage increased the base pressures approximately 10 percent and decreased the flow coefficient by 2 percent.

## Performance With Skewed Swirl Distribution

Since the axial flow configurations exhibited a much lower level of base pressure as compared to the swirling flow cases, the possibility that a skewed swirl distribution across the flow stream would improve the base pressures was investigated.

The axial vane assembly used to produce axial flow was reworked such that a similar level of swirl as observed with the swirl vane assembly existed at the tip of the vanes. At the hub, no rework was done so that axial flow would exist there, thus intending to produce comparable levels of base pressure as observed in the axial flow cases.

Figures 87 through 89 show the total and static pressure coefficients and swirl distributions for the Models 2, 6 and 10 with zero flow angle. As shown, the levels of base pressure are between those observed for the axial and swirl cases. Table IV contains a performance comparison for Models 2, 6 and 10 with the three types of flow fields tested. These results show that for the skewed swirl distributions, base pressure, thrust and flow coefficient all increased from the observed level with complete swirling flow, the largest increase occurring in the thrust and flow coefficients.

## APPLICATION OF ANALYTICAL METHODS

The analytical model developed for representation of the flow around blunt bases requires an evaluation of numerous empirical constants for completion of the mathematical model. The four most significant constants are:

FF - Effective friction or loss factor representative of losses associated with the boundary between the main and wake flows.

$C_2$ - The area occupied by the wake flow field at axial locations far downstream of the hub base. This constant represents the ratio of the wake flow diameter to the nozzle tip diameter.

$C_{PL}$ - The coefficient representative of the pressure gradients in the wake flow at the plane of the hub base. The parameter establishes the integrated average base pressure in terms of the pressures at the outer radius of the base.

$C_9$ - A coefficient that controls the initial rate of change of curvature of the wake flow.

The tests of the base pressure models with swirling flow provided the data necessary for evaluation of these constants. The initial step in the analysis was to determine the appropriate flow field parameters in a format compatible with the analytical model. The inlet flow to the model is represented as an average total pressure ratio, an air total temperature and the angular momentum distribution. The total pressure and temperature inputs were determined through test measurements and were assumed constant for all test models. The angular momentum in the analysis is represented by a tip momentum with a linear variation between the hub and tip. The test measurements were used to evaluate the required momentum distributions by fitting the measured profiles. The resulting variation of tip momentum and hub-to-tip momentum difference is given in Figure 90 for the range to test radius ratio. The total pressure ratio and temperature used during the analysis were 1.263 and 535° R (297° K), respectively.

Only one of the four empirical constants can be obtained directly from the test measurements. The wake area coefficient, $C_2$, can be obtained by referring to the test flow streamline distributions. Using the most downstream traverse location, the radius of the wake region was obtained and is summarized in Figure 91. The wake size appears to be independent of both model radius ratio and radial flow angle. An average value of 0.48 was selected for the coefficient, $C_2$, for evaluation of the test data using the mathematical model. A constant value of the wake size appears reasonable for the test model since the model employed one set of turning vanes upstream of the contoured nozzle and exhaust plane. The swirl vane had a hub-to-tip ratio of 0.5 with a tip radius of 4 inches (10.16 cm). Through observations of the downstream flow profiles, it appears that all models exhibit similar swirl and pressure distributions. Apparently, the flow field, as established at the plane of the swirling vanes, determines the downstream flow conditions and is not affected by the internal flowpath of the actual test model. This consistent flow field pattern can be expected since both axial and tangential momentum are conserved except for friction and mixing losses.

With one of the constants established, the problem was to determine the three remaining constants using the model test data. Through a process of trial and error, the friction factor was established at a level of 0.04 and the values of $C_9$ and $C_{PL}$ were determined to be a function of radius ratio and radial flow angle as shown in Figure 92. The justification for these characteristics is based on agreement of predicted and measured hub base pressure levels. A comparison of the hub base pressure coefficients as obtained from tests and theoretical analysis is given in Figures 93 through 95.

The agreement of test and theory is fair considering the small sampling of test configurations and the complexity of the analysis. A comparison of test and analytically derived nozzle velocity and flow coefficients shows similar agreement. The agreement of velocity coefficients is of prime importance since it includes the combined effects of swirl distributions in addition to stream and base pressure levels. The agreement between test and theory is within 2 percent.

-28-

The empirical constants, as derived for comparison of configurations with swirling flow, were then used to evaluate hub base pressure levels during axial flow. Without swirling flow, the value of the constant $C_2$ should be very small since the jet wake closes on itself at the hub base centerline. Likewise, the base pressure coefficient, $C_{PL}$, would be very small since the stream static pressures are uniform throughout the separated base regions. Using these assumptions, the comparison of test and analysis as shown in Figures 96 through 98 is possible. Again, the comparison shows fair agreement with the largest differences occurring for the 0.4 radius ratio configuration.

The configurations tested with the skewed swirl distribution and model "E" were compared with the analytical model using the empirical constants that were determined previously. Table V contains the comparison of test and theory. As shown, the theory predicts the test results reasonably well. This final comparison verifies the selection of the empirical constants derived from the 20 configurations previously tested and also confirms the validity of the analytical model.

Based on the comparison of test and analytical parameters such as velocity, flow and pressure coefficients, the analytical model appears to be an adequate representation of the exhaust flow downstream of annular nozzles with blunt bases. Considerable additional testing, including numerous models with variable swirl levels, along with further refinement of the analytical model, would be required to improve the levels of data correlation.

# CONCLUSIONS

An analytical model was developed to predict the base pressures established by axial or swirling flow through annular jets having blunt bases. Configurations consisting of various flow angularities, radius ratios and swirl distribution can be modeled by the computer program generated from the developed theory. Over 50 hours of scale model testing were conducted to assist in the selection of several empirical constants required by the analytical model. The significant conclusions which were derived from the results of this investigation are as follows:

- Three separate factors have been recognized as major contributors to the pressure at the base of an annular nozzle, i.e., the shear forces between the high velocity main stream flow and the relatively stagnant air mass composing the centerbody wake, the meridonal curvature of the flow streamlines in the vicinity of the nozzle exit, and the radial pressure gradient due to the swirl velocity component.

- Major differences in the flowfields between axial flow and swirling flow were observed. With axial flow, base pressure coefficients of -0.2 to 0.25 were measured while with swirling flow, base pressure coefficients of -0.4 to -0.8 were not uncommon.

- Base pressure levels are unaffected by changes in pressure ratio and only slightly affected by blockage downstream of the base.

- The agreement of test and theory is fair considering the small sampling of test configurations and the complexity of the analysis. The analytical model is an adequate representation of the exhaust flow downstream of annular nozzles with blunt bases based on the comparison of test and analytical parameters.

- Additional testing is required to refine the analytical model in order to improve the correlation between the theory and the test.

## NOMENCLATURE

| Symbol | Definition | Units |
|---|---|---|
| $a_n$ | Acceleration normal to a streamline | $ft/sec^2$ $(m/sec^2)$ |
| $A$ | Constant, $1 - R_{m2}$ | ft (m) |
| $A_m$ | Model measuring section effective flow area | $ft^2$ $(m^2)$ |
| $A_n$ | Nozzle exit annular area | $ft^2$ $(m^2)$ |
| AP | Surface area of wake mixing zone | $ft^2$ $(m^2)$ |
| $B$ | Constant, $A + L \tan \beta_{m1}$ | ft (m) |
| $c_m$ | Mean streamline curvature | 1/ft (1/m) |
| $C$ | Constant, $(-A + 3B + C_9)/6$ | ft (m) |
| $C_F$ | Nozzle flow coefficient, $\dot{M}/\dot{M}_i$ | |
| $C_P$ | Specific heat at constant pressure | BTU/lb-°R (joule/kg-°K) |
| $C_{PL}$ | Empirical coefficient $(\bar{P}_H - P_{H1})/[1/2 \ \rho_1 (RV_\theta)^2_H]$ | |
| $C_{PR}$ | Rotor static pressure rise coefficient, $(P_2 - P_1)/(P_{TR1} - P_1)$ | |
| CPS | Local static pressure coefficient, $(P_S - P_a)/(\bar{P}_{T1} - P_a)$ | |
| CPT | Local total pressure coefficient, $(P_T - \bar{P}_a)/(\bar{P}_{T1} - P_a)$ | |
| $C_{P1}$ | Hub base pressure coefficient at outer radius, $(P_{H1} - P_a)/(\bar{P}_{T1} - P_a)$ | |
| $C_{P2}$ | Average hub base pressure coefficient, $(\bar{P}_H - P_a)/(\bar{P}_{T1} - P_a)$ | |
| $C_T$ | Nozzle thrust coefficient, $F/F_i$ | |
| $C_V$ | Nozzle velocity coefficient, $C_T/C_F$ | |

| Symbol | Definition | Units |
|--------|-----------|-------|
| $C_2$ | Ratio of downstream to nozzle tip radius, $R_{T2}/R_{T1}$ | |
| $C_9$ | Empirical constant | ft (m) |
| d | Total differential | |
| DF | Rotor diffusion factor | |
| DRCUO | Angular momentum difference between hub and tip, $(RV_\theta)_H - (RV_\theta)_T$ | $ft^2/sec$ $(m^2/sec)$ |
| $e_1$ | Iteration error function in radius ratio | |
| $e_2$ | Iteration error function in axial force balance | |
| F | Total thrust | lb (kN) |
| $F_i$ | Ideal thrust | lb (kN) |
| FF | Wake shear stress coefficient, $F_S/(1/2\ \rho\ V_m^2)$ | |
| g | Gravitational constant | $ft/sec^2$ $(m/sec^2)$ |
| IPT | Print control parameter, 1 if flow-field print is desired, 0 if not | |
| J | Work equivalent of heat | ft-lb/BTU (N-m/joule) |
| K1 | Probe calibration coefficient, $(P_T - P_S)/(P_{TP} - P_{SP})$ | |
| K2 | Probe calibration factor, $P_{SP}/P_{SP}(\beta = 0°)$ | |
| L | Length parameter | ft (m) |
| $\dot{M}$ | Mass flow rate | lb-sec/ft (kg-sec/m) |
| $\dot{M}_i$ | Ideal mass flow rate | lb-sec/ft (kg-sec/m) |
| n | Distance normal to streamline | ft (m) |

| Symbol | Definition | Units |
|---|---|---|
| $P$ | Static pressure | $lb/ft^2$ $(kN/m^2)$ |
| $P_a$ | Ambient pressure | $lb/ft^2$ $(kN/m^2)$ |
| $\bar{P}_H$ | Area averaged hub base pressure | $lb/ft^2$ $(kN/m^2)$ |
| $P_S$ | Corrected probe static pressure | $lb/ft^2$ $(kN/m^2)$ |
| $P_{Sm}$ | Model flow section static pressure | $lb/ft^2$ $(kN/m^2)$ |
| $P_{SP}$ | Probe indicated static pressure | $lb/ft^2$ $(kN/m^2)$ |
| $P_T$ | Total or stagnation pressure | $lb/ft^2$ $(kN/m^2)$ |
| $\bar{P}_{T1}$ | Mean total pressure at nozzle exit based on ideal velocity, $V_i$ | $lb/ft^2$ $(kN/m^2)$ |
| $P_{TP}$ | Probe indicated total pressure | $lb/ft^2$ $(kN/m^2)$ |
| $P_{TR}$ | Relative total pressure | $lb/ft^2$ $(kN/m^2)$ |
| $Q$ | Dimensionless indicator (0, stator case; 1, rotor case) | |
| $r$ | Streamline radius of curvature | ft (m) |
| $r_m$ | Mean streamline radius of curvature | ft (m) |
| RCUO | Angular momentum at tip streamline, $RV_\theta$ | $ft^2/sec$ $(m^2/sec)$ |
| ROT | Control parameter, 0 if swirl is generated in stator, 1 if not. | |
| $R$ | Radius | ft (m) |
| $R_H$ | Hub radius | ft (m) |
| $R_m$ | Mean streamline radius | ft (m) |
| $R_T$ | Tip radius | ft (m) |
| $S$ | Distance along a streamline | ft (m) |
| $T$ | Static temperature | °R (°K) |
| $T_T$ | Total temperature | °R (°K) |

| Symbol | Definition | Units |
|--------|-----------|-------|
| $U$ | Wheel speed | ft/sec (m/sec) |
| VIN | Average rotor inlet absolute velocity | ft/sec (m/sec) |
| $V_1$ | Mass averaged ideal jet velocity | ft/sec (m/sec) |
| $V_m$ | Meridinal velocity component | ft/sec (m/sec) |
| $V_T$ | Total velocity component at tip | ft/sec (m/sec) |
| $V_z$ | Axial velocity component | ft/sec (m/sec) |
| $V_\theta$ | Tangential velocity component | ft/sec (m/sec) |
| $W$ | Integrated airflow from wake centerline | lb/sec (kg/sec) |
| $W_1$ | Rotor inlet relative velocity | ft/sec (m/sec) |
| $W_2$ | Rotor exit relative velocity | ft/sec (m/sec) |
| $W_T$ | Total integrated airflow at nozzle exit plane | lb/sec (kg/sec) |
| XIMM | Probe immersion | ft (m) |
| $Z$ | Axial distance downstream of nozzle plane | ft (m) |
| $\alpha$ | Yaw (swirl) angle | deg (deg) |
| $\beta$ | Streamline meridonal flow angle | deg (deg) |
| $\beta_m$ | Mean streamline meridonal flow angle | deg (deg) |
| $\gamma$ | Ratio of specific heats | |
| $\partial$ | Partial differential | |
| $\eta_R$ | Average rotor efficiency | |
| $\theta$ | Tangential flow angle | deg (deg) |
| $\lambda$ | Angular momentum distribution factor, $-[(RV_\theta)_T - (RV_\theta)_H]/\dot{M}$ | |

| Symbol | Definition | Units |
|---|---|---|
| $\rho$ | Mass density | $\text{lb-sec}^2/\text{ft}^4$ <br> $(\text{kg-sec}^2/\text{m}^4)$ |
| $\rho_i$ | Ideal mass density | $\text{lb-sec}^2/\text{ft}^4$ <br> $(\text{kg-sec}^2/\text{m}^4)$ |
| $\rho_T$ | Mass density based on stagnation conditions | $\text{lb-sec}^2/\text{ft}^4$ <br> $(\text{kg-sec}^2/\text{m}^4)$ |
| $\sigma$ | Solidity | |
| $\psi$ | Stream function | |
| $\bar{\omega}$ | Wake mixing loss coefficient, $(\bar{P}_{T1} - \bar{P}_T)/(\bar{P}_{T1} - P_a)$ | |
| $\omega_0$ | Nozzle model internal loss coefficient, $(P_{T0} - \bar{P}_{T1})/(P_{T0} - P_{Sm})$ | |

## Subscripts

| | |
|---|---|
| 0 | Upstream or reference station |
| 1 | Nozzle exit station, or rotor inlet station |
| 2 | Downstream station, or rotor exit station |
| H | Hub of flow field |
| m | Model flow or measuring station |
| T | Tip of flow field |

# REFERENCES

1.  Smith, E. G. and Uhl, W. R.; LF336/E Test Summary; General Electric Company Report No. R73AEG189; April, 1973.

2.  Smith, E. G.; LF336/E Design Summary; General Electric Company Report No. R72AEG293; December, 1972.

# APPENDIX I

## DERIVATION OF EQUATIONS OF EQUILIBRIUM NORMAL TO A STREAMLINE

### Angular Momentum Distribution

It is assumed in this analysis that the angular momentum distribution is known at the nozzle exit station and that it can be adequately represented as a linear function of the stream function $\Psi$ as follows:

$$RV_\theta = (RV_\theta)_T + \lambda \, \dot{M} \, (1 - \Psi) \tag{I1}$$

where

$$\lambda = - \, [(RV_\theta)_T - (RV_\theta)_H]/\dot{M} \tag{I2}$$

Assuming that angular momentum is conserved along any streamline, the above two equations can be applied at any point downstream of the nozzle exit station as well.

### Pressure-Temperature-Density Relations

Assuming uniform stagnation pressure and temperature at the upstream Station 0 and an isentropic process between Station 0 and the nozzle exit Station 1, we write

$$P_1 = P_{T0}(T_1/T_{T0})^{\gamma/(\gamma-1)}$$

which will apply to all streamlines at Station 1. Further, if we know the stagnation pressure loss between Station 1 and any downstream station, we may write

$$P/P_{T0} = (P_T/P_{T1}) \, (T/T_{T0})^{\gamma/(\gamma-1)} \tag{I3}$$

which will apply to any point downstream of the nozzle exit. Similarly, we may write for the density:

$$\rho/\rho_{T0} = (P_T/P_{T1}) \, (T/T_{T0})^{1/(\gamma-1)} \tag{I4}$$

Notice that the above three equations apply even though there may be energy addition (as by a fan rotor) between Stations 0 and 1 as long as the process is isentropic.

## Energy Relations

Case 1:

If no energy is added between Stations 0 and 1, then conservation of energy along a streamline results in

$$T/T_{TO} = 1 - (V_\theta^2 + V_m^2)/(2g\ J\ C_P\ T_{TO})$$

Case 2:

If the angular momentum at the nozzle exit is entirely the result of isentropic energy addition by a fan rotor, then conservation of energy along a streamline results in

$$T/T_{TO} = 1 + [V_{T1}^2(RV_\theta/(RV_\theta)_T) - V_\theta^2 - V_m^2]/(2g\ J\ C_P\ T_{TO})$$

where the energy added at the rotor tip is

$$\Delta T_T = V_T^2/(2g\ JC_P)$$

We may combine the above two cases into one equation

$$T/T_{TO} = 1 + [QV_{T1}^2(RV_\theta/RV_\theta)_T) - V_\theta^2 - V_m^2]/(2g\ J\ C_P\ T_{TO})$$

by defining

$Q = 0$ for no energy addition (stator case)

$Q = 1$ for rotor energy addition (rotor case)

Since $V_\theta = RV_\theta/R$ the above equation may be written as

$$T/T_0 = 1 + [QV_{T1}^2(RV_\theta/RV_\theta)_T) - \frac{(RV_\theta)^2}{R^2} - V_m^2]/(2g\ J\ C_P\ T_{TO}) \qquad (15)$$

## Continuity

By noting that

$$dR = -dn\ \cos\beta_m$$

we may express the continuity equation along any stream tube as follows:

$$d\Psi = 2_\pi\ R\ \rho\ V_m\ dR/\dot{M}\ \cos\beta_m$$

or

$$\frac{\partial R}{\partial \Psi} = \frac{\dot{M}\ \cos\beta_m}{2_\pi\ \rho\ V_m\ R} \qquad (16)$$

## Momentum Normal to a Streamline

The acceleration normal to a streamline of an element of fluid is given by

$$a_n = V_m^2/r - V_\theta^2 \cos \beta_m/R$$

The mass of this element is given by

$$dm = P \, R \, d\theta \, dS \, dn$$

The normal pressure force which balances the momentum force is given by

$$dF = R \, d\theta \, dS \, dP$$

Then since

$$dF = a_n \, dm$$

we may combine the above three equations to write

$$\frac{\partial P}{\partial n} = P \, (V_m^2/r - V_\theta^2 \cos \beta_m/R)$$

The derivative of stream function may be expressed as

$$\frac{d\Psi}{dn} = -2\pi \, R \, \rho \, V_m/\dot{M}$$

and the last two equations may be continued to yield

$$\frac{\partial P}{\partial \Psi} = (V_\theta^2 \cos \beta_m/R - V_m^2/R)/(2\pi \, R \, V_m) \tag{I7}$$

This equation gives the pressure gradient normal to a streamline required to balance the momentum forces normal to the streamline.

## Combined Equation

Equations I1 through I7 can be combined to eliminate pressure as a variable in Equation I7 and yield a new form for the momentum equation. This will then eliminate the need for Equation I3 in subsequent calculations. First, we differentiate Equation I3 with respect to the stream function to get

$$\frac{\partial P}{\partial \Psi} = \frac{\gamma}{\gamma-1} \, \rho_{TO}(P_T/P_{T1})(T/T_{TO})^{1/(\gamma-1)} \, \frac{\partial (T/T_{TO})}{\partial \Psi}$$

where we have assumed that the total pressure loss factor is constant in a direction normal to the streamlines so that $\partial(P_T/P_{T1})/\partial\Psi = 0$. Using the perfect gas equation of state and Equation I4 in the above result gives:

$$\frac{\partial P}{\partial \Psi} = g\ J\ C_p\ \rho\ T_{TO}\ \frac{\partial(T/T_{TO})}{\partial \Psi} \tag{I8}$$

Next, we differentiate Equation I5 with respect to stream function and use Equation I1 in the result to get

$$\frac{\partial(T/T_0)}{\partial\Psi} = \left[\ \frac{V_{T1}^2\ \dot{M}\ \lambda\ Q}{(R\ V_\theta)_T}\ -\ \frac{2R\ (RV_\theta)\ \dot{M}\lambda\ -\ (RV_\theta)^2\ \frac{\partial R}{\partial\Psi}}{R^3}\ -\ 2\ V_m\ \frac{\partial\ V_m}{\partial\Psi}\ \right]/$$

$$(2g\ J\ C_p\ T_{TO}) \tag{I9}$$

Using Equation I9 in Equation I8 to eliminate the temperature derivative and then replacing the left-hand side of Equation I7 with the result gives

$$\rho\ \left[\ \frac{V_{T1}^2\ \dot{M}\ \lambda Q}{(RV_\theta^-)_T}\ -\ \frac{2R\ (RV_\theta)\ \dot{M}\ \lambda\ -\ (RV_\theta)^2\ \frac{\partial R}{\partial\Psi}}{R^3}\ -\ 2\ V_m\ \frac{\partial\ V_m}{\partial\Psi}\ \right]\ =$$

$$\frac{V_\theta^2\ \cos\ \beta_m/R\ -\ V_m^2/r}{\pi\ R\ V_m}$$

Use of Equation I6 in the above and then solving for $\partial\ V_m/\partial\Psi$ finally gives a new form of the momentum equation as follows:

$$\frac{\partial\ V_m}{\partial\Psi} = \frac{\dot{M}}{2\pi\ \rho\ R\ r}\ +\ \frac{\dot{M}\ \lambda}{V_m}\ \left[\ \frac{V_{T1}^2\ Q}{2\ (RV_\theta)_T}\ -\ \frac{(RV_\theta)}{R^2}\ \right] \tag{I10}$$

This equation gives the meridional velocity gradient required to balance the momentum forces normal to a streamline.

## DATA ANALYSIS PROCEDURES

The exhaust flow of the various models was surveyed by radial traverses using the 3 element probe. The flow surveys for the various configurations consisted of approximately 20 discrete data points approximately 0.1 inch (0.254 centimeters) apart. The outer radial traverse boundary was established at the location where the total pressure was just equal to zero. The inner radial boundary was selected on the centerline of the particular model being surveyed.

The following discussion presents the calculation procedures used for analysis of the exhaust probe data. The calculations were performed using a time-sharing computer program.

The following data obtained from the exhaust probe was used as input to the data reduction program:

- XIMM, Probe Immersion
- $P_T$, Total Pressure (corrected for probe calibration)
- $P_S$, Static Pressure (corrected for probe calibration)
- $\alpha$, Yaw (Swirl) Angle

Additional fixed data input based on average conditions during the complete traverse cycle where:

- $T_{TO}$, Total or Plenum Temperature
- $P_a$, Barometric Pressure
- $P_{Sm}$, Model Flow Section Static Pressure
- $\beta$, Model Flow Angle
- $P_{TO}$, Upstream or Plenum Total Pressure

Several overall performance parameters were initially calculated as follows:

- Flow Section Mach Number, $M_m = [(\frac{2}{\gamma-1})(\frac{P_{TO}}{P_{Sm}})^{\frac{\gamma-1}{\gamma}} - 1)]^{1/2}$

- Flow Section Static Temperature, $T_{Sm} = T_T/(1 = \frac{\gamma-1}{\gamma} M_m^2)$

- Flow Section Velocity, $V_m - M_m(\gamma g R T_{Sm})^{1/2}$

- Flow Section Density, $\rho_m = P_{Sm}/g\,R\,T_{Sm}$

- Mass Flow, $\dot{M} = \rho_m V_m A_m$

- Nozzle Exit Total Pressure, $\overline{P}_{T1} = P_{TO} - \overline{\omega}_0 (P_{TO} - P_{Sm})$

- Ideal Mach Number, $M_i = [(\frac{2}{\gamma-1})(\frac{\overline{P}_{T1}}{P_a} \frac{\gamma-1}{\gamma} - 1)]^{1/2}$

- Static Temperature, $T_S = T_{TO}/(1 + \frac{\gamma-1}{2} M_i^2)$

- Ideal Velocity, $V_i = M_i(\gamma\,g\,P\,T_S)^{1/2}$

- Ideal Mass Flow, $\dot{M}_i = (P_a\,g\,R\,T_S)V_i$

- Ideal Thrust, $F_i = \dot{M}_i/V_i$

At each discrete point or immersion, the following parameters were calculated:

- Absolute Mach Number, $M = [\frac{2}{\gamma-1}(\frac{P_T}{P_S}^{\frac{\gamma-1}{\gamma}} - 1)]^{1/2}$

- Total Pressure Coefficient, $CPT = (P_T - P_a)/(\overline{P}_{T1} - P_a)$

- Static Pressure Coefficient, $CPS = (P_S - P_a)/(\overline{P}_{T1} - P_a)$

- Static Temperature, $T = T_T/(1 + \frac{\gamma-1}{2} M^2)$

- Absolute Velocity, $V = M(\gamma\,g\,R\,T)^{1/2}$

- Flow Per Unit Area, $W/A = (P_S/RT) V \cos \alpha \cos \beta$

- Thrust Per Unit Area, $F/A = W/A\,V \cos \alpha \cos \beta + (P_S - P_a)$

The total model exhaust flow was integrated to obtain the following performance:

- Airflow, $W = \Sigma (W/A) \Delta A$

- Total Thrust, $F = \Sigma (F/A) \Delta A$

- Mass Average Total Pressure, $\overline{P}_{T1} = (\Sigma P_T (W/A) \Delta A)/W$

- Hub Base Pressure, $\overline{P}_H = \Sigma(P_{SB}) \Delta A/A$

The following overall performance parameters were then calculated:

- Flow Coefficient, $C_F = \dot{M}/\dot{M}_i$

- Thrust Coefficient, $C_T = F/F_i$

-44-

- Base Pressure Coefficient at Hub Exit Radius, $C_{P1} = \dfrac{P_{H1} - P_a}{P_{T1} - P_a}$

- Average Base Pressure Coefficient Across Base, $C_{P2} = \dfrac{\overline{P}_H - P_a}{P_{T1} - P_a}$

The flow streamline locations were determined as follows: During the flow integration, the radius and the resulting integrated flow were stored in an array throughout the entire flow stream; then, for 10 to 100 percent flow, the appropriate radius was determined from the stored data by linear interpolation.

# APPENDIX III

## COMPUTER PROGRAM LISTING

```
1*#RUNH * =HBASE(NOGO,CORE=30)
100       COMMON PRATIO,PAM,ROTO,PLOSS,RHOI,RCU,PI,RHG0,V0,P0,MF,RCU0,LAM
110&      ,G1,G2,C3,C4,PTINT,DMF,T0,ROT,SOLT,SOLH,IND,VIN,EFF
120       REAL LAM,MF,DMF(11),MFI,L,RIP(4),ROP(4),ZIP(4),ZOP(4),BMP(4),ZMP(4)
130       INTEGER ROT
140       DIMENSION RPP(4),X(3),Y(3),VI(12),VI2(12),EI(3),E2(3),RCU(12),
150&      PRATIO(12),R(12)
160     1 PRINT 100 ; PRINT 100
170       PRINT, R/R,B0,FF,L,CPL,RCU0,DRCU0" ; READ,RR,B0,FF,L,CPL,RCU0,DRCU0
180       IF(RR.EQ.0.0) GO TO 999
190       PRINT, "P/P,TIN,ROT,IPT,C2,C9,C10,SOLT,SOLH,VIN,EFF"
191       READ,V0,TIN,ROT,IPT,C2,C9,C10,SOLT,SOLH,VIN,EFF
200       G=32.17405;IND=0
210       GAM=1.4 ; G1=GAM/(GAM-1) ; G2=1/(GAM-1)
211       T0=TIN*(1+(V0^(1/G1)-1)*(1/EFF-1)*ROT)
212       RG=53.35 ; RJ=778.16 ; C3=2*G*G1*RG*T0
215       V0=SQRT(C3*(V0^(1/G1)-1)*TIN/T0)
220       ROTO=0
230       IF(RCU0.NE.0.) ROTO=ROT/RCU0
240       C4=V0^2*.5*ROTO
250       PAM=14.696*144
260       P0=PAM
270       IF(ROT.EQ.0) P0=PAM*(1-V0^2/C3)^(-G1)
280       RHO0=P0/G/RG/T0
290       PI=3.14159 ; B0=B0*PI/180
310       ITR=1 ; MAXIT=10
320       C1=PI*(1-RR^2)/(1+RR^2)
322       VMAV=(V0^2-RCU0^2*(1+RR^2)/2)^.5
324       TRATIO=1+(V0^2*(RCU0+.5*DRCU0)*ROTO-(RCU0+.5*DRCU0)^2-VMAV^2)/C3
326       RHO=RHO0*TRATIO^G2
330       MF=2*C1*RHO*VMAV*COS(B0)
335       MF=.9*MF
340       RHI=RR*(2/(1+RR^2))^.5
350       RH2=C2*(2/(1+RR^2))^.5 ; RM2=1
360       V2=.99*V0
370       DO 4 I=1,12
380       RCU(I)=RCU0+DRCU0*(12-I)/10
385       RCU(I)=RCU0+DRCU0 ; RCU(2)=RCU0+.96*DRCU0
390       PRATIO(I)=(1+V0^2*RCU(I)*ROTO/C3)^G1*P0/PAM
400     4 CONTINUE
401       Z=2
404*
405       PLOSS=(1-V2^2/(C3+V0^2*ROT))^(-G1)/PRATIO(12)
430     5 CALL ROTFLO(1,RM2,0.,0.,RT2,RH2,V2,FP2,FPH2,FM2)
490       A=1-RM2
500       B=A+L*TAN(B0)
505       C=(-A+3*B+C9)/6
510       I=1 ; DZM=Z/10 ; Z=0
520       V2=V0 ; AP=0 ; FFZ=0 ; PFZ=0 ; PLOSS=1 ; IT=0
525       BMAX=ABS(B0)
530    10 EP=EXP(-Z/L)
540       RM=(A+B*Z/L+C*Z*Z/L/L)*EP+RM2
550       RMP=-(A-B+(B-2*C)*Z/L+C*Z*Z/L/L)*EP/L
560       RMPP=(A-2*B+2*C+(B-4*C)*Z/L+C*Z*Z/L/L)*EP/L/L
570       BM=ATAN(RMP)
575       IF(ABS(BM).GT.BMAX) BMAX=ABS(BM)
```

```
580        CM=RMPP/(1+RMP^2)^1.5
590        CALL ROTFLO(3,RM,BM,CM,RT,RH,V2,VMT,VMH,PH)
600        IF((ABS((RM2-RM)/(RM2-1)).GT..01).OR.(ABS(BM).GT..2*BMAX))
602&       GO TO 13
610        IF(IT.EQ.1)GO TO 13
620        Z=Z-DZM*(RM2+.01*ABS(1-RM2)*ABS(RML-RM2)/(RML-RM2)-RM)/(RML-RM)
630        IT=1
640        GO TO 10
650     13 IF(IPT+IND.EQ.2) PRINT 2,Z,RM,BM*180/PI,CM,RT,RH,V2,VMT,VMH,PH-PAM
660      2 FORMAT(1H ,F6.3,F7.3,F6.1,F9.4,2F7.3,3F7.1,F8.0)
670        ZH=Z+(RM-RH)*SIN(BM)
680        ZT=Z-(RT-RM)*SIN(BM)
690        IF(I.EQ.1) GO TO 12
700        BH=ATAN((RH-RHL)/(ZH-ZHL))
710        DAP=PI*(RH+RHL)*(ZH-ZHL)/COS(BH)
720        AP=AP+DAP
730        DFF=.5*RHO1*FF*DAP*(VMH^2+VMHL^2)/2
740        PLOSS=PLOSS*(1-DFF/PTINT)
750        V2=((C3+V0^2*ROT)*(1-(PLOSS*PRATIO(12))^(-1/G1)))^.5
760        FFZ=FFZ+DFF*COS(BH)
770        PFZ=PFZ+((PH+PHL)/2-PAM)*DAP*SIN(BH)
780
790        IF((IT.EQ.1).OR.(I.GT.50))GO TO 20
800     12 RHL=RH ; RML=RM ; ZHL=ZH ; VMHL=VMH ; PHL=PH
810        IF(I.GT.3) GO TO 15
820        RIP(I)=RHL ; ROP(I)=RT ; ZIP(I)=ZHL ; ZOP(I)=ZT ; ZMP(I)=Z
830        RPP(I)=RM
840     15 I=I+1 ; Z=Z+DZM
850        GO TO 10
860
870     20 ZIP(4)=0 ; ZOP(4)=0
880        CALL INT(RIP,ZIP)
890        CALL INT(ROP,ZOP)
900        RRT=RIP(4)/ROP(4)
910        CALL INT(ZMP,ZIP)
920        CALL INT(RPP,ZIP)
930        RHI=RIP(4) ; RMI=RPP(4) ; ZMI=ZMP(4)
950        EP=EXP(-ZMI/L)
960        RMP=-(A-B+(B-2*C)*ZMI/L+C*ZMI*ZMI/L/L)*EP/L
970        RMPP=(A-2*B+2*C+(B-4*C)*ZMI/L+C*ZMI*ZMI/L/L)*EP/L/L
980        BMI=ATAN(RMP)
990        CMI=RMPP/(1+RMP^2)^1.5
1000       CALL ROTFLO(2,RMI,BMI,CMI,RTI,RHI,V0,FPI,FPHI,FMI)
1010       CALL ROTFLO(1,RM2,0.,0.,RT2,RH2,V2,FF2,FPH2,FM2)
1020
1030       ERR1=(RRT-RR)/RR
1040       FPHX=CPL*RHO1/2*PI*(RCU0+LAM*MF)^2
1045       FPHY=C10*FPHX
1050       ERR2=(FP2+FPH2-FM2-FP1+FPHY-FPH1+FM1-FPHX)/FM1
1060       IF(((ABS(ERR1).LT..003).AND.(ABS(ERR2).LT..003))
1061&      .AND.((IND.EQ.1).OR.(IPT.EQ.0))) GO TO 30
1065       IF((ABS(ERR1).LT..003).AND.(ABS(ERR2).LT..003)) IND=1
1070       IF(ITR.EQ.MAXIT) GO TO 26
1080    23 DO 40 I=1,2
1090       X(4-I)=X(3-I)
1100       Y(4-I)=Y(3-I)
```

```
1110      E1(4-I)=E1(3-I)
1120   40 E2(4-I)=E2(3-I)
1130      X(1)=MF ; Y(1)=L ; E1(1)=ERR1 ; E2(1)=ERR2
1140      IF(ITR.EQ.1) GO TO 41 ; IF(ITR.EQ.2) GO TO 42
1150      CALL INT2(X,Y,E1,E2,MF,L)
1155   43 PRINT,X(1),Y(1),ERR1,ERR2
1160      ITR=ITR+1 ; LAM=DRCU0/MF
1165      IF(IND.EQ.1) PRINT 100
1170      GO TO 5
1180   41 L=L*(1-.05*ABS(ERR2)/ERR2) ; GO TO 43
1190   42 MF=MF*(1-RR^2)/(1+RR^2)/(1-RRT^2)*(1+RRT^2) ; GO TO 43
1200   26 PRINT 101,MAXIT,ERR1,ERR2
1210      PRINT,"ADDITIONAL ITERATIONS" ; READ,NIT
1220      IF(NIT.EQ.0) GO TO 30
1230      MAXIT=MAXIT+NIT ; GO TO 23
1240
1250   30 MFI=0 ; FI=0
1260      RHOI=RHO0*(PAM/P0)^(1/GAM)
1270      DO 32 I=1,12
1280      VI2(I)=C3*(1-(PRATIO(I))^(-1/G1))*(PRATIO(I)^(ROT/G1))
1290      VI(I)=VI2(I)^.5
1300   32 CONTINUE
1310      C6=.2*VI(1)+.5*VI(2)+.3*VI(3)
1320      DO 34 I=3,11
1330      C6=C6+(VI(I)+VI(I+1))/2
1350   34 CONTINUE
1360      MFI=PI*RHOI*(ROP(4)*ROP(4)-RIP(4)*RIP(4))*C6/10
1370      FI=MFI*C6/10
1380      CF=MF/MFI
1390      CT=(FM2-FP2-FPH2-FPHY)/FI
1400      CV=CT/CF
1410      VIB2=(FI/MFI)^2
1420      C5=C3+V0^2*RCU(7)*ROTO
1430      DELPT=((1-VIB2/C5)^(-G1)-1)*PAM
1440      CP1=-FPHI/DELPT/PI/RH1^2
1450      CP2=CP1*(FPH1+FPHX)/FPH1
1460      PRINT 100
1470      PRINT,"     RR     B0     FF    CPL    RCU0    DRCU0
1480&     VI     T0    ROT ITR"
1490      PRINT 102,RR,B0*180/PI,FF,CPL,RCU0,DRCU0,C6/10,T0,ROT,ITR
1500      PRINT 100
1510      PRINT,"     CF     CV     CT    CP1    CP2     Z     AP     L
1515&     MF     FI"
1520      PRINT 103,CF,CV,CT,CP1,CP2,Z,AP,L,MF,FI
1530      GO TO 1
1540  100 FORMAT(1H )
1550  101 FORMAT(1H ,"AFTER ",I2," ITERATIONS ERR1= ",F6.3," , ERR2= ",F6.3)
1560  102 FORMAT(1H ,F7.3,F7.1,F8.4,F7.3,4F8.1,I5,I4)
1570  103 FORMAT(1H ,5F7.3,2F7.2,F7.3,F7.2,F7.0)
1580  999 STOP ; END
1590*
1600      SUBROUTINE INT(R,Z)
1610      DIMENSION R(4),Z(4)
1620      C3=((R(3)-R(1))/(Z(3)-Z(1))-(R(2)-R(1))/(Z(2)-Z(1)))/(Z(3)-Z(2))
1630      C2=(R(2)-R(1))/(Z(2)-Z(1))-C3*(Z(2)+Z(1))
```

```
1640      C1=R(1)-C2*Z(1)-C3*Z(1)^2
1650      R(4)=C1+C2*Z(4)+C3*Z(4)^2
1660      RETURN ; END
1670*
1680      SUBROUTINE ROTFLO(KR,RM,BM,CM,RT,RH,V2,PR1,PR2,PR3)
1690      COMMON PRATIO,PAM,ROTO,PLOSS,RHO1,RCU,PI,RHO0,V0,P0,MF,RCU0,LAM
1700&     ,G1,G2,C3,C4,PTINT,DMF,T0,ROT,SOLT,SOLH,IND,VIN,EFF
1710      REAL LAM,VM(12),R(12),P(12),RCU(12),PRATIO(12),MF,DMF(11),VX(12)
1712      INTEGER ROT
1715      DATA VX/1.,1.,1.,1.,1.,1.,1.,1.,1.,1.,1.,1./
1720      KS=7 ; PLOS=PLOSS
1730      IF(KR.EQ.1)KS=1
1735      IF(KR.EQ.2) PLOS=1.0
1740      K=0 ; PR1=0 ; PR3=0
1742      DO 3 I=1,11
1744    3 DMF(I)=.1*MF
1746      DMF(1)=.04*MF ; DMF(2)=.06*MF
1750      VM(KS)=V2 ; R(1)=RH ; R(7)=RH
1760      IF(ABS(CM).LT.2.E-18) CM=2.E-18
1770    5 DO 10 I=KS,11
1780      TRATIO=1+(V0^2*RCU(I)*ROTO-(RCU(I)/R(I))^2-VM(I)^2)/C3
1790      RHO=RHO0*TRATIO^G2*PLOS
1800      F1=1/CM+(RM-R(I))/COS(BM)
1810      F2=SIN(BM)^2 ; F3=R(I)^2-RM^2
1820      F4=R(I)^2+(RM*SIN(BM))^2
1830      CV=1/F1+F2*F3/F4^1.5 ; IF(ABS(CV).LT.2.E-18) CV=2.E-18
1840      F5=CV/2/PI/RHO/R(I)
1850      F6=LAM/VM(I)*(RCU(I)/R(I)^2-C4)
1860      DVM1=F5+F6
1870      DR1=.5/PI/RHO/VM(I)/R(I)*COS(BM)
1880      DTRATIO=(-C4*LAM+RCU(I)/R(I)^2*(LAM+RCU(I)/R(I)*DR1)-VM(I)*DVM1)
1890&     *2/C3
1900      DRHO=G2*DTRATIO/TRATIO
1910      DCV=(DR1/COS(BM)/F1^2-2*R(I)*DR1*F2/F4^1.5*(1-1.5*F3/F4))/CV
1915      DRSQ=DR1*2*R(I)
1920      DDRSQ=-DRSQ*(DRHO+DVM1/VM(I))
1930      DDVM1=-F5*(DRHO+DR1/R(I)-DCV)-F6*DVM1/VM(I)
1940&     -LAM/VM(I)/R(I)^2*(LAM+2*RCU(I)*DR1/R(I))
1950      VM1=VM(I)+(DVM1+DDVM1*DMF(I)/2)*DMF(I)
1960      R1=(R(I)^2+(DRSQ+DDRSQ*DMF(I)/2)*DMF(I))^.5
1970      TRATIO=1+(V0^2*RCU(I+1)*ROTO-(RCU(I+1)/R1)^2-VM1^2)/C3
1980      RHO=RHO0*TRATIO^G2*PLOS
1990      CV1=1/(1/CM+(RM-R1)/COS(BM))+(R1^2-RM^2)*SIN(BM)^2/
2000&     (R1^2+RM^2*SIN(BM)^2)^1.5
2010      DVM2=CV1/2/PI/RHO/R1+LAM/VM1*(RCU(I+1)/R1^2-C4)
2020      DR2=.5/PI/RHO/VM1/R1*COS(BM)
2030      VM(I+1)=VM(I)+(DVM1+DVM2)*DMF(I)/2
2040      R(I+1)=R(I)+(DR1+DR2)*DMF(I)/2
2050   10 CONTINUE
2060
2070      CU0=RCU0/R(12) ; V22=V21 ; VM2T=VM1T ; VM1T=VM(KS) ; K=K+1
2075      RM2=RM1 ; RM1=R(7)
2080      V21=(CU0^2+VM(12)^2)^.5
2090      IF(K.GT.20) GO TO 32
2100      IF(ABS(1-V21/V2).LT..00001)GO TO 18
```

```
2110        IF(K.NE.1) GO TO 15
2120        VM(KS)=.95*VM(KS)
2130        GO TO 5
2140    15  VM(KS)=VM1T+(VM1T-VM2T)/(V21-V22)*(V2-V21)
2150        DEC=VM(KS)/VM1T-1
2160        IF(ABS(DEC).GT..2) VM(KS)=VM1T*(1+.2*DEC/ABS(DEC))
2165        IF(KR.EQ.1)RM=RM1-(RM2-RM1)/(VM2T-VM1T)*(VM1T-VM(1))
2170        GO TO 5
2180
2190    18  IF(KR.EQ.1) GO TO 21
2200*
2210        DO 20 J=1,6
2220        I=8-J
2230        TRATIO=1+(V0^2*RCU(I)*ROTO-(RCU(I)/R(I))^2-VM(I)^2)/C3
2240        RHO=RHO0*TRATIO^G2*PLOS
2250        F1=1/CM+(RM-R(I))/COS(BM)
2260        F2=SIN(BM)^2 ; F3=R(I)^2-RM^2
2270        F4=R(I)^2+(RM*SIN(BM))^2
2280        CV=1/F1+F2*F3/F4^1.5 ; IF(ABS(CV).LT.2.E-18) CV=2.E-18
2290        F5=CV/2/PI/RHO/R(I)
2300        F6=LAM/VM(I)*(RCU(I)/R(I)^2-C4)
2310        DVM1=F5+F6
2320        DR1=.5/PI/RHO/VM(I)/R(I)*COS(BM)
2330        DTRATIO=(-C4*LAM+RCU(I)/R(I)^2*(LAM+RCU(I)/R(I)*DR1)-VM(I)*DVM1)
2340&       *2/C3
2350        DRHO=G2*DTRATIO/TRATIO
2360        DCV=(DR1/COS(BM)/F1^2-2*R(I)*DR1*F2/F4^1.5*(1-1.5*F3/F4))/CV
2365        DRSQ=DR1*2*R(I)
2370        DDRSQ=-DRSQ*(DRHO+DVM1/VM(I))
2380        DDVM1=-F5*(DRHO+DR1/R(I)-DCV)-F6*DVM1/VM(I)
2390&       -LAM/VM(I)/R(I)^2*(LAM+2*RCU(I)*DR1/R(I))
2400        VM1=VM(I)-(DVM1+DDVM1*DMF(I-1)/2)*DMF(I-1)
2410        R1=(R(I)^2-(DRSQ-DDRSQ*DMF(I-1)/2)*DMF(I-1))^.5
2420        TRATIO=1+(V0^2*RCU(I+1)*ROTO-(RCU(I+1)/R1)^2-VM1^2)/C3
2430        RHO=RHO0*TRATIO^G2*PLOS
2440        CV1=1/(1/CM+(RM-R1)/COS(BM))+(R1^2-RM^2)*SIN(BM)^2/
2450&       (R1^2+RM^2*SIN(BM)^2)^1.5
2460        DVM2=CV1/2/PI/RHO/R1+LAM/VM1*(RCU(I-1)/R1^2-C4)
2470        DR2=.5/PI/RHO/VM1/R1*COS(BM)
2480        VM(I-1)=VM(I)-(DVM1+DVM2)*DMF(I-1)/2
2490        R(I-1)=R(I)-(DR1+DR2)*DMF(I-1)/2
2500    20  CONTINUE
2510*
2520        IF(KR.EQ.2) GO TO 21
2530*
2540        RT=R(12) ; RH=R(1) ; PR1=VM(12) ; PR2=VM(1)
2550        TRATIO=1+(V0^2*RCU(1)*ROTO-(RCU(1)/R(1))^2-VM(1)^2)/C3
2560        PR3=P0*TRATIO^G1*PLOS
2570        RHO1=RHO0*TRATIO^G2*PLOS
2580        PTINT=0
2590        DO 22 I=1,11
2600        PTINT=PTINT+(PRATIO(I)+PRATIO(I+1))/2*(R(I+1)^2-R(I)^2)
2610    22  CONTINUE
2620        PTINT=PTINT*PAM*PLOS*PI
2630        GO TO 35
```

```
2640
2650   21 DO 25 I=1,12
2660      TRATIO=1+(V0^2*RCU(I)*ROTO-(RCU(I)/R(I))^2-VM(I)^2)/C3
2670      P(I)=P0*TRATIO^G1*PLOS
2680      IF(I.EQ.1)RHOI=RHO0*TRATIO^G2*PLOS
2690   25 CONTINUE
2700      RH=R(1) ; RM=R(7) ; RT=R(12)
2710      DO 30 I=1,11
2720      PR1=PR1+PI*(R(I+1)-R(I))*(R(I+1)+R(I))*(PAM-(P(I)+P(I+1))/2)
2730      PR3=PR3+DMF(I)*(VM(I)+VM(I+1))/2/(1+RM^2*SIN(BM)^2/R(I)^2)
2740   30 CONTINUE
2750      PR2=PI*RH^2*(PAM-P(1))
2755      IF(ABS(KR-2)+ABS(IND-1)+ABS(ROT-1))35,34,35
2770   32 PRINT 33,KS,VM(KS),VM(12),R(KS),R(12)
2775      GO TO 35
2780   33 FORMAT(1H ,"ROTFLO2 NOT CONVERGED K=20",I1,2F7.1,2F7.3)
2785   34 PRINT 38
2790      DO 37 I=1,12
2800      VI=VX(I)*VIN
2810      DTI=(1-EFF)*V0^2/C3*T0
2815      TSI=T0-DTI-VI^2/C3*T0
2820      PSI=P0*(TSI/(T0-DTI))^G1
2830      UB=V0^2*R(I)/2/RCU0/EFF
2840      TTR2=T0+(V0^2*RCU(I)*ROTO/EFF-(RCU(I)/R(I))^2+(UB-RCU(I)/R(I))^2
2841&     )/C3*T0
2850      CPR=((P(I)/PSI)^(1/G1)-1)/(TTR2/TSI-1)
2852      SOL=SOLT+(SOLH-SOLT)*(R(12)/R(I)-1)/(R(12)/R(1)-1)
2853      WI=(VI^2+UB^2)^.5
2854      WO=(VM(1)^2+(RCU(I)/R(I))^2)^.5
2855      DFACT=1-WO/WI+RCU(I)/2/SOL/R(I)/WI
2860      PRINT 36,I,R(I),P(I)-PAM,WI,WO,VI,UB,SOL,CPR,DFACT
2865   37 CONTINUE
2870   36 FORMAT(1H ,I2,F8.3,F8.0,4F7.0,3F8.3)
2875   38 FORMAT(1H )
2880   35 RETURN ; END
2890*
2900      SUBROUTINE INT2(X,Y,E1,E2,MF,L)
2910      REALMF,L
2920      DIMENSION X(3),Y(3),E1(3),E2(3)
2930      DIMENSION C1(3),C2(3)
2940      CALL COEF(X,Y,E1,C1)
2950      CALL COEF(X,Y,E2,C2)
2960      D1=C1(2)*C2(3)-C1(3)*C2(2)
2970      D2=C1(3)*C2(1)-C1(1)*C2(3)
2980      D3=C1(1)*C2(2)-C1(2)*C2(1)
2990      DF1=1 ; DF2=1
3000      MF=X(1)+DF1*(D1/D3-X(1))
3010      L=Y(1)+DF2*(D2/D3-Y(1))
3020      DEL1=1-MF/X(1) ; DEL2=1-L/Y(1)
3030      IF(ABS(DEL1).GT..1) MF=(1-.1*ABS(DEL1)/DEL1)*X(1)
3040      IF(ABS(DEL2).GT..2) L=(1-.2*ABS(DEL2)/DEL2)*Y(1)
3050      RETURN ; END
3060*
```

```
3070      SUBROUTINE COEF(X,Y,E,C)
3080      DIMENSION X(3),Y(3),E(3)
3090      DIMENSION C(3)
3100      D1=X(1)*Y(2)+X(2)*Y(3)+X(3)*Y(1)-X(3)*Y(2)-X(2)*Y(1)-X(1)*Y(3)
3110      D2=E(1)*Y(2)+E(2)*Y(3)+E(3)*Y(1)-E(3)*Y(2)-E(2)*Y(1)-E(1)*Y(3)
3120     ·D3=X(1)*E(2)+X(2)*E(3)+X(3)*E(1)-X(3)*E(2)-X(2)*E(1)-X(1)*E(3)
3130      D4=X(1)*Y(2)*E(3)+X(2)*Y(3)*E(1)+X(3)*Y(1)*E(2)
3140&     -X(3)*Y(2)*E(1)-X(2)*Y(1)*E(3)-X(1)*Y(3)*E(2)
3150      C(1)=D2/D1
3160      C(2)=D3/D1
3170      C(3)=D4/D1
3180      RETURN ; END
3190      FUNCTION TAN(XXX);TAN=SIN(XXX)/COS(XXX); RETURN ; END
```

## TABLE I

### Base Pressure Model Descriptions

| Model | R/RT | Flow* Angle | Outer Flowpath Exit Diameter In. | (Cm) | Inner Flowpath Exit Diameter In. | (Cm) |
|-------|------|------|------|------|------|------|
| 1 | 0.4 | 10 | 3.116 | 7.915 | 1.246 | 3.165 |
| 2 | 0.4 | 0 | 3.116 | 7.915 | 1.246 | 3.165 |
| 3 | 0.4 | -10 | 3.116 | 7.915 | 1.246 | 3.165 |
| 4 | 0.4 | -20 | 3.116 | 7.915 | 1.246 | 3.165 |
| 5 | 0.55 | 10 | 3.420 | 8.687 | 1.879 | 4.773 |
| 6 | 0.55 | 0 | 3.420 | 8.687 | 1.880 | 4.773 |
| 7 | 0.55 | -10 | 3.420 | 8.687 | 1.878 | 4.773 |
| 8 | 0.55 | -20 | 3.420 | 8.687 | 1.879 | 4.773 |
| 9 | 0.70 | 10 | 4.000 | 10.160 | 2.795 | 7.099 |
| 10 | 0.70 | 0 | 4.000 | 10.160 | 2.803 | 7.099 |
| **E | 0.638 |  | 3.710 | 8.052 | 2.366 | 6.010 |

*  Radially out designated positive angle

** Scaled from LF336/E lift fan (see Reference 2)

TABLE II

Inner and Outer Exit Contour Geometries of the Base Pressure Models

| MODEL: | 1 | | 2 | | 3 | | 4 | |
|---|---|---|---|---|---|---|---|---|
| $z/_{RT}$ | $(R/_{RT})_H$ | $(R/_{RT})_T$ | $(R/_{RT})_H$ | $(R/_{RT})_T$ | $(R/_{RT})_H$ | $(R/_{RT})_T$ | $(R/_{RT})_H$ | $(R/_{RT})_T$ |
| 0 | 0.400 | 1.000 | 0.400 | 1.000 | 0.400 | 1.000 | 0.400 | 1.000 |
| -0.128 | 0.356 | 0.983 | 0.400 | 1.000 | 0.440 | 1.016 | 0.479 | 1.033 |
| -0.258 | 0.306 | 0.967 | 0.400 | 1.000 | 0.478 | 1.034 | 0.549 | 1.068 |
| -0.385 | 0.263 | 0.951 | 0.402 | 1.003 | 0.517 | 1.053 | 0.612 | 1.105 |
| -0.513 | 0.237 | 0.950 | 0.411 | 1.019 | 0.563 | 1.087 | 0.674 | 1.155 |
| -0.642 | 0.225 | 0.962 | 0.430 | 1.048 | 0.599 | 1.137 | 0.688 | 1.206 |
| -0.770 | 0.229 | 0.990 | 0.459 | 1.096 | 0.625 | 1.191 | 0.703 | 1.254 |
| -0.899 | 0.245 | 1.033 | 0.499 | 1.155 | 0.639 | 1.239 | 0.703 | 1.284 |
| -1.027 | 0.278 | 1.091 | 0.548 | 1.205 | 0.642 | 1.284 | 0.689 | 1.284 |
| -1.155 | 0.327 | 1.151 | 0.589 | 1.253 | 0.642 | 1.284 | 0.664 | 1.284 |
| -1.284 | 0.387 | 1.202 | 0.618 | 1.284 | 0.642 | 1.284 | 0.648 | 1.284 |
| -1.412 | 0.447 | 1.249 | 0.635 | 1.284 | 0.642 | 1.284 | 0.642 | 1.284 |
| -1.540 | 0.507 | 1.284 | 0.642 | 1.284 | 0.642 | 1.284 | 0.642 | 1.284 |
| -1.669 | 0.558 | 1.284 | 0.642 | 1.284 | 0.642 | 1.284 | 0.642 | 1.284 |
| -1.797 | 0.596 | 1.284 | 0.642 | 1.284 | 0.642 | 1.284 | 0.642 | 1.284 |
| -1.926 | 0.623 | 1.284 | 0.642 | 1.284 | 0.642 | 1.284 | 0.642 | 1.284 |
| -2.054 | 0.637 | 1.284 | 0.642 | 1.284 | 0.642 | 1.284 | 0.642 | 1.284 |
| -2.182 | 0.642 | 1.284 | 0.642 | 1.284 | 0.642 | 1.284 | 0.642 | 1.284 |

TABLE II (continued)

| MODEL: | 5 | | 6 | | 7 | | 8 | |
|---|---|---|---|---|---|---|---|---|
| $Z/RT$ | $(R/RT)_H$ | $(R/RT)_T$ | $(R/RT)_H$ | $(R/RT)_T$ | $(R/RT)_H$ | $(R/RT)_T$ | $(R/RT)_H$ | $(R/RT)_T$ |
| 0 | 0.550 | 1.000 | 0.550 | 1.000 | 0.550 | 1.000 | 0.550 | 1.000 |
| -0.128 | 0.520 | 0.984 | 0.550 | 1.000 | 0.580 | 1.016 | 0.608 | 1.033 |
| -0.258 | 0.488 | 0.968 | 0.550 | 1.000 | 0.608 | 1.034 | 0.662 | 1.065 |
| -0.385 | 0.457 | 0.953 | 0.551 | 1.001 | 0.635 | 1.053 | 0.712 | 1.101 |
| -0.513 | 0.435 | 0.950 | 0.560 | 1.015 | 0.649 | 1.085 | 0.748 | 1.145 |
| -0.642 | 0.422 | 0.961 | 0.575 | 1.042 | 0.651 | 1.127 | 0.769 | 1.170 |
| -0.770 | 0.418 | 0.984 | 0.584 | 1.083 | 0.639 | 1.170 | 0.777 | 1.170 |
| -0.899 | 0.422 | 1.023 | 0.585 | 1.126 | 0.616 | 1.170 | 0.771 | 1.170 |
| -1.027 | 0.436 | 1.073 | 0.585 | 1.169 | 0.596 | 1.170 | 0.753 | 1.170 |
| -1.155 | 0.458 | 1.117 | 0.585 | 1.170 | 0.585 | 1.170 | 0.720 | 1.170 |
| -1.284 | 0.490 | 1.160 | 0.585 | 1.170 | 0.585 | 1.170 | 0.674 | 1.170 |
| -1.412 | 0.528 | 1.170 | 0.585 | 1.170 | 0.585 | 1.170 | 0.636 | 1.170 |
| -1.540 | 0.557 | 1.170 | 0.585 | 1.170 | 0.585 | 1.170 | 0.609 | 1.170 |
| -1.669 | 0.575 | 1.170 | 0.585 | 1.170 | 0.585 | 1.170 | 0.592 | 1.170 |
| -1.797 | 0.584 | 1.170 | 0.585 | 1.170 | 0.585 | 1.170 | 0.585 | 1.170 |
| -1.926 | 0.585 | 1.170 | 0.585 | 1.170 | 0.585 | 1.170 | 0.585 | 1.170 |
| -2.054 | 0.585 | 1.170 | 0.585 | 1.170 | 0.585 | 1.170 | 0.585 | 1.170 |
| -2.182 | 0.585 | 1.170 | 0.585 | 1.170 | 0.585 | 1.170 | 0.585 | 1.170 |

TABLE II (continued)

| MODEL: | 9 | | 10 | | E | |
|---|---|---|---|---|---|---|
| $Z/_{RT}$ | $(R/_{RT})_H$ | $(R/_{RTT})$ | $(R/_{RT})_H$ | $(R/_{RT})_T$ | $(R/_{RT})_H$ | $(R/_{RT})_T$ |
| 0 | 0.700 | 1.000 | 0.700 | 1.000 | 0.638 | 1.000 |
| -0.128 | 0.679 | 0.985 | 0.700 | 1.000 | 0.595 | 1.029 |
| -0.258 | 0.657 | 0.970 | 0.700 | 1.000 | 0.564 | 1.058 |
| -0.385 | 0.633 | 0.957 | 0.699 | 1.000 | 0.545 | 1.078 |
| -0.513 | 0.598 | 0.953 | 0.688 | 1.000 | 0.539 | 1.078 |
| -0.642 | 0.560 | 0.961 | 0.665 | 1.000 | 0.539 | 1.078 |
| -0.770 | 0.532 | 0.981 | 0.629 | 1.000 | 0.539 | 1.078 |
| -0.899 | 0.513 | 1.000 | 0.585 | 1.000 | 0.539 | 1.078 |
| -1.027 | 0.502 | 1.000 | 0.550 | 1.000 | 0.539 | 1.078 |
| -1.155 | 0.500 | 1.000 | 0.525 | 1.000 | 0.539 | 1.078 |
| -1.284 | 0.500 | 1.000 | 0.509 | 1.000 | 0.539 | 1.078 |
| -1.412 | 0.500 | 1.000 | 0.501 | 1.000 | 0.539 | 1.078 |
| -1.540 | 0.500 | 1.000 | 0.500 | 1.000 | 0.539 | 1.078 |
| -1.669 | 0.500 | 1.000 | 0.500 | 1.000 | 0.539 | 1.078 |
| -1.797 | 0.500 | 1.000 | 0.500 | 1.000 | 0.539 | 1.078 |
| -1.926 | 0.500 | 1.000 | 0.500 | 1.000 | 0.539 | 1.078 |
| -2.054 | 0.500 | 1.000 | 0.500 | 1.000 | 0.539 | 1.078 |
| -2.182 | 0.500 | 1.000 | 0.500 | 1.000 | 0.539 | 1.078 |

## TABLE III

## TEST RUN SUMMARY

| | | 1.3 | 1.3 | 1.3 | 1.3 | 1.3 | 1.3 | 1.2 | 1.4 | 1.3 |
|---|---|---|---|---|---|---|---|---|---|---|
| PRESSURE RATIO | | | | | | | | | | |
| TRAVERSE AXIAL (IN.) | | 0.1 | 0.625 | 1.625 | 2.625 | 3.625 | 4.625 | 0.1 | 0.1 | 0.1 |
| DISTANCE (CM.) | | 0.254 | 1.588 | 4.128 | 6.668 | 9.208 | 11.778 | 0.254 | 0.254 | 0.254 |
| BLOCKAGE | | | | | | | | | | X |
| MODEL: | A1 | X | X | X | X | | | | | |
| | A2 | X | X | X | X | | | | | X |
| | A3 | X | X | X | X | | | | | |
| | A4 | X | X | X | X | | | | | |
| | A5 | X | X | | X | X | | | | |
| | A6 | X | X | X | X | | | | | X |
| | A7 | X | X | X | X | | | | | |
| | A8 | X | X | X | X | | | | | |
| | A9 | X | X | | X | | X | | | |
| | A10 | X | X | | X | X | | | | X |
| | AE | X | X | | X | | | | | |
| | S1 | X | X | X | X | | | | | |
| | S2 | X | X | X | X | | | X | X | X |
| | S3 | X | X | X | X | | | | | |
| | S4 | X | X | X | X | | | | | |
| | S5 | X | X | X | X | | | | | |
| | S6 | X | X | X | X | | | X | X | X |
| | S7 | X | X | X | X | | | | | |
| | S8 | X | X | X | X | | | | | |
| | S9 | X | X | X | X | X | | | | |
| | S10 | X | X | X | X | X | | X | X | X |
| | SE | X | X | X | X | | | | | |
| | SA2 | X | | | | | | | | |
| | SA6 | X | | | | | | | | |
| | SA10 | X | | | | | | | | |

## TABLE IV

### Performance Comparisons for Axial, Swirling
### and Skewed Flow Distributions

| Model | Average Base Pressure Coefficient $C_{P2}$ | Thrust Coefficient $C_T$ | Flow Coefficient $C_F$ |
|-------|------------------|------------------|------------------|
| A2    | -.166            | .979             | .972             |
| S2    | -.840            | .695             | .827             |
| SA2   | -.484            | .903             | .954             |
|       |                  |                  |                  |
| A6    | -.195            | .964             | .991             |
| S6    | -.740            | .684             | .888             |
| SA6   | -.341            | .981             | .993             |
|       |                  |                  |                  |
| A10   | -.211            | .888             | .980             |
| S10   | -.500            | .660             | .942             |
| SA10  | -.240            | .861             | 1.009            |

## TABLE V

### Comparison of Test and Theory for Configurations

### SA2, SA6, SA10, SE

| Model | Average Base Pressure Coefficient $C_{P2}$ | Thrust Coefficient $C_T$ | Flow Coefficient $C_F$ | |
|-------|------|------|------|--------|
| SA2 | -.484 | .903 | .954 | Test |
|     | -.463 | .910 | 1.006 | Theory |
| SA6 | -.341 | .981 | .993 | Test |
|     | -.400 | .871 | 1.008 | Theory |
| SA10 | -.240 | .861 | 1.009 | Test |
|      | -.272 | .858 | 1.019 | Theory |
| SE  | -.535 | .688 | .868 | Test |
|     | -.553 | .628 | .941 | Theory |
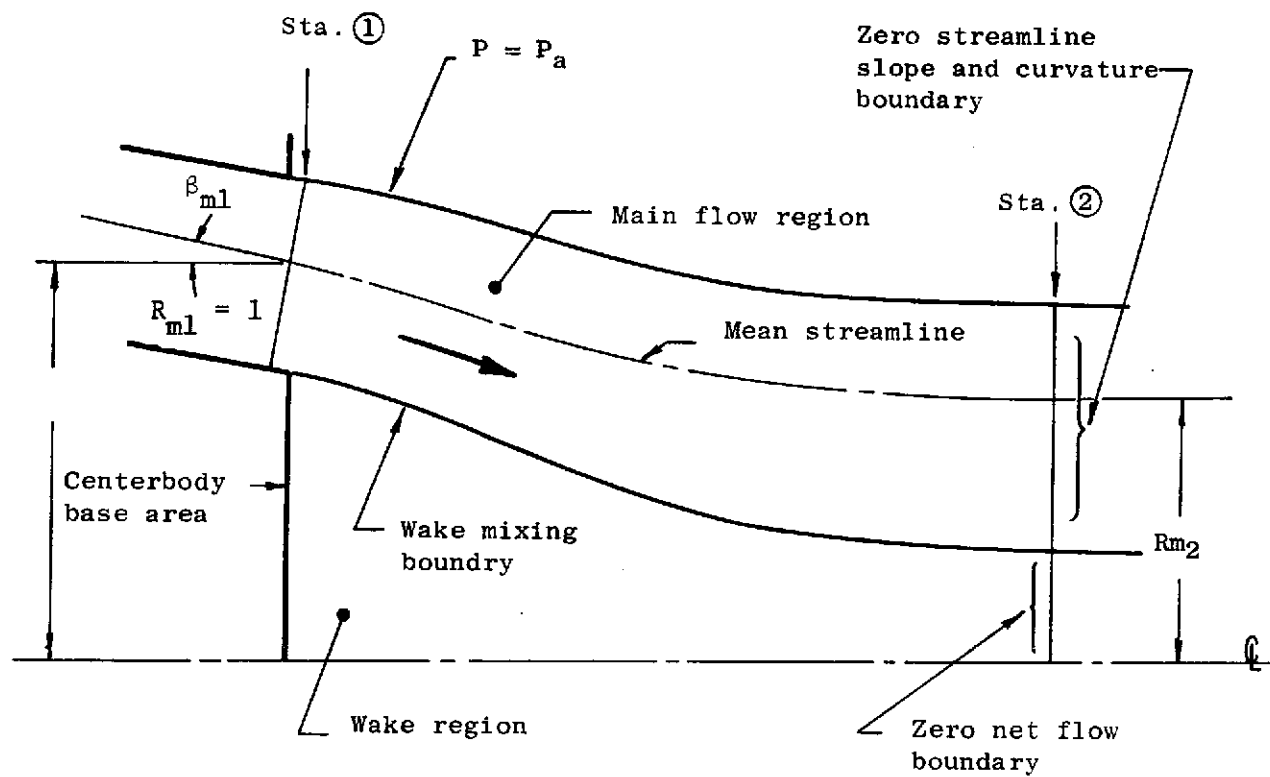
Figure 1.  Analytical Model

**Case 1.** Parallel Streamlines and $r_m \neq 0$
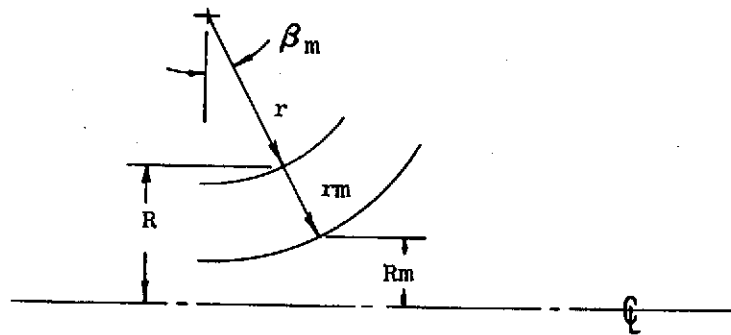


$$r = r_m - (R - R_m)/\cos \beta_m$$

**Case 2.** Constant Area Between Streamlines and $r_m = 0$
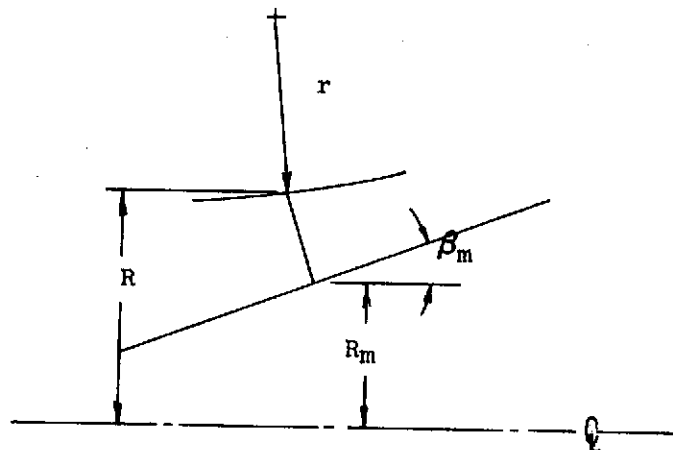


$$r = \frac{(R^2 + R_m^2 \sin^2 \beta_m)^{1.5}}{(R^2 - R_m^2) \sin^2 \beta_m}$$

Figure 2. Streamline Curvature Approximations

Specification Statements

1. Ask for input data ← Terminal Input

Is R/R = 0 ?  →yes→ Stop

no

Do preliminary calculations

Estimate starting values for MF, ᵹ, V2, PLOS

5 Calculate constants in meanline equation

Subroutine ROTFLO

Initialize parameters to values for ᵹ = 0

Subroutine COEP

10 Calculate normal equilibrium and continuity at successive downstream stations

Calculate R/R and axial forces at stations ① and ②

Subroutine INI

Calculate error in R/R and axial force balance

Are both errors ≤ .3%?  →yes→  Is IPT = 0?  →yes→

no                                        no

Is ITR = MAXIT?  →yes→  More iterations?  →no→

no                          yes

23 Select new MF and L  ←  Subroutine INT2

30 Do final calculations and print results

Figure 3. Computer Program Block Diagram

-62-

(a)

(b)
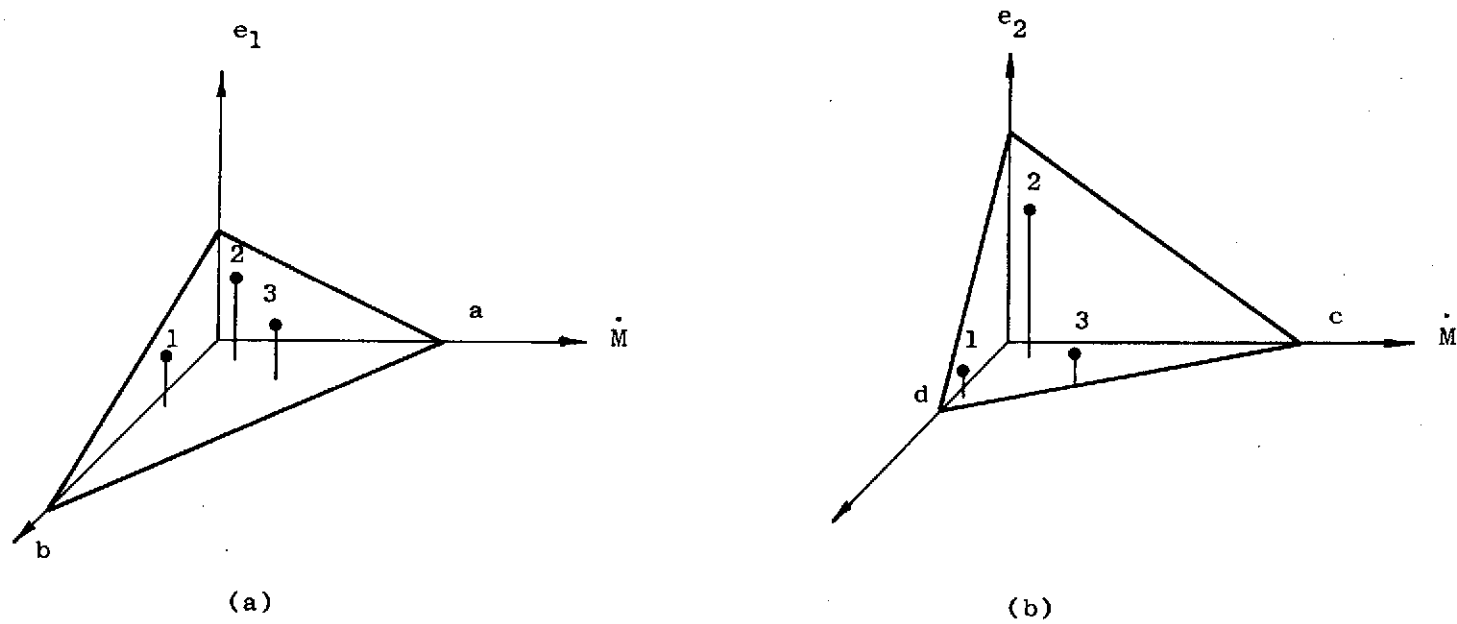
Figure 4.  Secant Iteration Scheme
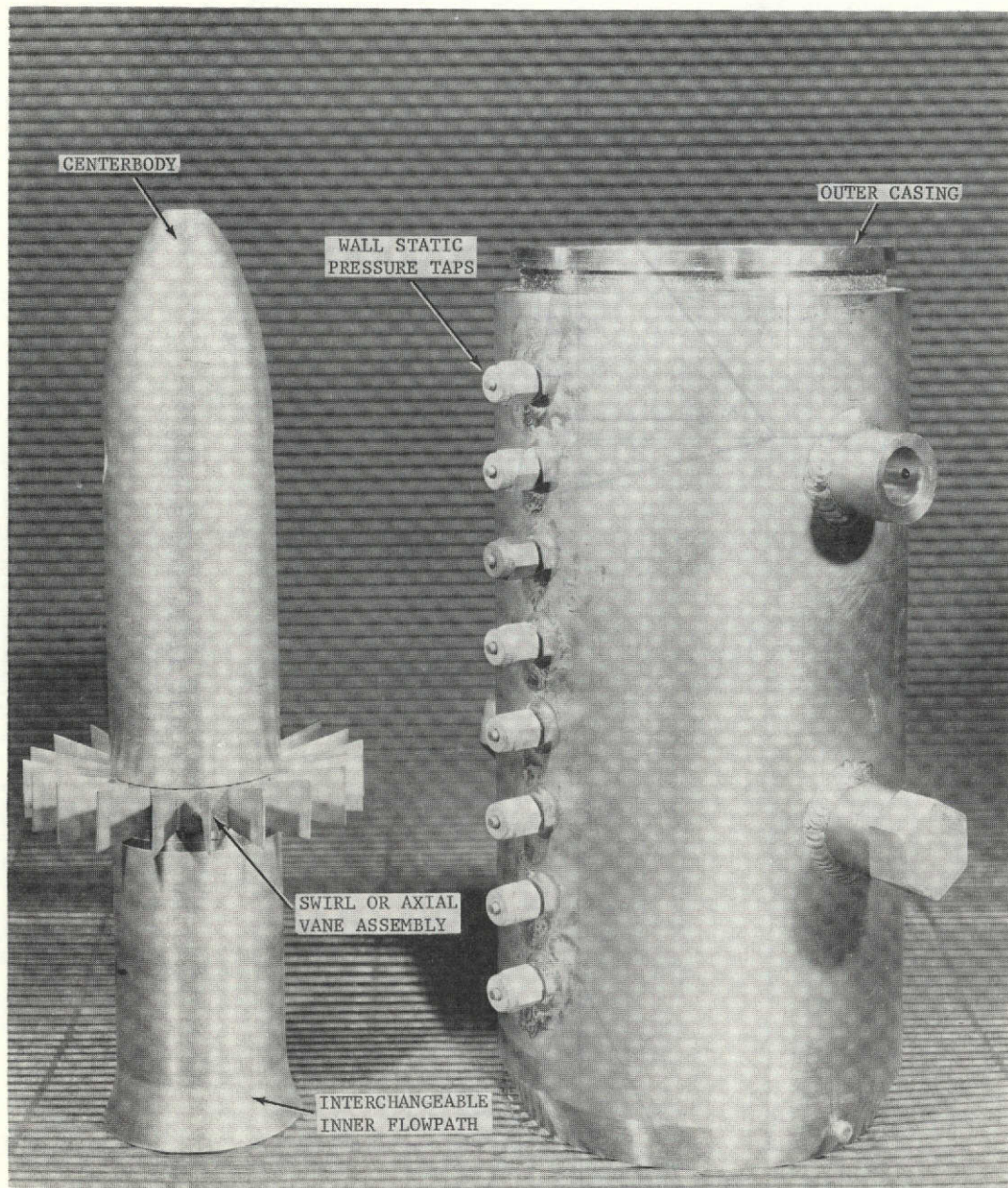
Figure 5. Photograph of the Base Pressure Model Assembly

65
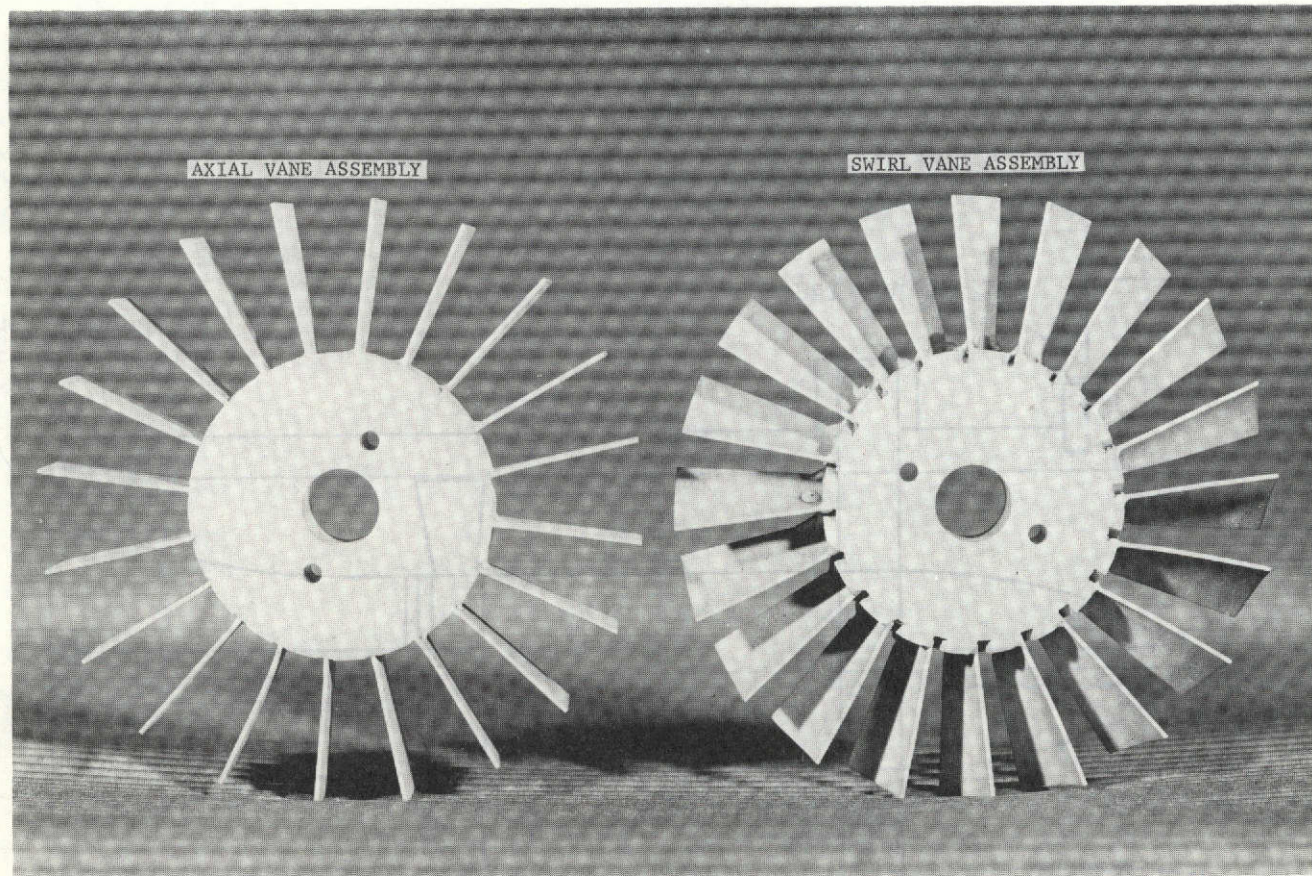


Figure 6.  Photograph of the Axial and Swirl Vane Assemblies
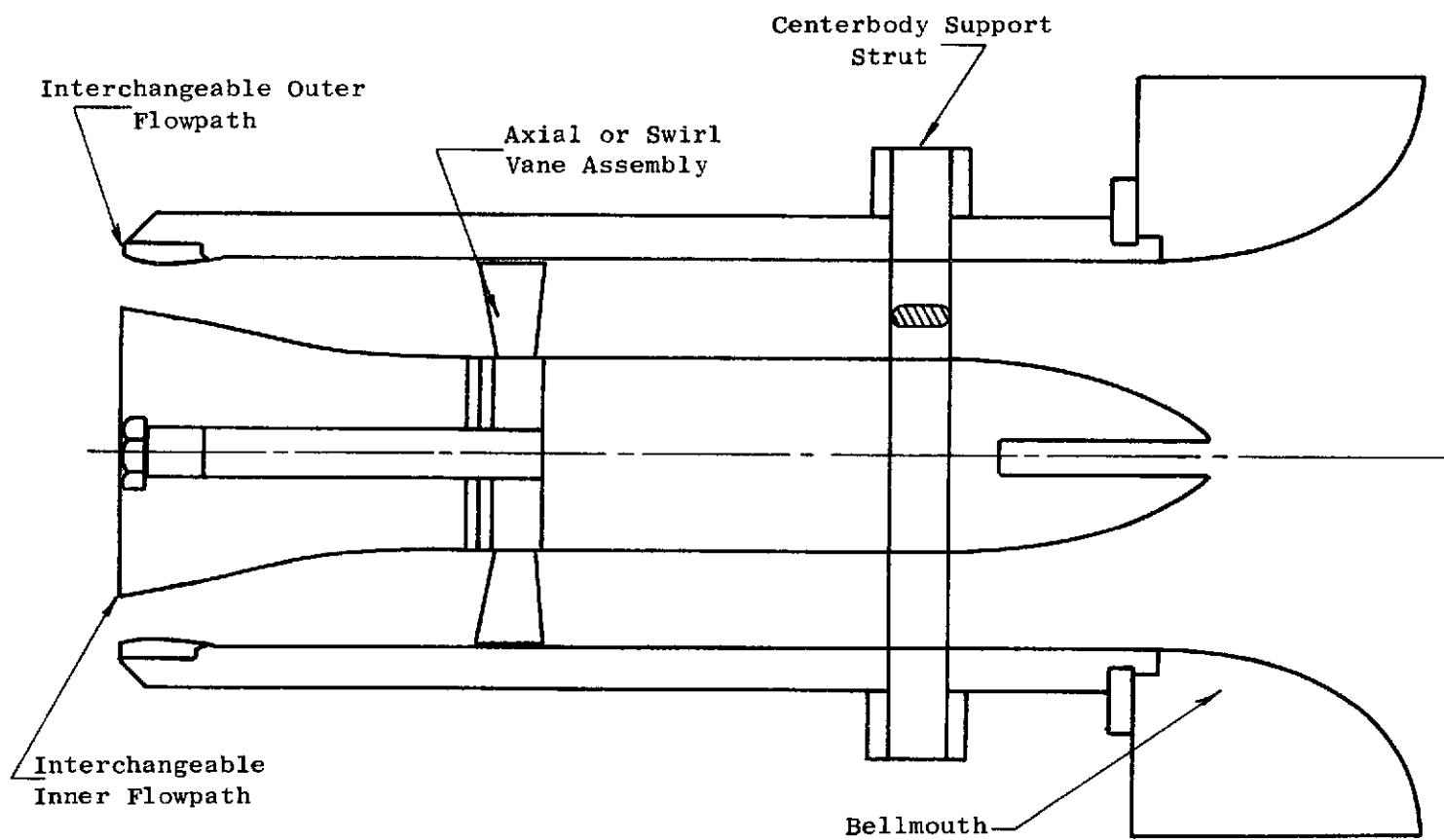
Figure 7. Hub Base Pressure Test Model Schematic
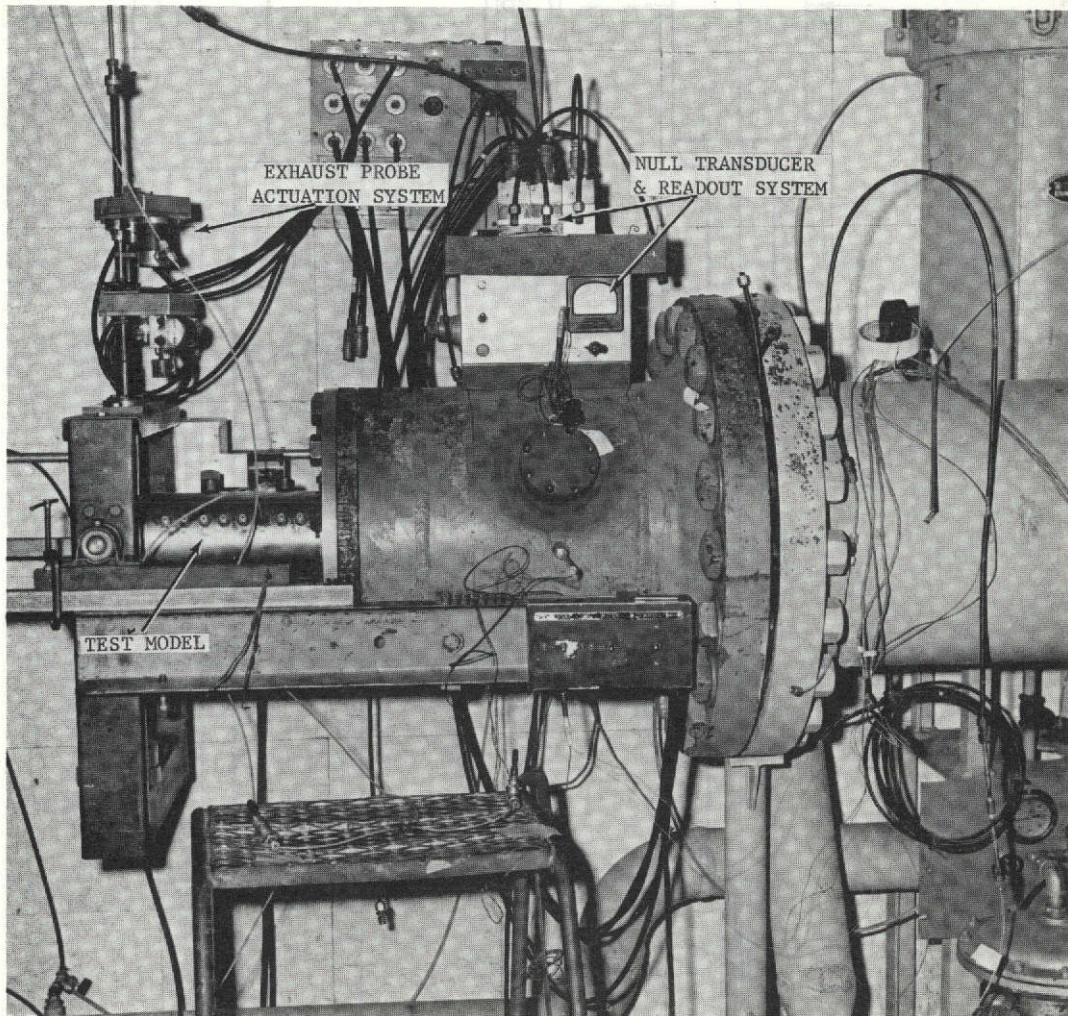
Figure 8. Photograph of the Base Pressure Model Installed in the Test Stand

0.250
(0.635)

0.120
(0.305)

2.00
(5.08)

All units in
inches except those
in parentheses
which are
centimeters.

0.100
(0.254)

0.032 (0.081) O.D.
0.020 (0.051) I.D.

0.500
(1.270)

0.120 (0.305)

45°
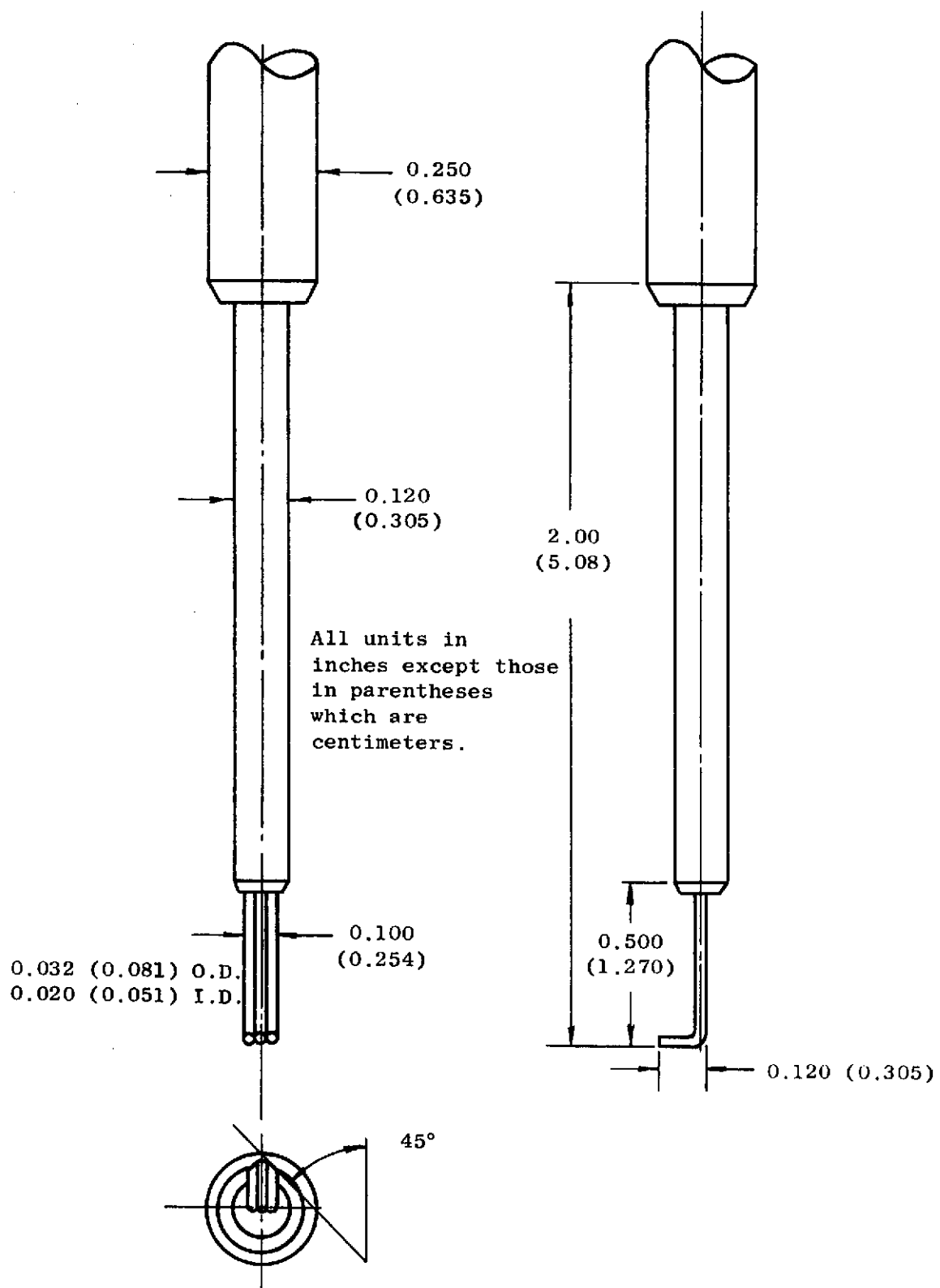
Figure 9.  Schematic of Exhaust Traverse Probe
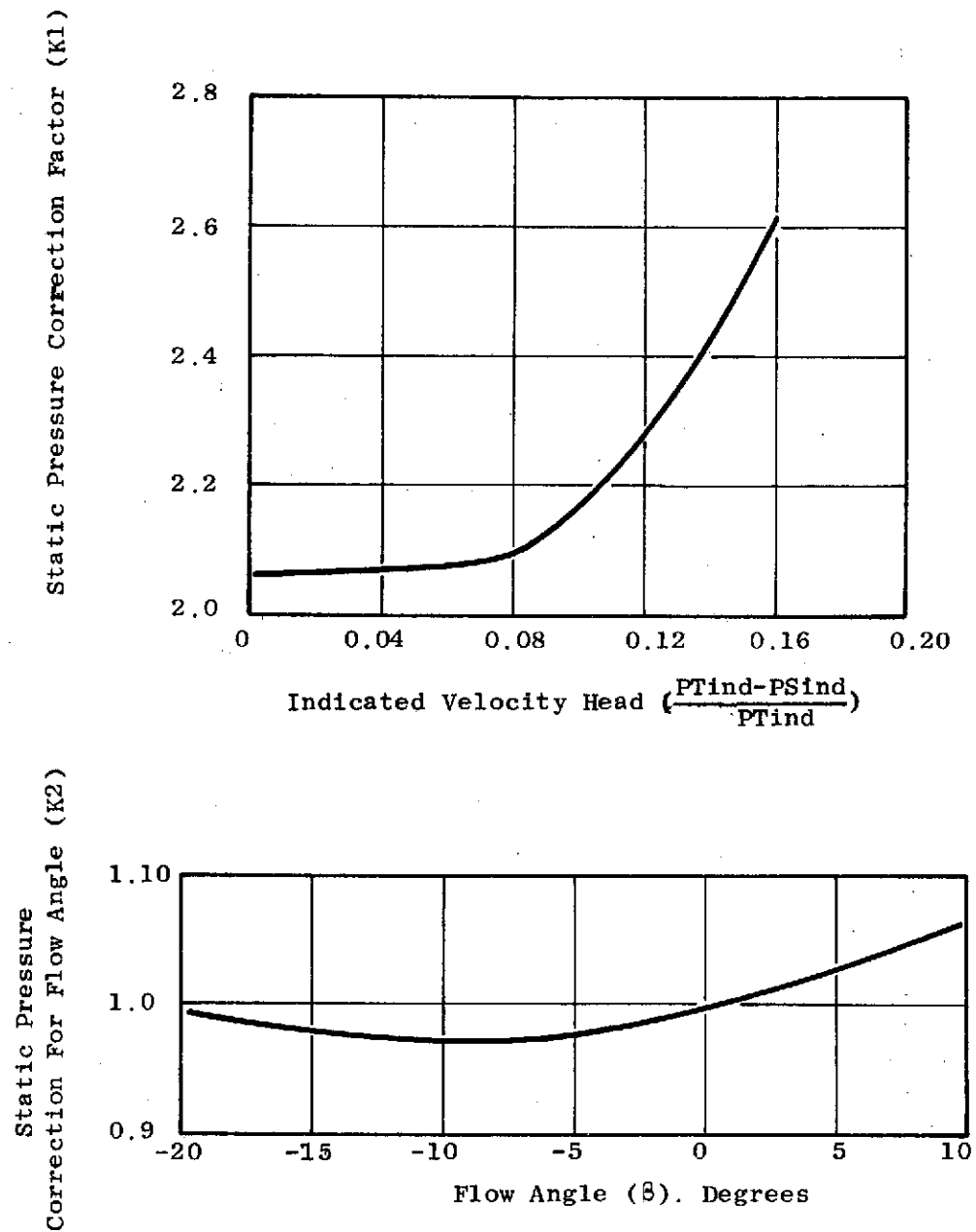
Figure 10. Probe Calibration for Static Pressure
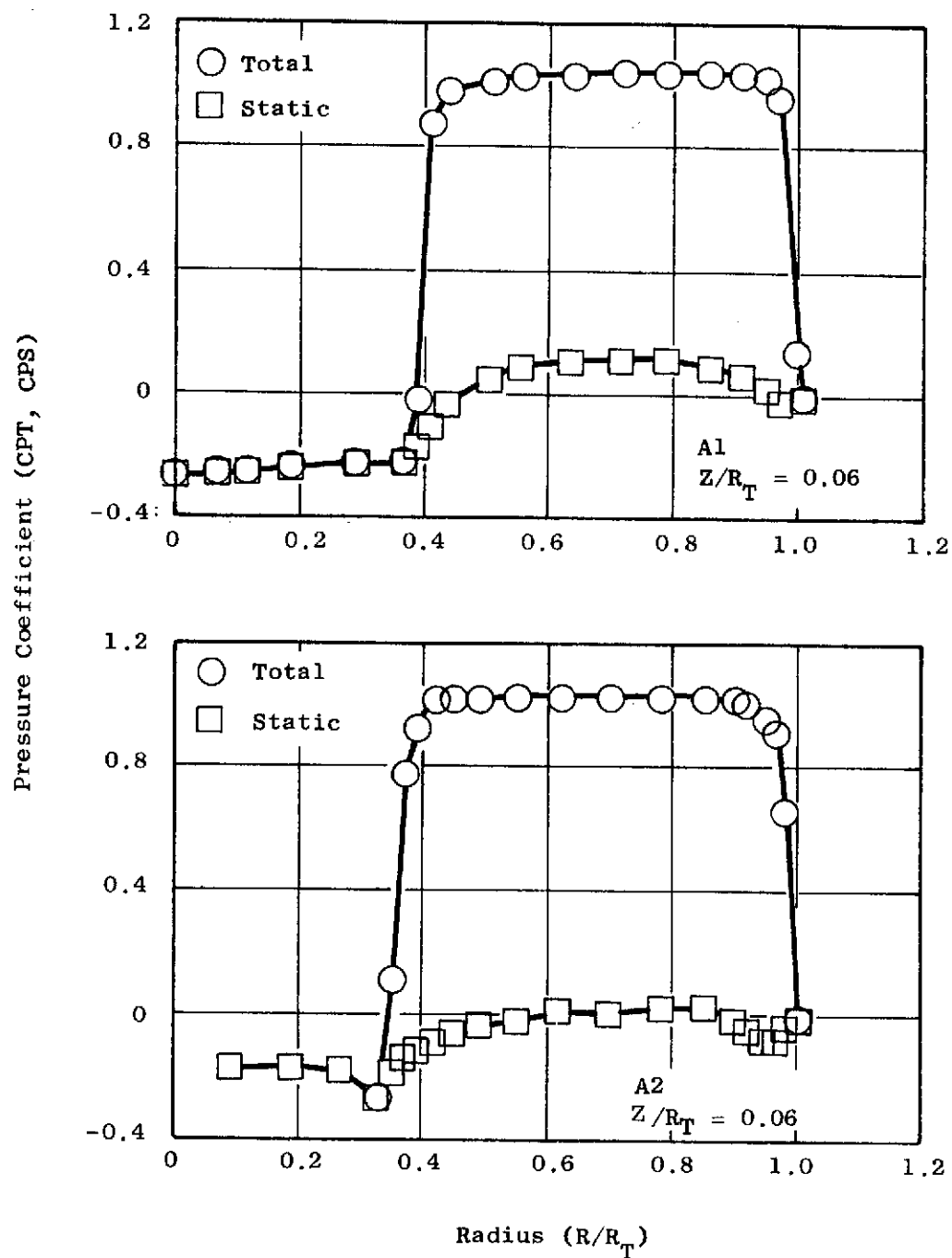
Figure 11. Total and Static Pressure Coefficient
Distribution for Models 1 and 2, Axial Flow
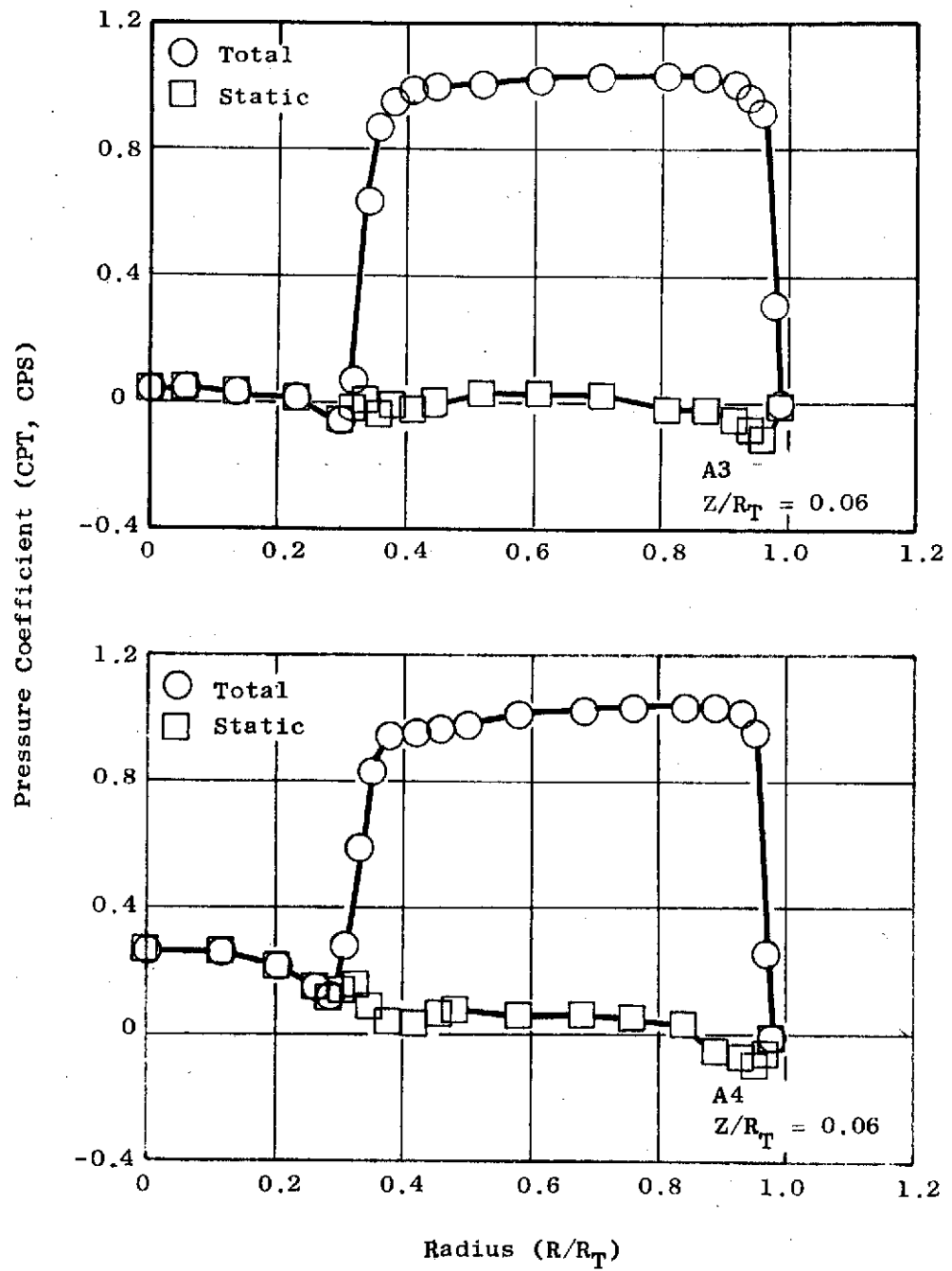
Figure 12. Total and Static Pressure Coefficient
Distribution for Models 3 and 4, Axial Flow
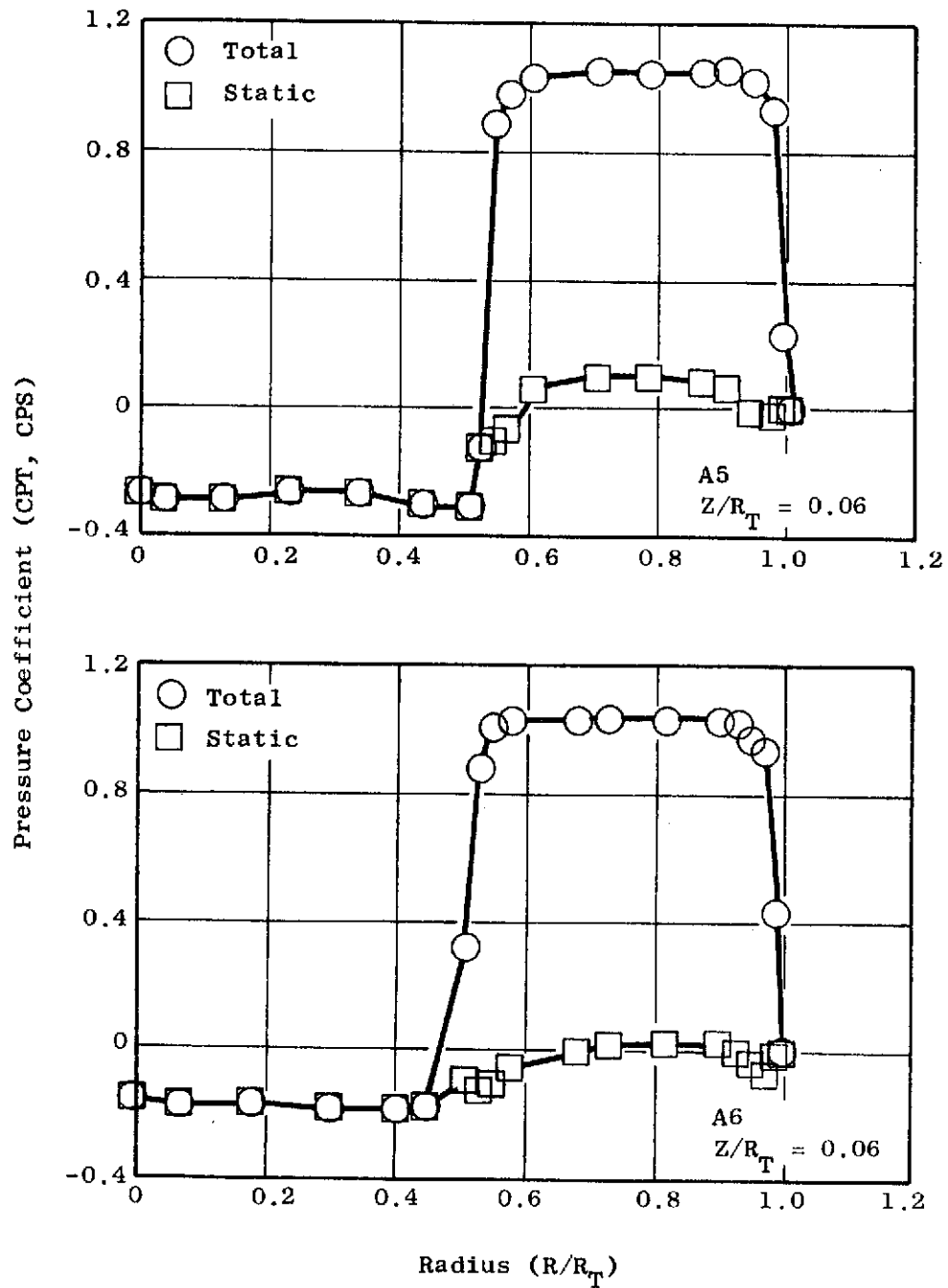
Figure 13. Total and Static Pressure Coefficient
Distribution for Models 5 and 6, Axial Flow
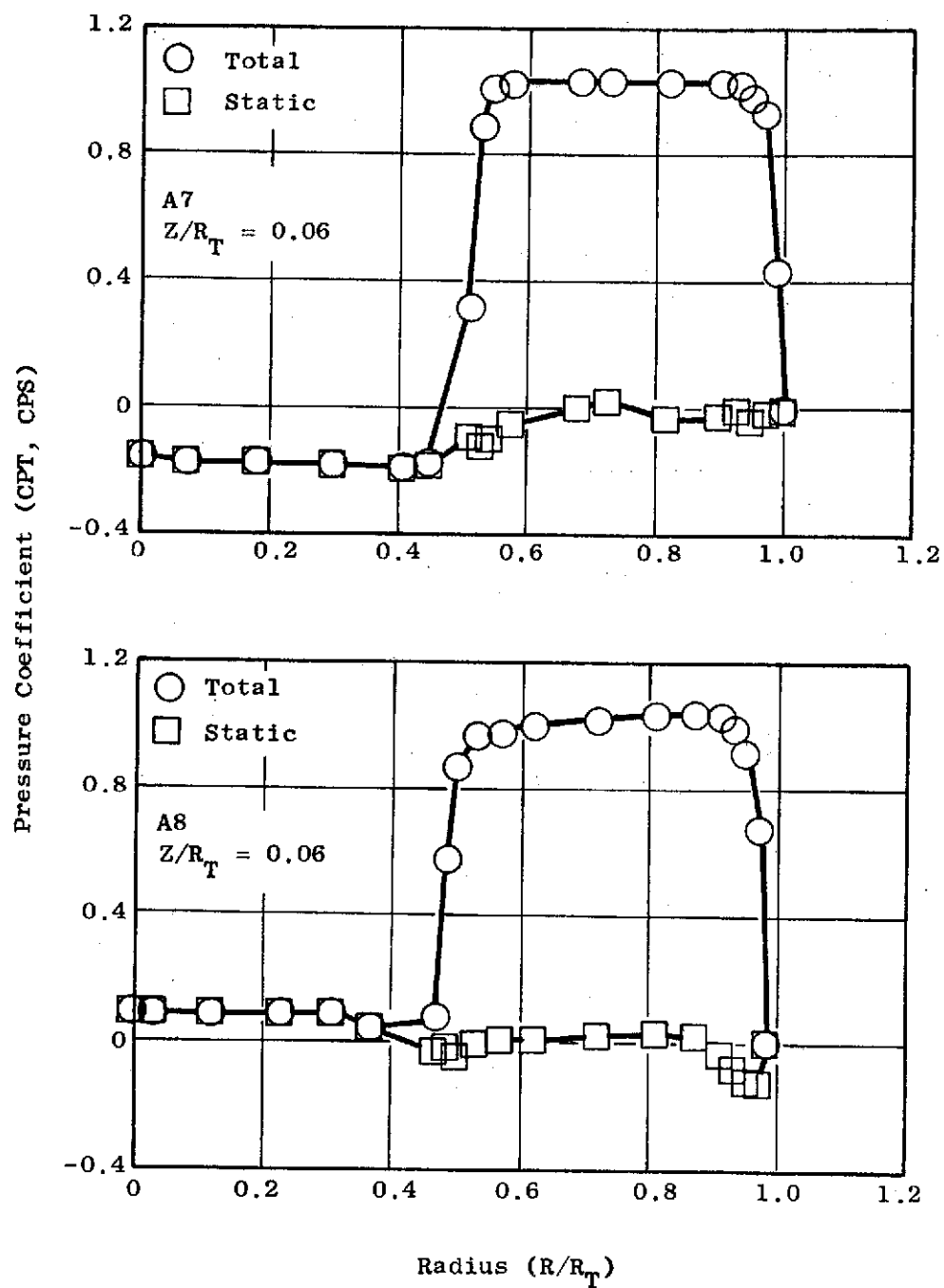
Figure 14.   Total and Static Pressure Coefficient
Distribution for Models 7 and 8, Axial Flow
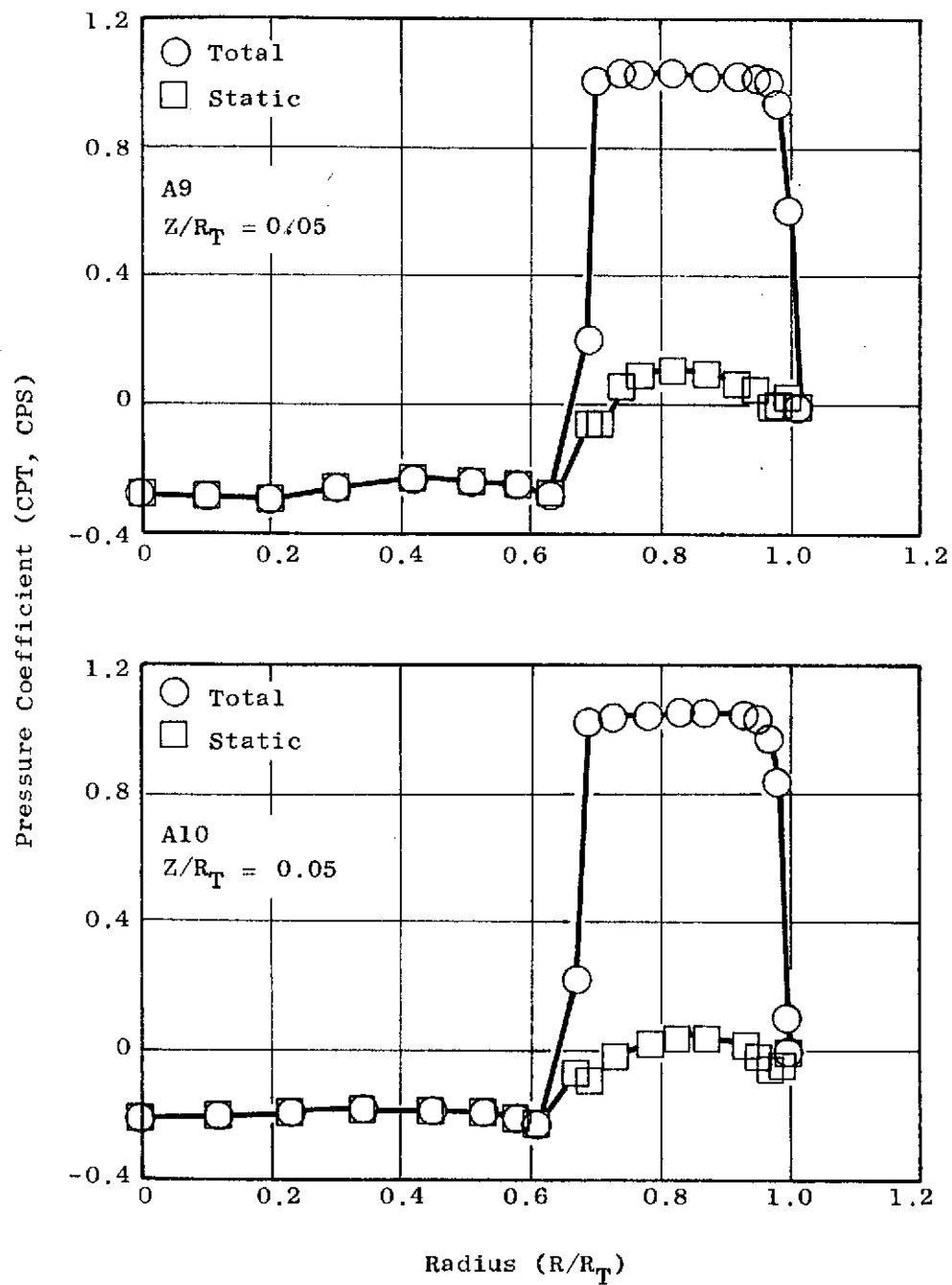
Figure 15.  Total and Static Pressure Coefficient
            Distribution for Models 9 and 10, Axial Flow
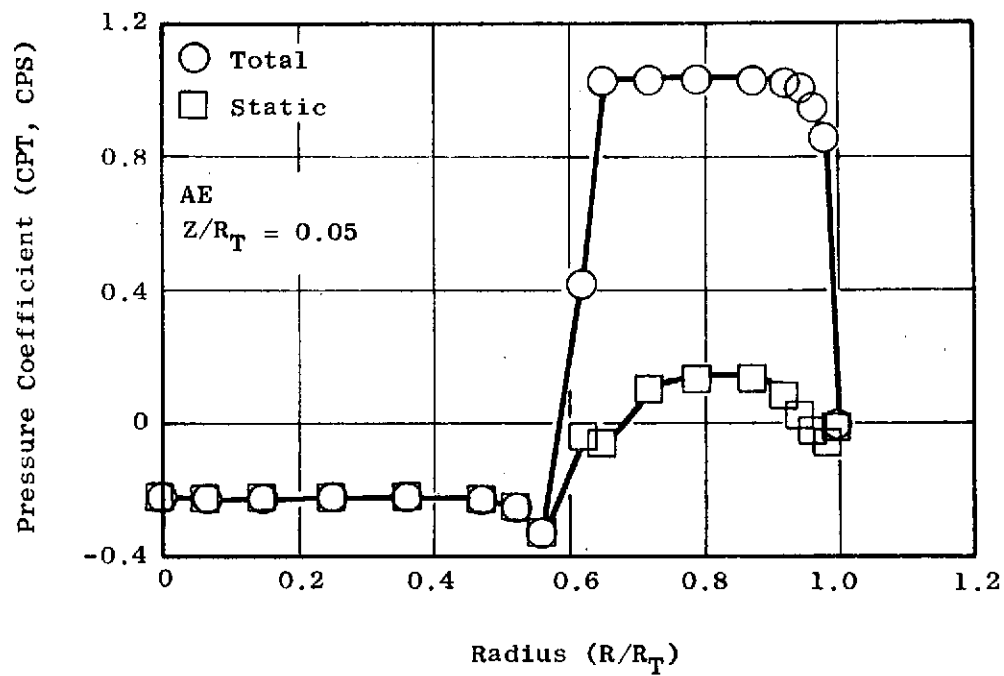
Figure 16.  Total and Static Pressure Coefficient
Distribution for Model E, Axial Flow
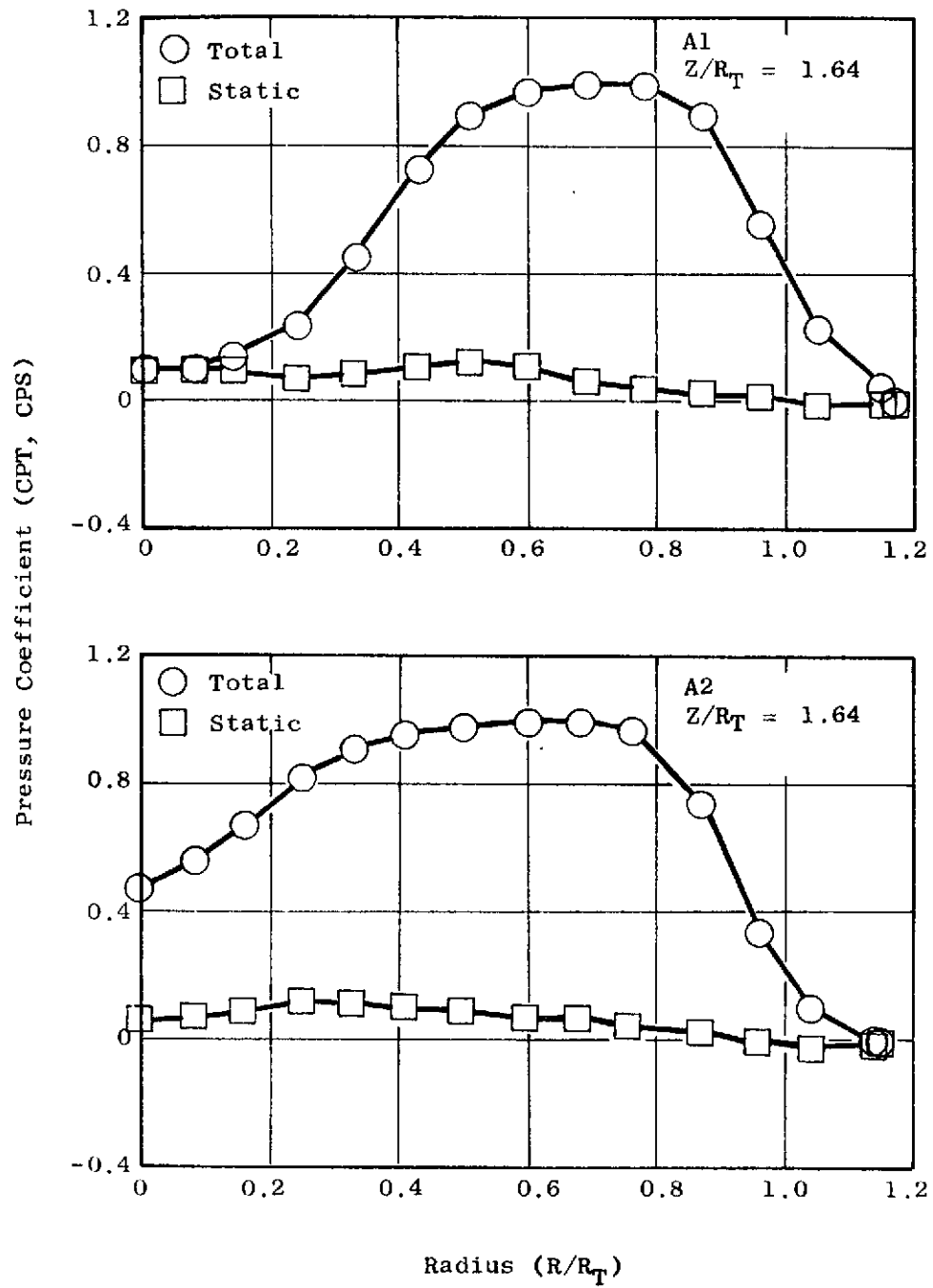
Figure 17. Total and Static Pressure Coefficient
Distribution for Models 1 and 2, Axial Flow
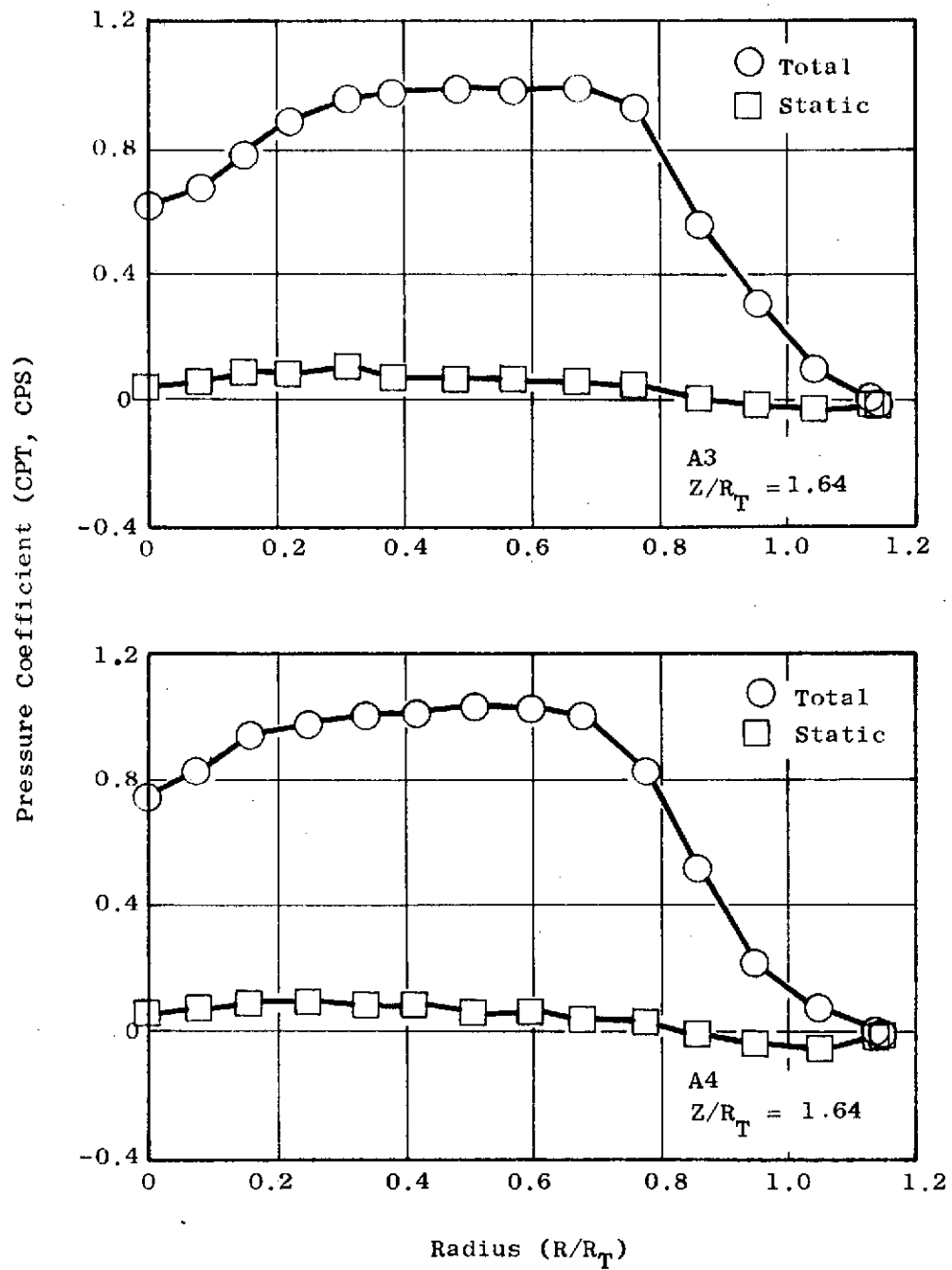
Figure 18. Total and Static Pressure Coefficient Distribution for Models 3 and 4, Axial Flow
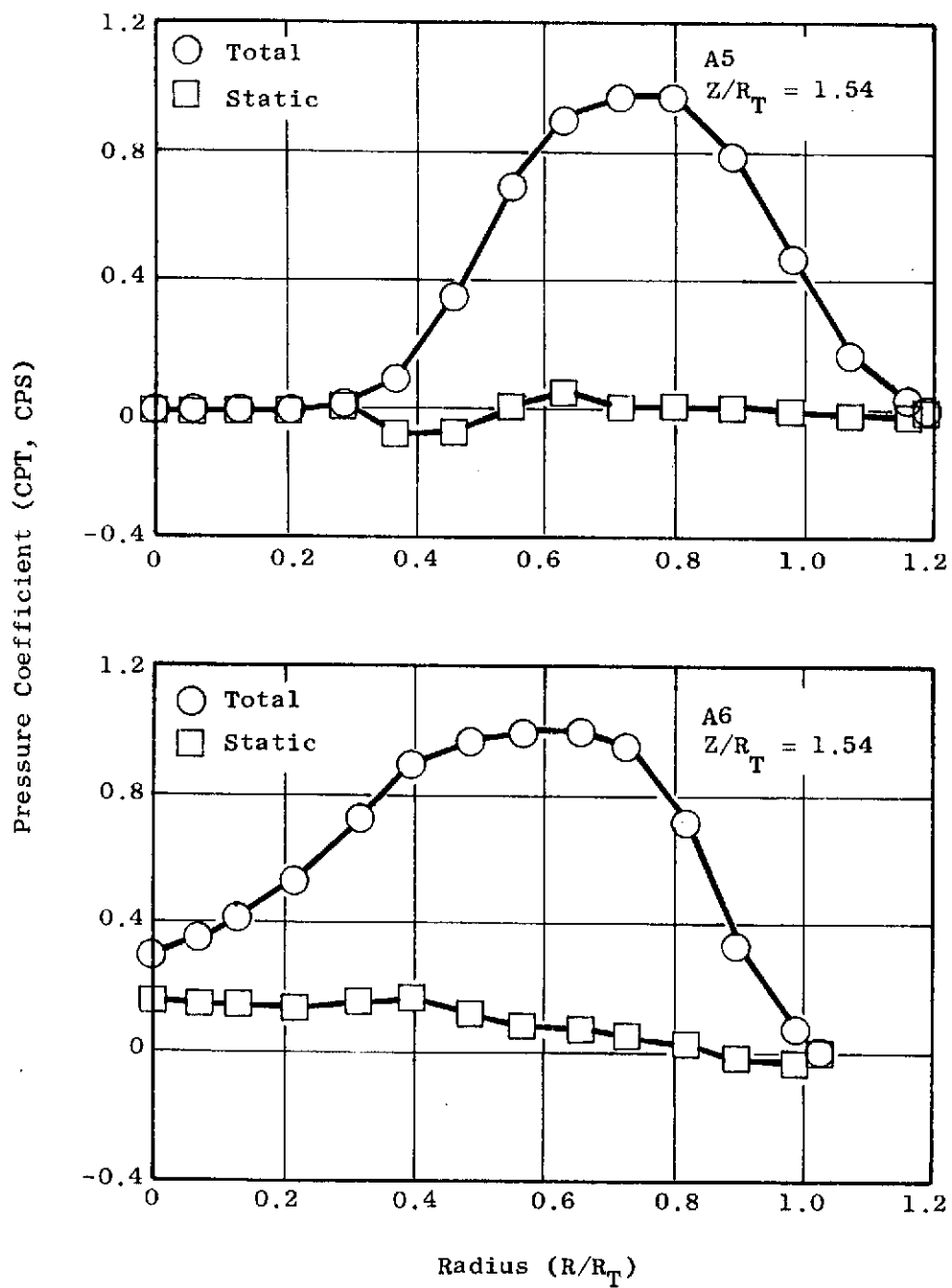
Figure 19. Total and Static Pressure Coefficient
Distribution for Models 5 and 6, Axial Flow
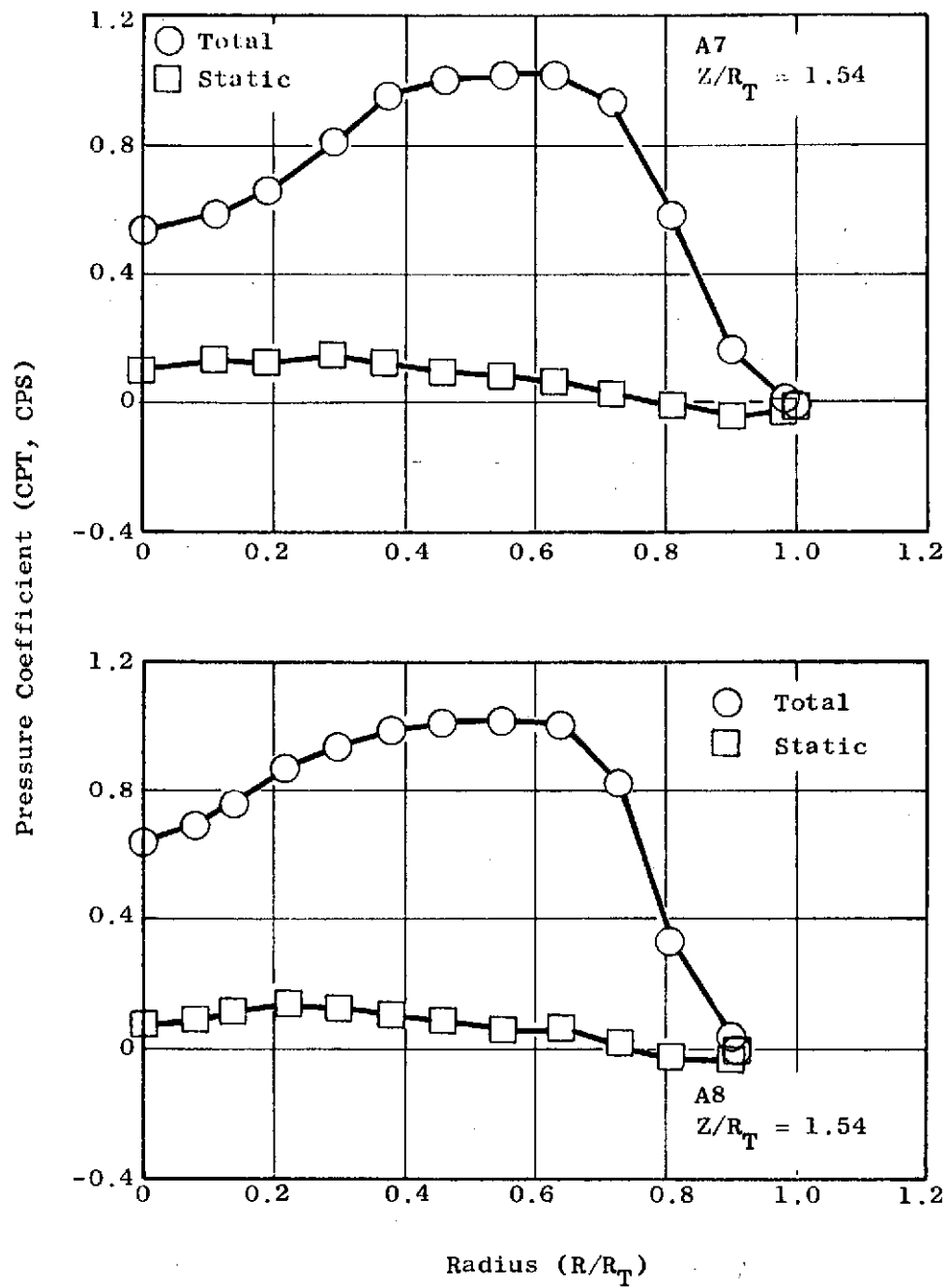
Figure 20. Total and Static Pressure Coefficient
Distribution for Models 7 and 8, Axial Flow
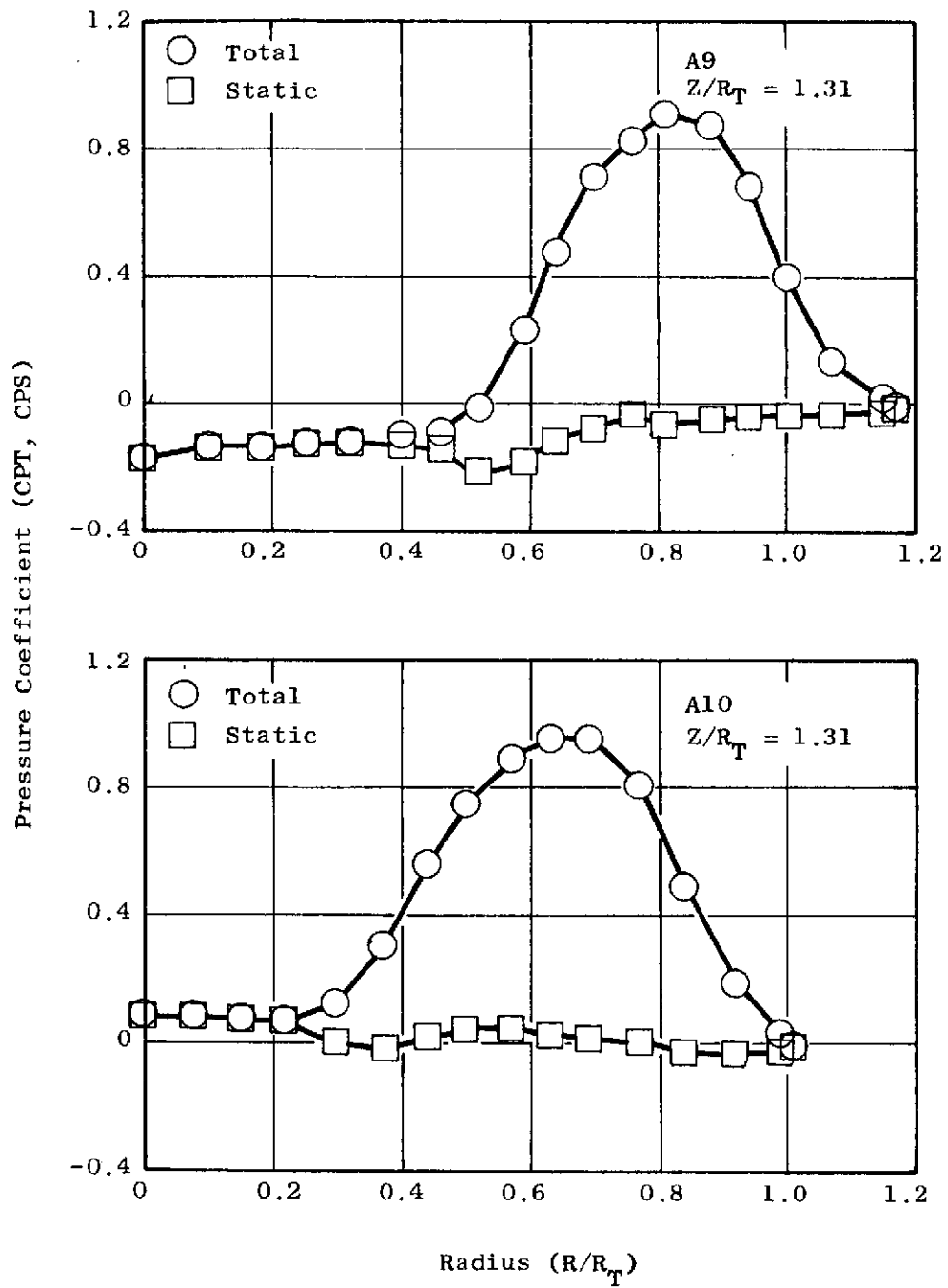
Figure 21.   Total and Static Pressure Coefficient
             Distribution for Models 9 and 10, Axial Flow
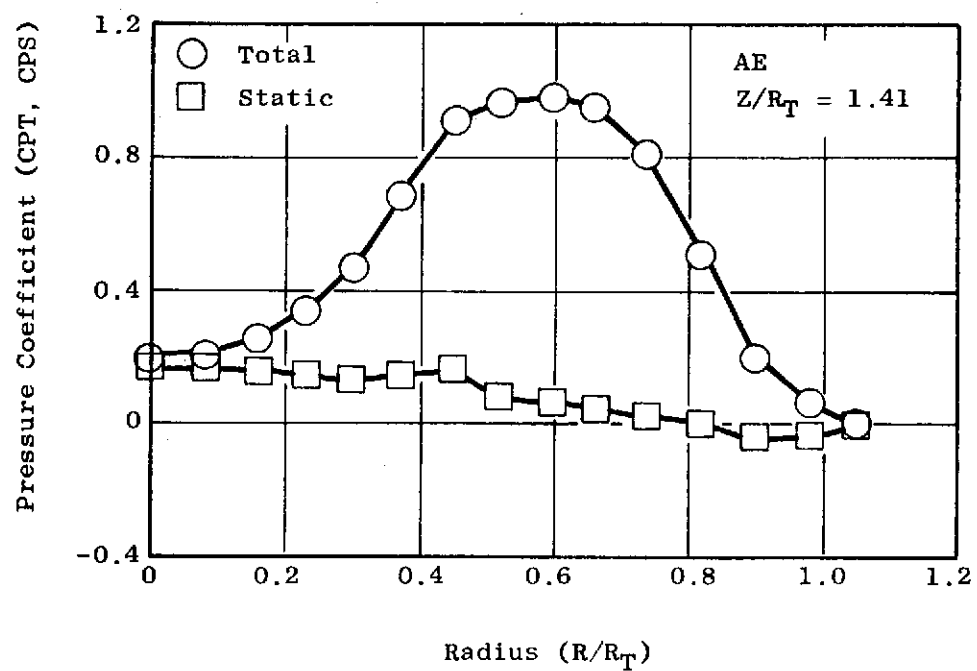
Figure 22. Total and Static Pressure Coefficient
Distribution for Model E, Axial Flow

**A1**

W/W$_T$(%)

100
80
60
40
20

0

Mixing
Region

**A2**

W/W$_T$ (%)

100
80
60
40
20

0
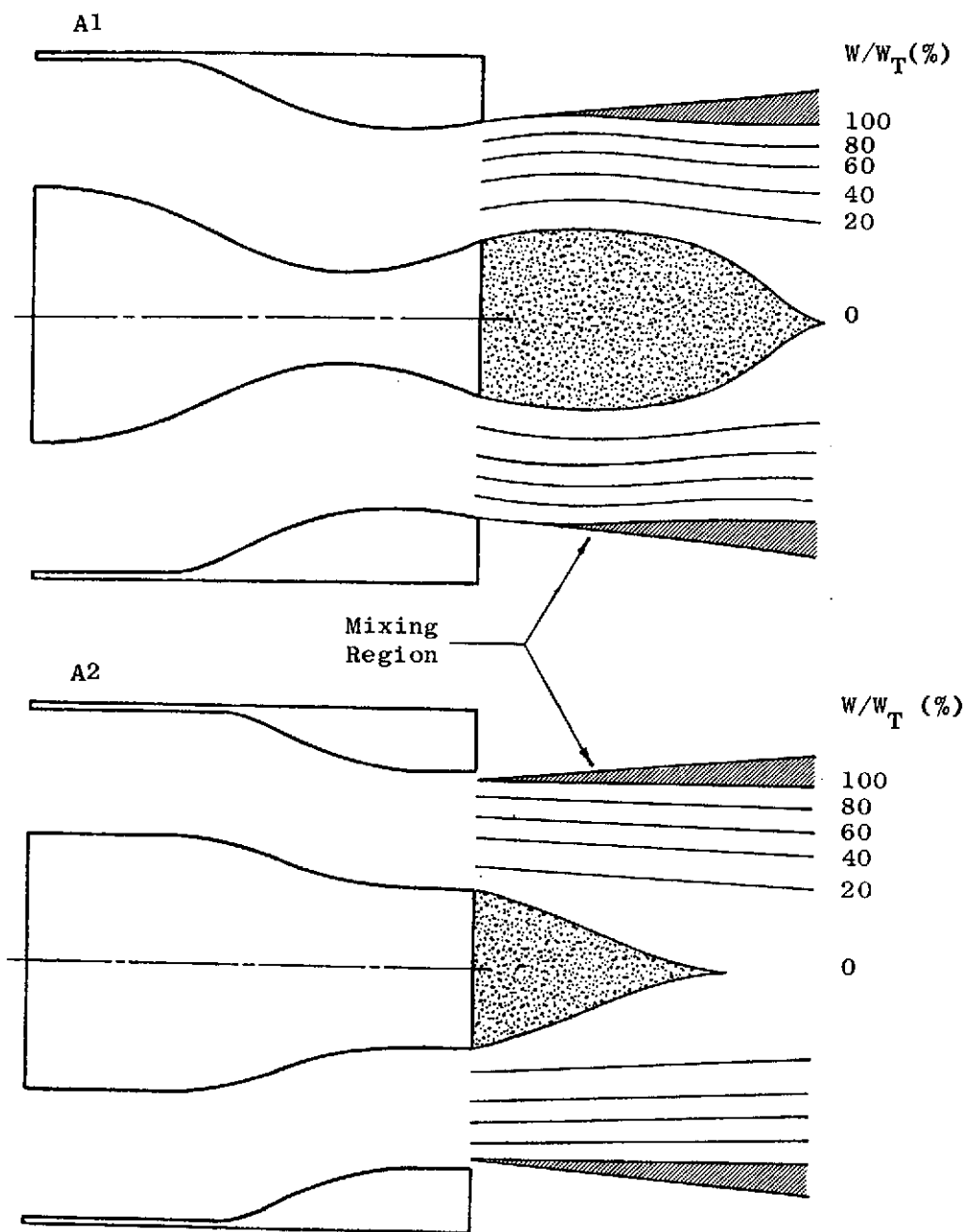
Figure 23. Graphical Representation of the Flow Field for
Models 1 and 2, Axial Flow

A3

W/W$_T$(%)

100
80
60
40
20

0

Mixing
Region

A4

W/W$_T$(%)

100
80
60
40
20

0
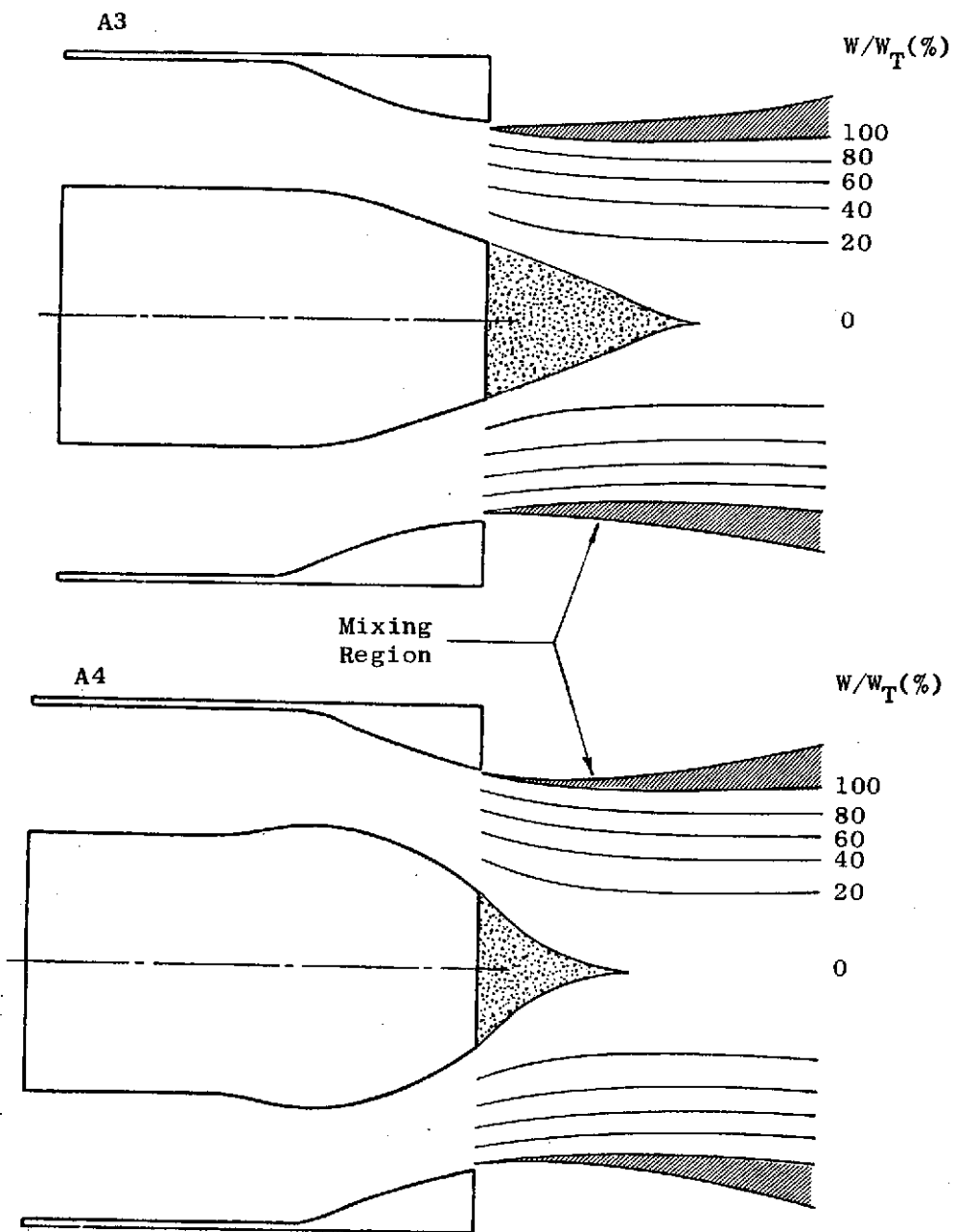
Figure 24.   Graphical Representation of the Flow Field for
Models 3 and 4, Axial Flow
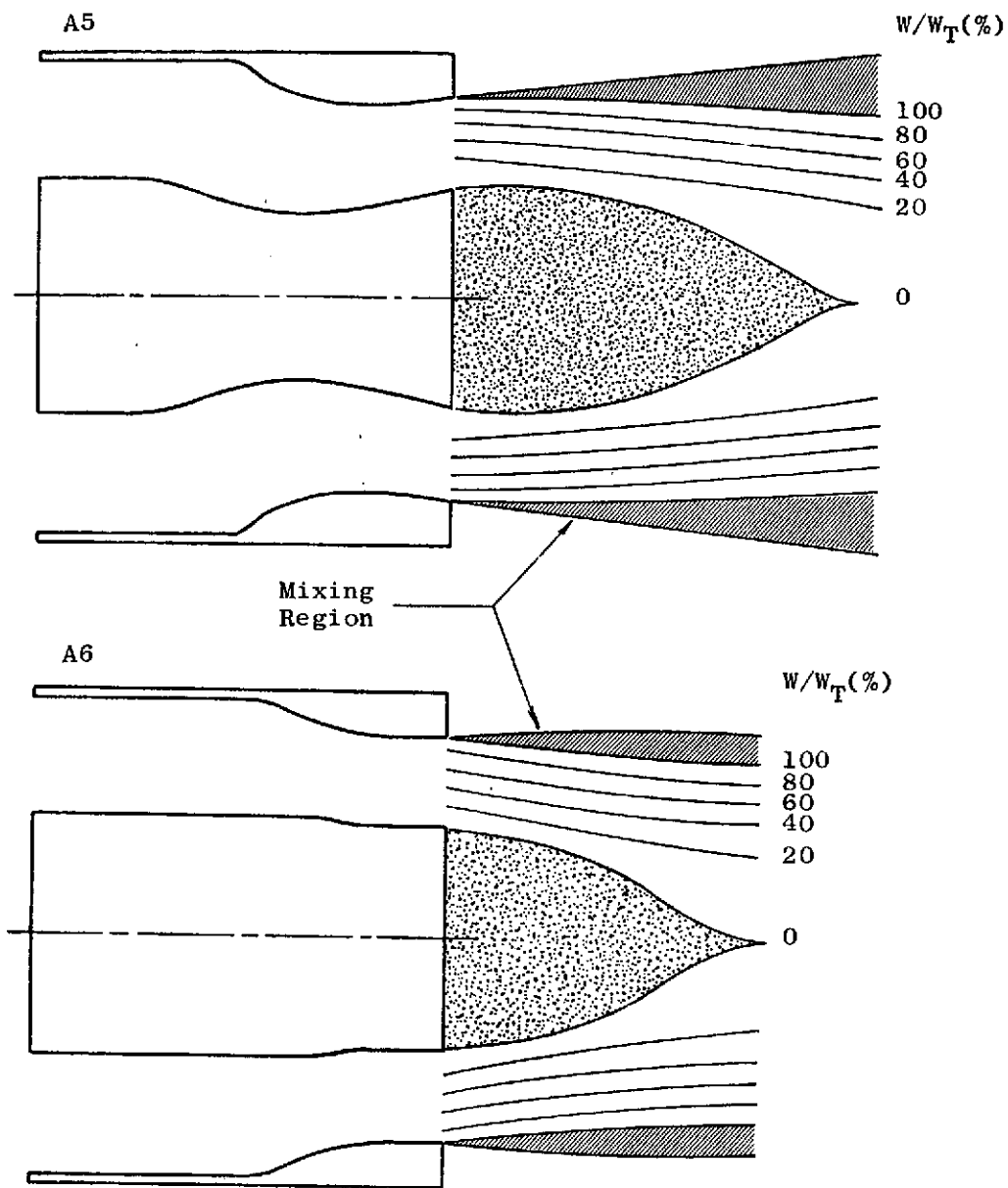
Figure 25. Graphical Representation of the Flow Field for Models 5 and 6, Axial Flow

A7

$W/W_T(\%)$

100
80
60
40
20

0

Mixing
Region

A8

$W/W_T(\%)$

100
80
60
40
20

0
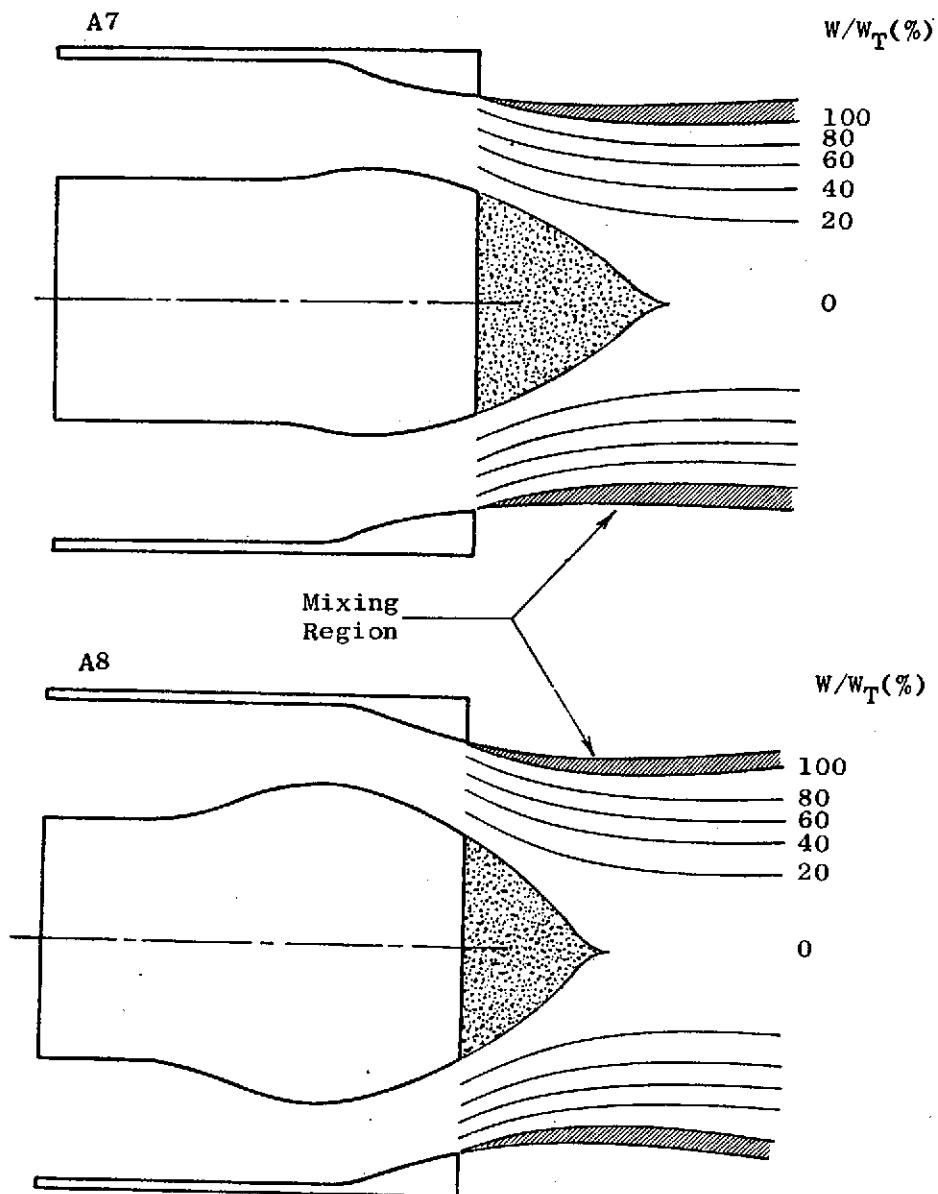
Figure 26. Graphical Representation of the Flow Field for
Models 7 and 8, Axial Flow

A9

W/W$_T$(%)

100
80
60
40
20

0

Mixing
Region

A10

W/W$_T$(%)

100
80
60
40
20

0
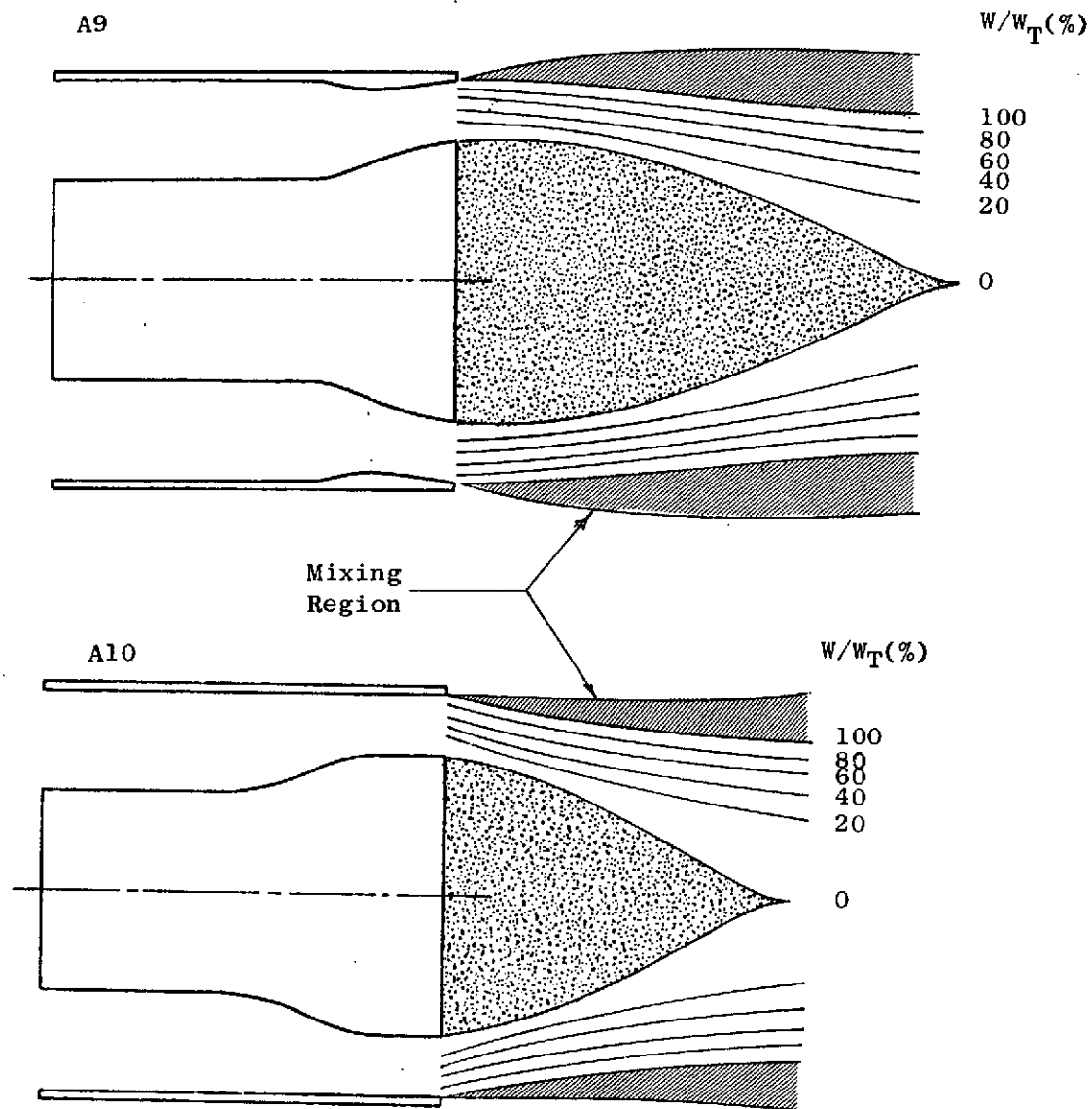
Figure 27. Graphical Representation of the Flow Field for
Models 9 and 10, Axial Flow
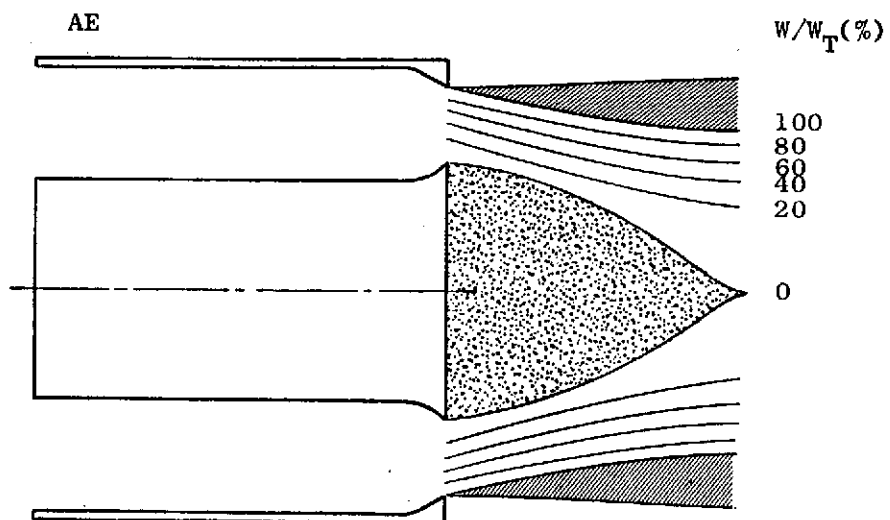
Figure 28. Graphical Representation of the Flow Field for Model E, Axial Flow
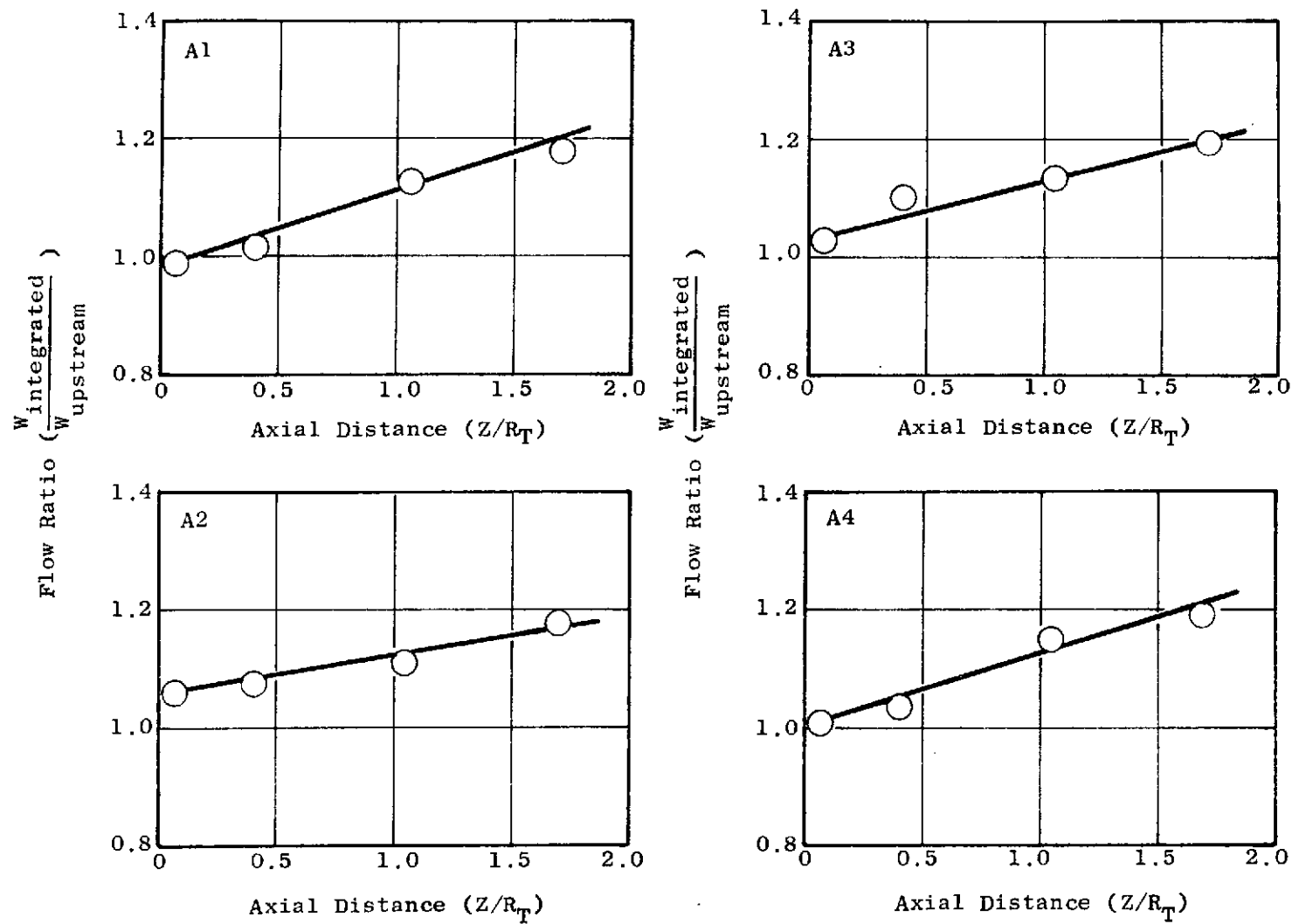
Figure 29. Flow Entrainment Characteristics for Models 1 through 4, Axial Flow
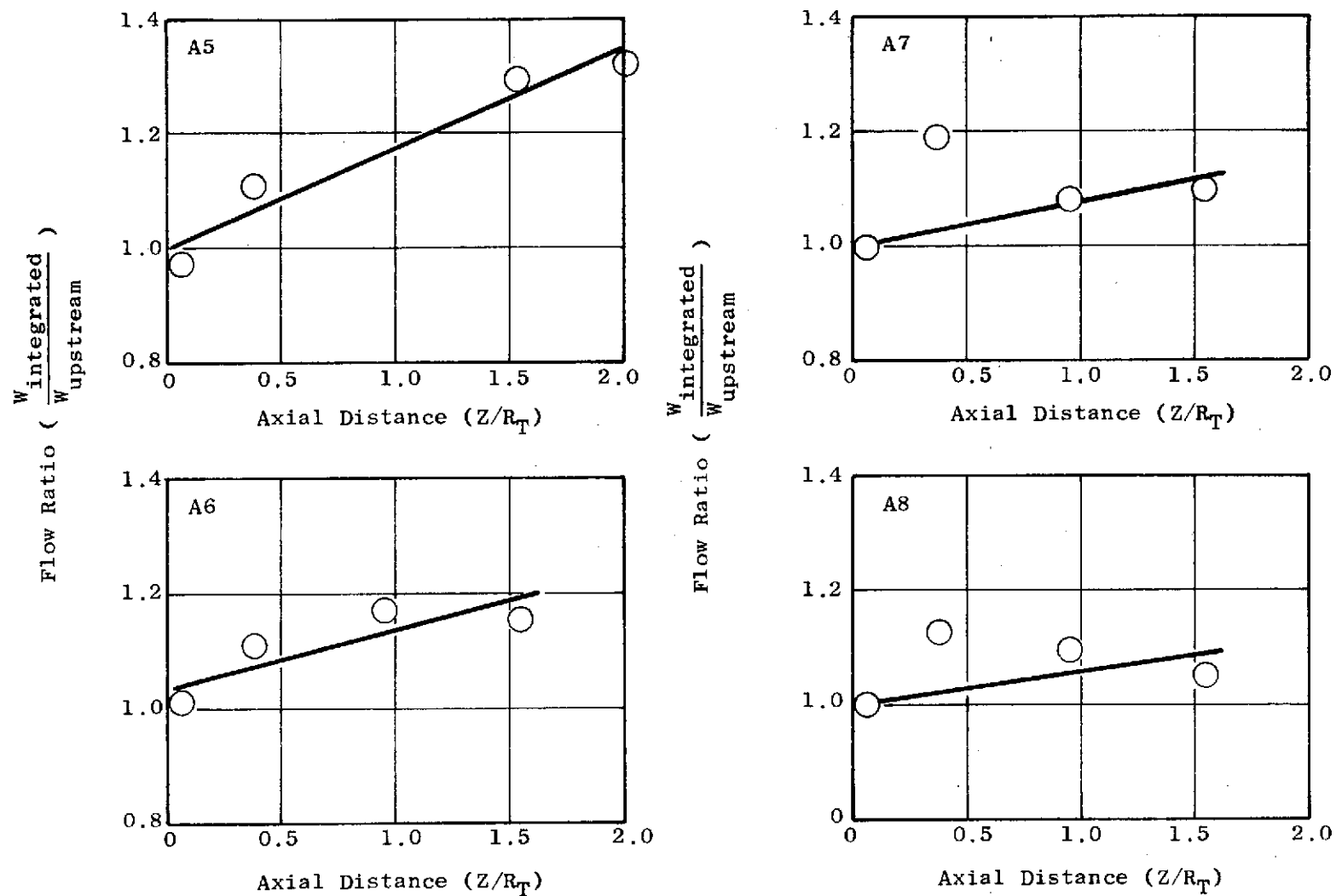
Figure 30.  Flow Entrainment Characteristics for Models 5 through 8, Axial Flow
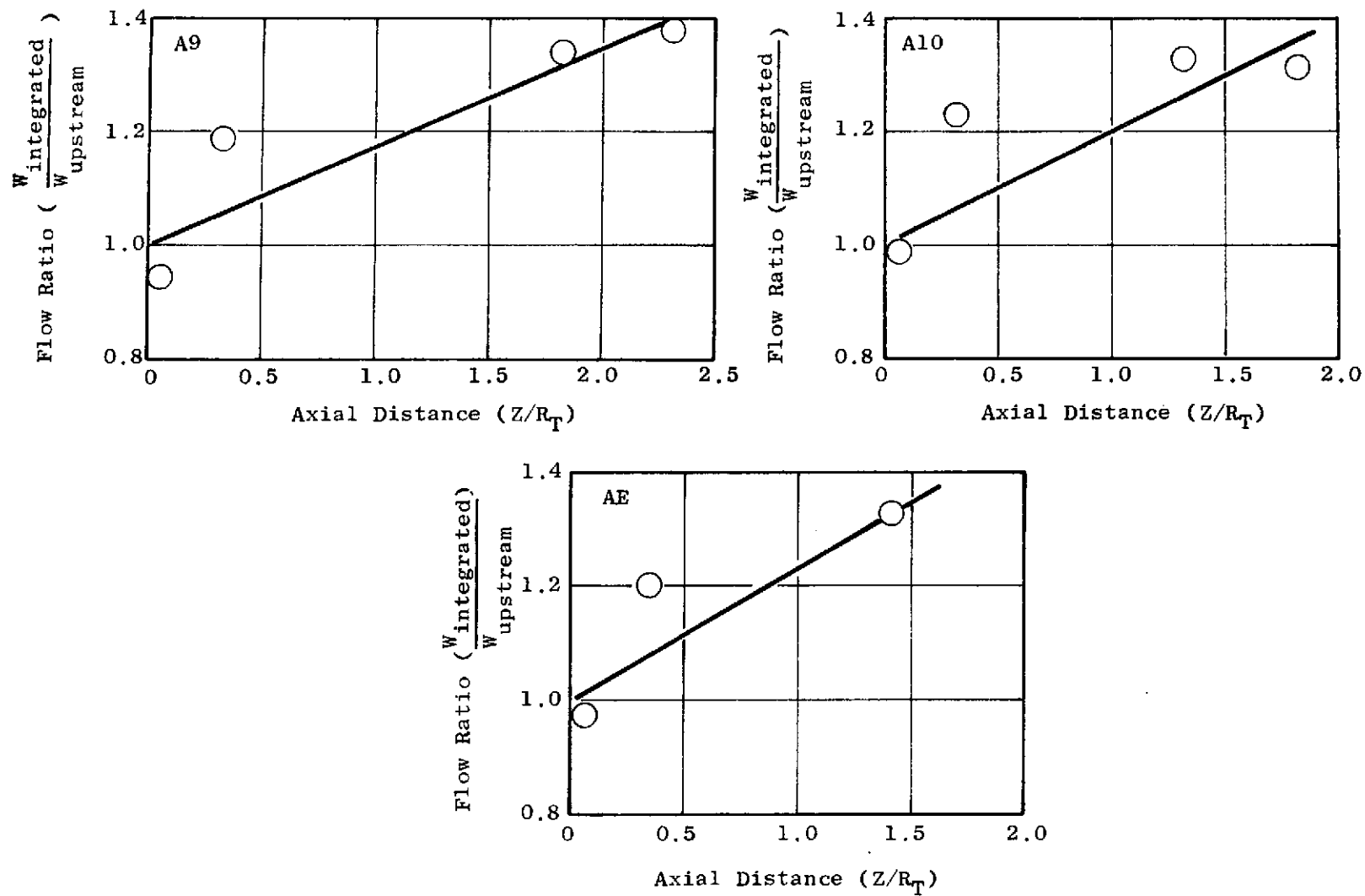
Figure 31. Flow Entrainment Characteristics for Models 9, 10 and AE, Axial Flow
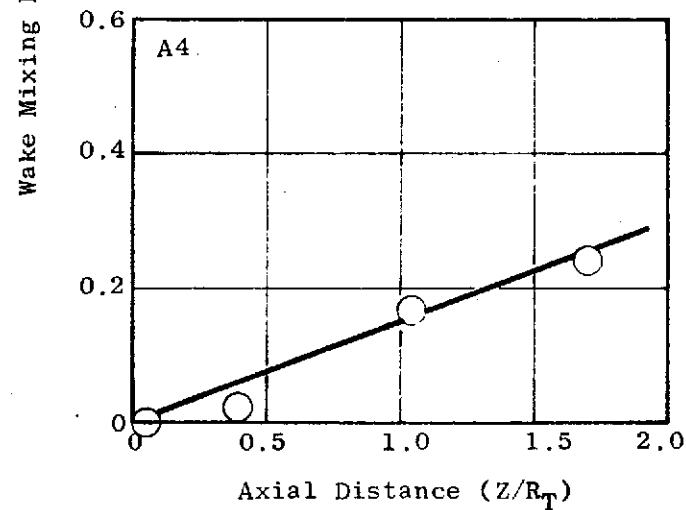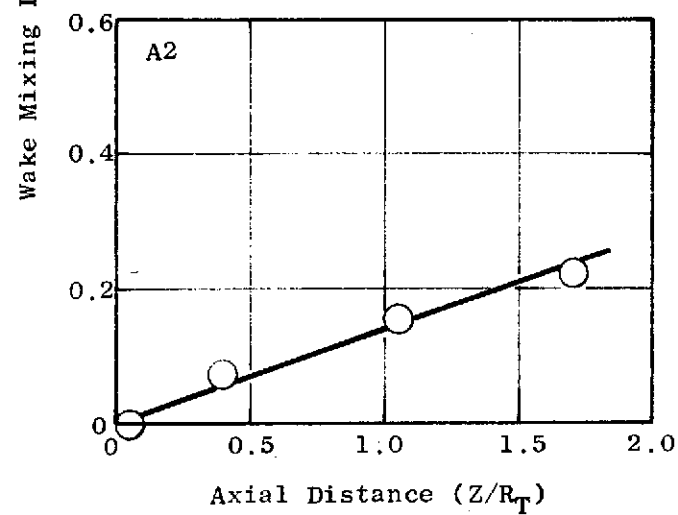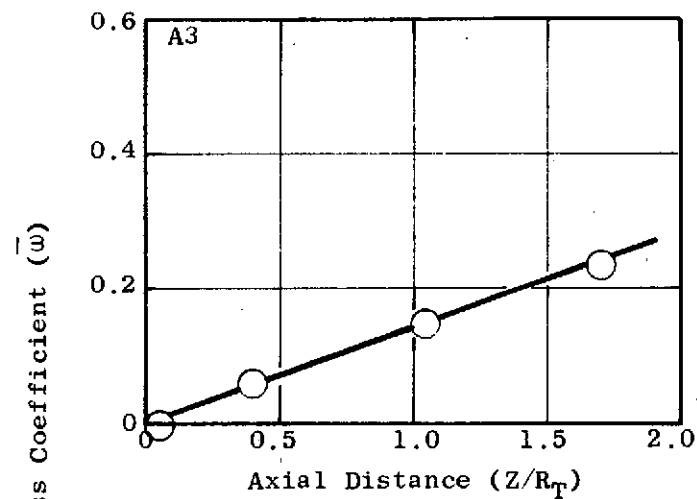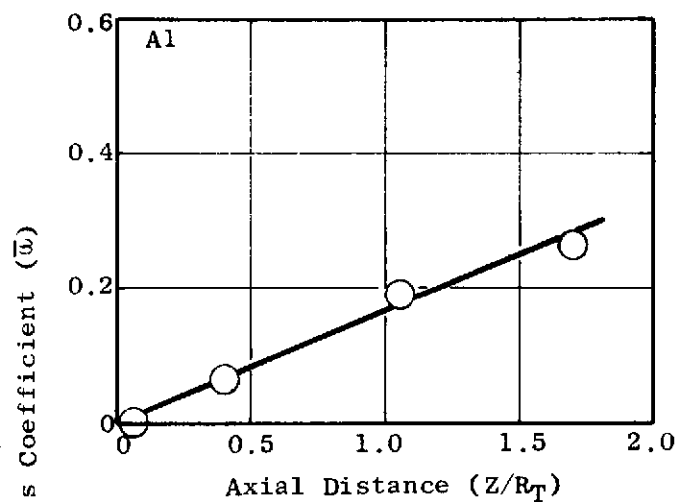
Figure 32 . Wake Mixing Loss Characteristics for Models A1 through A4, Axial Flow
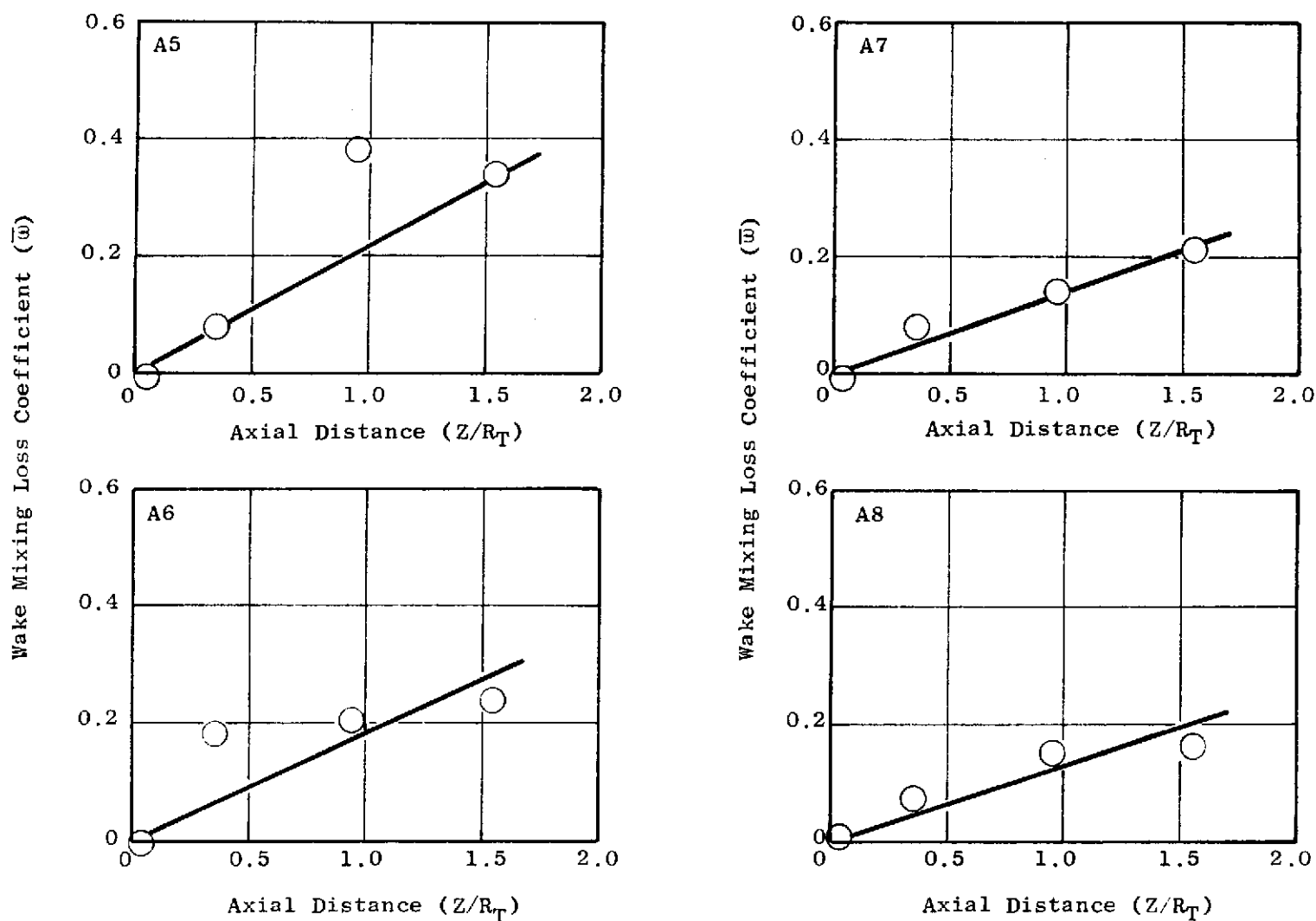
Figure 33.   Wake Mixing Loss Characteristics for Models 5 through 8, Axial Flow
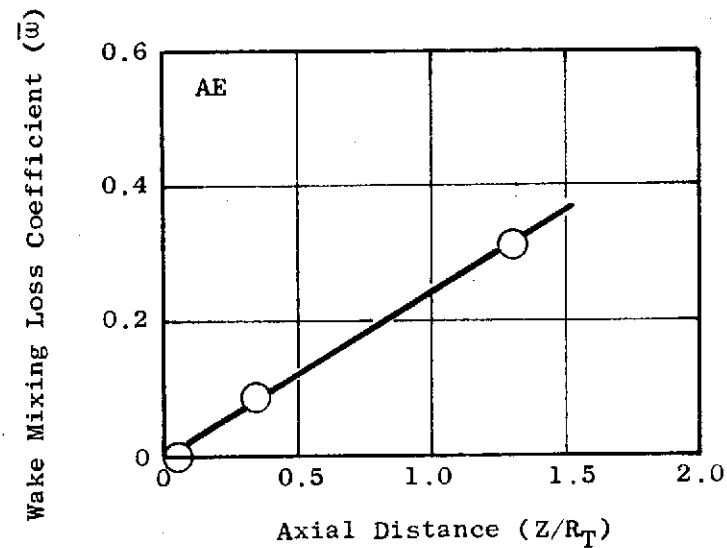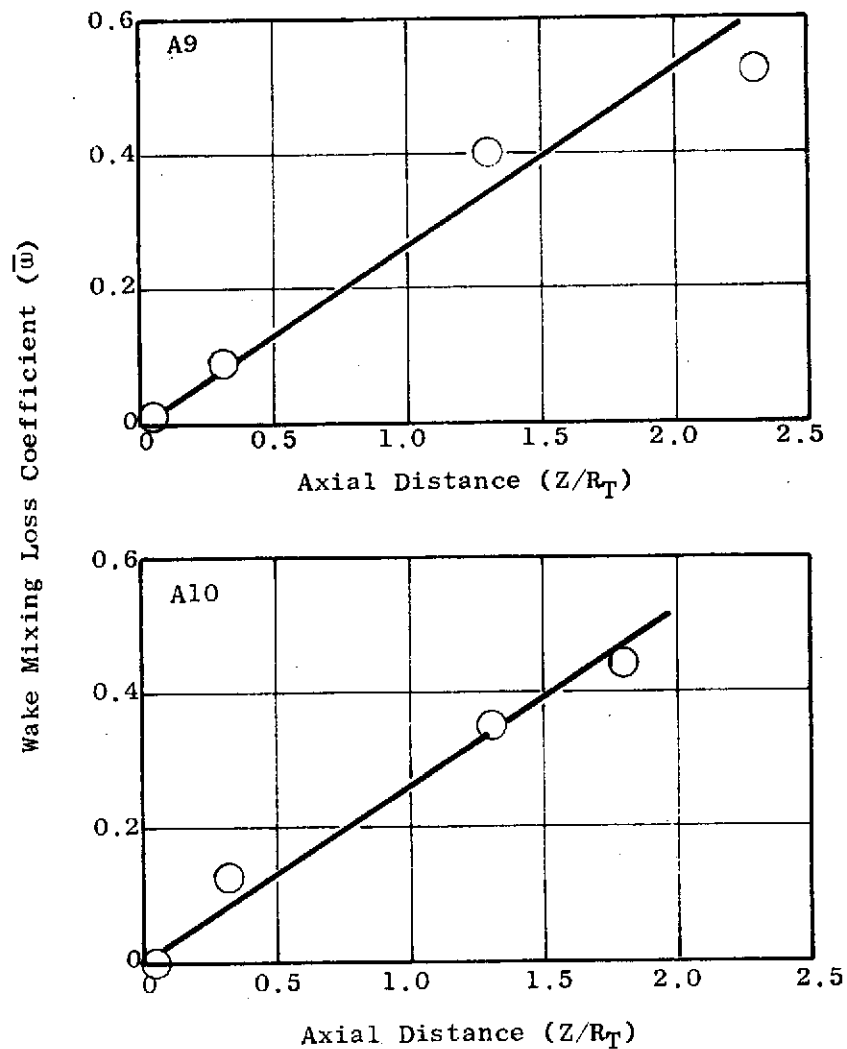
Figure 34. Wake Mixing Loss Characteristics for Models 9, 10, and AE, Axial Flow
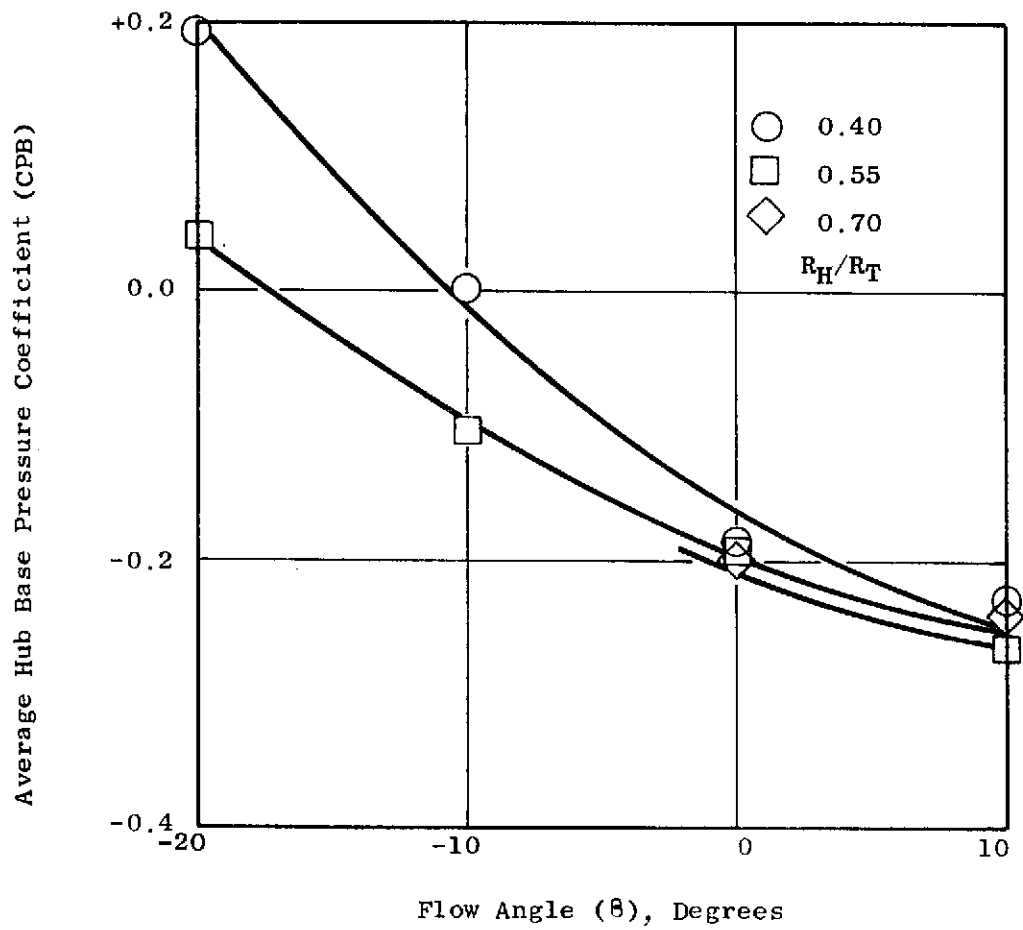
Figure 35.    Effects of Geometry on Average Hub Base
              Pressure, Axial Flow
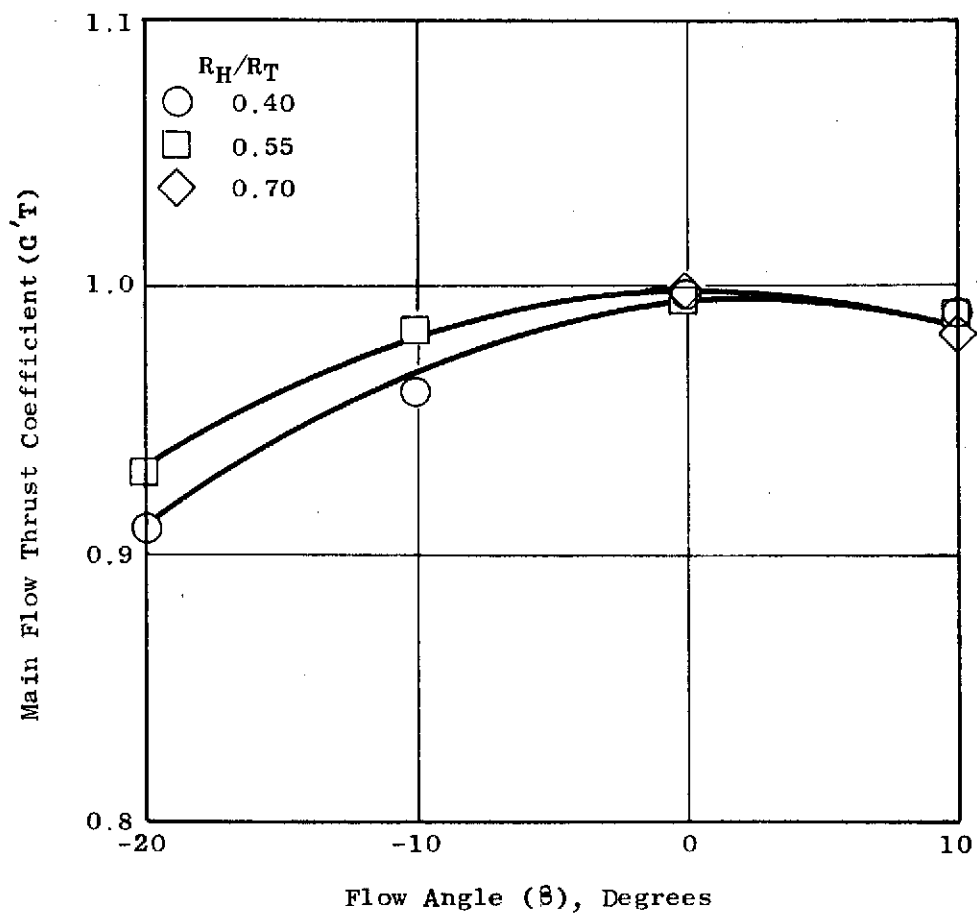
Figure 36. Effects of Geometry on Main Flow Thrust Coefficient, Axial Flow
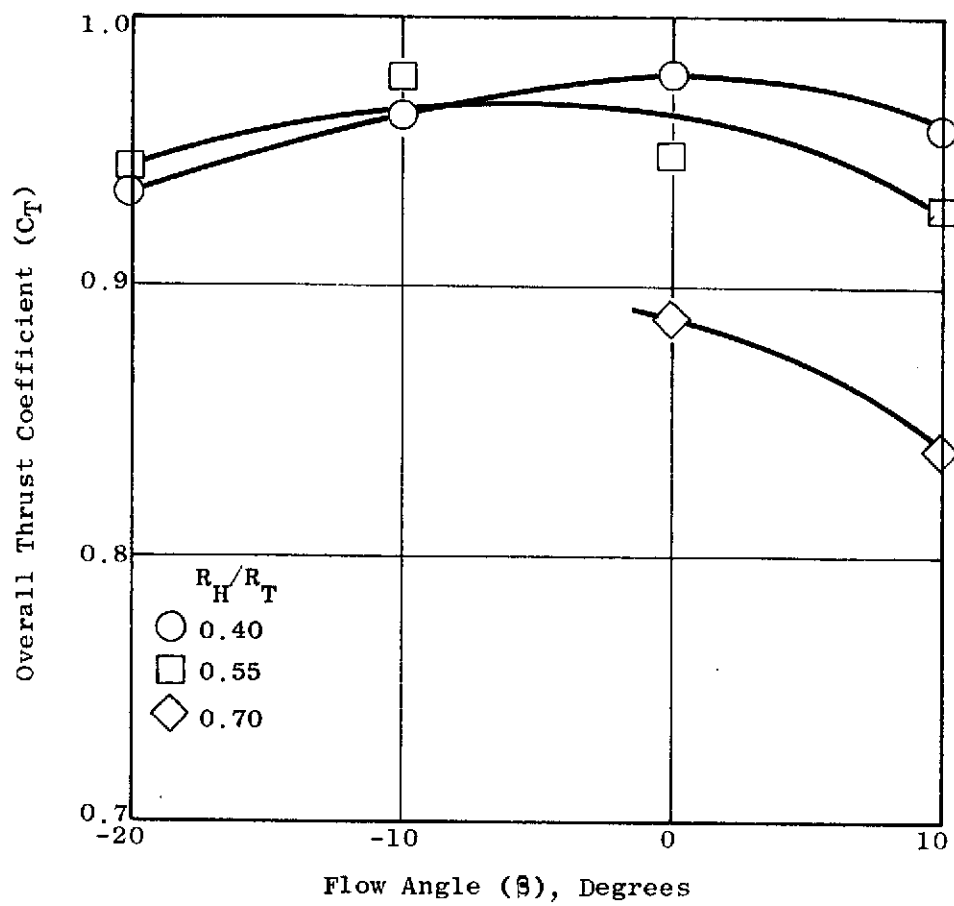
Figure 37.    Effects of Geometry on Overall Thrust, Axial Flow
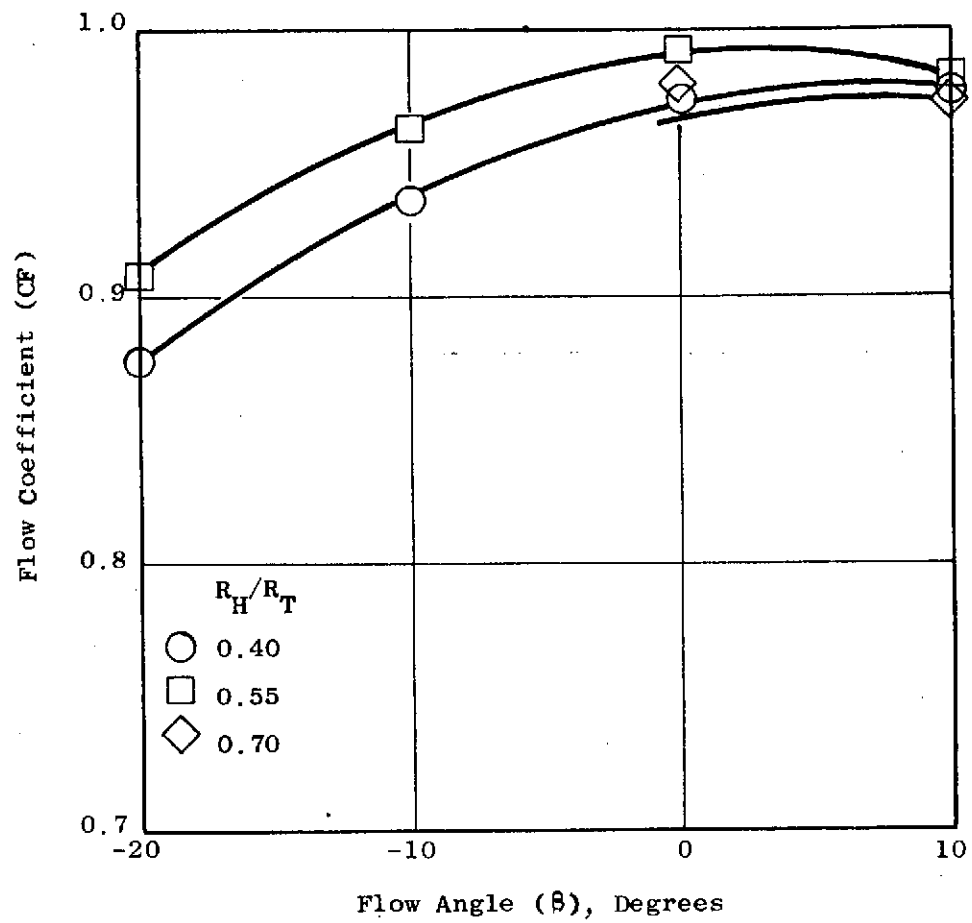
Figure 38.  Effects of Geometry on Flow Coefficient,
Axial Flow
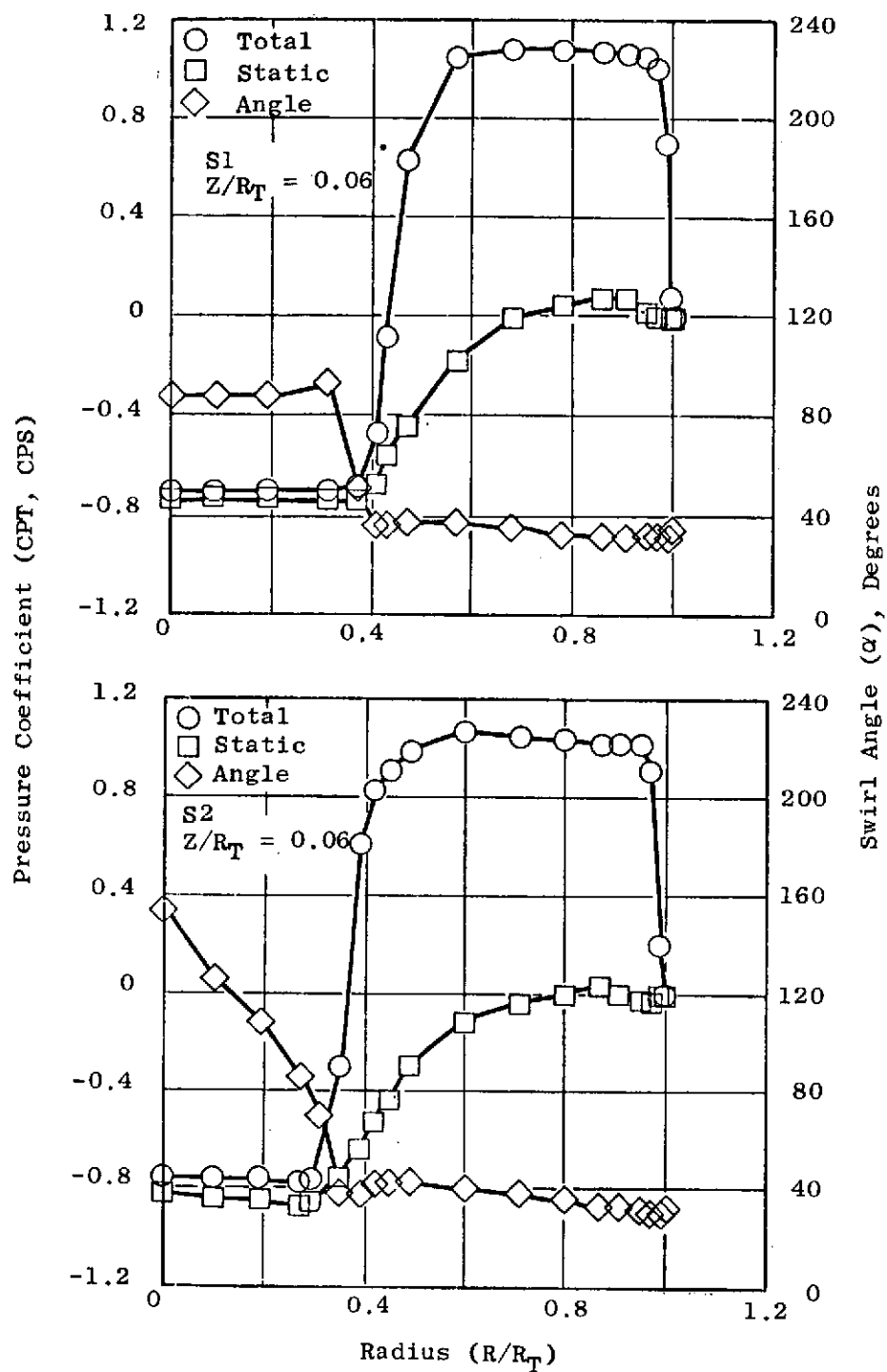
Figure 39.  Total and Static Pressure Coefficient
and Swirl Angle Distribution for Models
1 and 2, Swirling Flow, Close-Up Traverse
Position
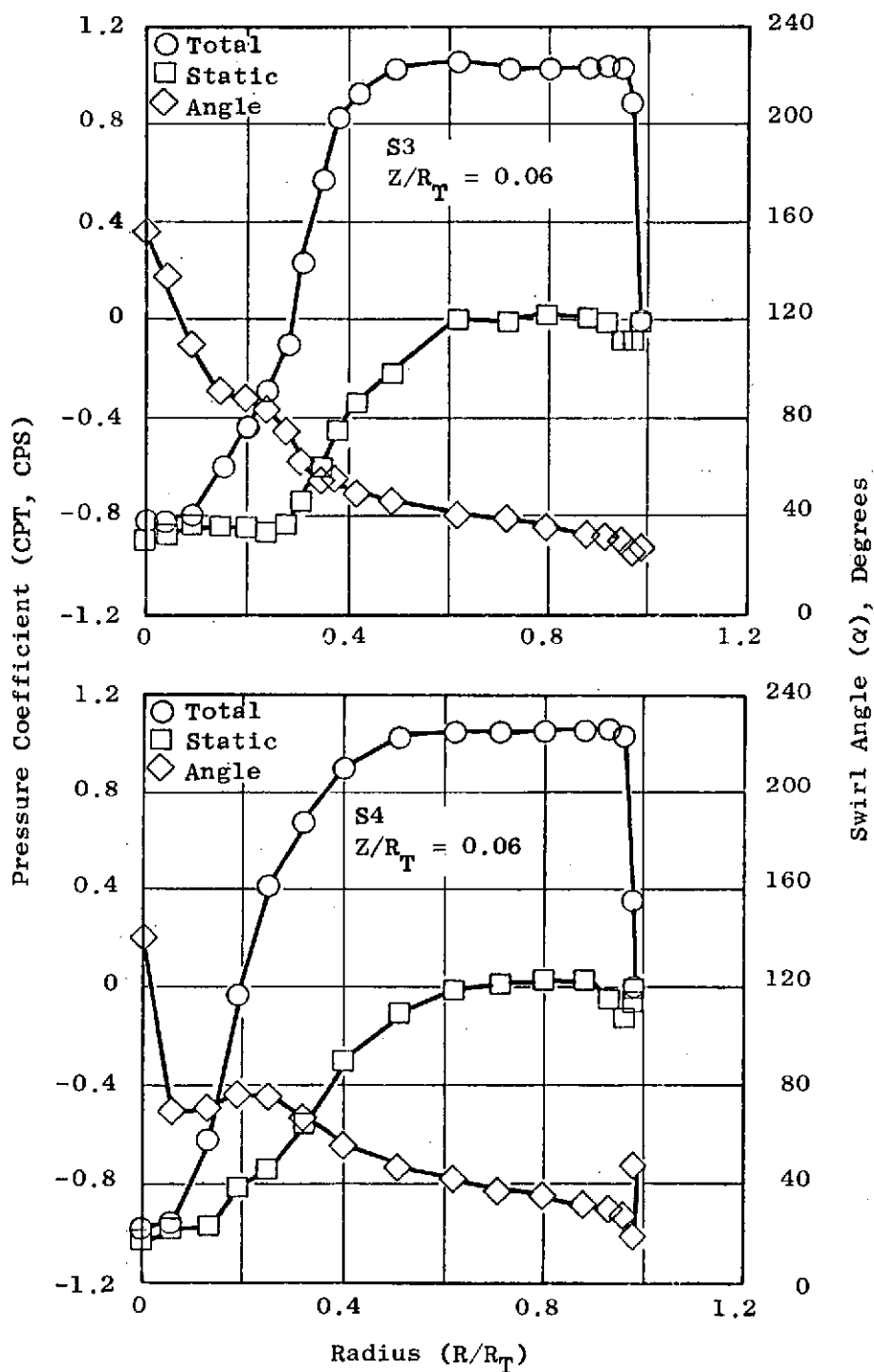
Figure 40.   Total and Static Pressure Coefficient
             and Swirl Angle Distribution for Models
             3 and 4, Swirling Flow, Close-Up Traverse
             Position
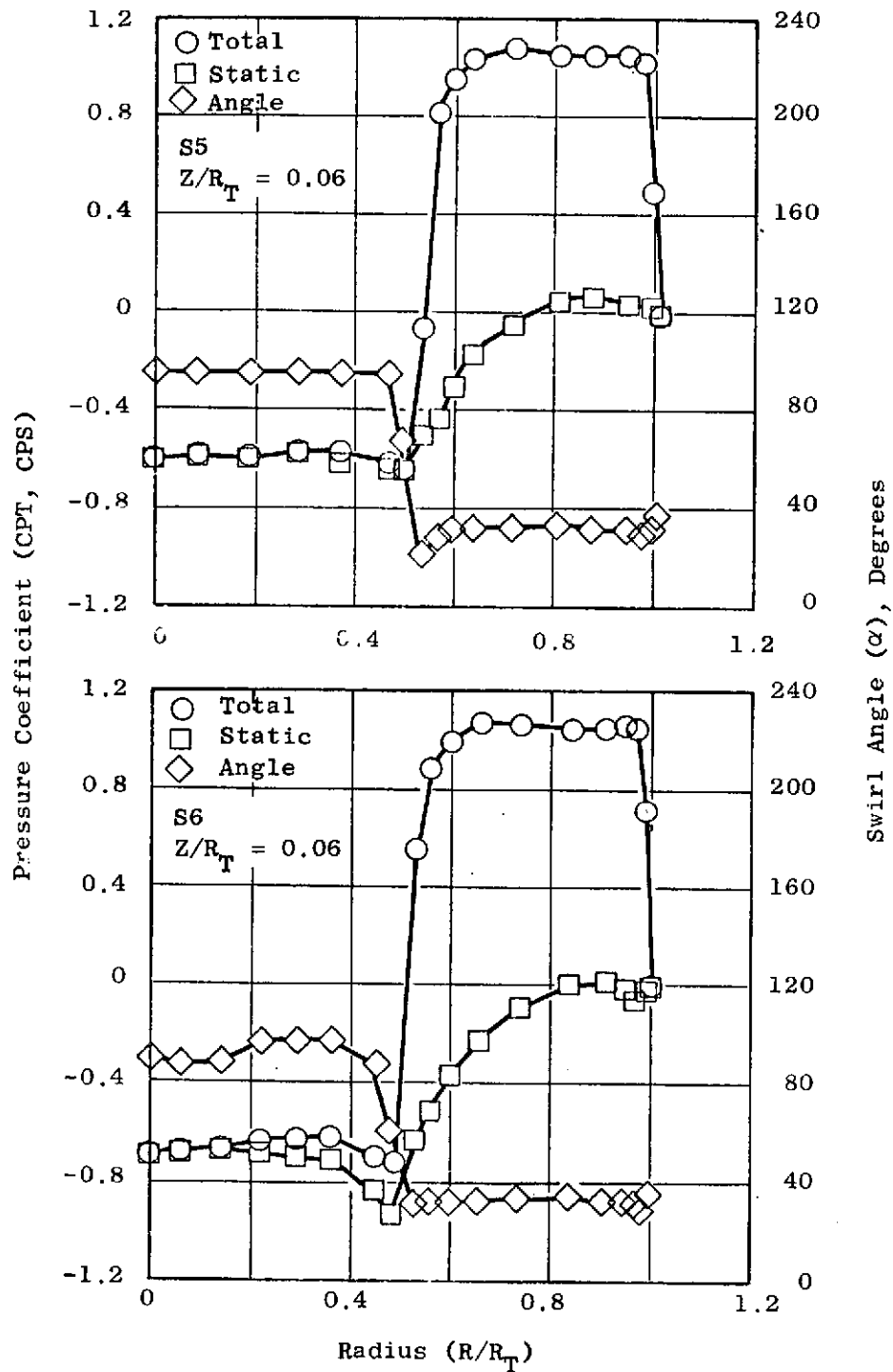
Figure 41. Total and Static Pressure Coefficient
and Swirl Angle Distribution for Models
5 and 6, Swirling Flow, Close-Up Traverse
Position
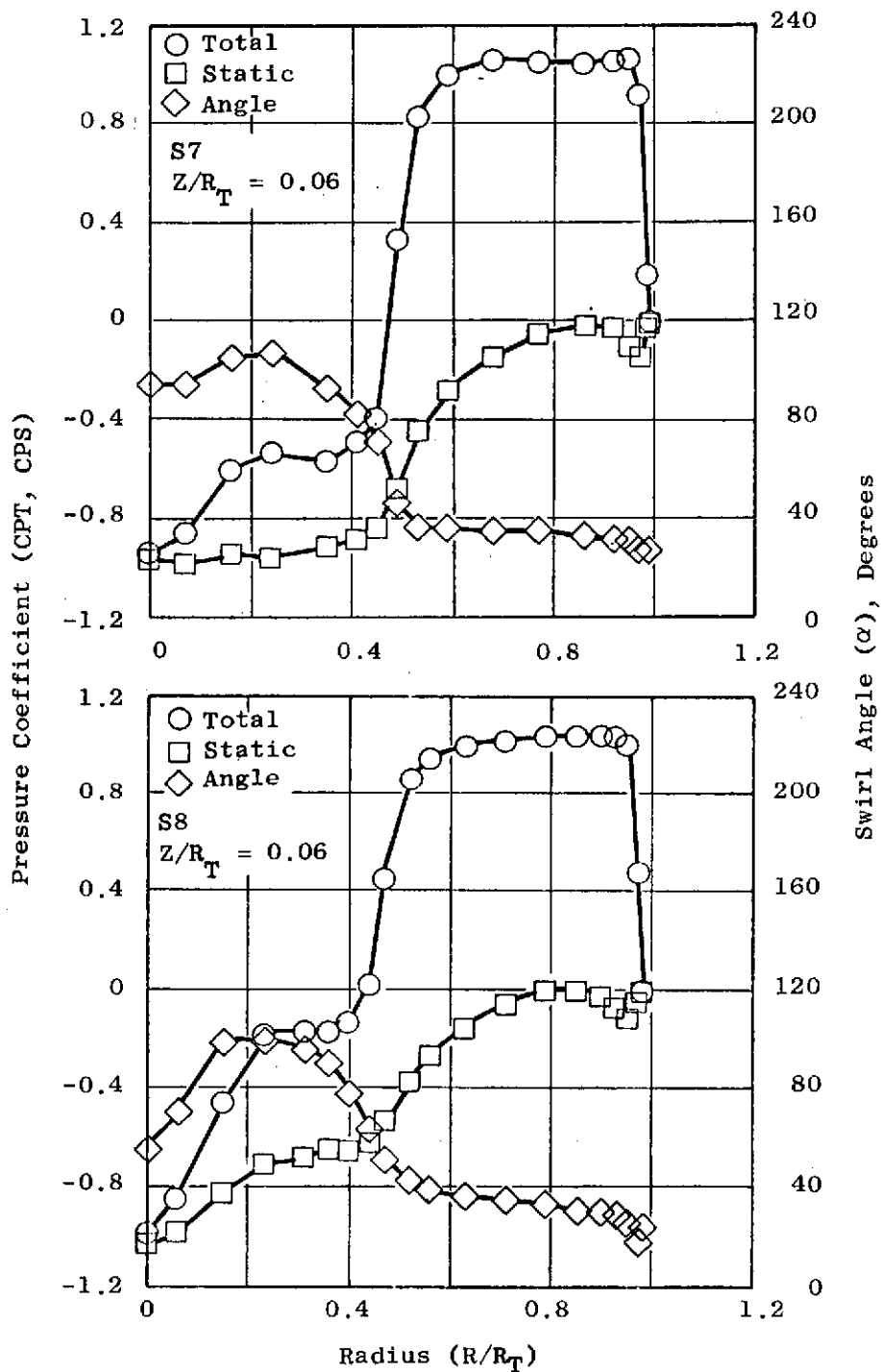
Figure 42. Total and Static Pressure Coefficient
and Swirl Angle Distribution for Models
7 and 8, Swirling Flow, Close-Up Traverse
Position
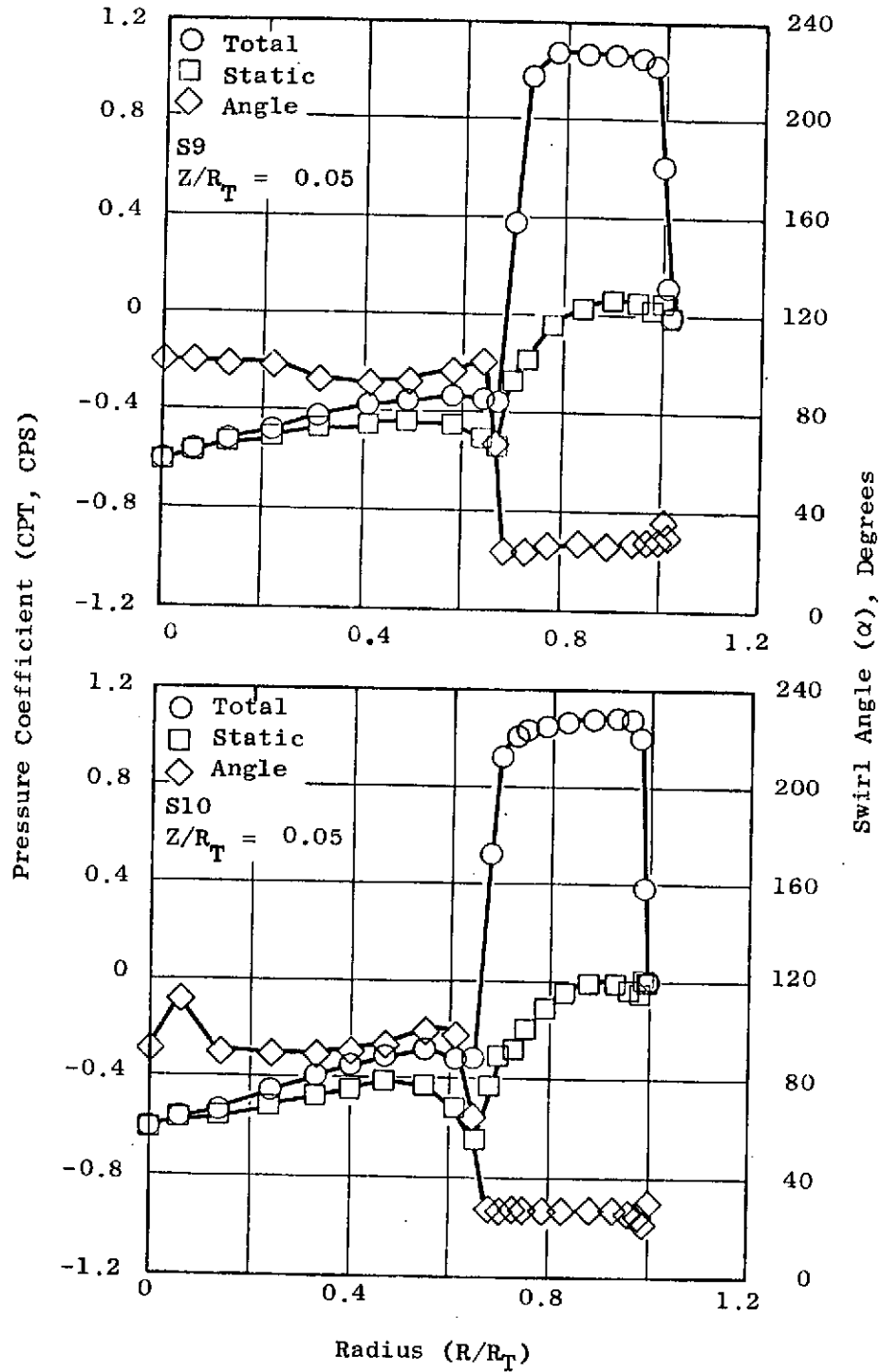
Figure 43. Total and Static Pressure Coefficient and Swirl Angle Distribution for Models 9 and 10, Swirling Flow, Close-Up Traverse Position
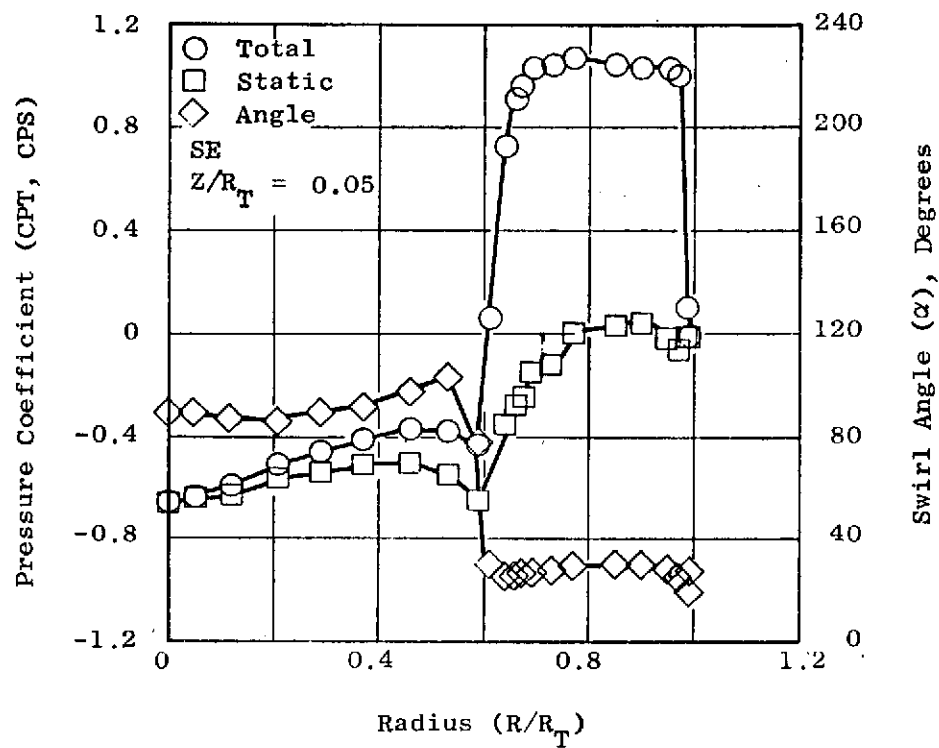
Figure 44  Total and Static Pressure Coefficient
and Swirl Angle Distribution for Models
E, Swirling Flow, Close-Up Traverse
Position
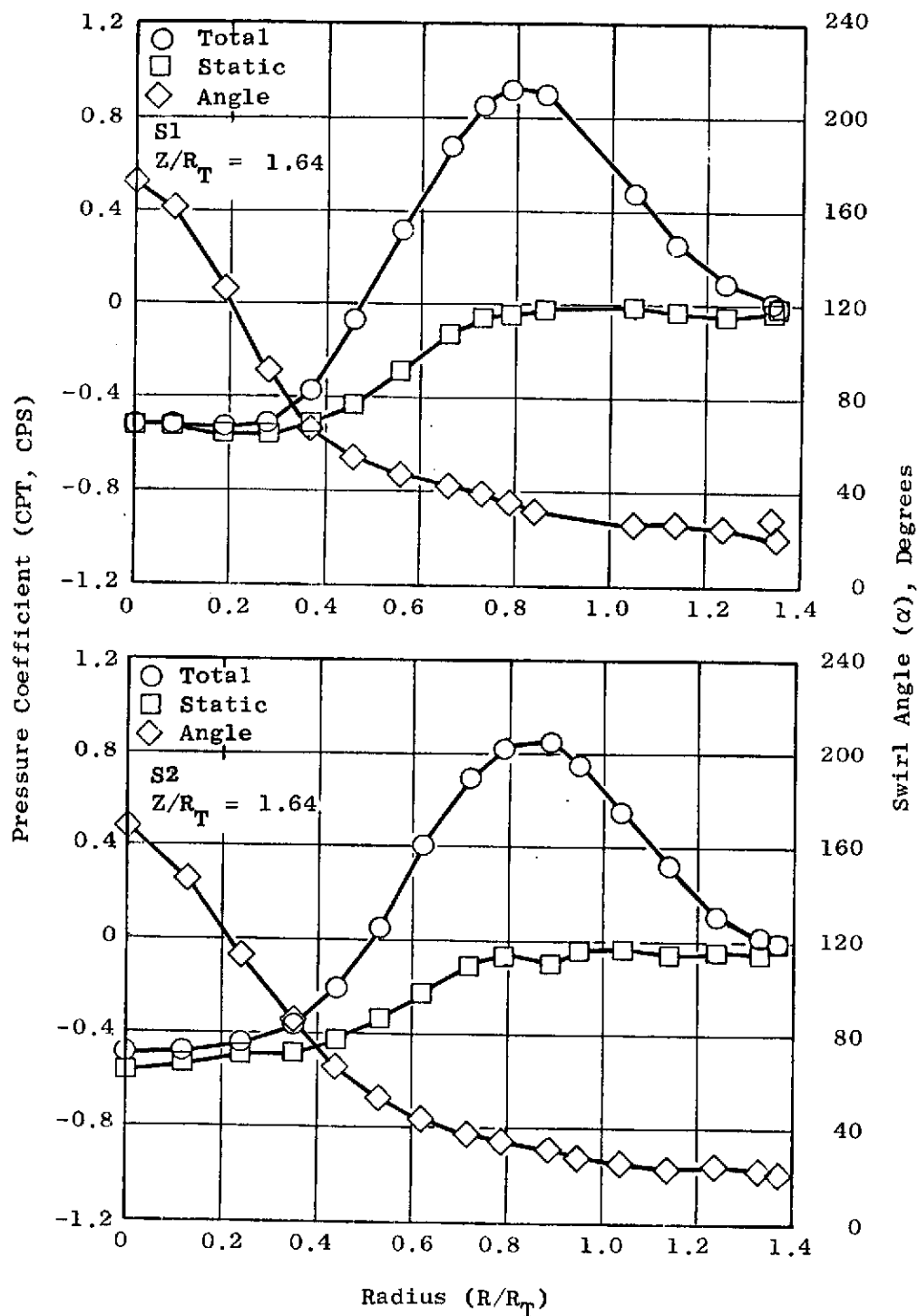
Figure 45. Total and Static Pressure Coefficient and Swirl Angle Distribution for Models 1 and 2, Swirling Flow, Downstream Traverse Location
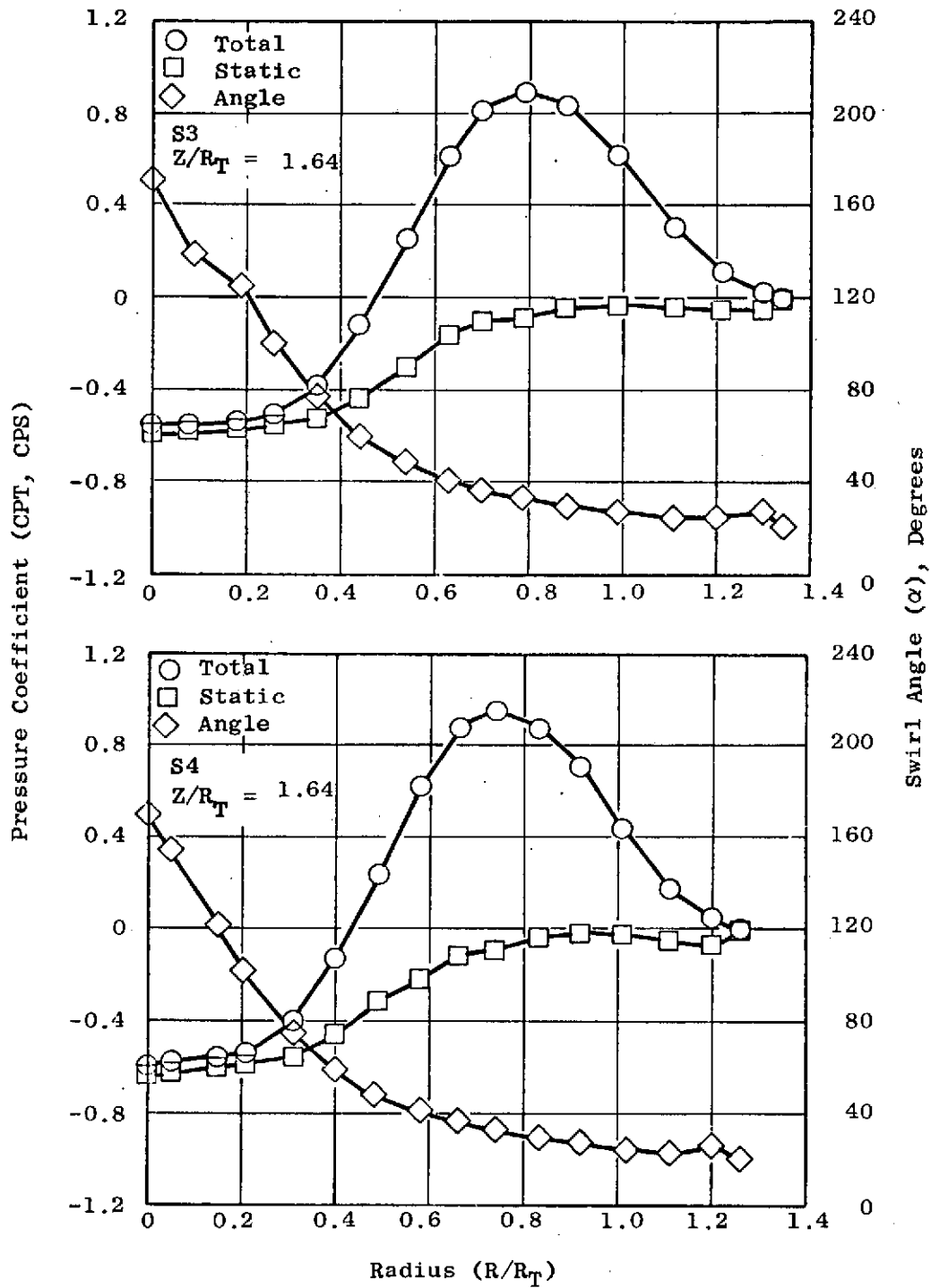
Figure 46. Total and Static Pressure Coefficient and
Swirl Angle Distribution for Models 3 and 4,
Swirling Flow, Downstream Traverse Location
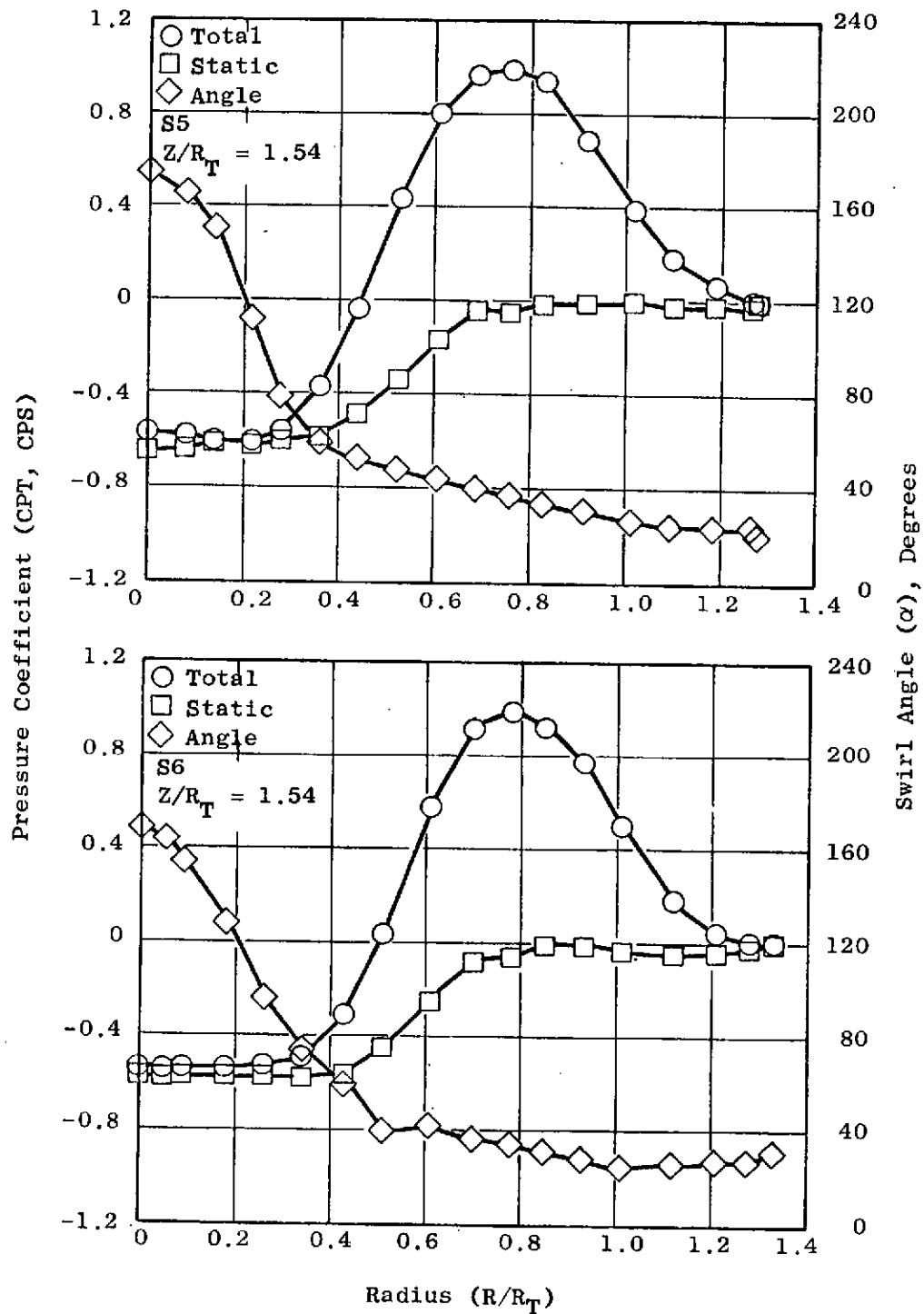
Figure 47.  Total and Static Pressure Coefficient and
Swirl Angle Distribution for Models 5 and 6,
Swirling Flow, Downstream Traverse Location
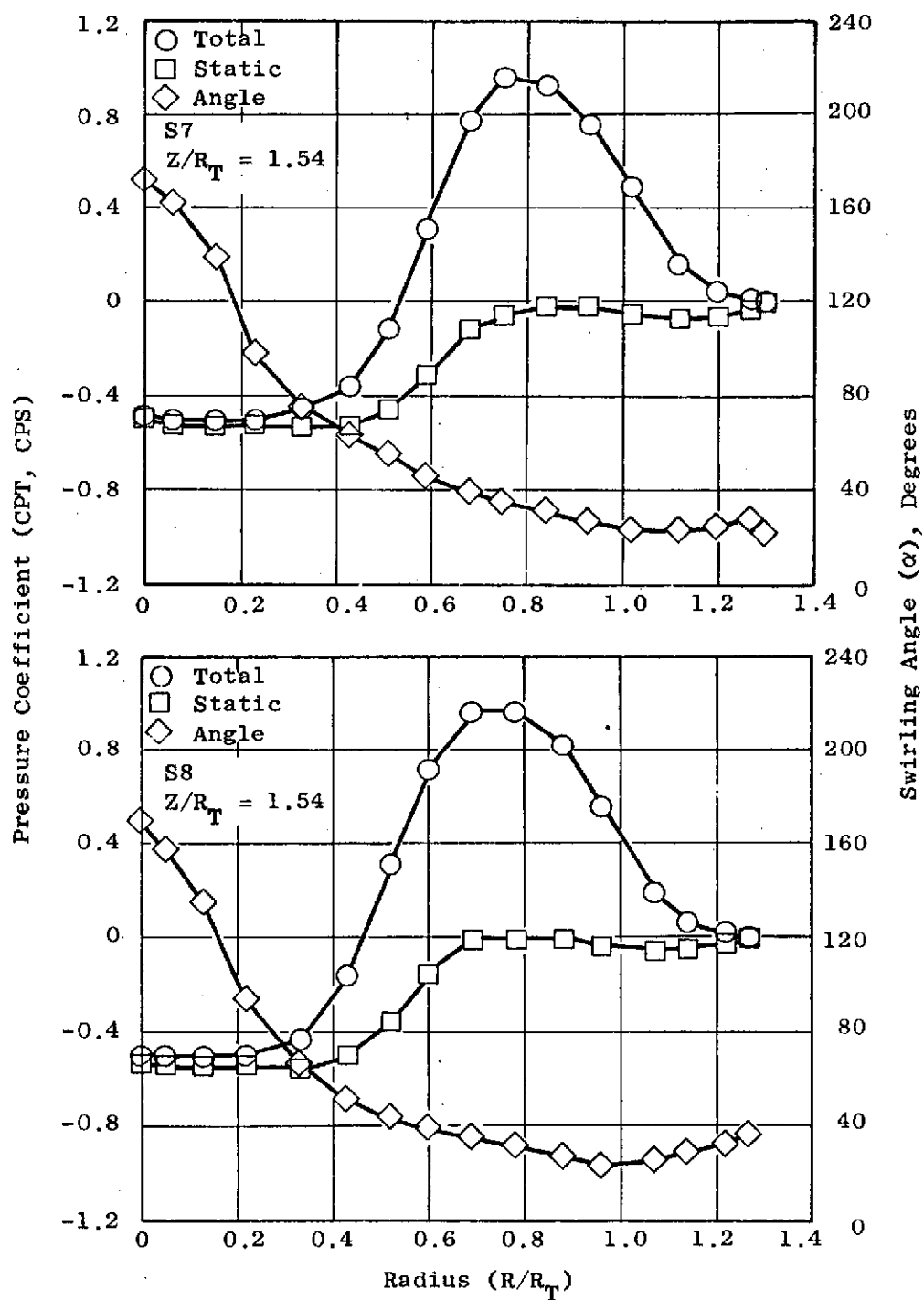
Figure 48. Total and Static Pressure Coefficient and
Swirl Angle Distribution for Models 7 and 8,
Swirling Flow, Downstream Traverse Location
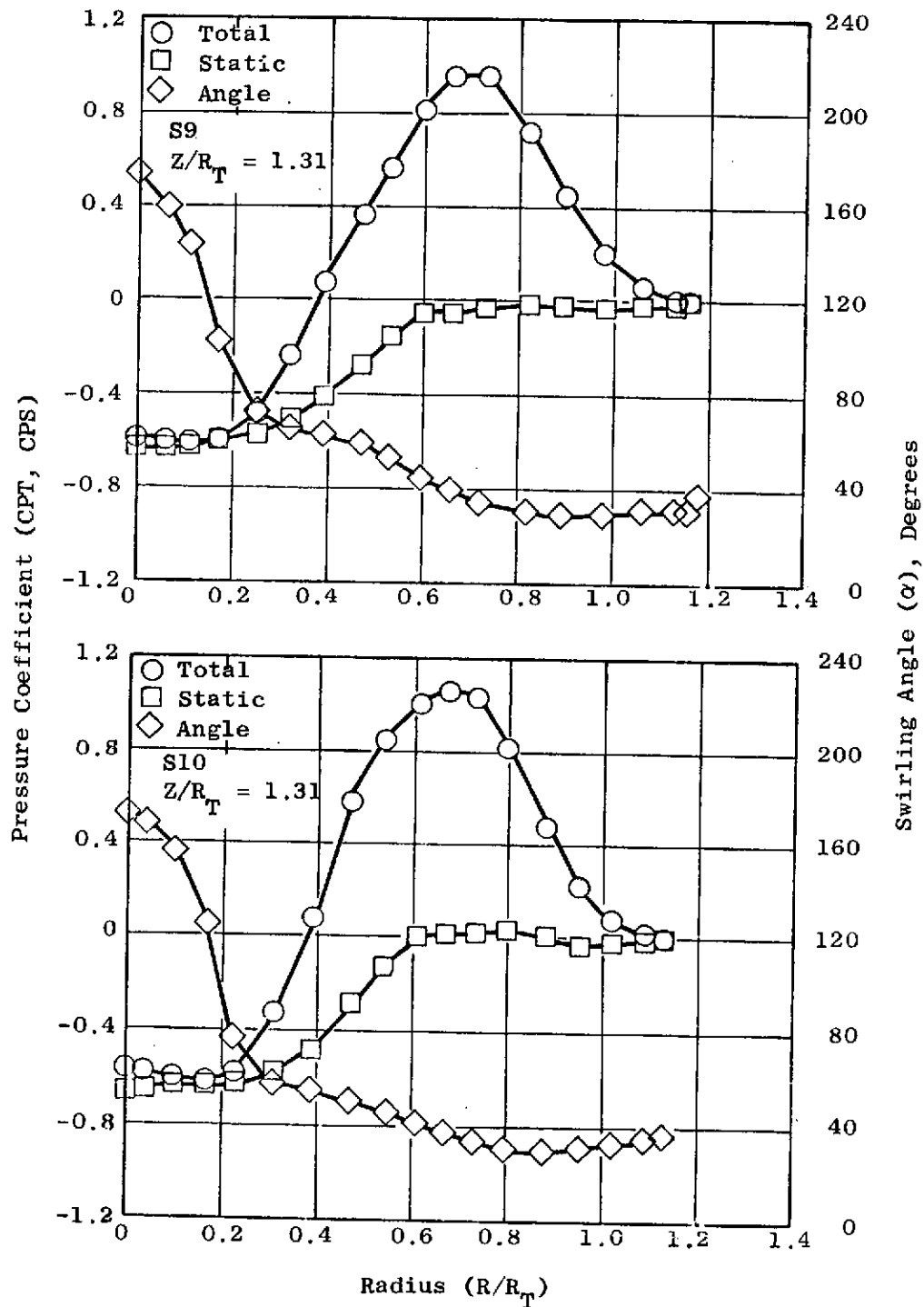
Figure 49. Total and Static Pressure Coefficient and Swirl Angle Distribution for Models 9 and 10, Swirling Flow, Downstream Traverse Location
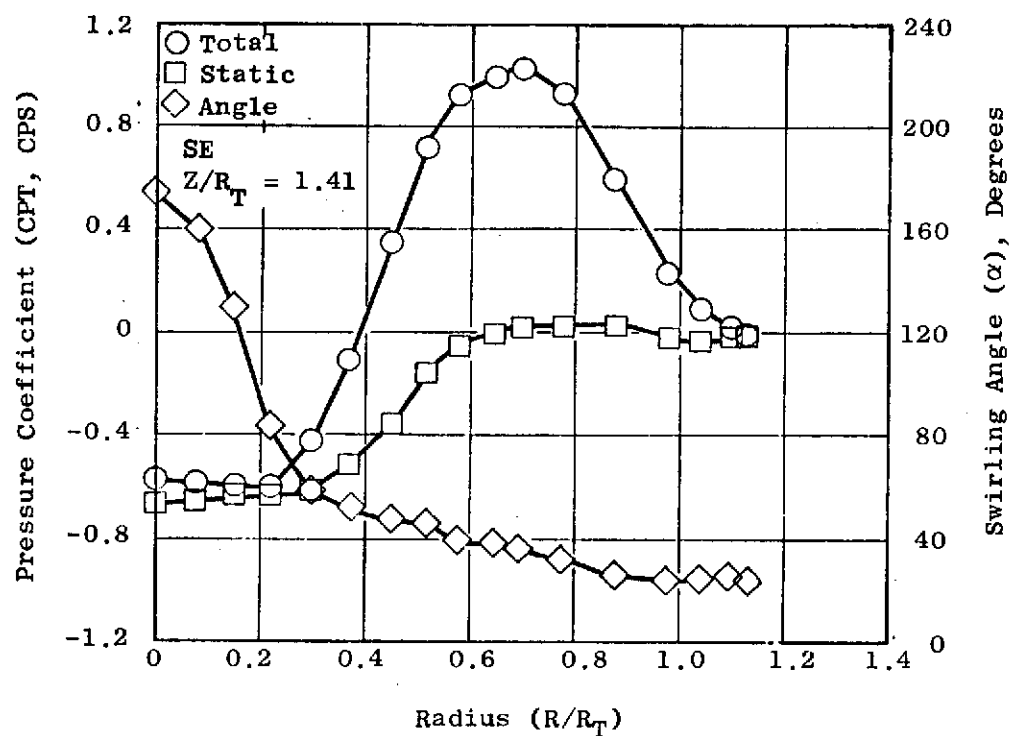
Figure 50. Total and Static Pressure Coefficient and Swirl Angle Distribution for Model E, Swirling Flow, Downstream Traverse Location
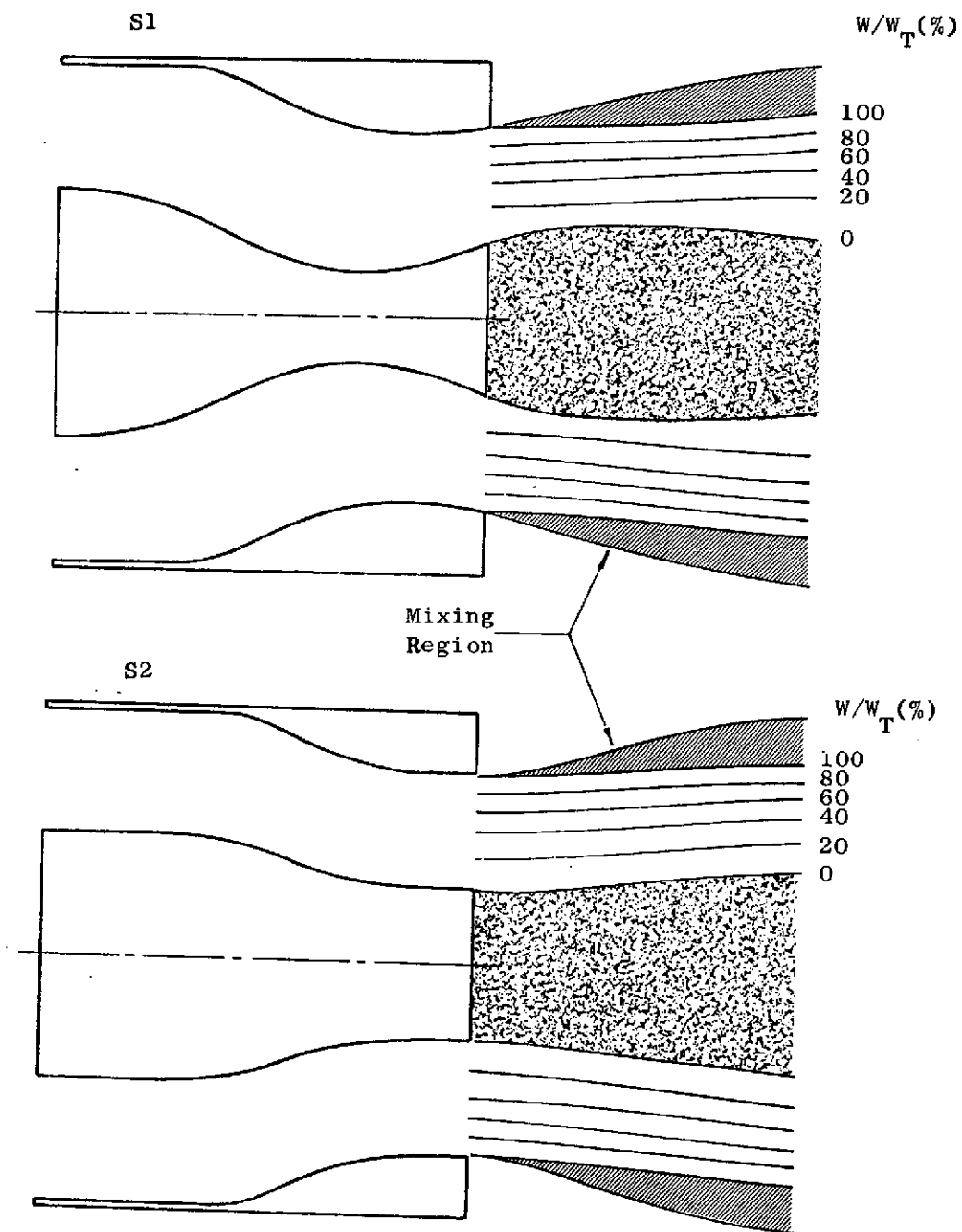
Figure 5 1.  Graphical Representation of the Flow Field for Models
1 and 2, Swirling Flow
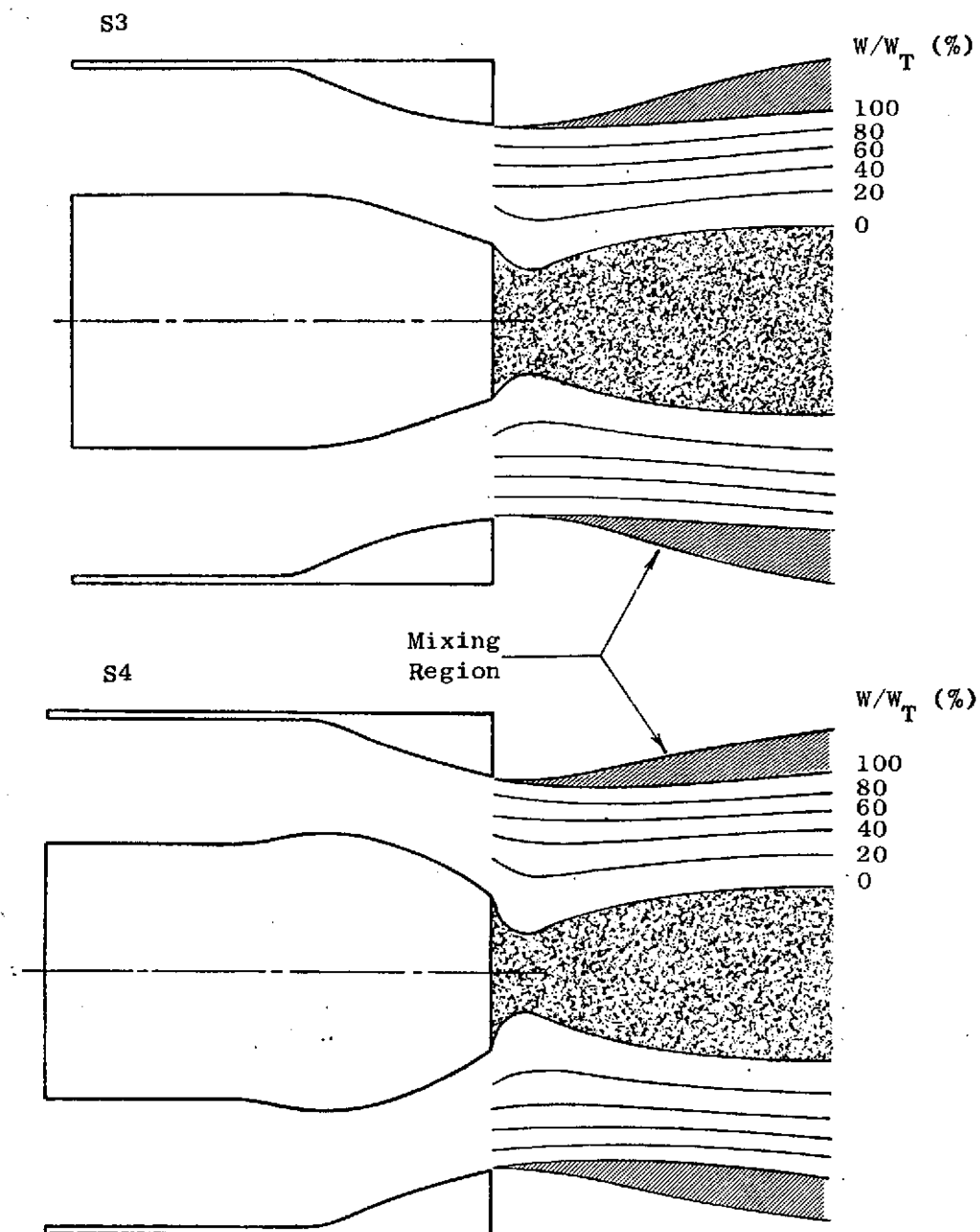
Figure 52. Graphical Representation of the Flow Field for Models
3 and 4, Swirling Flow

S5

W/W$_T$ (%)

100
80
60
40
20
0

Mixing
Region

S6

W/W$_T$(%)

100
80
60
40
20
0
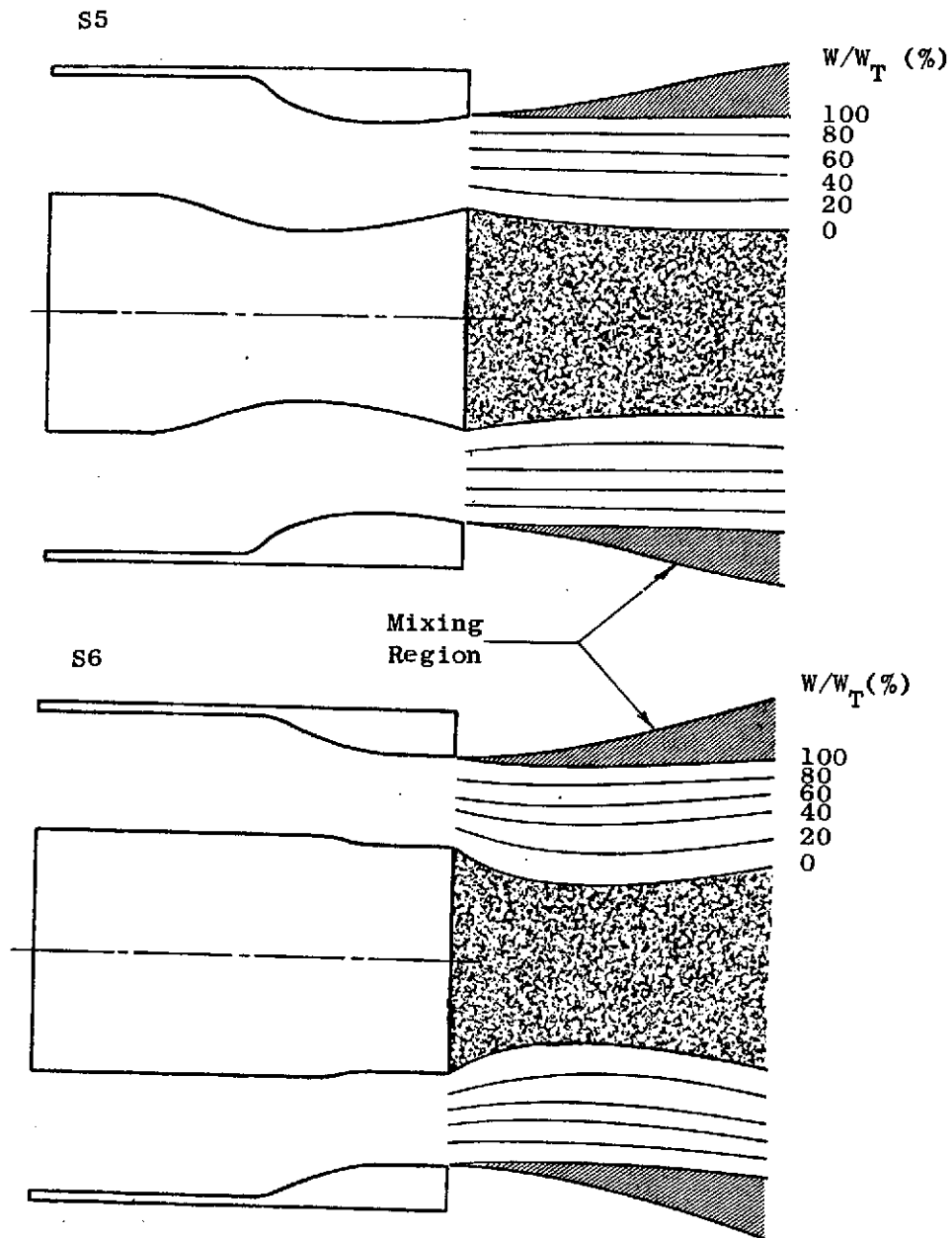
Figure 53. Graphical Representation of the Flow Field for
Models 5 and 6, Swirling Flow
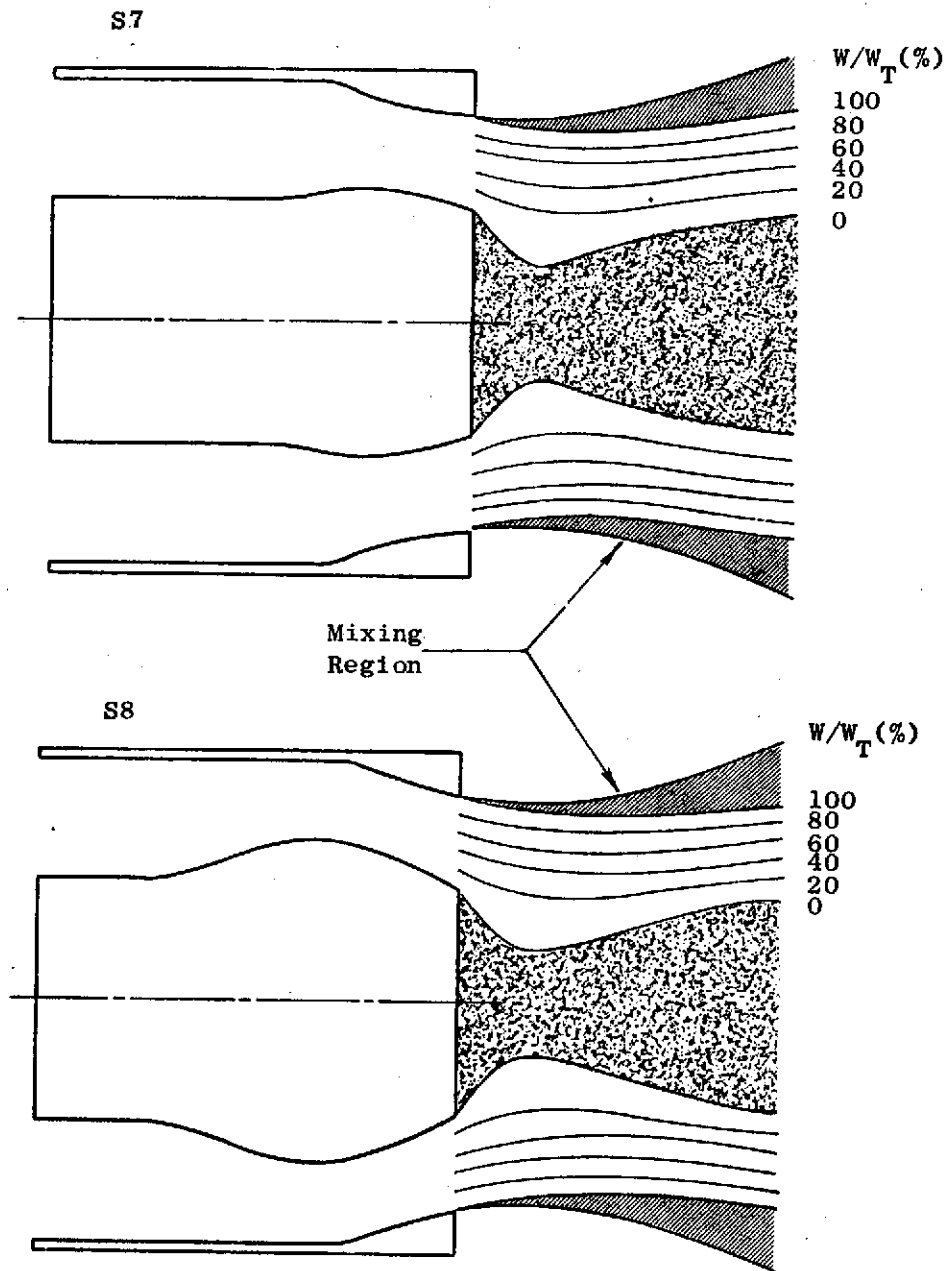
Figure 54. Graphical Representation of the Flow Field for
Models 7 and 8, Swirling Flow
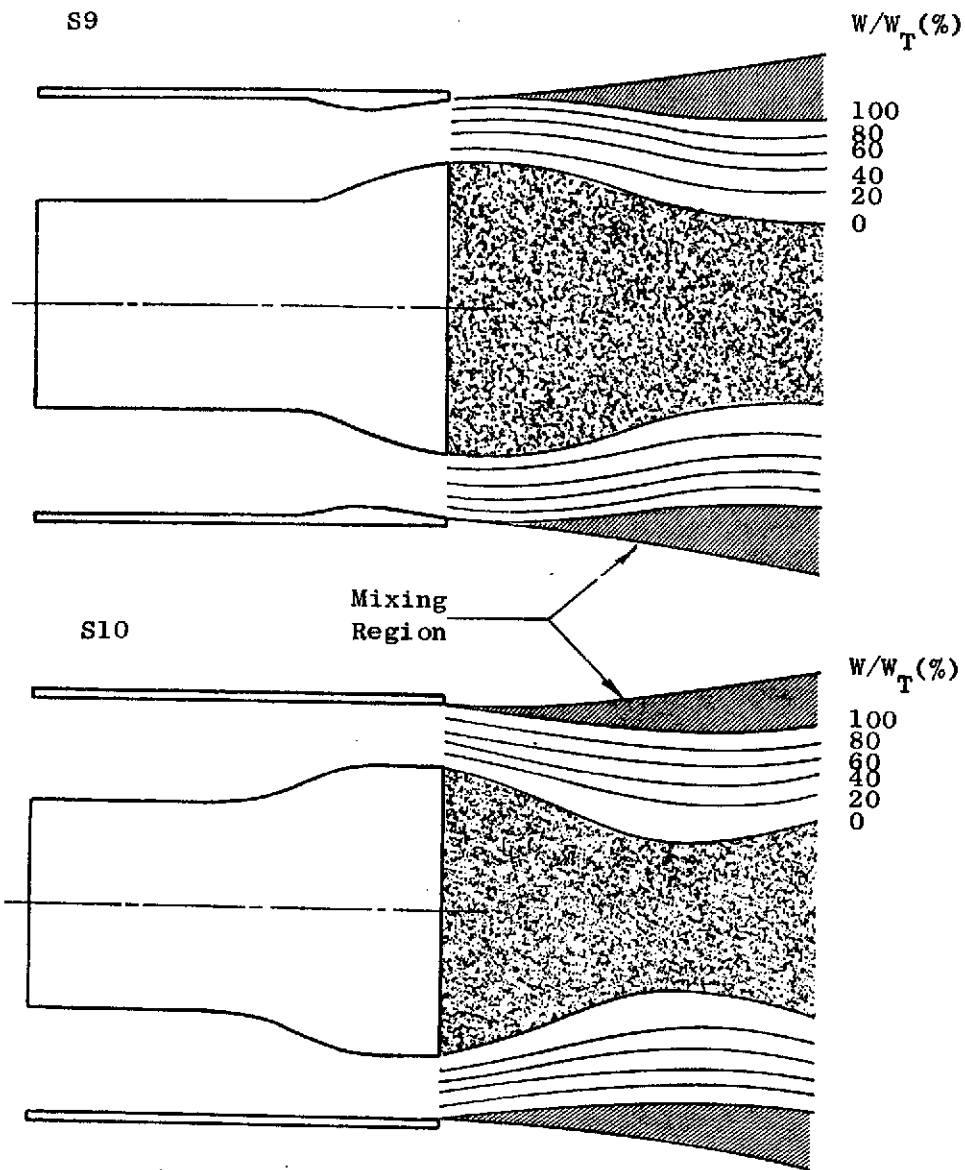
Figure 55.  Graphical Representation of the Flow Field for
Models 9 and 10, Swirling Flow

SE

W/W$_T$(%)

100
80
60
40
20
0
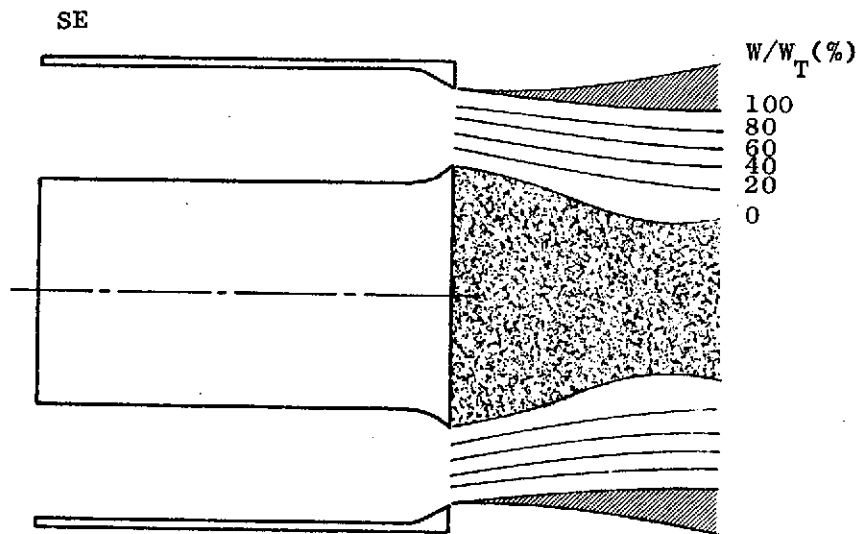
Figure 56.  Graphical Representation of the Flow Field
for Model E, Swirling Flow
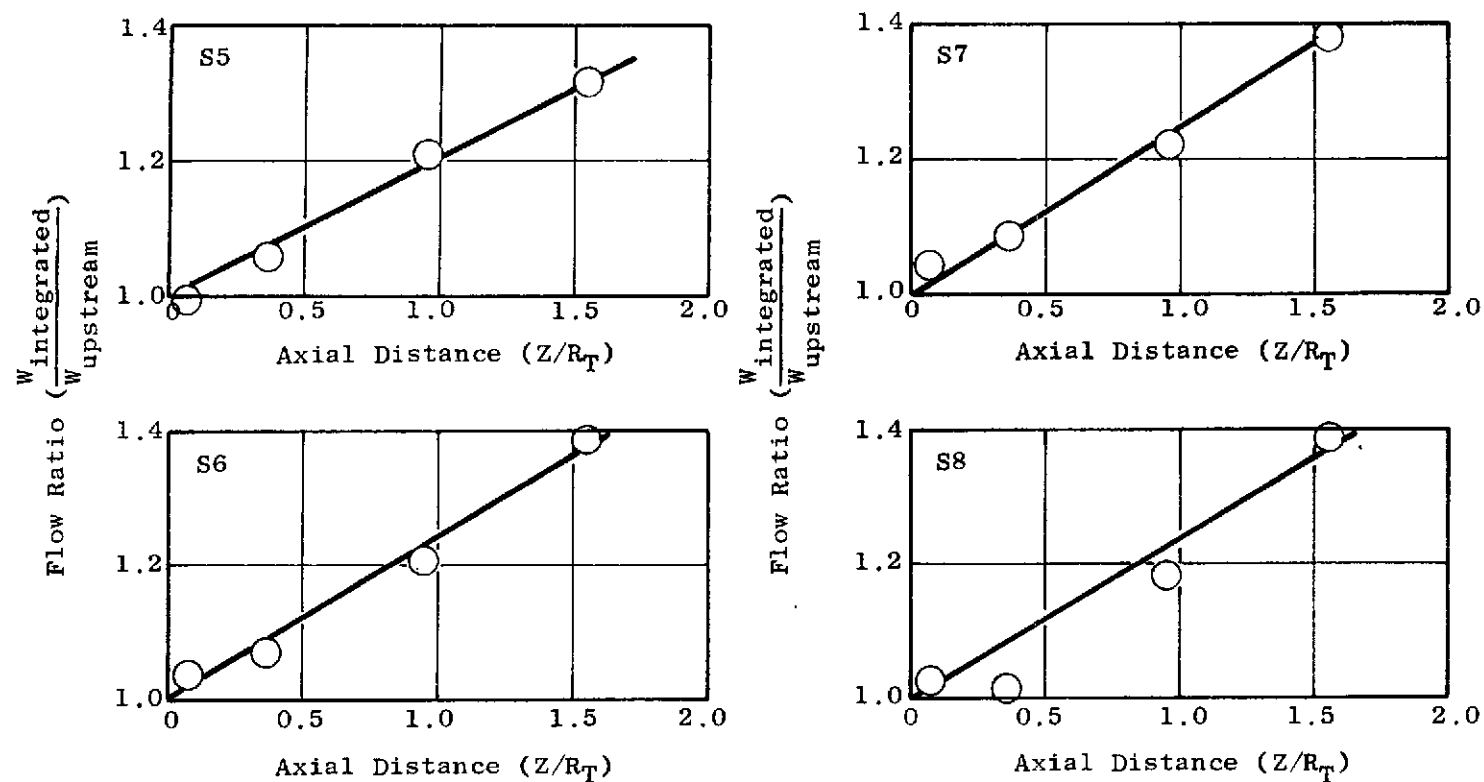
Figure 57. Flow Entrainment Characteristics for Models 5 through 8, Swirling Flow
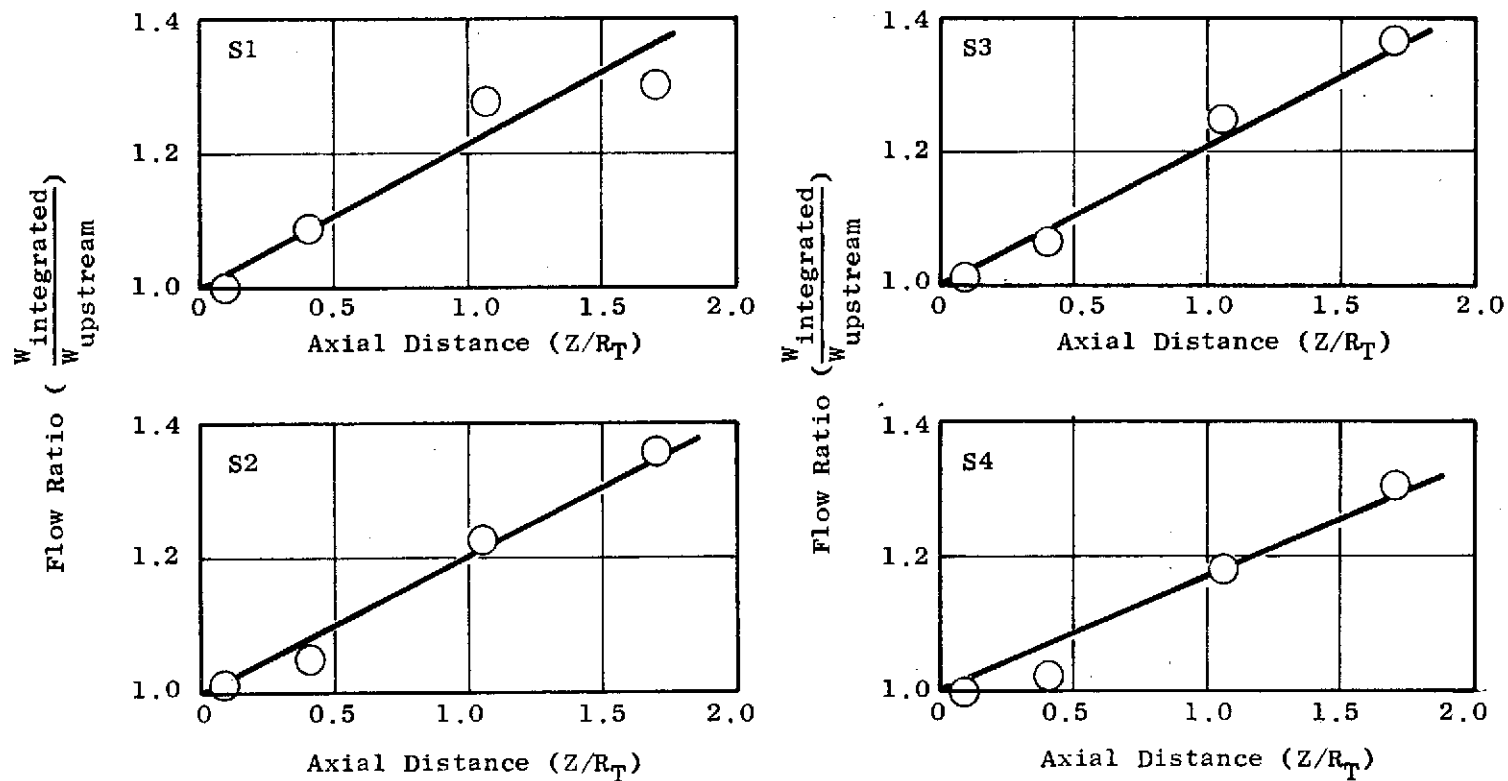
Figure 58.  Flow Entrainment Characteristics for Models 1 through 4, Swirling Flow
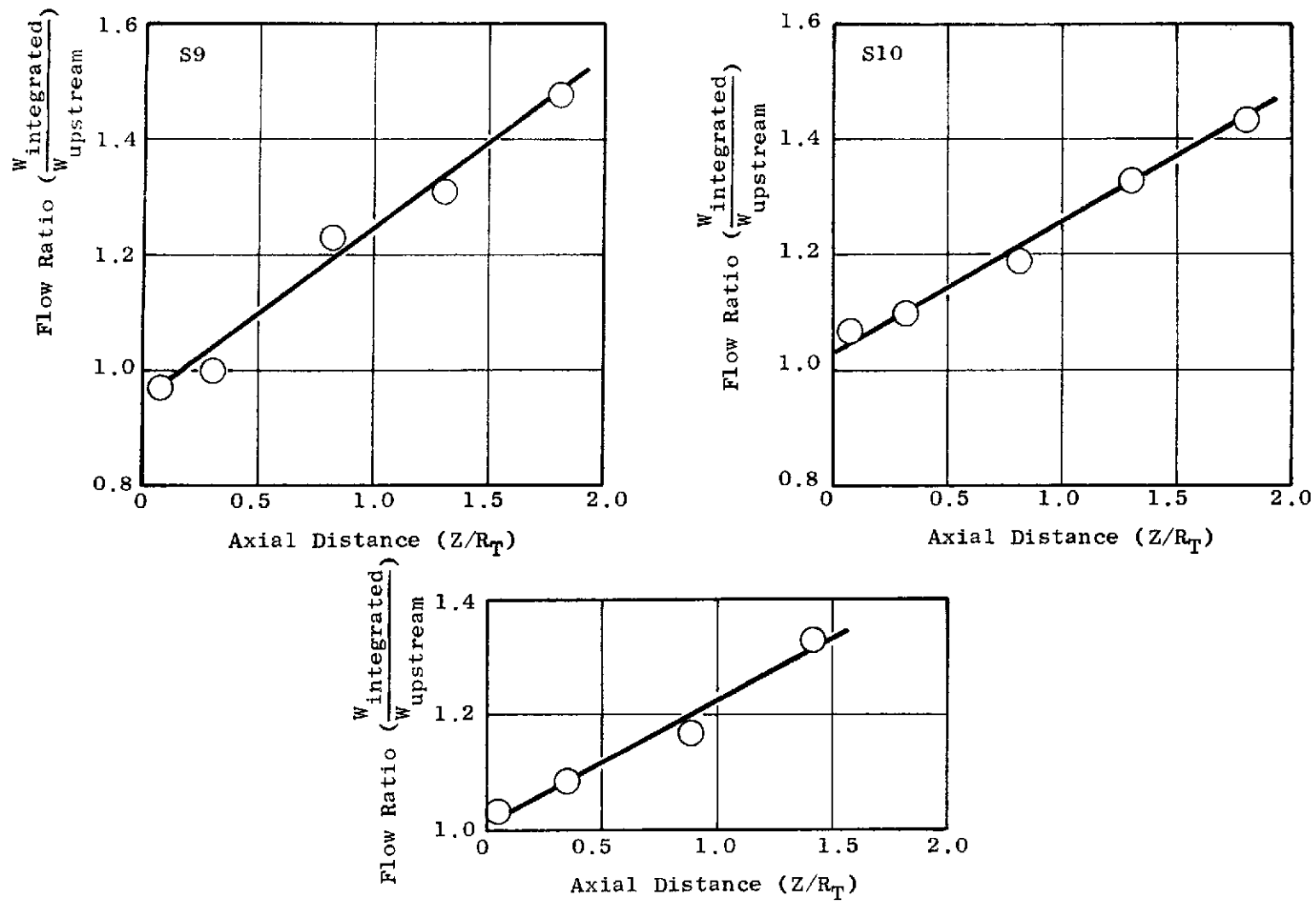
Figure 59. Flow Entrainment Characteristics for Models 9, 10, and E, Swirling Flow
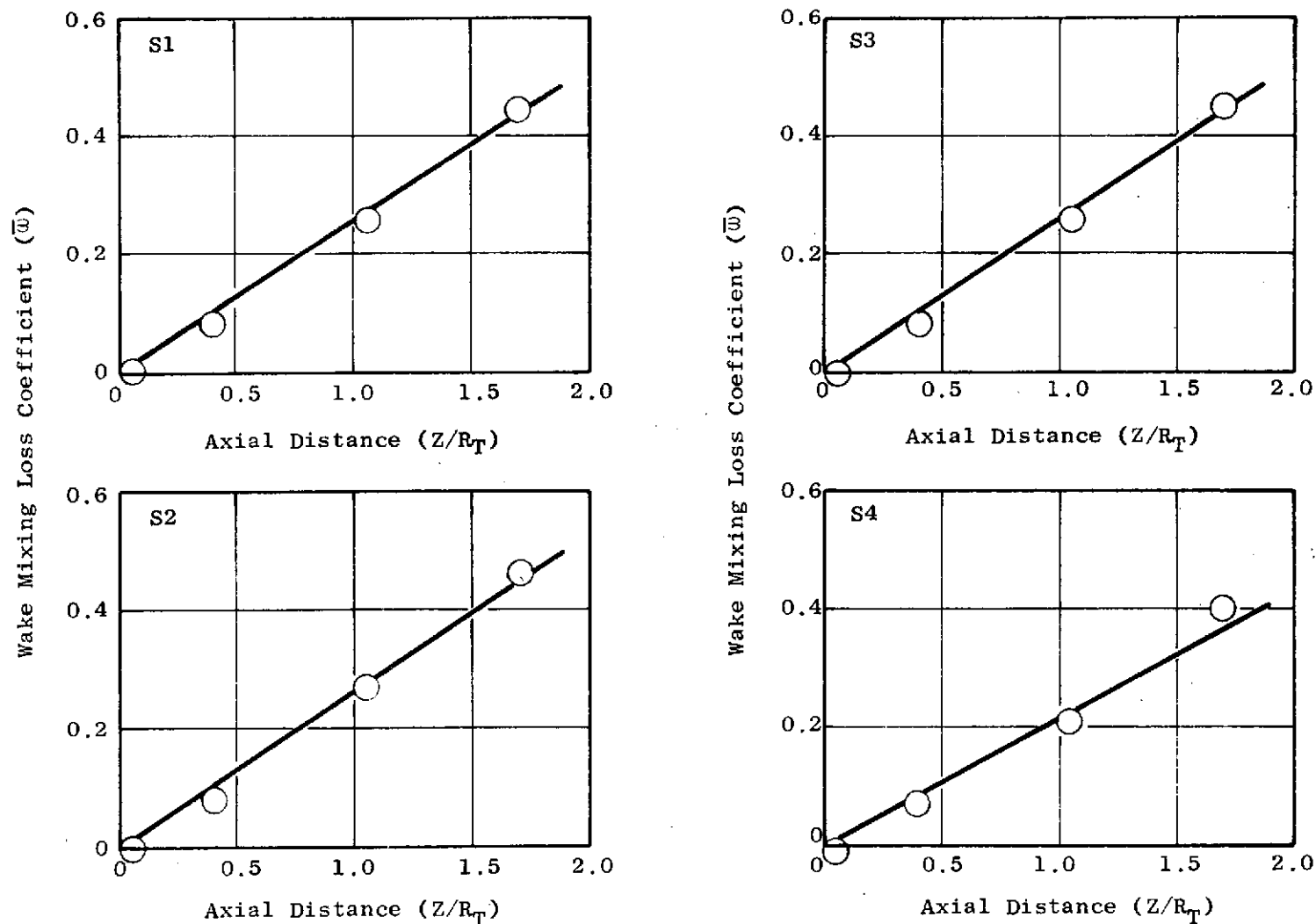
Figure 60. Wake Mixing Loss Characteristics for Models 1 through 4, Swirling Flow
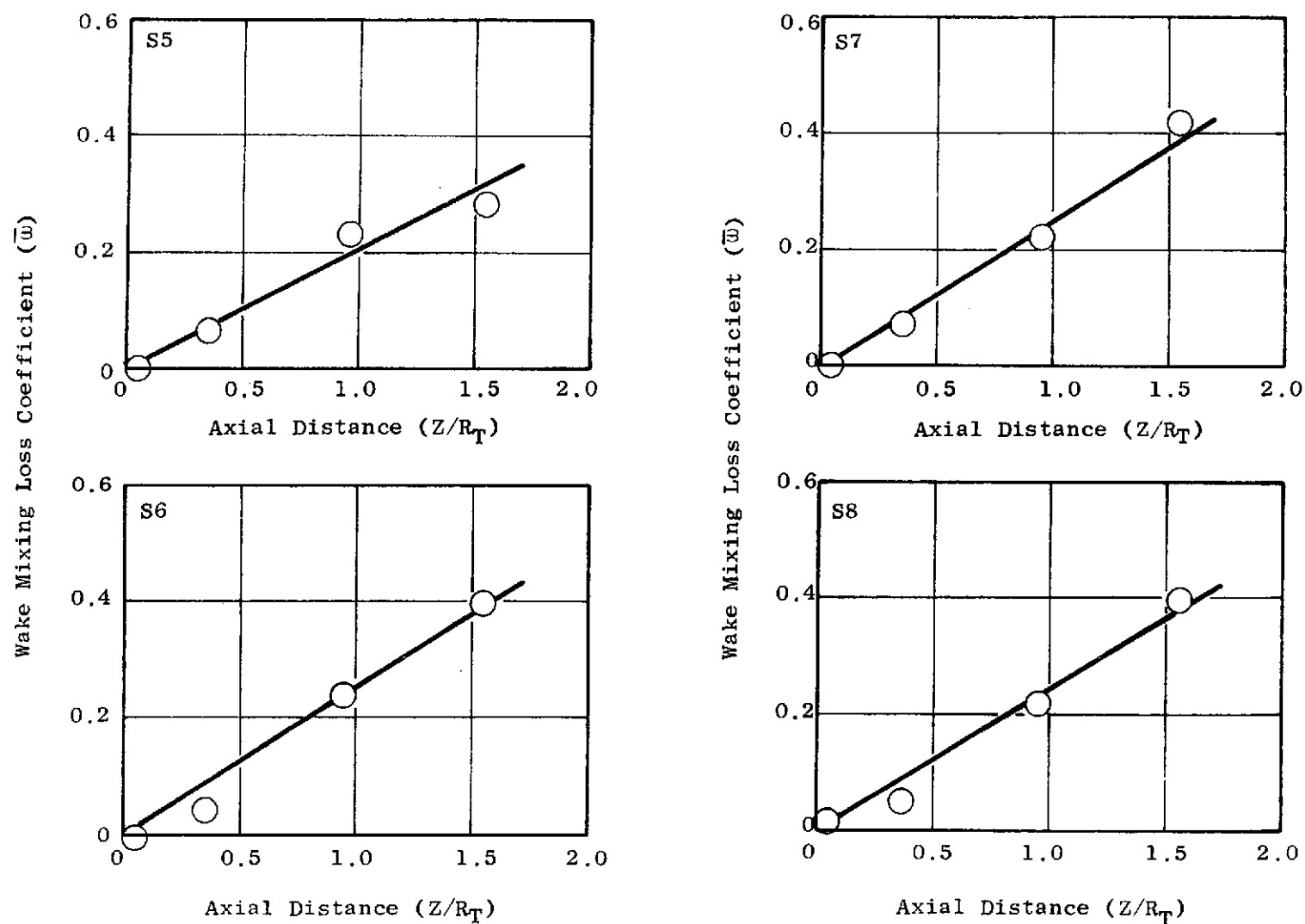
Figure 61.   Wake Mixing Loss Characteristics for Models 5 through 8, Swirling Flow
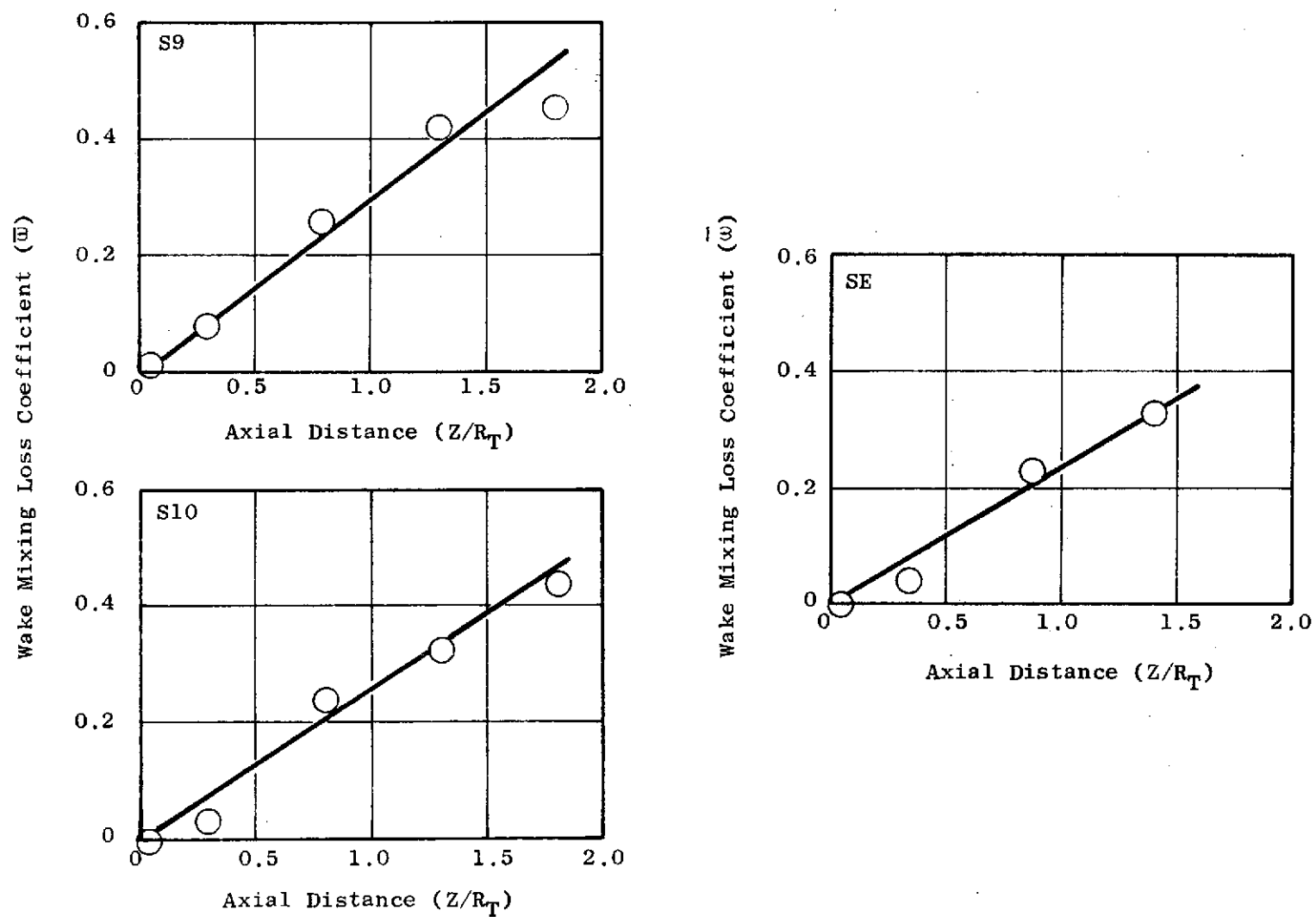
Figure 62. Wake Mixing Loss Characteristics for Models 9, 10 and SE, Swirling Flow
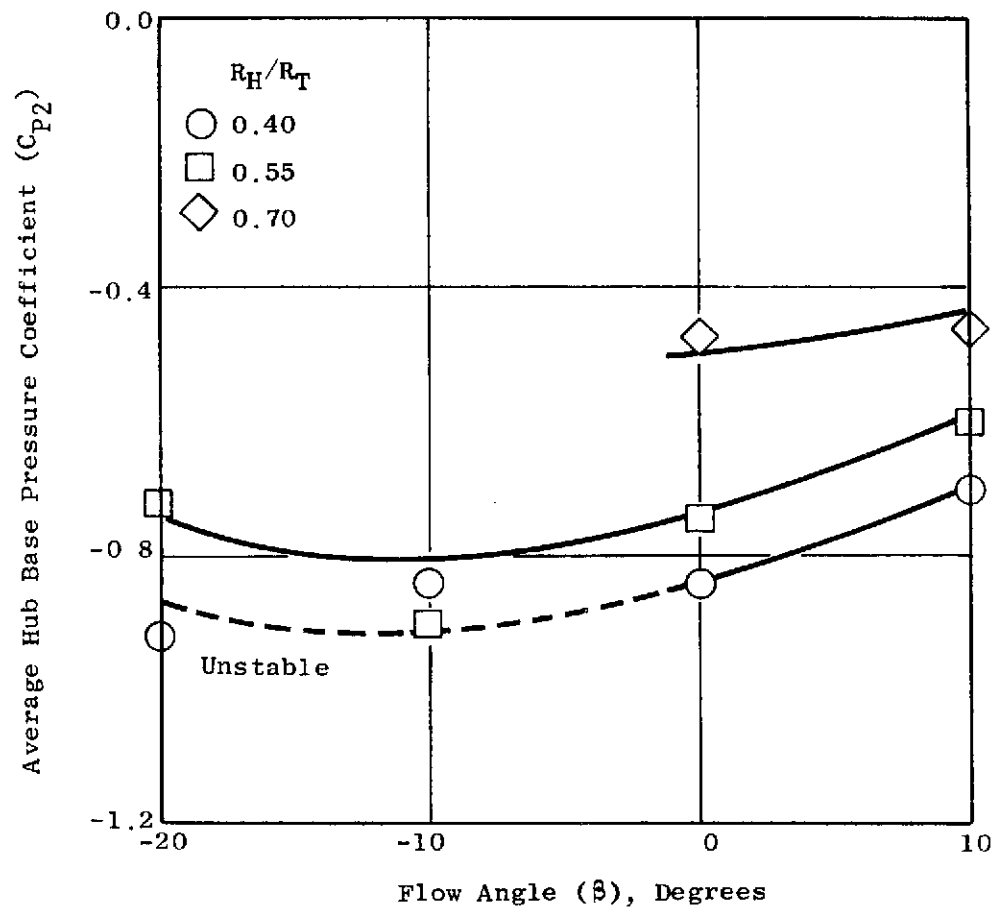
Figure 63. Effects of Geometry on Average Hub Base
Pressure, Swirling Flow
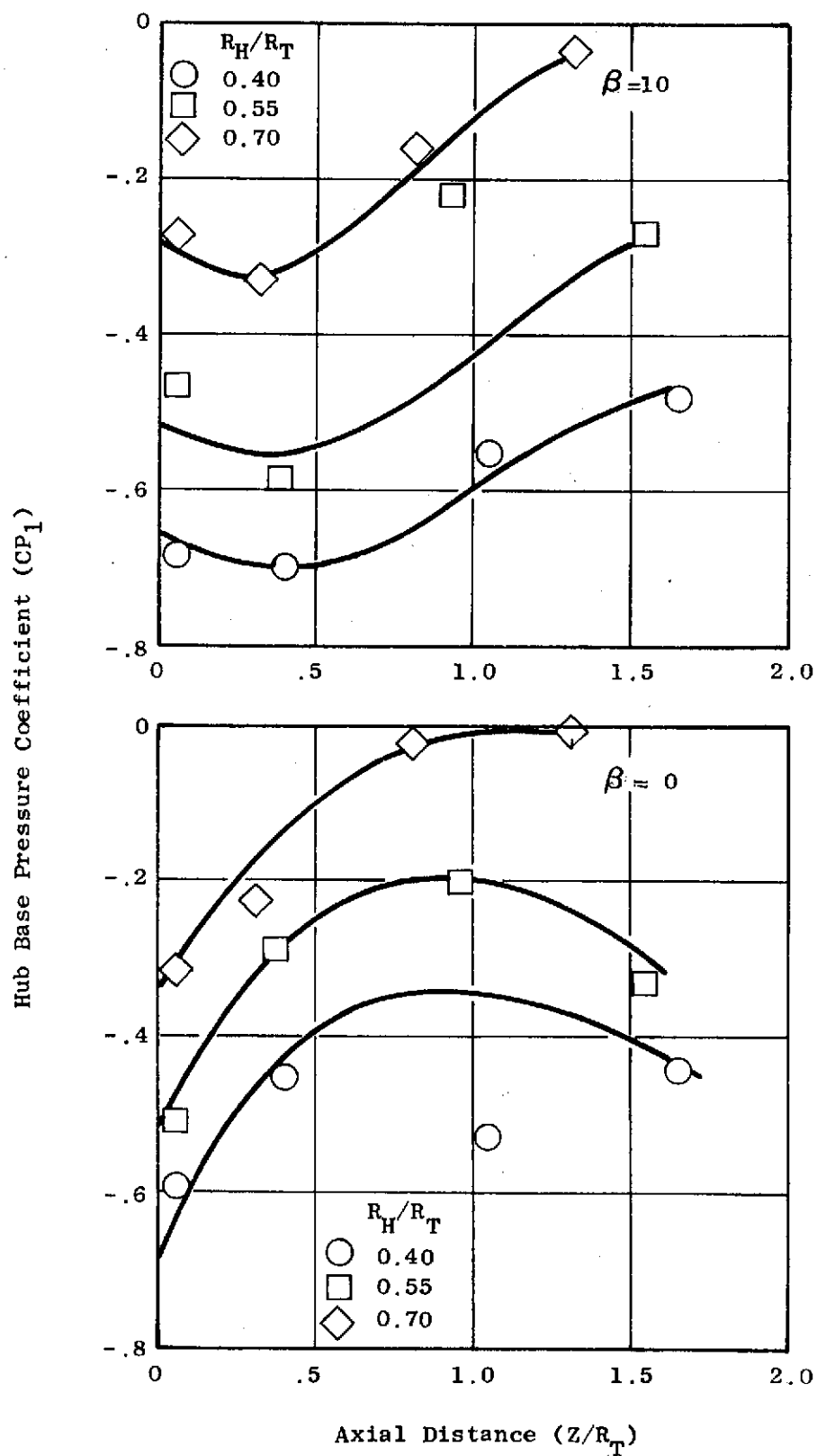
Figure 64.    Effects of Geometry on the Hub Outer Radius Base
Pressure Coefficient,  $\beta$ = 10 & 0, Swirling Flow
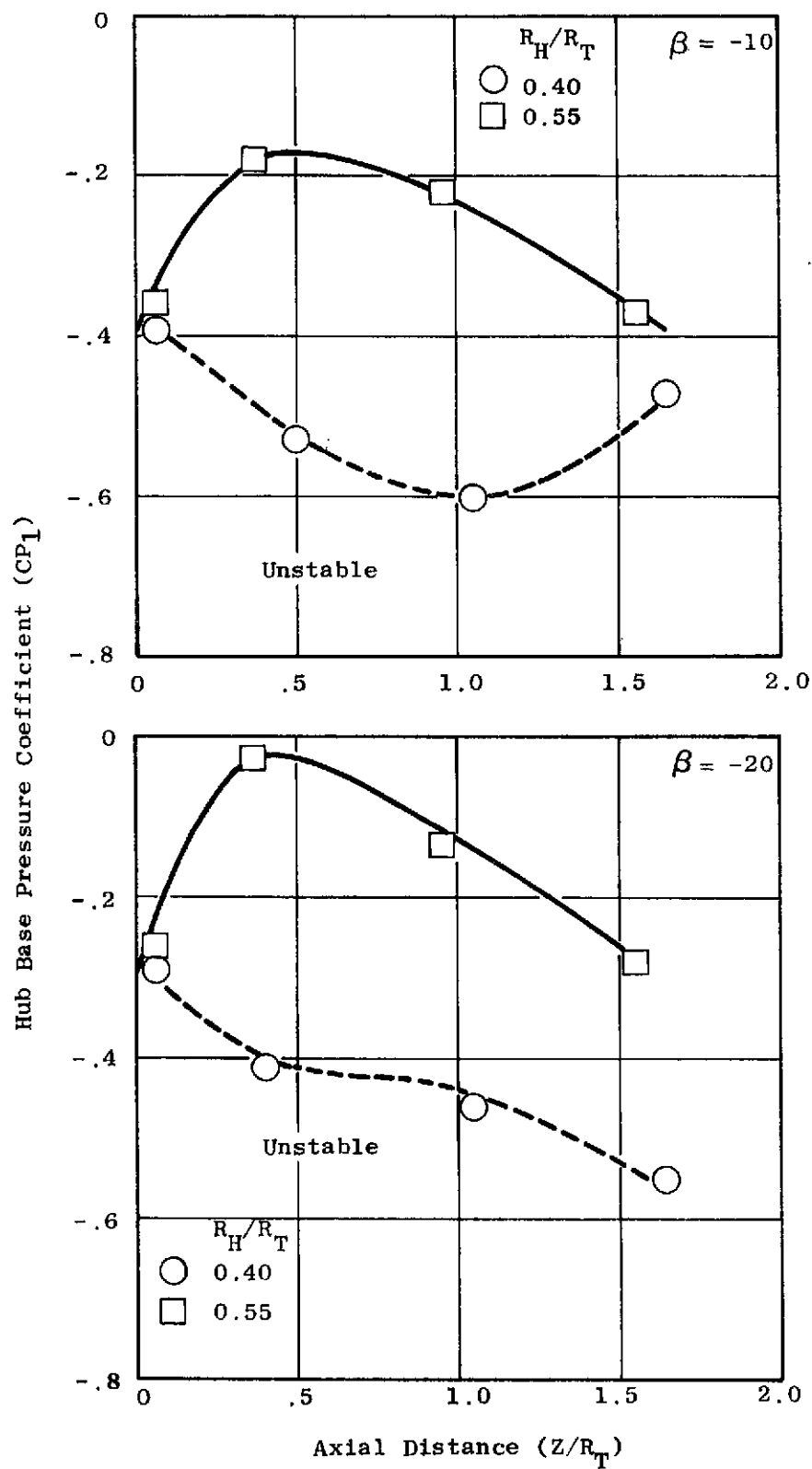
Figure 65. Effects of Geometry on the Hub Outer Radius Base Pressure Coefficient, $\beta$ = -10 & -20, Swirling Flow
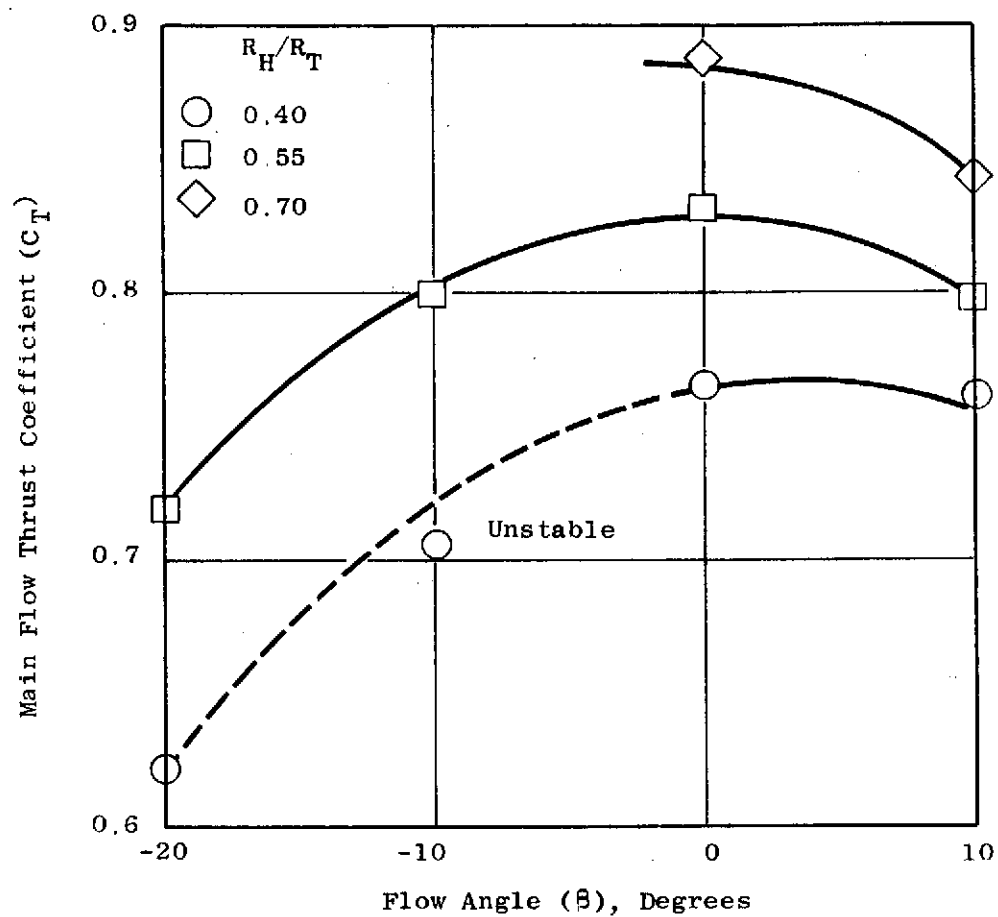
Figure 66. Effects of Geometry on Main Flow Thrust, Swirling Flow
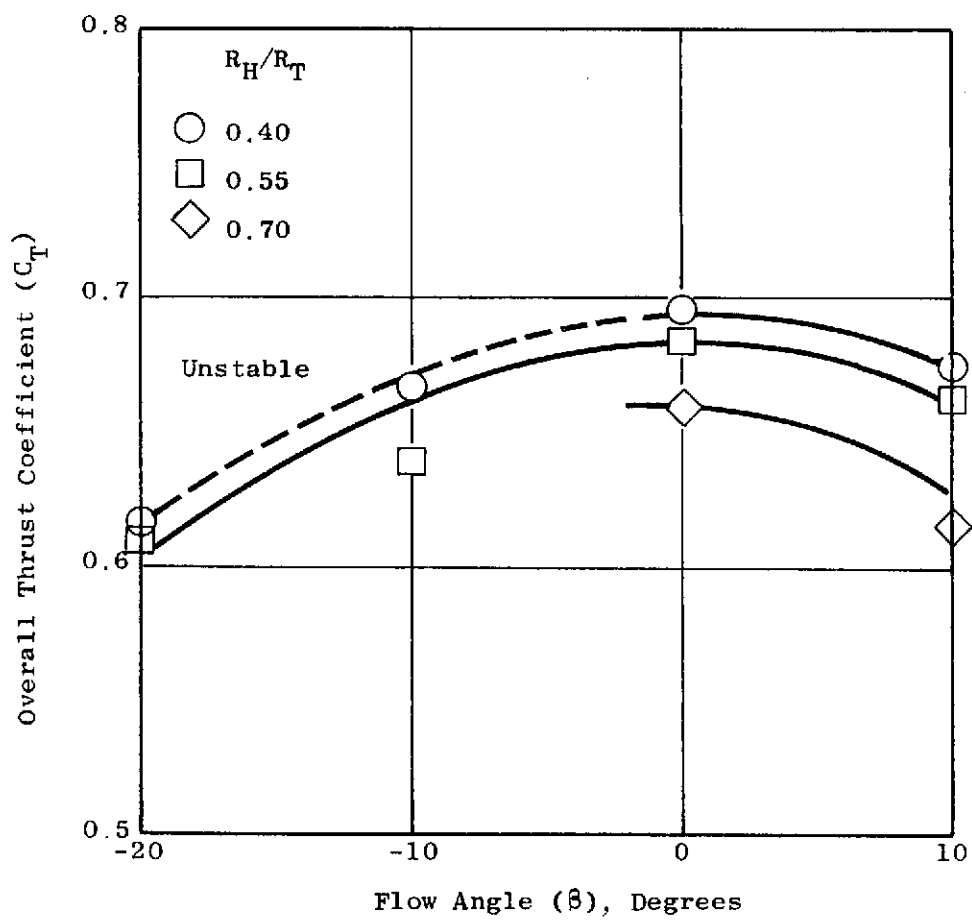
Figure 67. Effects of Geometry on Overall Thrust, Swirling Flow
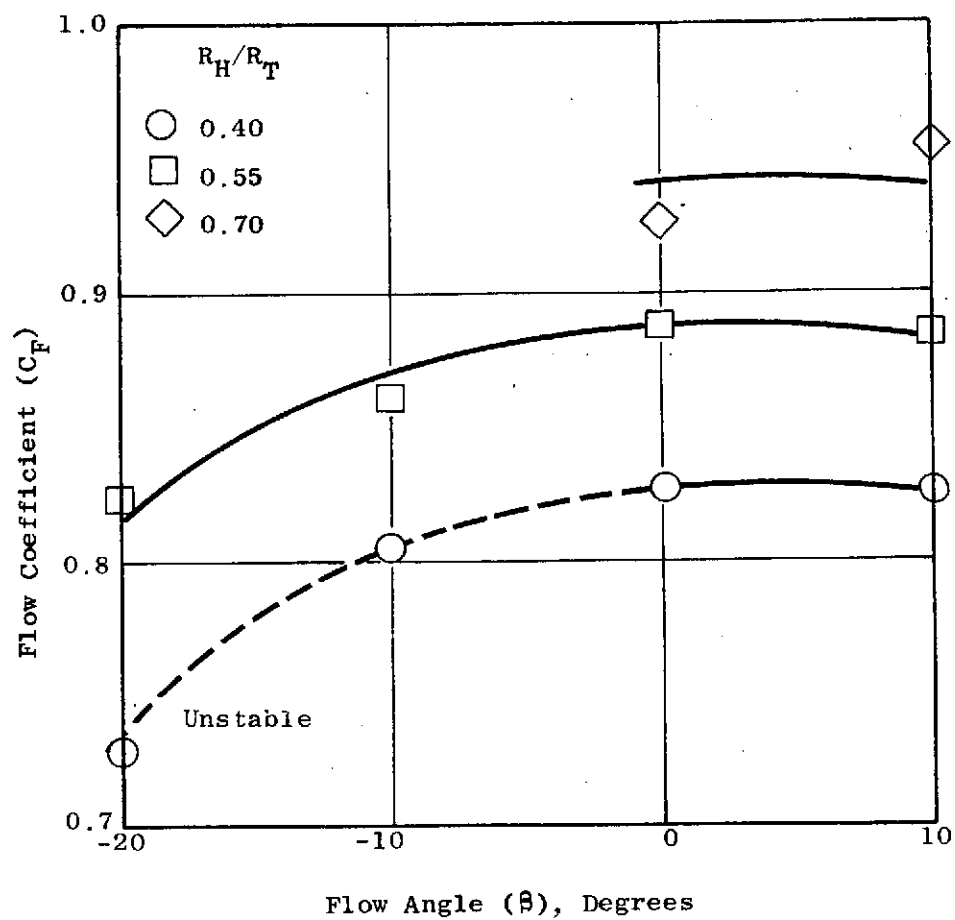
Figure 68. Effects of Geometry on Flow Coefficient, Swirling Flow
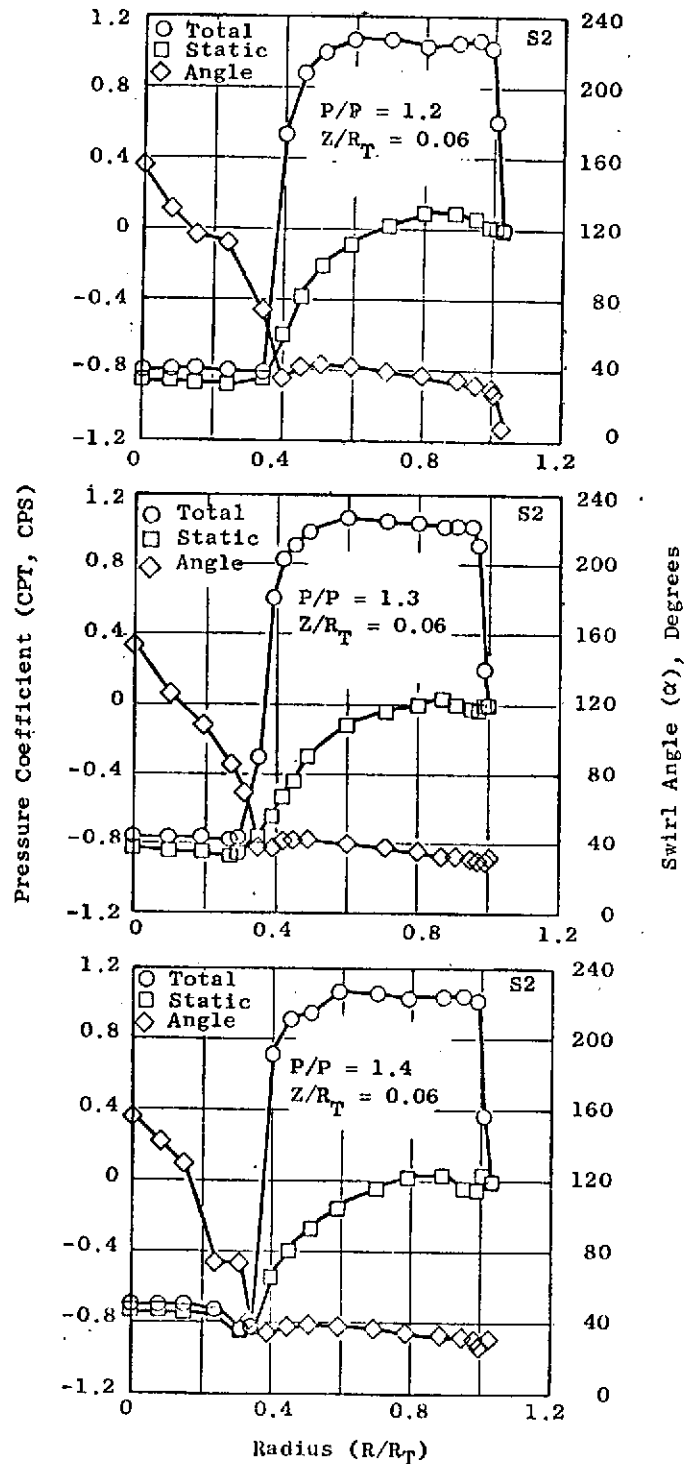
Figure 69. Effects of Pressure Ratio on Total and Static Pressure Coefficients and Swirl Distribution for Model 2, Swirling Flow
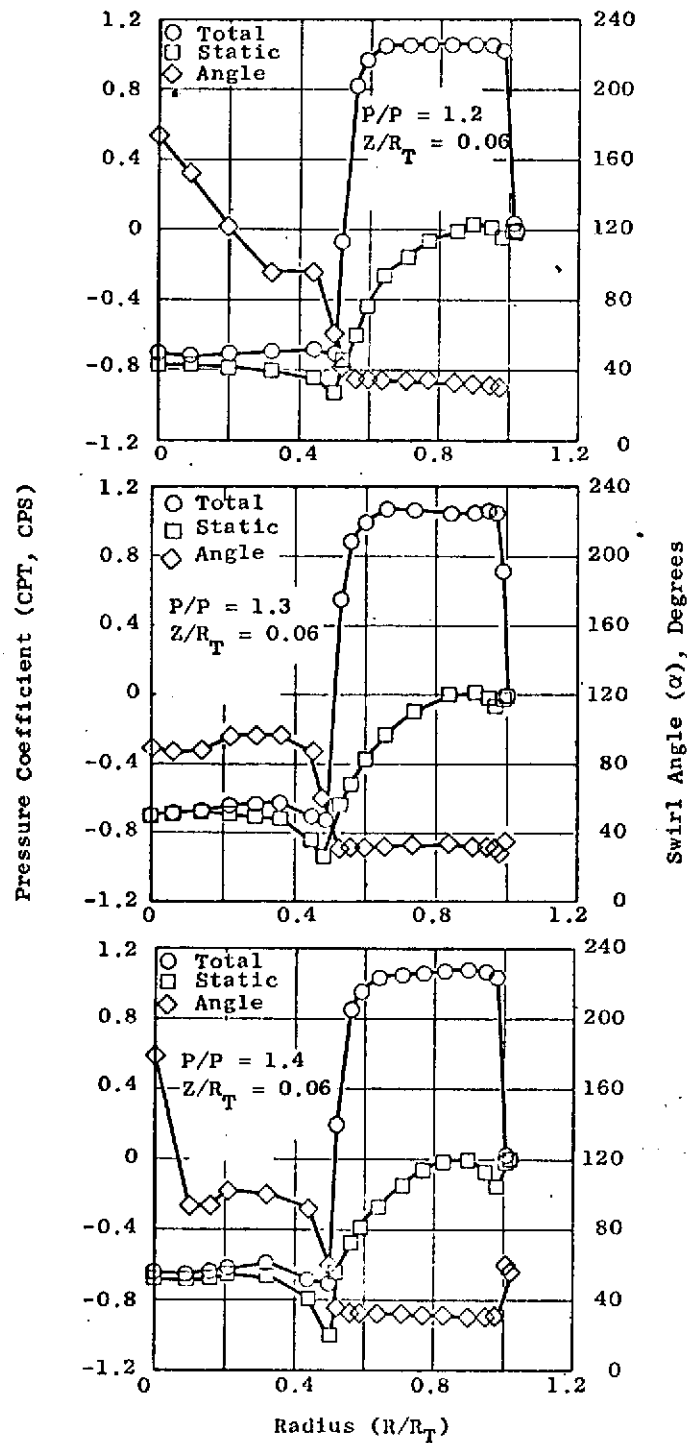
Figure 70. Effects of Pressure Ratio on Total and Static
Pressure Coefficients and Swirl Distribution
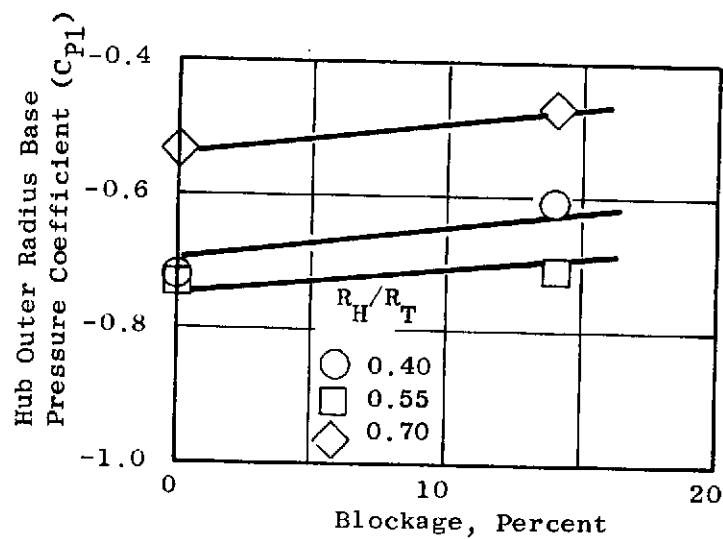for Model 6, Swirling Flow
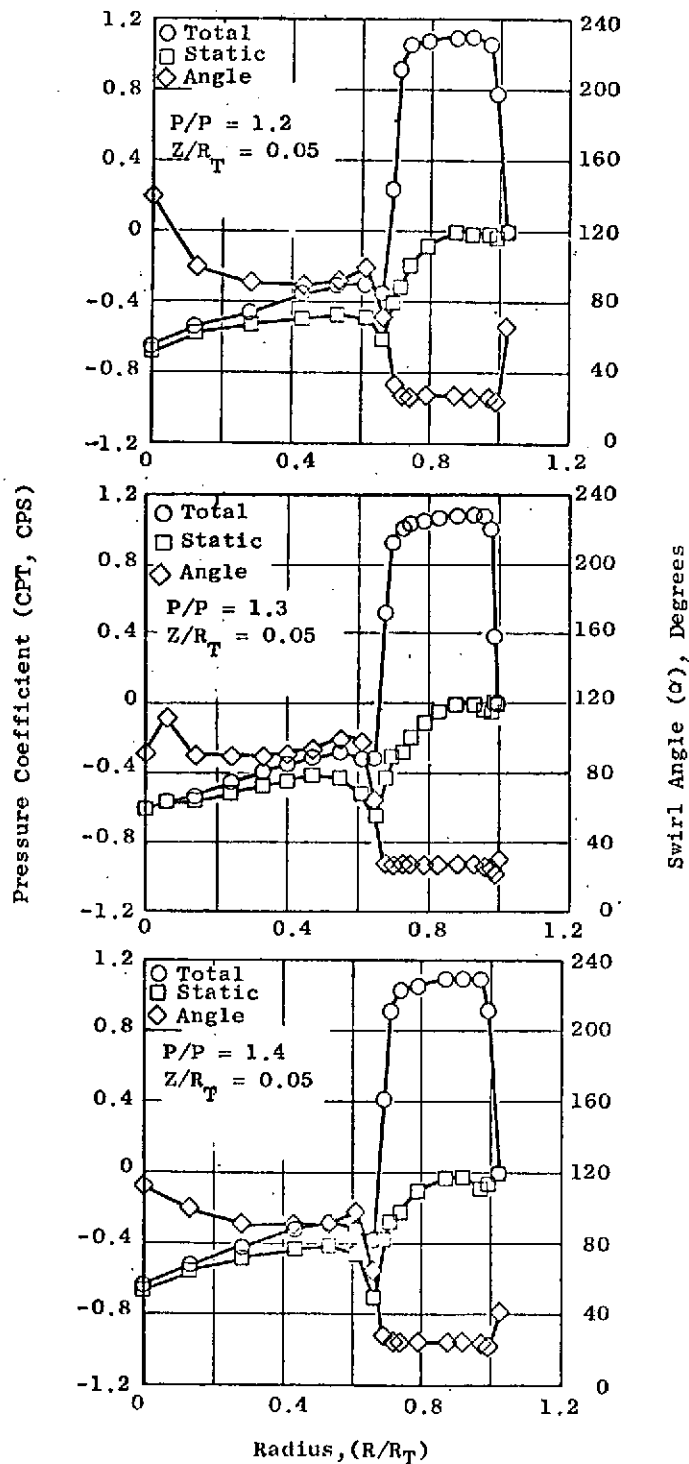
Figure 71. Effects of Pressure Ratio on Total and Static
Pressure Coefficients and Swirl Distribution
for Model 10, Swirling Flow
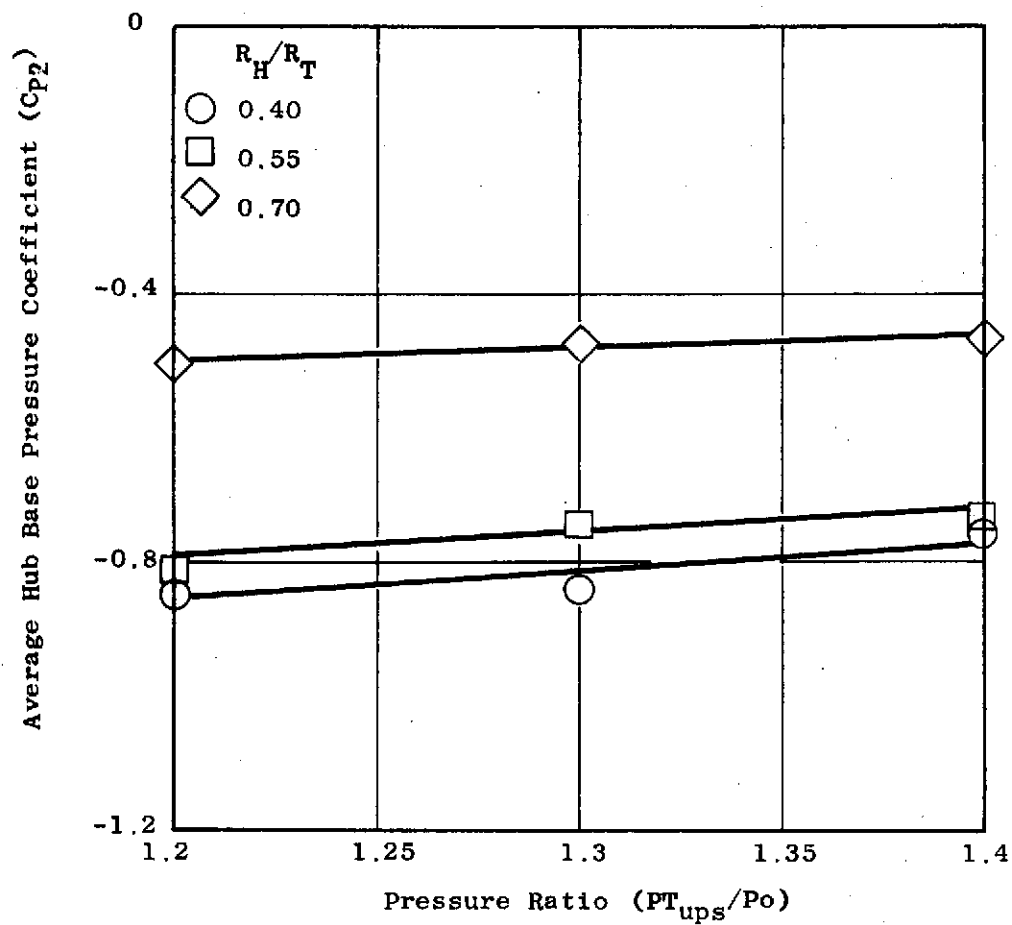
Figure 72.    Effects of Pressure Ratio on the Average Hub
Base Pressure Coefficient, Swirling Flow
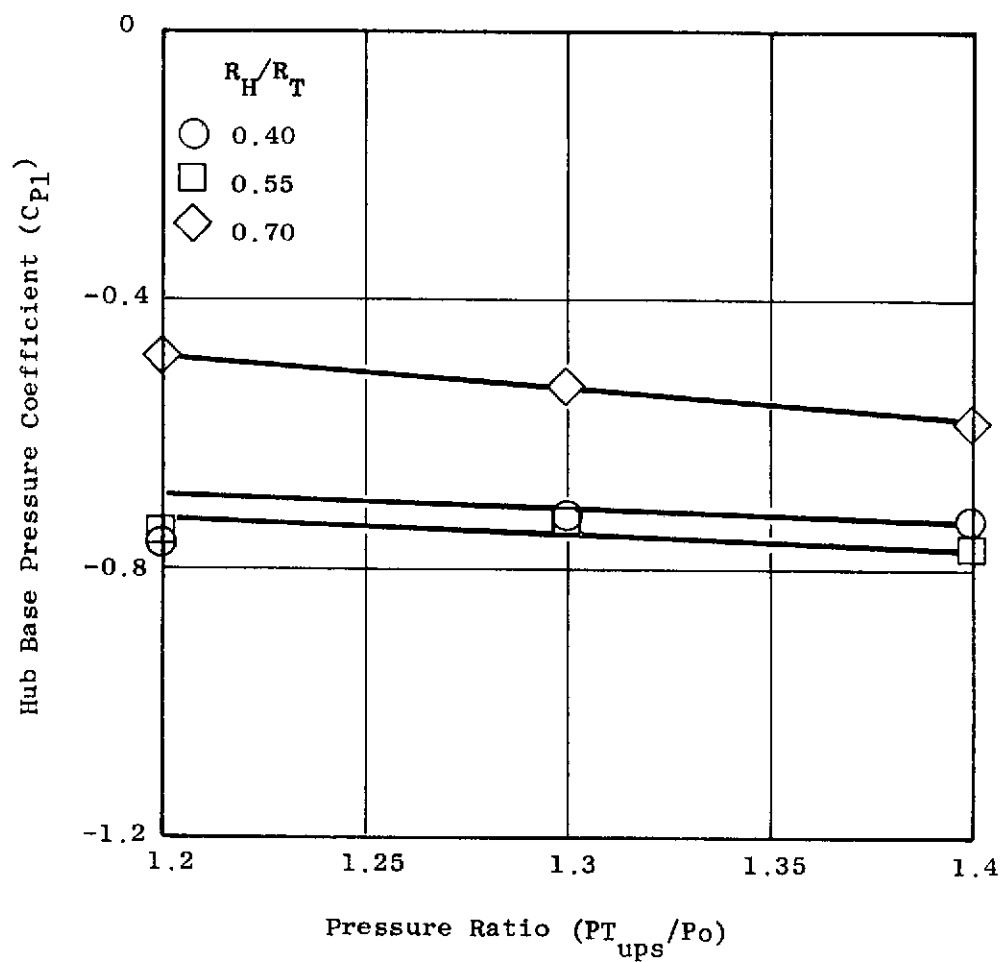
Figure 73. Effects of Pressure Ratio on the Hub Outer Radius Base Pressure Coefficient, Swirling Flow
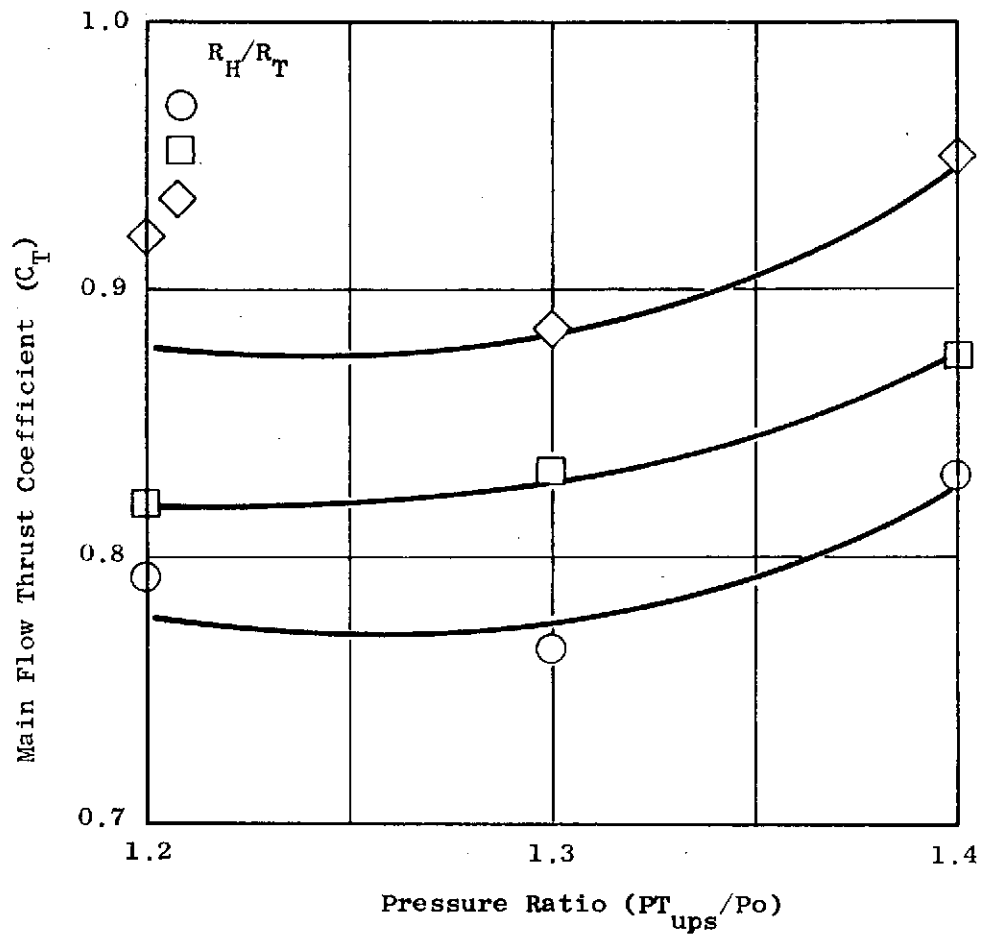
Figure 74.    Effects of Pressure Ratio on the Main Flow
             Thrust Coefficient, Swirling Flow
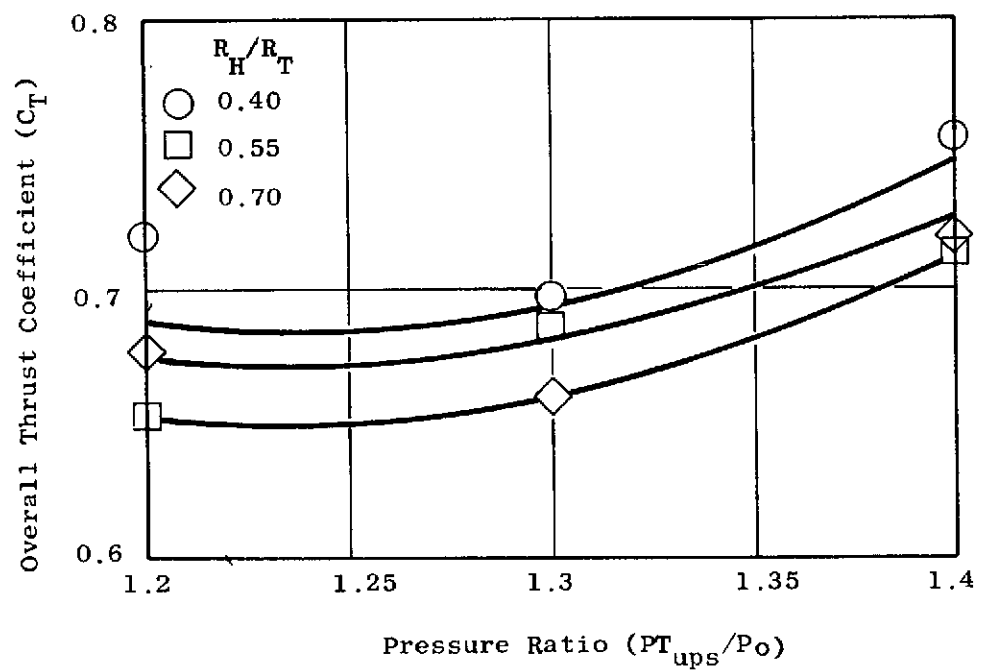
Figure 75. Effects of Pressure Ratio on the Overall Thrust Coefficient, Swirling Flow
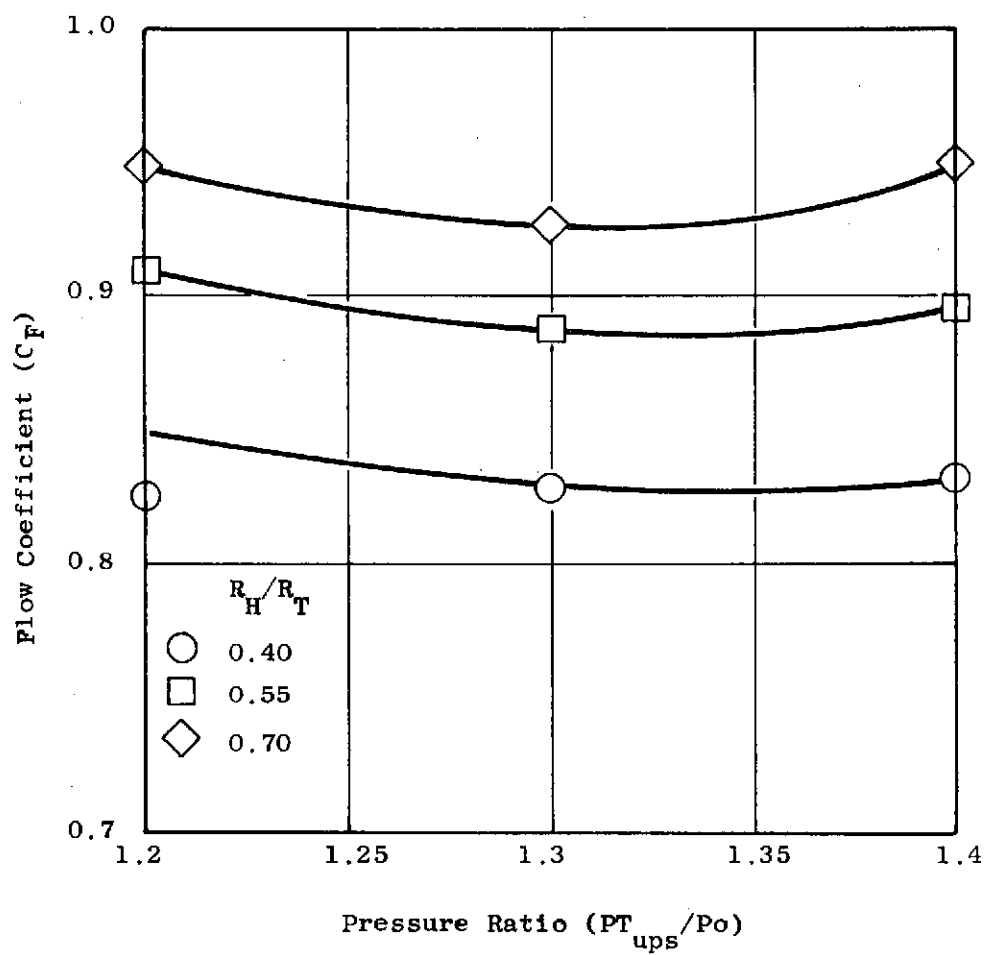
Figure 76. Effects of Pressure Ratio on The Flow
Coefficient, Swirling Flow
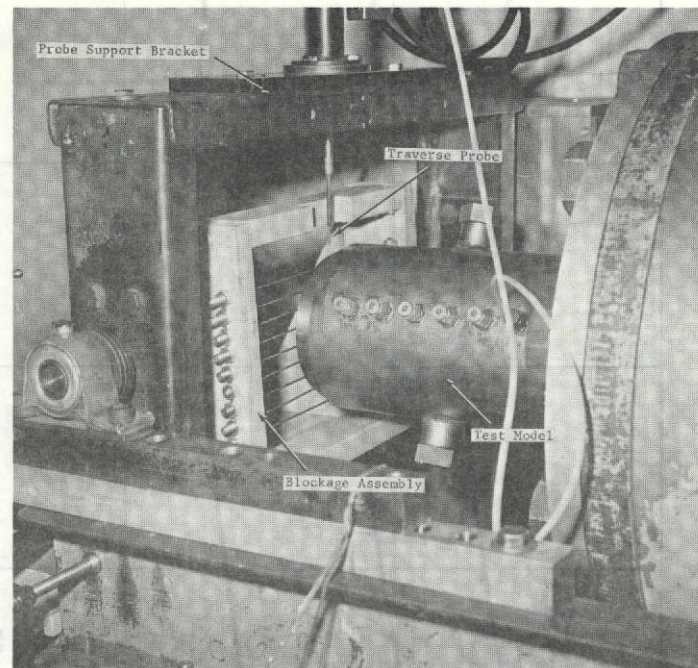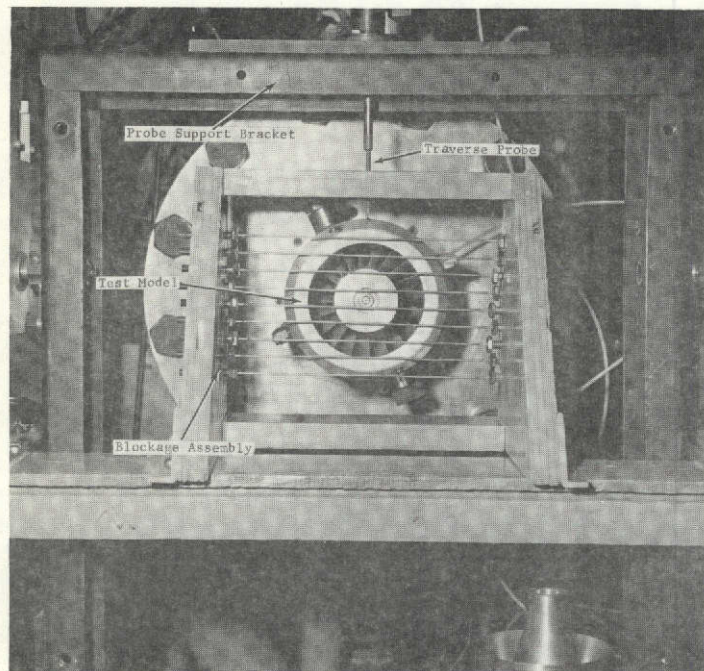
Figure 77. Photograph of the Blockage System Installed in the
Test Stand
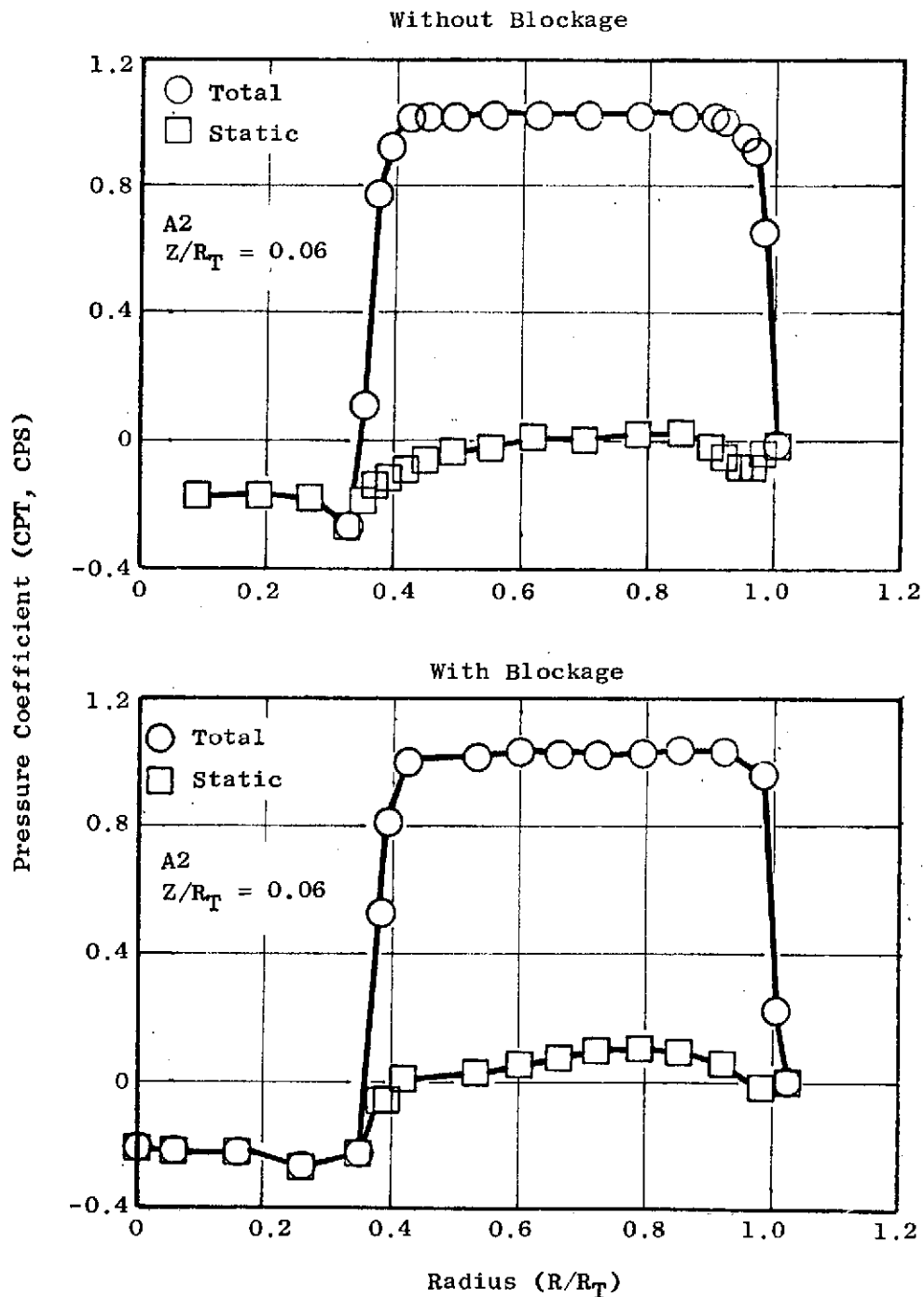
Figure 78. Effects of Blockage on Total and Static Pressure Coefficients for Model 2, Axial Flow
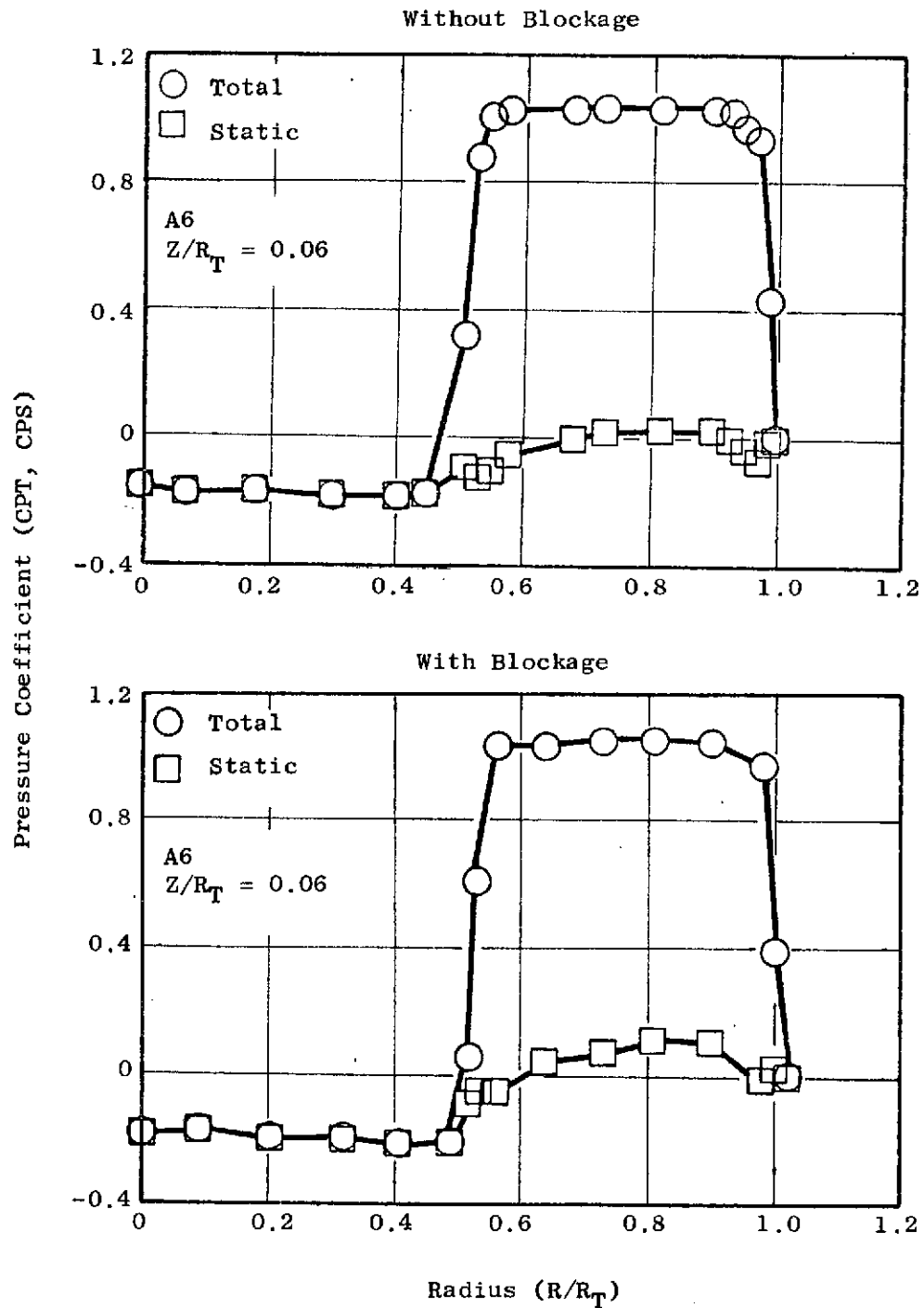
Figure 79. Effects of Blockage on Total and Static Pressure
Coefficients for Model 6, Axial Flow
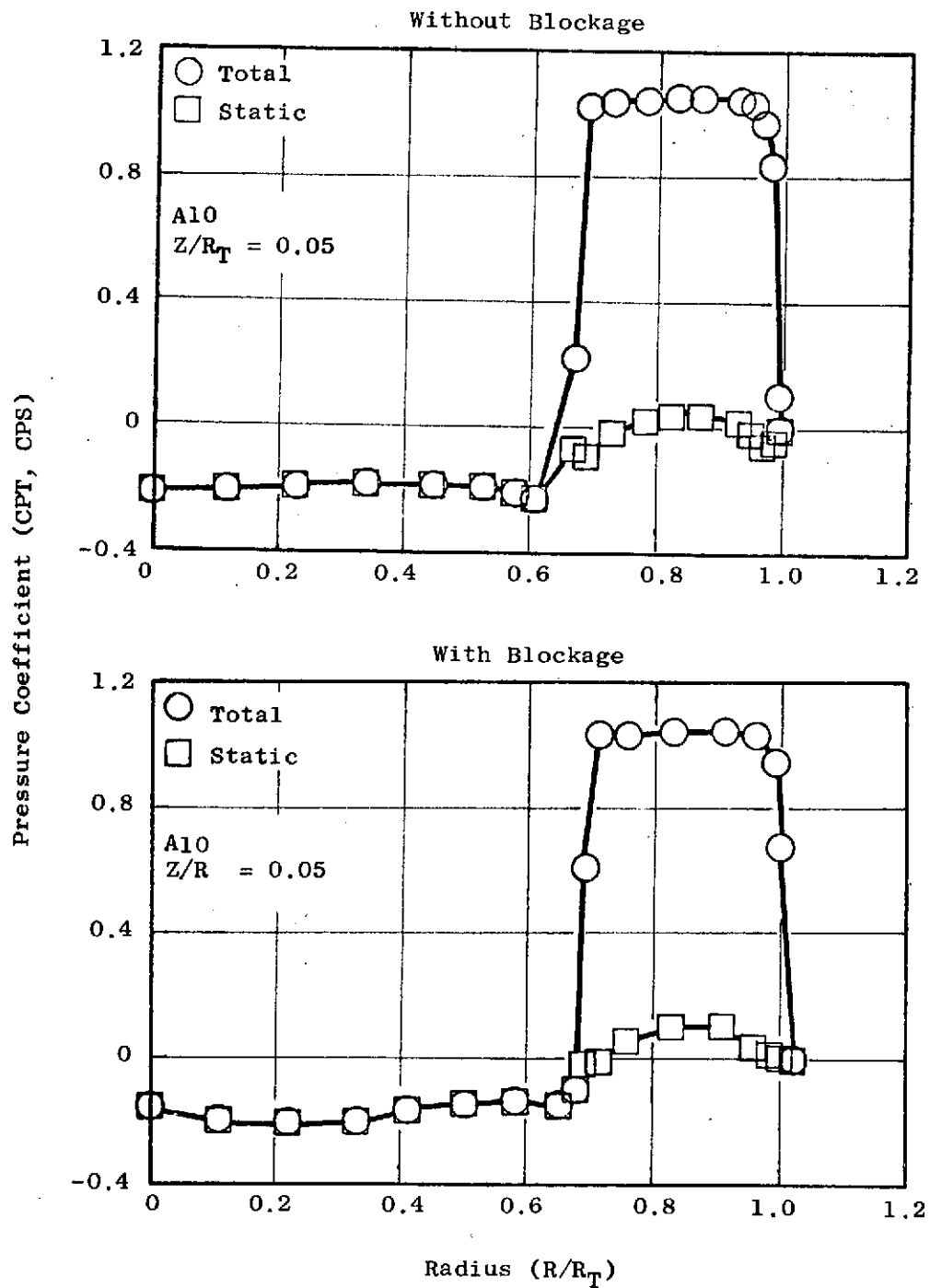
Figure 80.  Effects of Blockage on Total and Static Pressure Coefficients for Model 10, Axial Flow
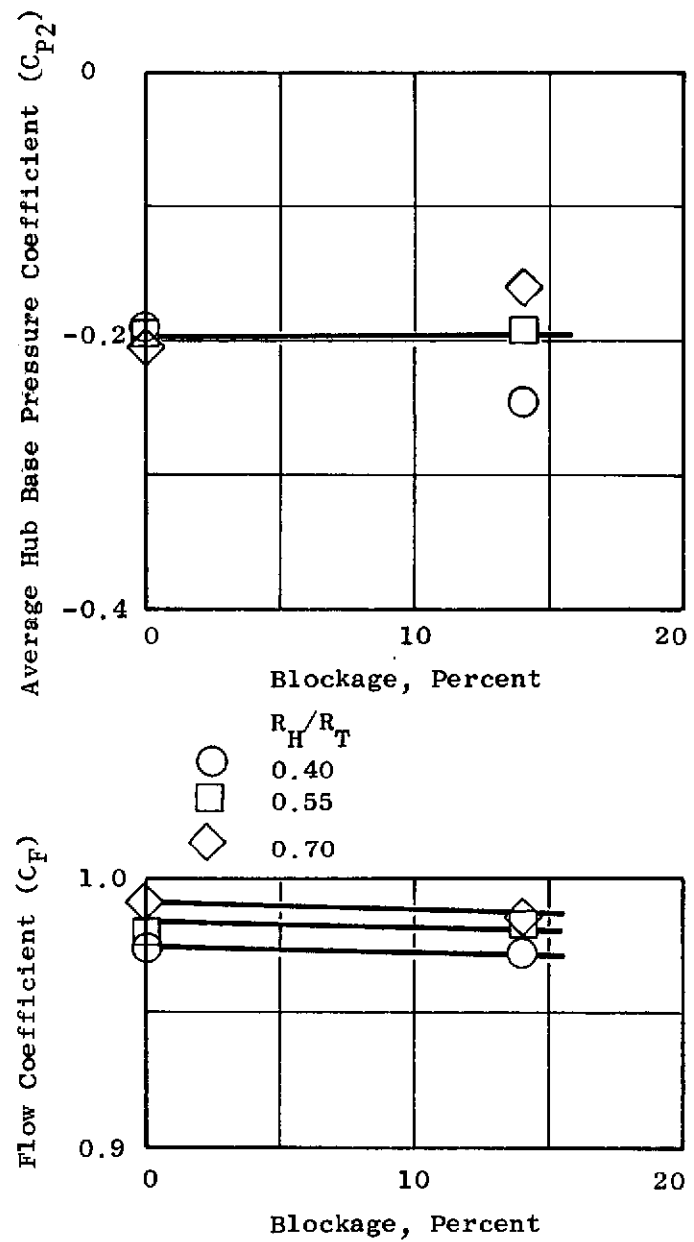
Figure 81.    Effects of Blockage on the Base
Pressure and Flow Coefficient for
Models 2,6 and 10, Axial Flow
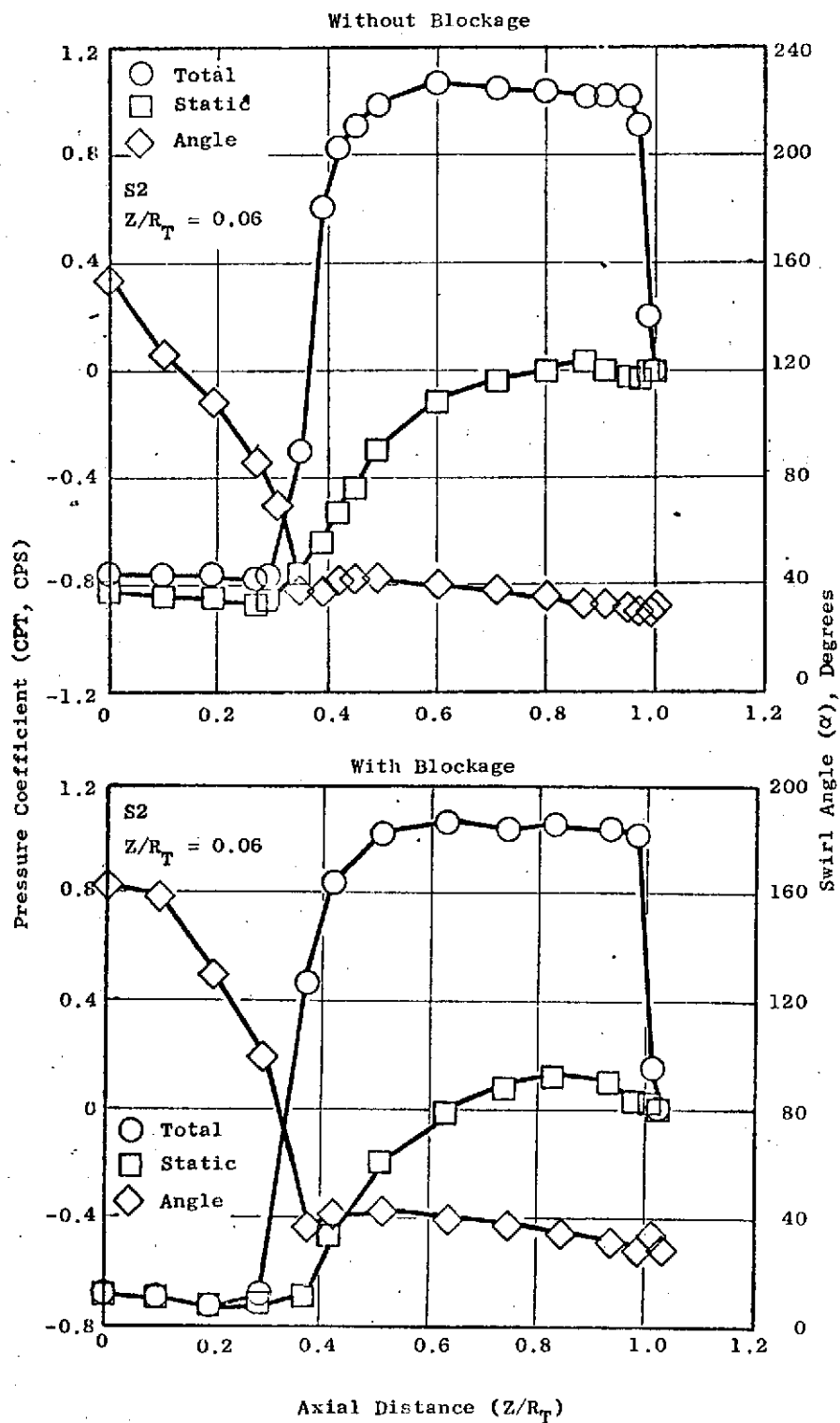
Figure 82. Effects of Blockage on Total and Static Pressure Coefficients and Swirl Distribution for Model 2, Swirling Flow
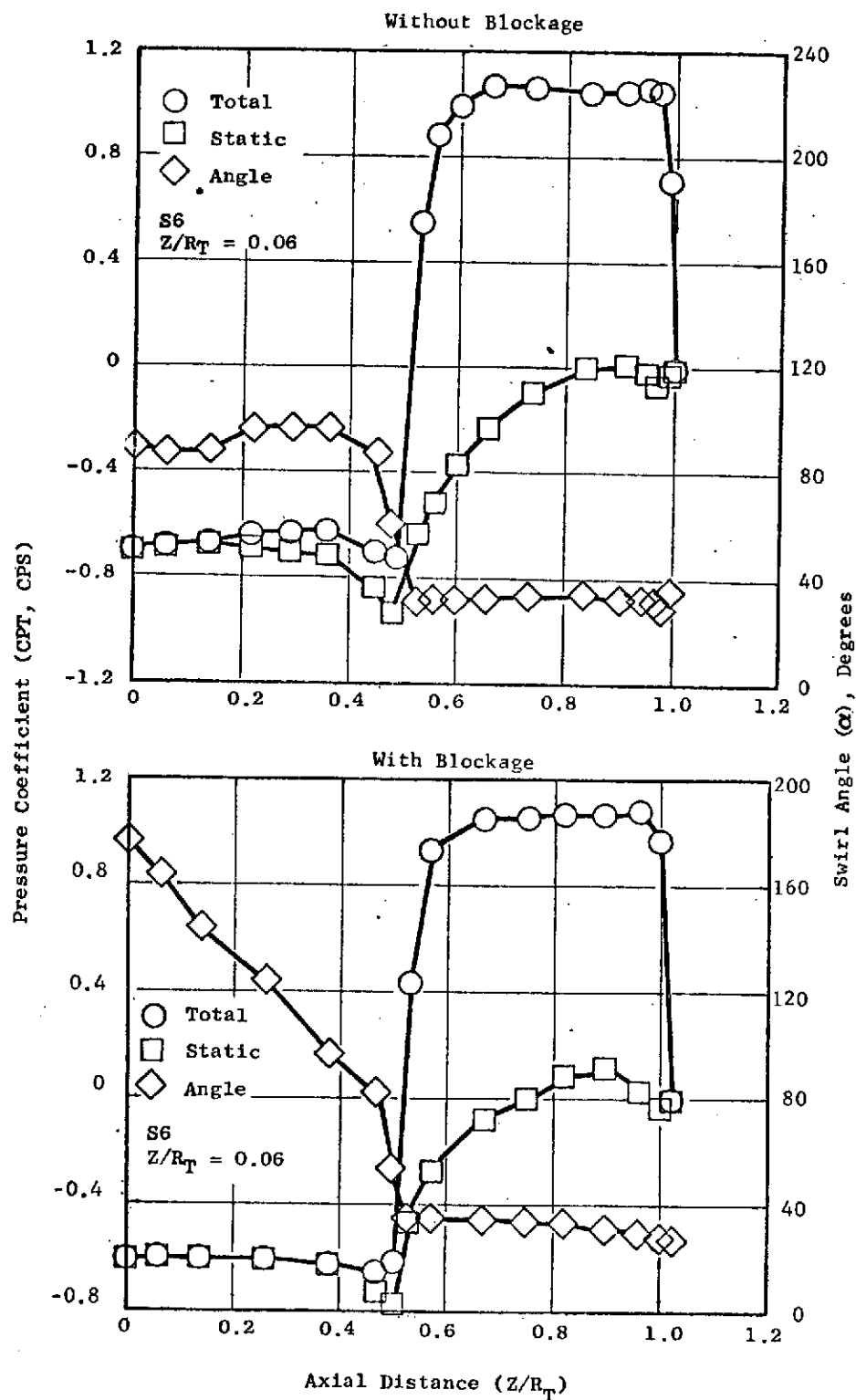
Figure 83. Effects of Blockage on Total and Static Pressure Coefficients and Swirl Distribution for Model 6, Swirling Flow
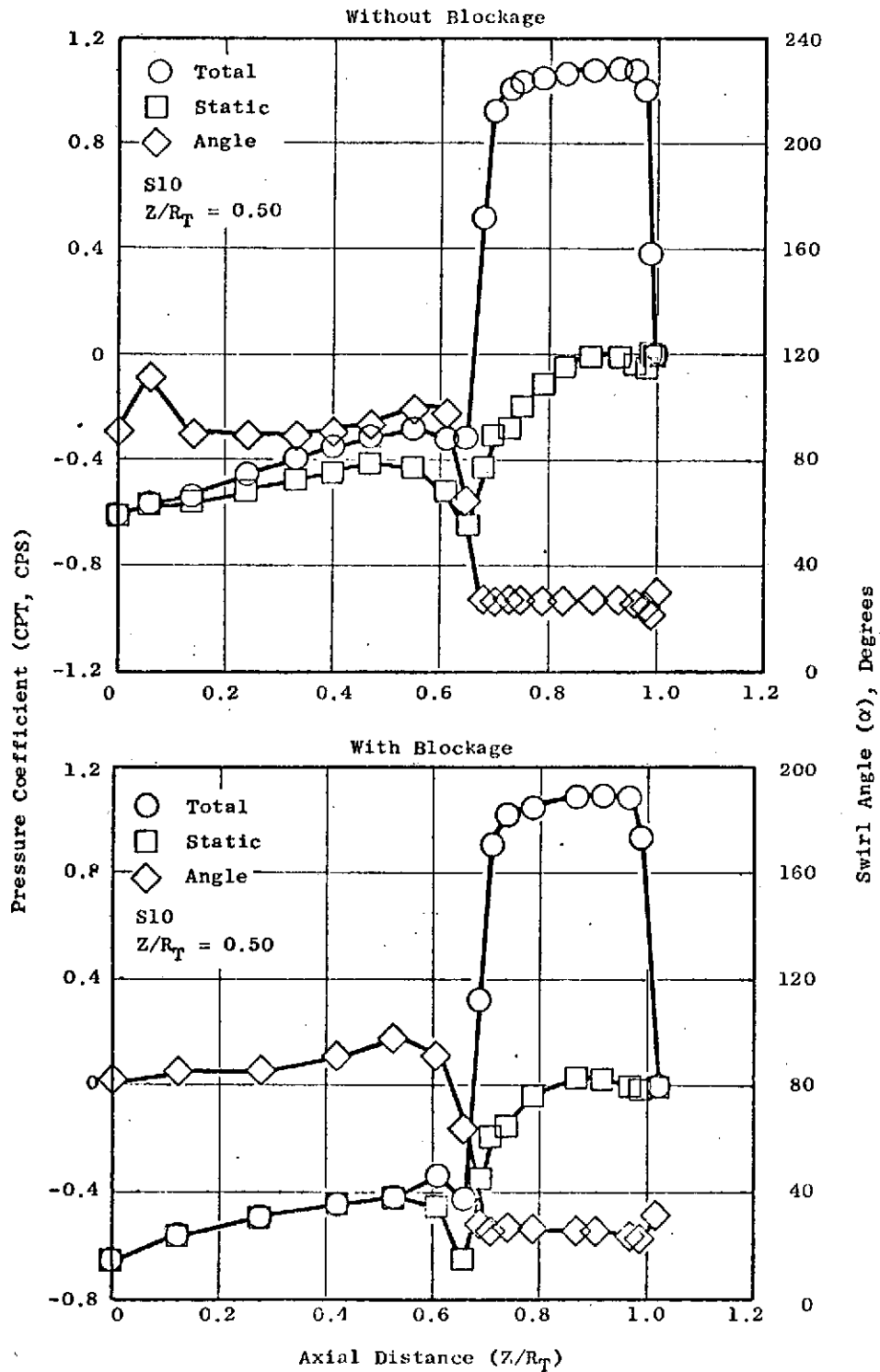
Figure 84. Effects of Blockage on Total and Static Pressure Coefficients and Swirl Distribution for Model 10, Swirling Flow
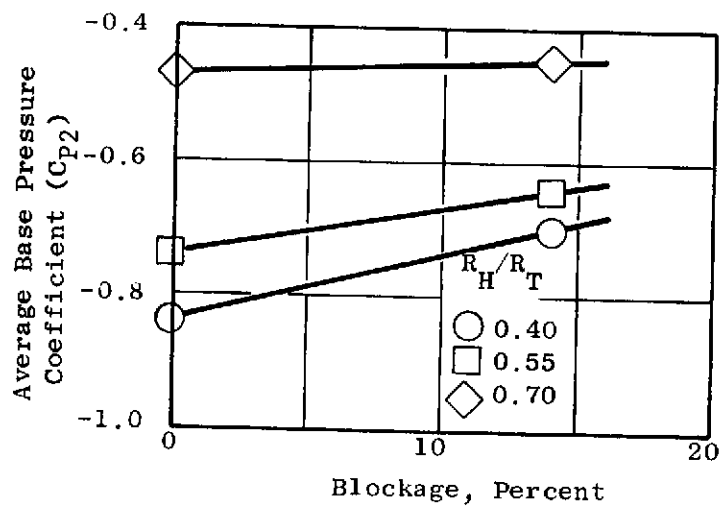
Figure 85. Effects of Blockage on the Base Pressure
Coefficients, Swirling Flow
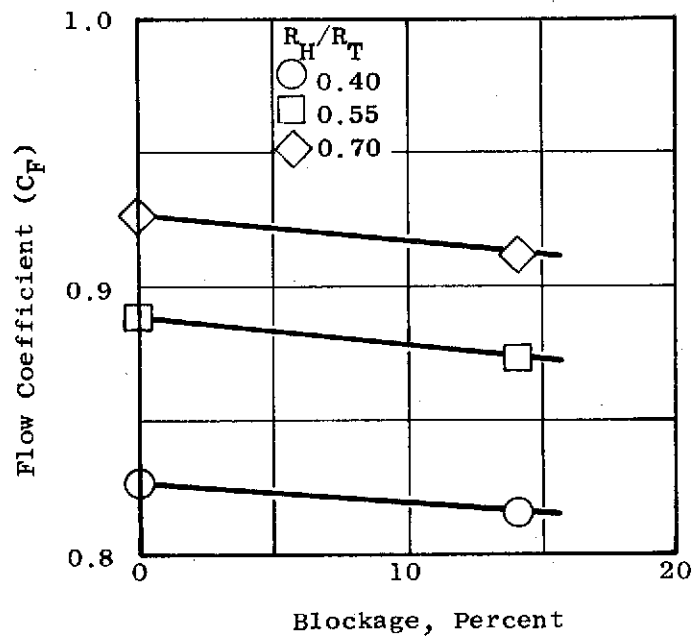
Figure 86. Effects of Blockage on The Flow Coefficient, Swirling Flow
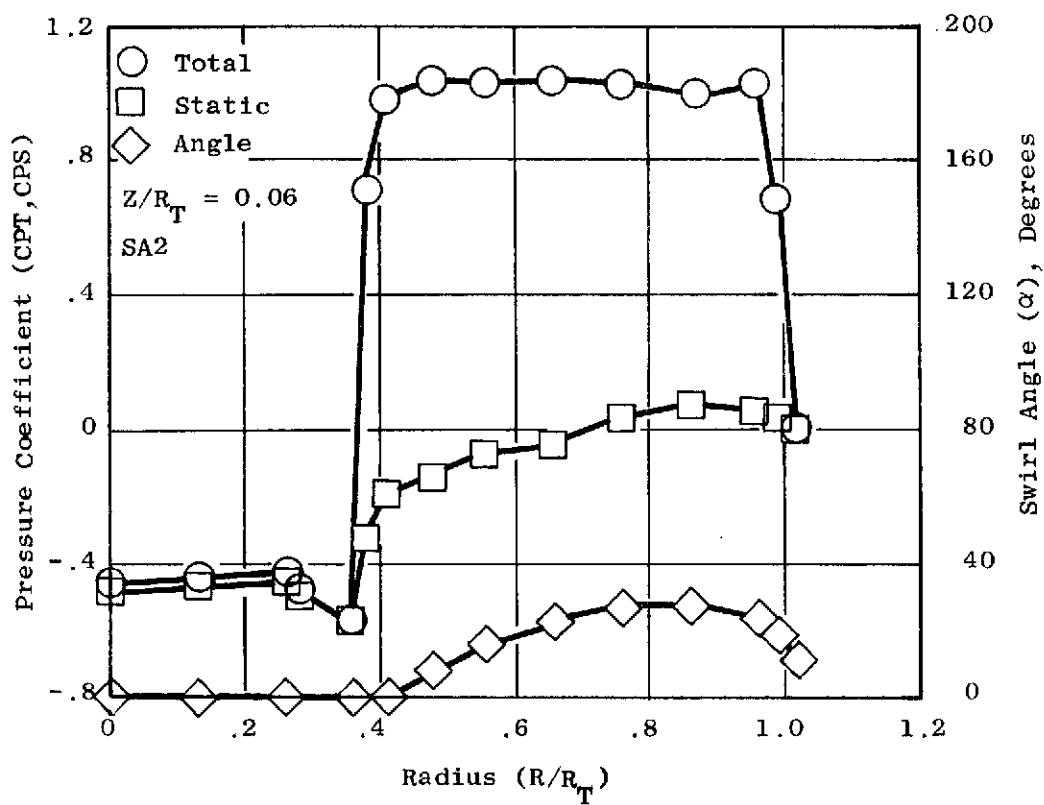
Figure 87.    Total and Static Pressure Coefficient and
             Swirl Angle Distribution for Model 2,
             Skewed Flow Distribution
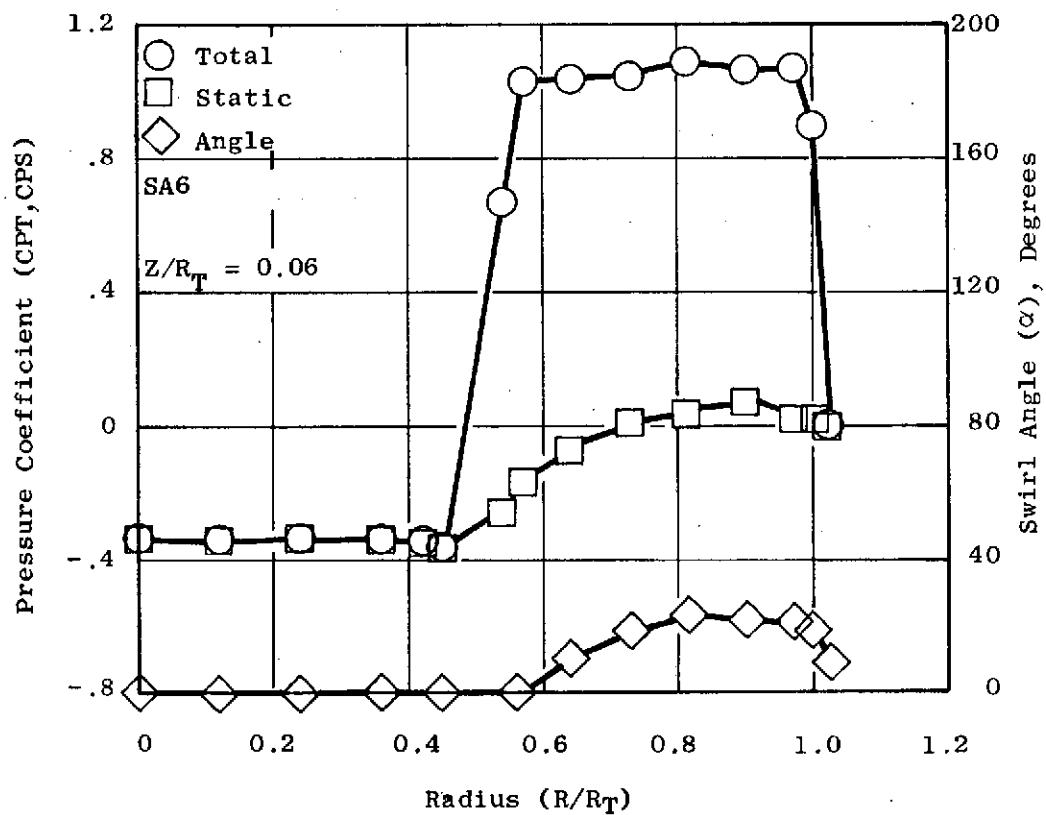
Figure 88. Total and Static Pressure Coefficient
and Swirl Angle Distribution for Model 6,
Skewed Flow Distribution
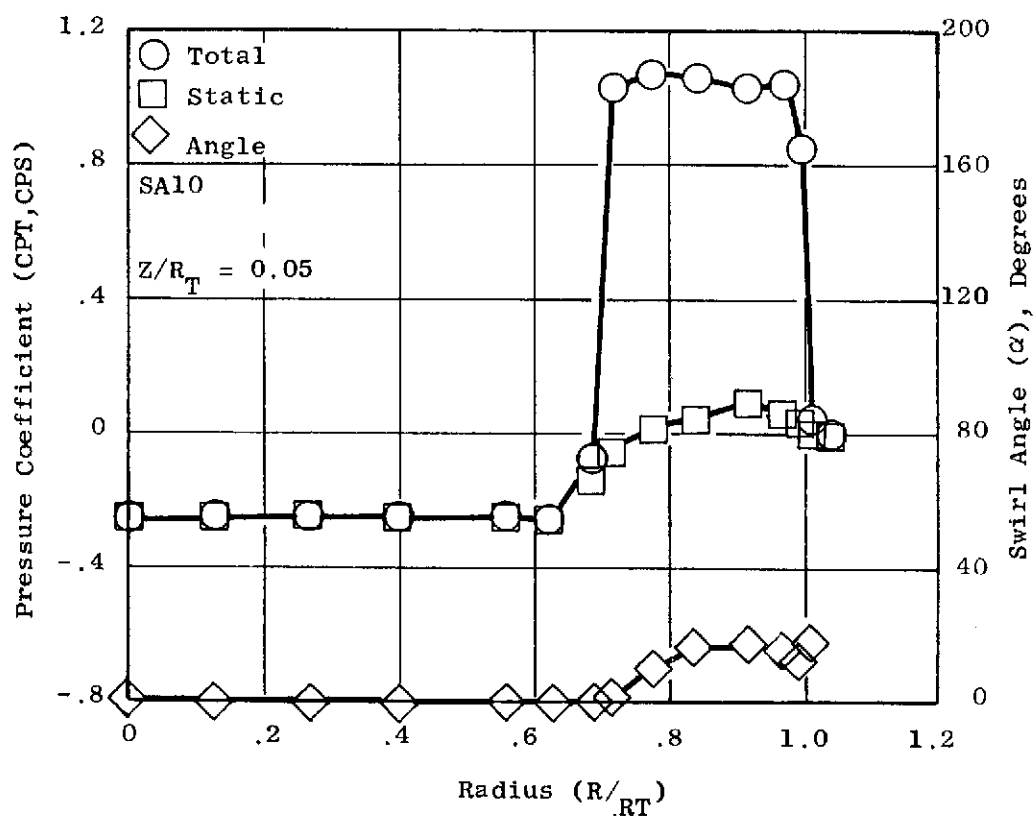
Figure 89. Total and Static Pressure Coefficient and Swirl Angle Distribution for Model 10, Skewed Flow Distribution
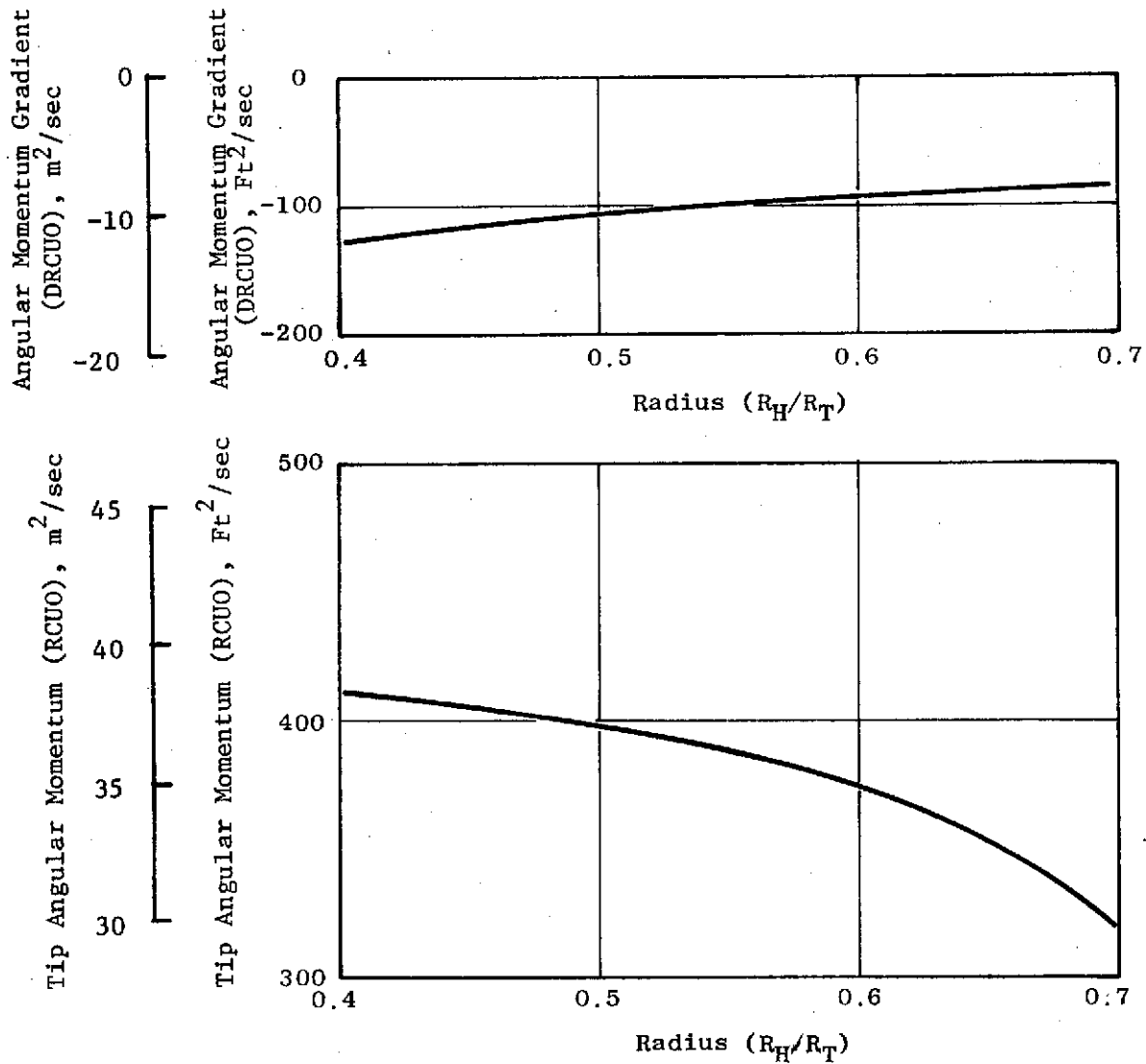
Figure 90.  Angular Momentum Distribution From Test
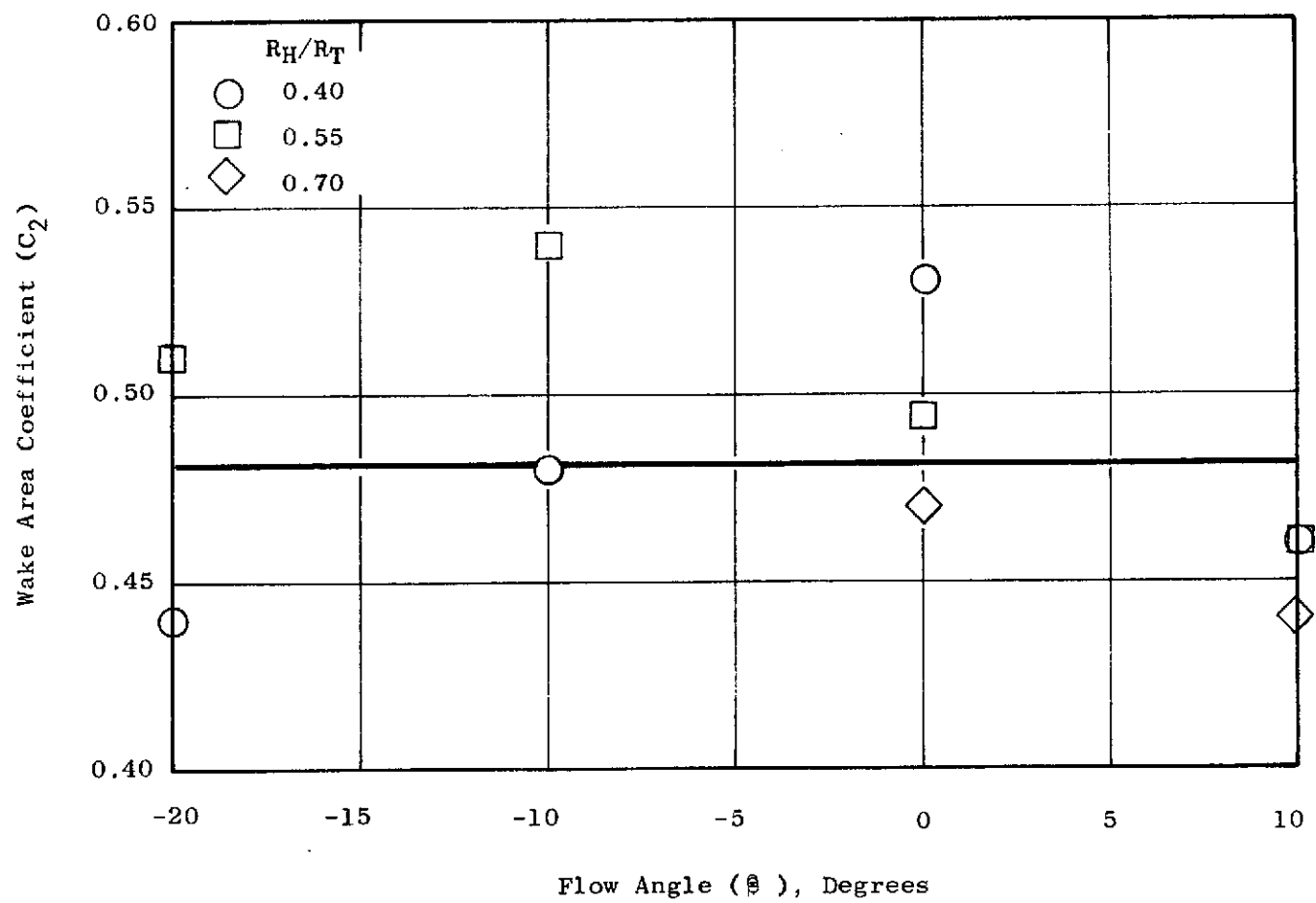
Figure 91.  Wake Area Coefficient
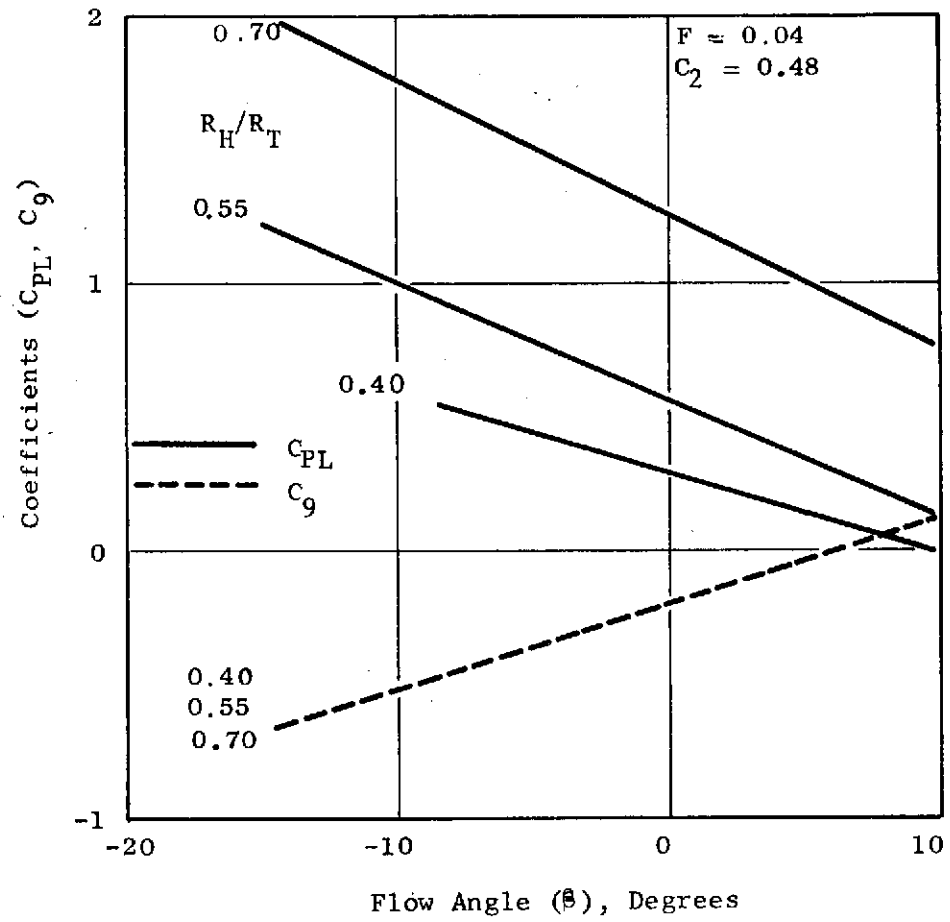
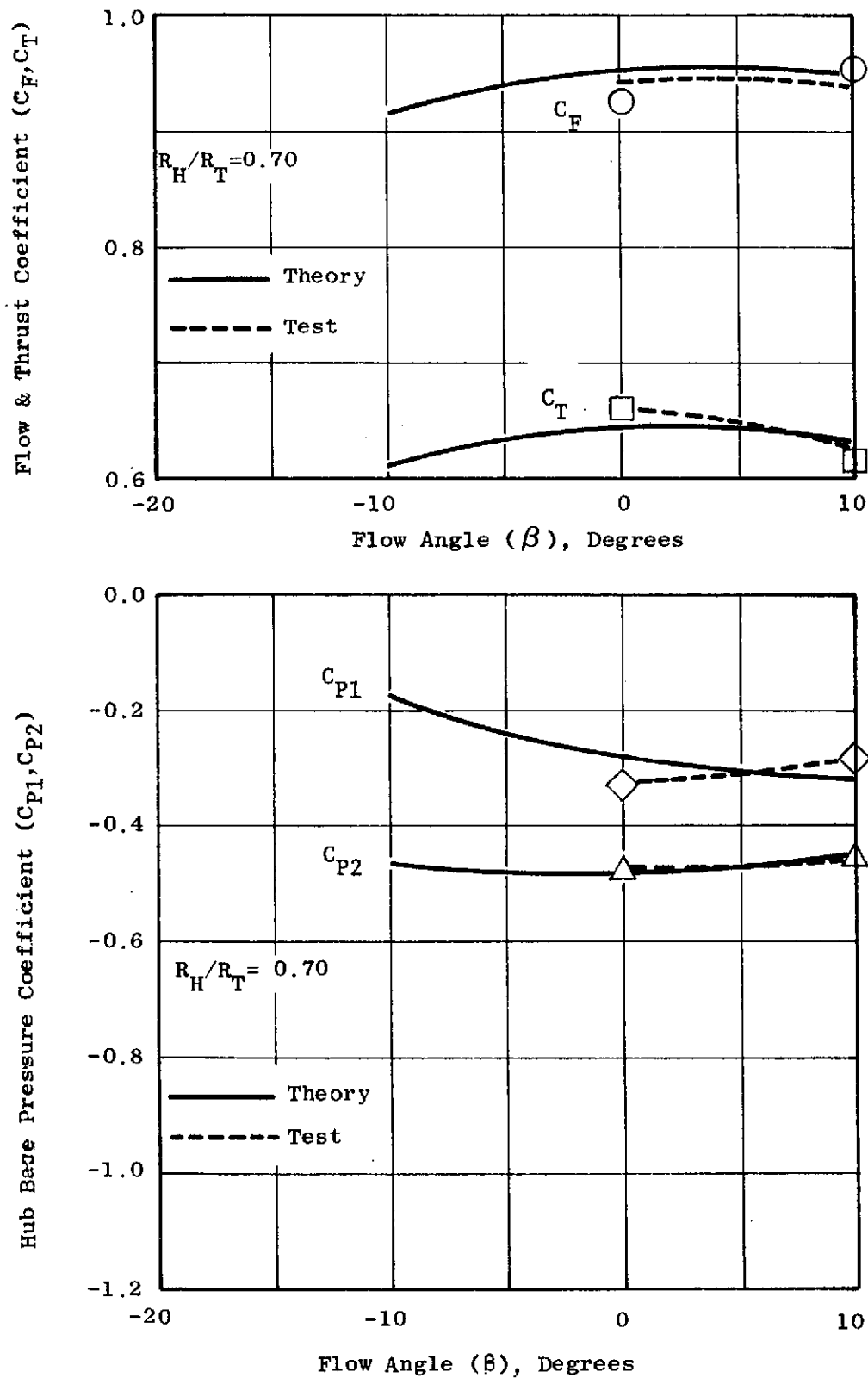Figure 92. Variation of $C_{PL}$ and $C_9$ with Geometry
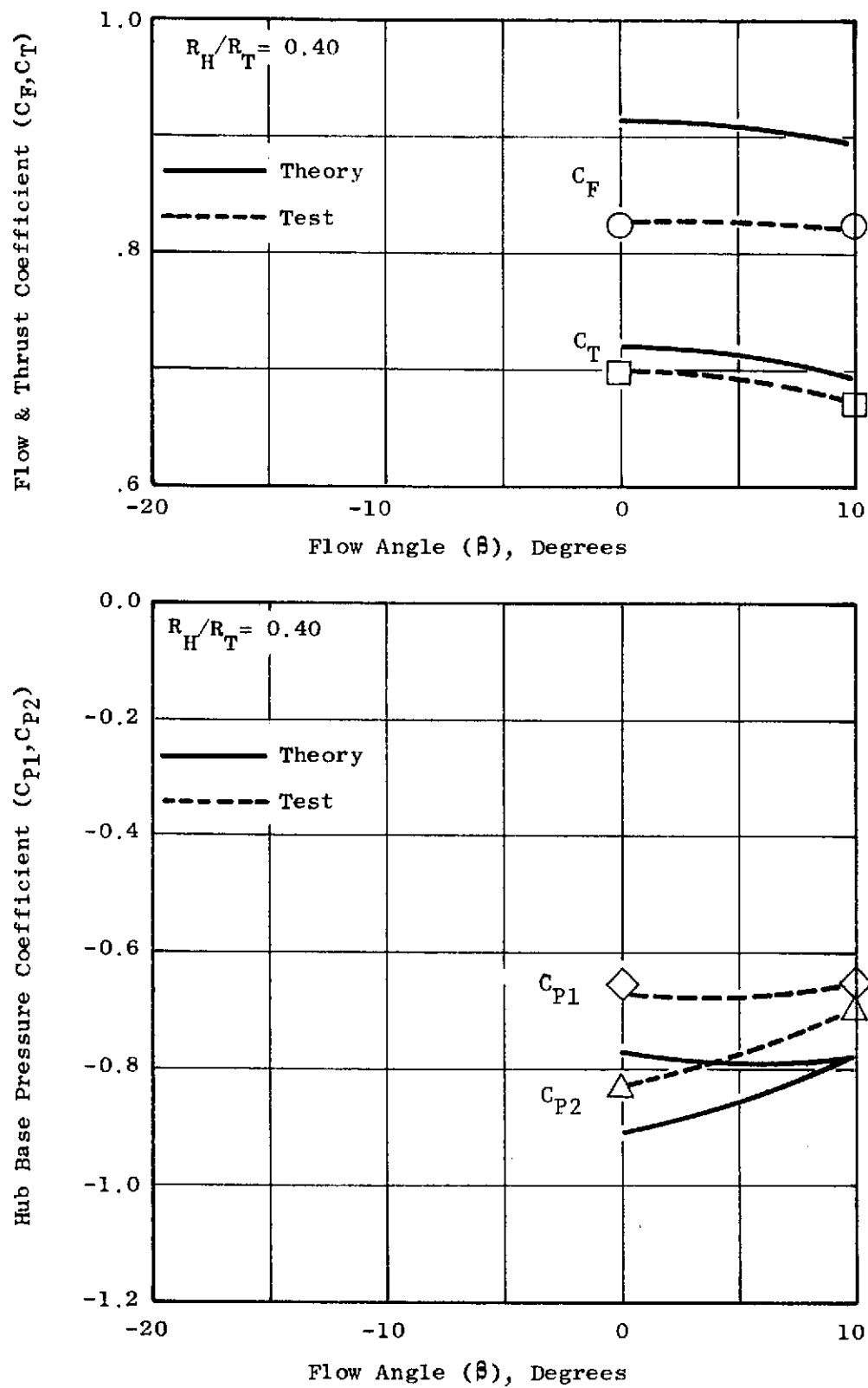
Figure 93.    Comparison of Theoretical Predictions to Test Results
for the Base Pressure, Flow and Thrust Coefficients,
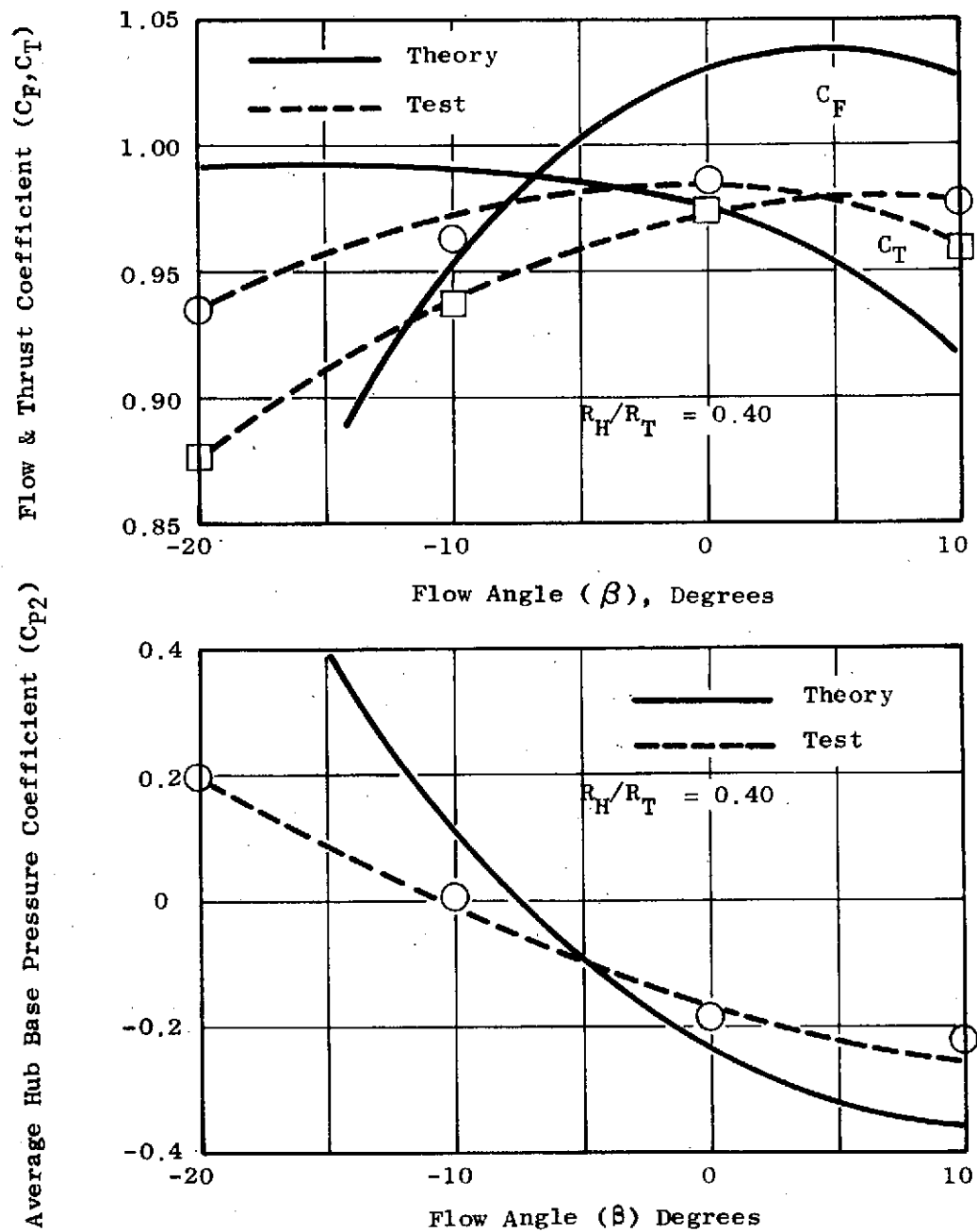$R_H/R_T$ = 0.40, Swirling Flow
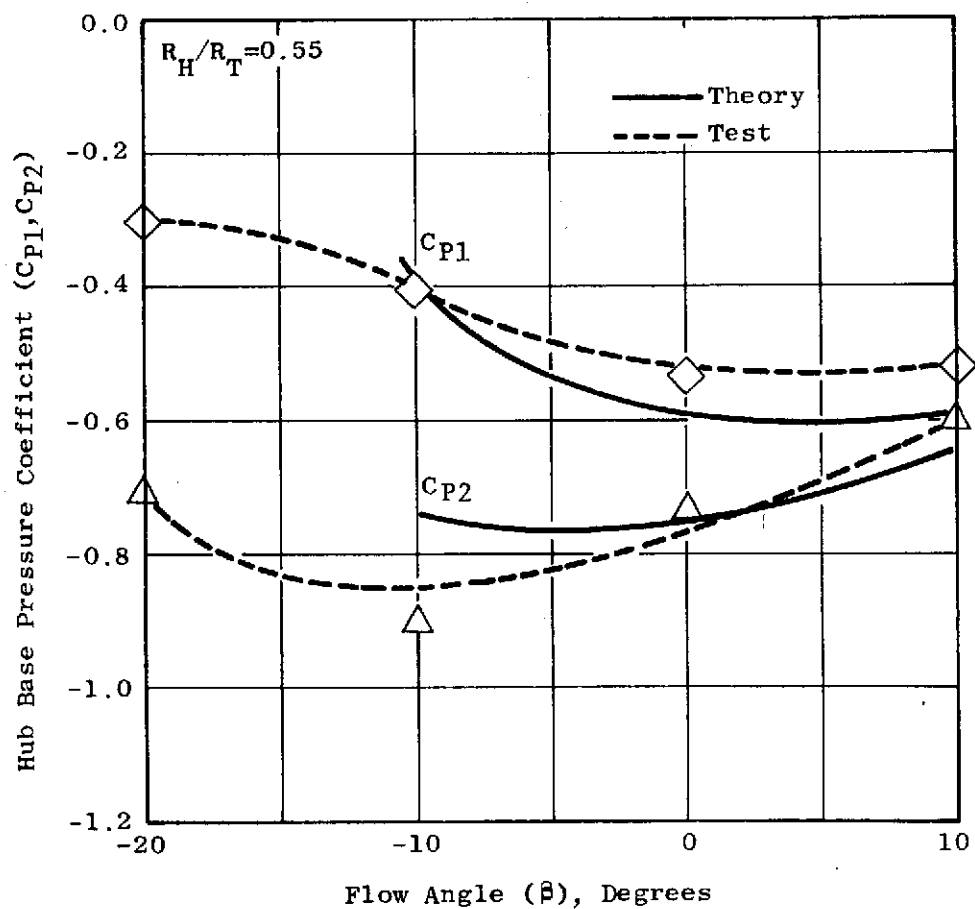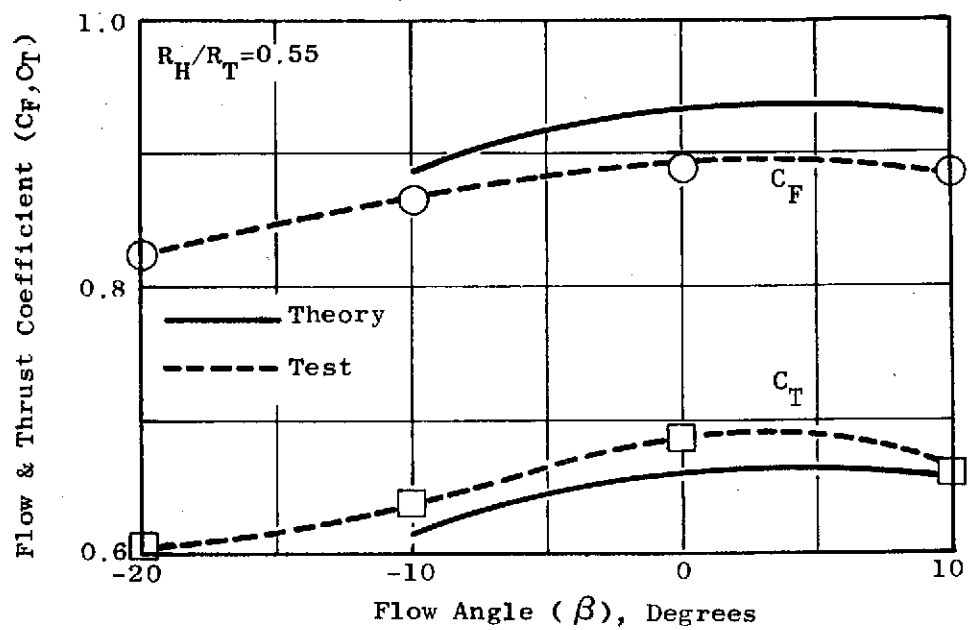
Figure 94.   Comparison of Theoretical Predictions to Test Results
for the Base Pressure, Flow and Thrust Coefficients,
$R_H/R_T=0.55$, Swirling Flow

Figure 95. Comparison of Theoretical Predictions to Test Results for the Base Pressure, Flow and Thrust Coefficients, $R_H/R_T = 0.70$, Swirling Flow

Figure 96.    Comparison of Theoretical Predictions to Test Results
for the Base Pressure, Flow and Thrust Coefficients,
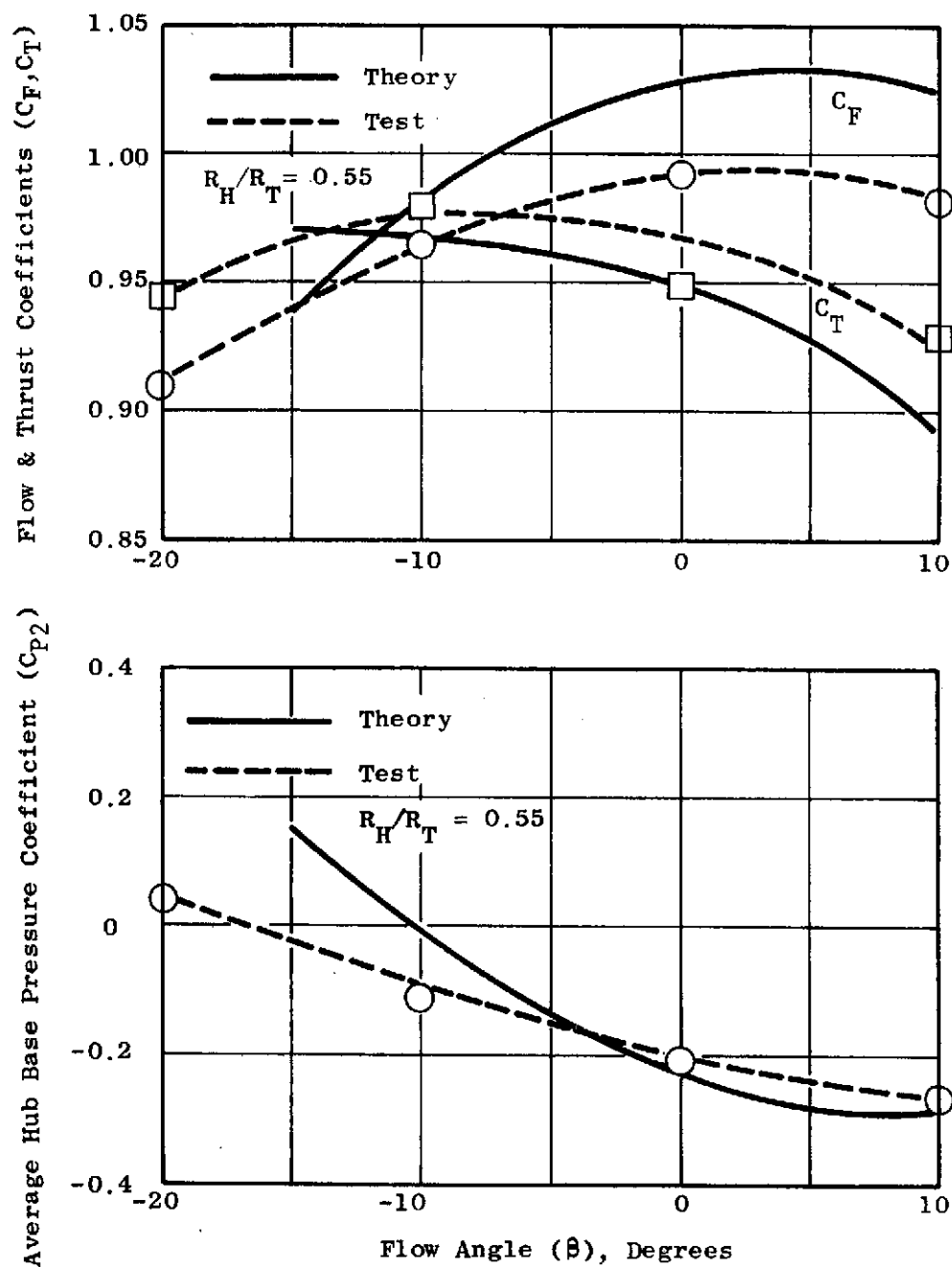$R_H/R_T$ = 0.40, Axial Flow

Figure 97.   Comparison of Theoretical Predictions to Test Results
for Base Pressure, Flow and Thrust Coefficients,
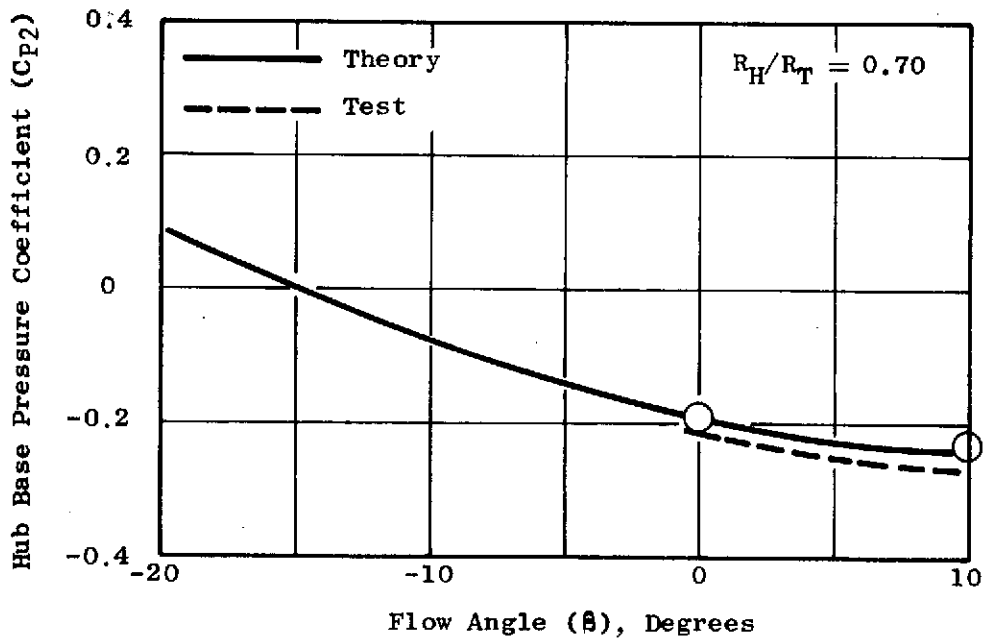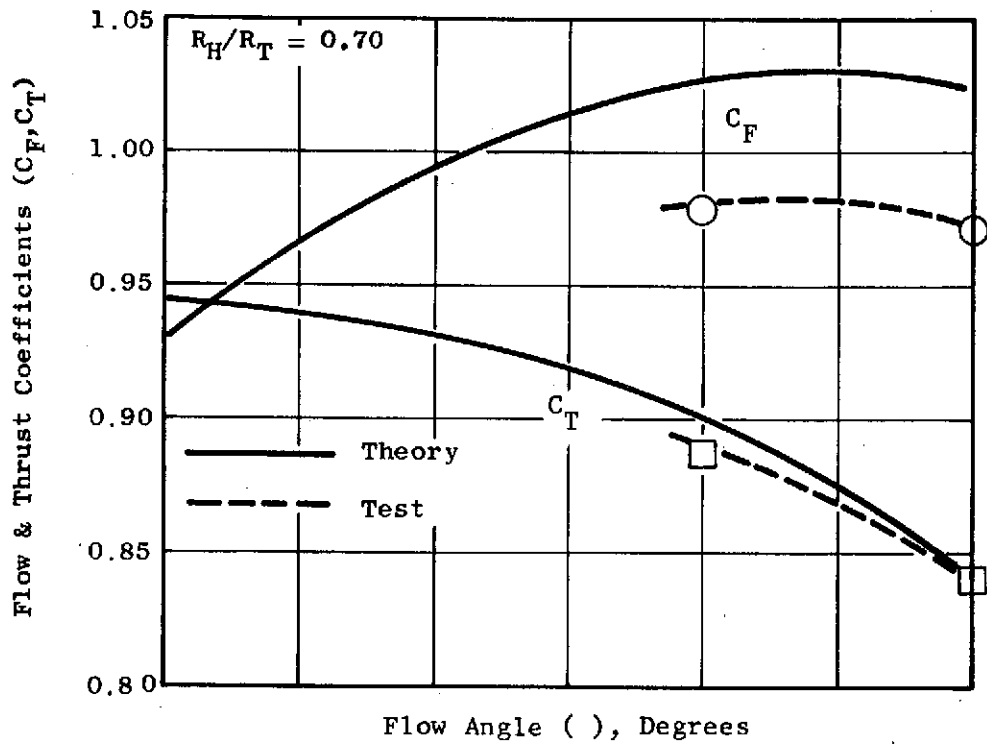$R_H/R_T$ = 0.55, Axial Flow

Figure 98. Comparison of Theoretical Predictions to Test Results
for Base Pressure, Flow and Thrust Coefficients,
$R_H/R_T = 0.70$, Axial Flow